Thermoplastic Composites for Underwater Applications

Maël Arhant

To cite this version:

Maël Arhant. Thermoplastic Composites for Underwater Applications. Matériaux composites et construction. École centrale de Nantes, 2016. English. NNT : 2016ECDN0029 . tel-03237825

HAL Id: tel-03237825
https://theses.hal.science/tel-03237825v1
Submitted on 26 May 2021

Thèse de Doctorat

Mael ARHANT

Mémoire présenté en vue de l'obtention
du grade de Docteur de l'École Centrale de Nantes
sous le sceau de l'Université Bretagne Loire

École doctorale : Sciences pour l'Ingénieur, Géosciences, Architecture

Discipline : Mécanique des solides, des matériaux des structures et des surfaces
Unité de recherche : Institut de Recherche en Génie Civil et Mécanique

Soutenue le 9 Décembre 2016

COMPOSITES THERMOPLASTIQUES POUR ENCEINTES SOUS-MARINES

JURY

Président :	**Philippe OLIVIER**, Professeur des universités, Université de Toulouse
Rapporteurs :	**Federica DAGHIA**, Maître de Conférences- HDR, Ecole Normale Supérieure de Cachan
	BrunoFAYOLLE, Professeur des universités, ENSAM Paris
Examinateur:	**Fréderic JACQUEMIN**, Professeur des universités, Université de Nantes
Invité:	**Christophe BRIANÇON**, Docteur, CETIM, Technocampus EMC2, Bouguenais
Directeur de thèse :	**Christian BURTIN**, Maître de Conférences - HDR, Ecole Centrale de Nantes
Co-directeur de thèse :	**Peter DAVIES**, Chargé de recherche - HDR, IFREMER Centre de Brest

Acknowledgments

I've heard several times that one can feel lonely during a PhD, which was absolutely not the case for me. As a result, I do not consider this work as my own but the fruit of an amazing collaboration between everyone involved in this project. I hope this short but important section will show you, brave reader, that all the persons and cat cited in this section deserve a lot of credit.

First, I would like to thank my advisors, Christian Burtin, Peter Davies and Christophe Briançon for supporting me during these three years. Special thanks go to Peter, who always made himself available and always accepted answering the millions of questions I asked.

Second, I would like to thank the members of my PhD committee, Philippe Olivier for presiding the jury and Federica Daghia, Bruno Fayolle and Frederic Jacquemin for the time they spent reviewing the manuscript in details.

Special thanks also go to Maelenn Le Gall and Pierre-Yves Le Gac. This work would not have been possible without you two. Your guidance throughout this PhD made it what it is today. I would also like to thank Benoit Bigourdan and Nicolas Dumergue for their help and guidance throughout this PhD.

I would like to thank the entire LCSM department and the RDT unit at Ifremer for helping me whenever I needed help, either concerning science or other crucial matters (coffee...!). I would especially like to thank the technicians of the LCSM laboratory: Nico, Mick, Luc, Christophe, Arnaud, Patrick and Bertrand for the technical help they provided all along this study.

Grateful thanks also go to Benoit Courtemanche, Didier Mastain and the other collaborators at CETIM for all the help they provided all along this study concerning the manufacture of the different cylinders.

Then, I would like to thank my roommates and colleagues Corentin Humeau and Aurélien Gangloff for their help throughout this PhD. You just saw what it's like to finish one. Now, it's your turn to enter the final year and I'll be here to see you defend next year.

Grateful thanks also go to Eric Lolive and Thomas Bonnemains from the IUT of Brest, who helped me manufacture the different composite panels that were produced during this PhD. A significant part of this work would not have been possible without you two.

I wish to express my thanks to Professor Dayakar Penumadu from the University of Tennessee, whom I had the chance to visit during this PhD. I have learned a lot during our collaboration and I hope that we will be able to work together again in the future. Special thanks also go to Nathan Meek who contributed a lot in this work. Apart from work, you made this trip to Knoxville a real blast.

Concerning my friends from Binic, Saint Brieuc, Paimpol, Rennes and Nantes, I am not sure whether I should thank you or not, since you guys are the reason why I am mostly tired on Monday mornings.

I also need to thank Patrick and Laurence Quemar for the suit I wore during the defense...! You will get it back, I promise...!

We now enter the sensitive part, the family. First, I would like to thank my parents, Isabelle and Goulven Arhant and my little sister, Léna, who always supported and guided me in all of my choices. Growing up in such a positive environment makes everything much easier. This PhD wouldn't have been possible otherwise. I would also like to thank my cat, Neige, for being...around... Then, just a few words to my younger self, who I'm sure is laughing so hard knowing that I just finished a PhD.

Grateful thanks also go to my grandmothers, Mireille Verlynde and Yvonne Arhant. Concerning the latter, I made you sign a contract at the beginning of this PhD stating that you weren't allowed to leave this planet until the end of this contract. You made it through ! We probably need to sign another one now...!

My final word goes to my grandfather, Jacques Vitse, who passed away at the very beginning of my PhD. At the time, when I told you that I would become a Doctor, you were already so proud. You first understood that I was studying at med school and that I would be able to heal you from your long illness. Unfortunately, thermoplastic composites were not exactly a solution to your cancer. However, I will never forget you and what you said. You were and still are a true model for me. I hope this work would have made you proud. It is dedicated to you.

Contents

Introduction

The year 2015 has been recognised as being the warmest year ever recorded in modern history. While this information is only related to the surface temperature (atmosphere), the main concern today is focussed on the oceans that absorb more than 90% of the energy linked to global warming. This long term warming trend raises several questions, in particular on how the latter will influence the future climate changes. Understanding and predicting these changes is essential, however, 70% of the oceans still remain unexplored and deep water masses possess very specific properties (temperature, salinity) that have to be measured in real time. Therefore, with an average depth of over 3800 meters, it is necessary to design exploration and monitoring devices that are able to withstand high hydrostatic pressures.

For many years, metals have been used underwater. However, due to their excellent specific properties, composite materials are starting to replace existing deep sea structures. Those used today in a marine environment are almost exclusively thermoset-based composites (polyester, epoxy). These pressure vessels, manufactured by filament winding, require high thicknesses (more than 10 mm) and obtaining such thicknesses without defects is a real challenge; residual stresses and delaminations are common and can lead to premature failures.

There is an increasing number of thermoplastic matrix polymers available on the market (PP, polyamide, PPS, PEEK, PEKK…), which offer possibilities for forming by local heating, attractive mechanical properties, good environmental resistance and the potential for end of life recycling. More ductile, and reparable by melting, they offer a real potential for greatly improved devices. From a scientific point of view, most of the previous studies conducted on these materials were focused on aircraft structures, i.e. thin structures, and several studies have made connections between manufacture and microstructure. However, their influence on the biaxial compression for thick pressure vessels has not been studied yet. In 2013, the CETIM (Technical Centre of the Mechanical Industries), located in Nantes (France), invested in a Laser Assisted Tape Placement (LATP) machine. Controlling the process and its parameters (placement velocity, temperature, roller pressure, etc.) allows a thorough evaluation of the potential of these materials for such applications. Thermoplastic composites are a family of materials in which the manufacturing parameters have a strong influence on the microstructure and the mechanical performance. The understanding and the control of these relationships are essential to optimise structures and this requires a strong collaboration between the manufacturer and the testing laboratory, which is a feature of the current study. Additionally, little work is found in the literature concerning the aging behaviour of carbon reinforced thermoplastic composites and it is not clear what their durability will be in such harsh environments. Understanding and being able to predict the effect of prolonged deep sea immersion on both the water diffusion and the mechanical properties is essential when long service lives (several years) are considered.

The principal objective of the current study is to manufacture thick thermoplastic composite cylinders (over 10mm) by Laser Assisted Tape Placement that can resist high hydrostatic pressures (above 400 bar). Their behaviour will be compared to that of the existing carbon/epoxy cylinder used at Ifremer for deep sea applications, called the DEEP ARVOR profiler that can dive down to 4500 meters, which will be presented in detail later in the study. It is 1.2 meters long, has an inner diameter of 120 mm, and a thickness of 12 mm. To achieve such a goal, the study has been divided into seven sections, that will investigate the behaviour of these new thermoplastic materials subjected to extreme conditions (immersion at low temperatures ranging from 4 to 15°C coupled with high hydrostatic pressures). The project is a collaboration based on the manufacturing experience of the CETIM and the testing facilities and knowledge of Ifremer and the Ecole Centrale de Nantes.

In Chapter 1, particular emphasis will be placed on published knowledge of composite cylinders for underwater applications, both concerning thermoset and thermoplastic based composites. From this, several difficulties are highlighted, associated with the manufacturing process used to produce the cylinders, the way to measure the compression properties, and the effect of water aging.

In Chapter 2, the different materials and the experimental techniques used in this study are presented.

In Chapter 3, water diffusion has been investigated, first in the unreinforced matrix and then in the laminate. Diffusion kinetics are identified and then used to predict the water diffusion in the real structure, i.e. a thick thermoplastic cylinder immersed at low temperatures for several years.

In Chapter 4, an extensive experimental study is described to study the effect of water diffusion on the tensile, compressive and out-of-plane mechanical properties. These are then used to predict how water absorption could limit the use of thermoplastic cylinders for deep sea applications.

In Chapter 5, the effect of processing conditions is investigated. The effect of cooling rate on the crystallization kinetics has been examined and associated modelling is presented. Then, the influence of crystallinity on the mechanical properties is presented. Finally, differences between properties obtained by hot press forming and Laser Assisted Tape Placement are discussed.

In Chapter 6, residual stresses and strains have been investigated both on composites manufactured by press forming and by Laser Assisted Tape Placement. Moreover, the effects of environmental conditions (temperature and humidity) have been investigated in detail using different techniques.

Chapter 7 describes the manufacture of thermoplastic composite cylinders by Laser Assisted Tape Placement, and presents results from pressure vessel testing to implosion. The implosion pressures were then compared to values measured on the C/Epoxy reference used today at Ifremer.

Finally, a general conclusion is given to highlight the main achievements of this work and discuss prospects for future studies.

A schematic diagram illustrating the study is presented in Figure 1.

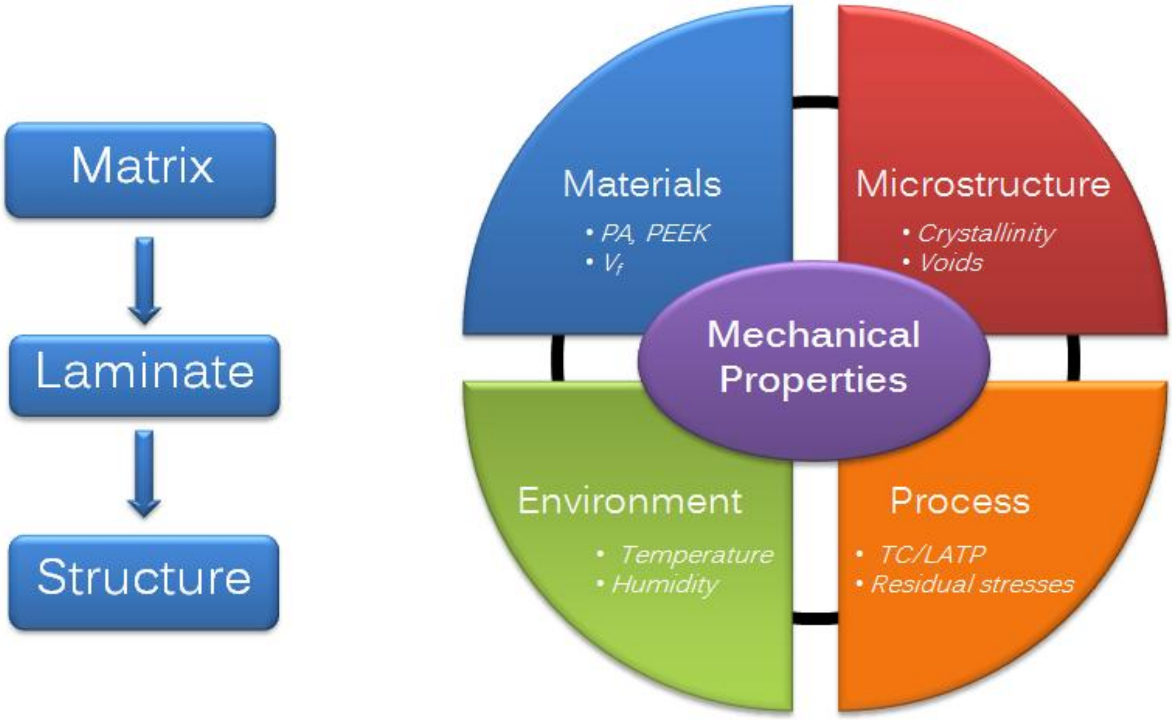

Figure 1 : Schematic diagram of the study

Chapter 1

Context and Literature review

Studying the performance of thick thermoplastic composite cylinders for underwater applications is a complex subject in which several aspects have to be investigated separately.

First, the manufacturing step has to be studied carefully to ensure that the cylinders are of good quality. Even though the Laser Assisted Tape Placement process has been used for several years and has significant potential, it has not reached its full maturity and further work is needed to fully master this manufacturing process. Another difficulty is that these composite cylinders have to be of a certain thickness (over 10 mm) to resist high hydrostatic pressures (above 400 bars). However, manufacturing thick composite parts is not an easy subject due to residual stresses, property gradients and induced defects such as delaminations. Therefore, this aspect also has to be studied in parallel.

Then, cylinders under hydrostatic pressures are subjected to compression loadings. Therefore, the compression properties of the composite have to be determined and this is known to be a controversial subject. The compressive properties are highly dependent on the test fixture, and various other parameters affect these values as will be discussed in the literature review.

Finally, these cylinders will be immersed in sea water, which is known to be a severe environment, so aging will occur. This aspect is known to have a significant effect on the mechanical properties and it can severely limit the use of such materials. Therefore, understanding the effects of aging on the long term behaviour of these thermoplastic composite materials is essential.

Therefore, in this chapter, existing results for all these aspects will be discussed and missing data will then be highlighted.

1. Composites for underwater applications

1.1.Thermoset composites for underwater applications

The use of composites for pressure hulls of underwater vehicles and submarines has been an ongoing research topic for many years, since early work in the UK by Smith and colleagues in the 1970's [1]. They focused on glass reinforced thermoset composites, but subsequently their work was extended to carbon fibre reinforced thermosets in the 1990's as the potential of these materials for weight saving became apparent.

Over the last 30 years, several metallic pressure hulls started being replaced by composite materials, for some unmanned submersibles (autonomous underwater vehicles) for instance. Two examples are AUTOSUB [2] and the AUSS [3]. Design of the AUTOSUB started in 1988 for the UK Natural Environment Research Council and the first complete vehicle was built between October 1995 and May 1996. It undertook its first autonomous mission in July 1996, it is 7 meters long and has a depth limit of 1600 meters. The AUSS (Advanced Unmanned Search System) vehicle, developed for the US Navy in the 1980's, was designed to operate down to 6000 meter depth. It is 5 meters long, 0.8 meters in diameter, and weighs 1.2 tons. The centre section is a cylindrical carbon/epoxy pressure hull (wound at $0/90_2$) with titanium hemispherical ends.

Large quantities of composites are also used for military submarines. While many of the details are confidential, some published information is available [4], [5]. Lemière [4] relates that external decks of conventional French submarines were made of glass reinforced composite from 1974. For the "Triomphant", a missile-launching nuclear submarine, composite applications include the sonar dome, the propulsion unit and fins, and the outer deck. Additional information is found in [6].

Various US Navy and ONR (Office of Naval Research) programmes and several European projects (e.g. EUCLID RTP 3.8, DEVILS, MAST-AUV, MAST-Composite Housings), all of which IFREMER was involved in, have resulted in a solid database of test results from implosion studies on a range of materials and geometries [7]–[10]. Other more academic studies have included buckling [11], [12], failure envelope determination [13]–[15], post-buckling behaviour [16], and studies of winding angles [17].

The use of composite cylinders for oceanographic containers has been developing for many years. At Ifremer these materials have been employed for various prototypes. The first application in the 1990’s was the SAR magnetometer, a 100mm diameter glass fibre reinforced tube. In the GEOSTAR project 55mm diameter glass/epoxy tubes were used as buoyancy units at 4000m depth. Composites were also considered for the instrumentation protection in the ANTARES neutrino telescope project, and some tests were performed at sea in 2500 metres water depth [18], but titanium alloy was finally adopted for cost reasons.

1.2. Application of interest

The application of interest here is the casings of autonomous ocean profilers. These are tubes containing sensors which follow ocean currents at different depths taking measurements (temperature, salinity…) and rise to the surface periodically to send the data. They then return to their programmed depth, as shown in Figure 2.

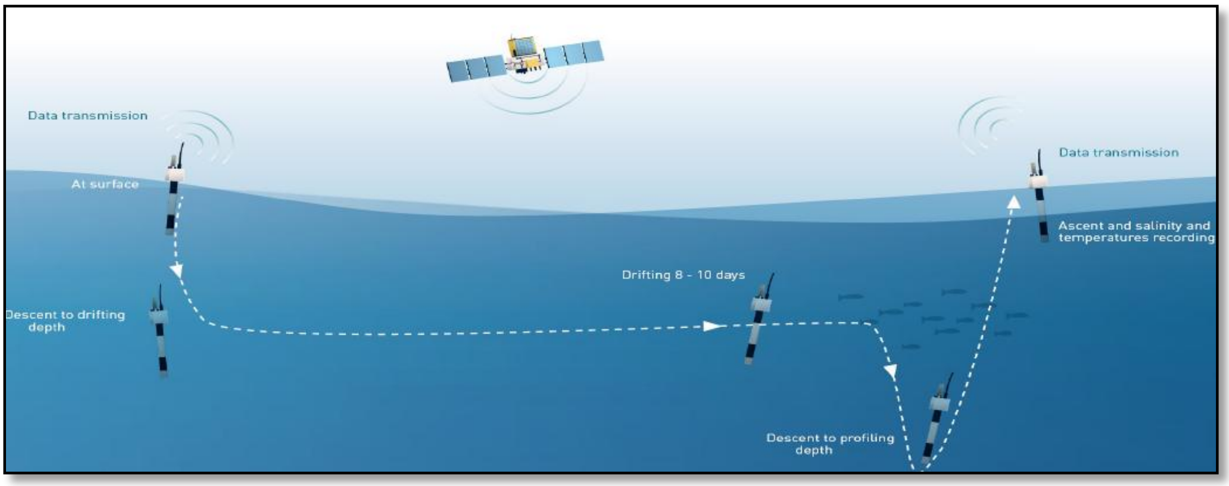

Figure 2 : Profiler program

At shallow depths (2000 metres) aluminium alloy was used, but for 4500 metres depth the recent DEEP ARVOR project has resulted in the development of a carbon/epoxy profiler, Figure 3. These cylinders are 1.2 meters long, have an inner diameter of 120 mm and a thickness of 12.7 mm. The aim is to manufacture thermoplastic counterparts that could replace the thermoset cylinders used today.

Figure 3 : DEEP ARVOR profiler used at Ifremer for deep sea applications

These profilers are manufactured by Filament Winding, an automated process where the fibres are passed through a resin bath and are then wound on a rotated mandrel to a given orientation, as shown on Figure 4. This process is used to manufacture composite cylinders at low cost and at relatively high production rates, even though a postcuring stage is needed. However, manufacturing thick thermoset composite cylinders is not an easy task because of the significant exothermic reaction occurring during crosslinking that is responsible for significant voids inside the cylinders. These are currently a major problem for the application.

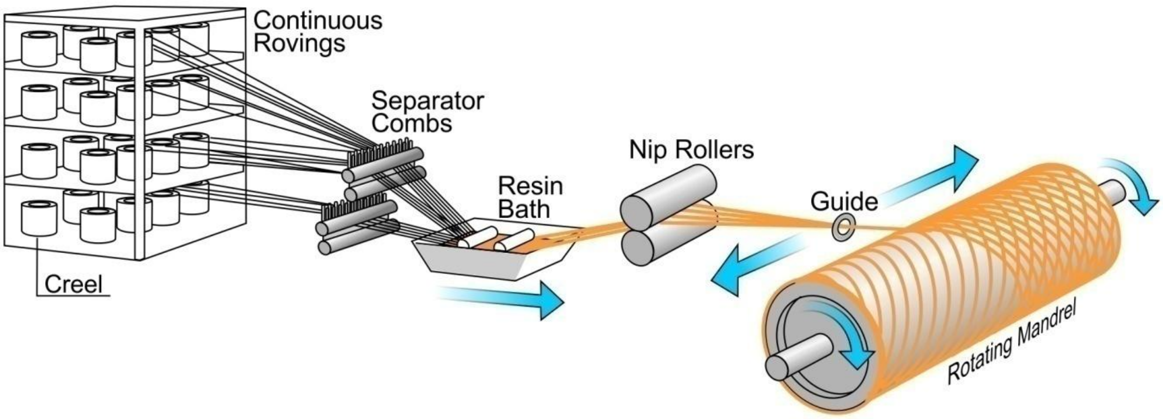

Figure 4 : Filament winding process

1.3.Thermoplastic composites for underwater applications

Results concerning thermoplastic composite cylinders subjected to hydrostatic pressure are quite rare. A study in the USA on carbon/PEEK was described by Gruber et al [19]. At Ifremer, studies were performed from 2000 onwards, to examine different thermoplastic matrix polymers for cylinders [20]. These tubes were supplied by American companies, first small diameter (55mm, 6mm wall thickness) then larger (175mm diameter, 20mm thick). Two were retained for hydrostatic pressure testing, carbon/PEEK and glass/PEI. The former were very promising, implosion pressures similar to those for carbon/epoxy were obtained, while the latter suffered from poor manufacturing quality (high porosity) and imploded at much lower pressures than glass/epoxy of similar geometry.

Concerning offshore applications, these are not the aim of the present project, but it should be noted that considerable work has been performed on long tubular composites both for risers and other flow-lines. Early work by IFP and Aerospatiale [21] in the 1980's was followed by various other projects over the last 25 years [22]–[25] to develop thermoset composite tubes with metal liners, and the publication of guidelines by the DNV. Other groups have focused on thermoplastic matrix composites, in particular the Dutch company Airborne[1] which supplies down-lines for sub-sea intervention with various thermoplastic polymers and the British company Magma[2] which is developing PEEK composites.

2. Benefits of Thermoplastics over Thermoset matrix polymers

Fundamental differences exist between thermoset and thermoplastic polymers. Concerning the former, these are formed through a chemical reaction between a monomer, an accelerator and a catalyst or between a pre-polymer and a hardener that will start the reaction. The liquid resin then passes into the solid state through a crosslinking process and this reaction is irreversible. Once this reaction has occurred, it is no longer possible to reshape the thermoset resin. Exposures to high temperature will degrade the material rather than melting it, unlike thermoplastic polymers. Thermoplastic polymers are fundamentally different from their thermoset counterparts because the matrix has already undergone polymerisation prior to processing. Semi-crystalline polymers are mostly characterised by two main properties, the glass transition temperature T_g and the melting temperature T_m. The melting temperature is characteristic of semi-crystalline polymers as thermosets are not able to crystallize.

---

[1] http://airborne-oilandgas.com/

[2] https://www.magmaglobal.com/technology/

Concerning composite materials, continuous fibre reinforced thermoset composites have been used in industry for more than 50 years, either in aircraft structures, naval structures or in automotive applications. However, fewer thermoplastic composite parts are found in industry, even though these materials have been studied for more than 30 years. Difficulties are mainly associated with the manufacturing process where high temperatures are needed to lower the viscosity of the matrix. Also, these materials are usually more expensive than their thermoset counterparts. However, they generally offer increased impact resistance and have an infinite shelf life, which is a non-negligible advantage over thermosets. Additionally, they are much safer during processing than the thermoset counterparts which can release toxic emissions during manufacture. The main advantages and drawbacks of thermoset and thermoplastic materials are presented in Table 1.

Table 1 : Advantages and drawbacks of thermoset and thermoplastic composites

	Thermoset composites	**Thermoplastic composites**
Advantages	High temperature resistance	Infinite Shelf Life
	Relatively cheap	Recyclable
	Low viscosity	Impact resistance
	Well established properties	Chemical resistance
	Excellent bonding with fibres	No emissions
Drawbacks	Limited shelf life	High viscosity
	Difficult to manufacture thick composite parts	High manufacturing temperatures
	Non recyclable	Generally more expensive

Semi-crystalline polymers such as PEEK and Polyamides show a distinct microstructure and are able to crystallize upon cooling. A degree of crystallinity X_c can be measured. During cooling, the crystallites that are formed can have different shapes and sizes and this has an influence on the degree of crystallinity and mechanical properties [26], [27]. The faster the cooling rate the lower the degree of crystallinity and the smaller the crystallites. Moreover, in the case of composite materials, the fibres (either carbon or glass for instance) may have a strong effect on the degree of crystallinity but also on the geometry of the crystallites, as fibres are known to have an effect on the nucleation of crystallites and transcrystalline region may grow out from the fibres [28]. Therefore, understanding this behaviour and being able to describe it is of primary interest when investigating different manufacturing processes, for which the thermal conditions (cooling rates) are very specific and different.

3. Processing Thermoplastic composite cylinders

3.1. Laser Assisted Tape Placement (LATP)

Automated Tape Placement is a process used for both thermoset and thermoplastic composite materials. It was first developed in the 1960s but mainly for thermoset composite materials in aircraft structures [29].

This process uses narrow bands (tapes) of prepregs (typically 1 inch, ½ inch or ¼ inch wide) that are laid ply-by-ply on a mandrel or surface (flat or curved). These are consolidated upon deposition using a compaction roller. Intimate contact between the plies is ensured by a local increase of the tape temperature. In the case of thermoplastics, this temperature is above the melting temperature to lower the viscosity of the matrix. A schematic illustration of the process is shown in Figure 5 and an actual picture of the Laser Assisted Tape Placement machine used in this study is shown in Figure 6.

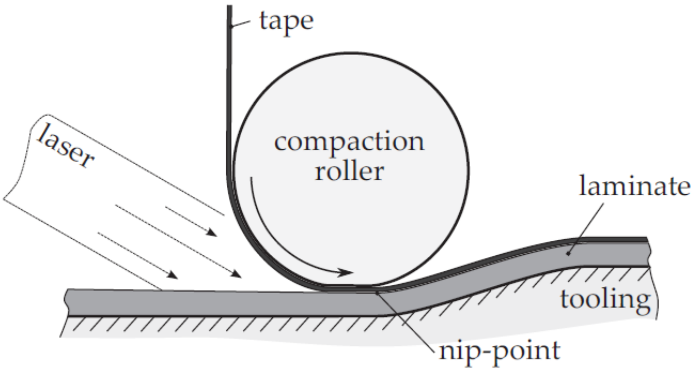

Figure 5 : Principle of the Laser Assisted Tape Placement process

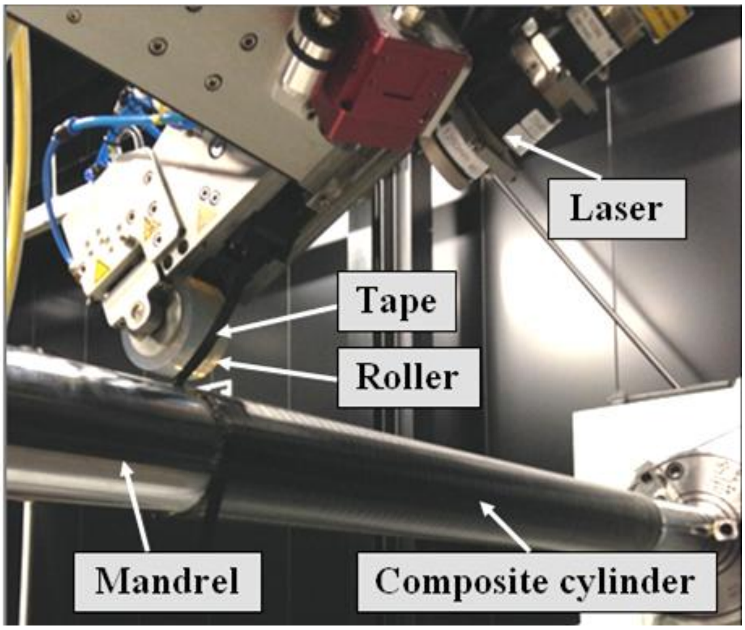

Figure 6 : Thermoplastic composite cylinder manufactured by Laser Assisted Tape Placement at the CETIM Composite facility

Several difficulties can be highlighted with this process. First, contrary to other processes, many parameters have to be mastered such as the laser angle, the tape back tension, the manufacturing speed, the mandrel temperature, compaction pressure. Additionally, parameters related to the hardware itself (heat source, roller type), material aspects (fibre distribution through the tape thickness, tape surface roughness, void content [30], [31]) and to the composite structure (edge connections between tapes: gaps, overlaps [32]) have also proved to have a significant influence. All these aspects show that manufacturing composite parts using this new process is not an easy task. For each material of interest, optimal parameters have to be determined and the time needed to obtain these depends on the operator/lab/company's experience with LATP [33]. Extensive studies have been conducted to investigate the effects of all these parameters. It may be noted that most of the results reported in the literature focused on C/PEEK laminates. For instance, optimum heating temperatures [31], [33] are to be found to reach the maximal mechanical properties as well as optimum mandrel temperatures that have been shown to reduce residual stresses [34]. It has been shown that lower laying speeds usually lead to improved mechanical properties [35], [36] as the increased healing time leads to a better intimate contact [35]. However, as stated by Pitchumani et al.[37], lowering the laying speed results in better properties but does not lead to time optimal solutions. Therefore, depending on the application of interest, a compromise must be made. Moreover, increased laying speeds lead to much higher cooling rates that can have a significant influence on the degree of crystallinity. Difficulties associated to through-thickness differences in degrees of crystallinity can arise due to the multiple passes of the laser head and can induce unwanted re-crystallizations. Top layer compaction has been shown to reduce the void content and led to higher mechanical properties, although it still did not reach the thermocompression properties. However, several studies have shown that after an autoclave reconsolidation process, the autoclave mechanical properties were recovered [34]. An excellent review was recently conducted by Stokes-Griffin and Compston [38] which grouped different interlaminar shear strength results obtained by many authors; that highlighted a significant effect of the manufacturing process parameters on strength, as shown in Figure 7. They also showed that it is very difficult to obtain mechanical properties as high as those obtained by autoclave or thermo-compression.

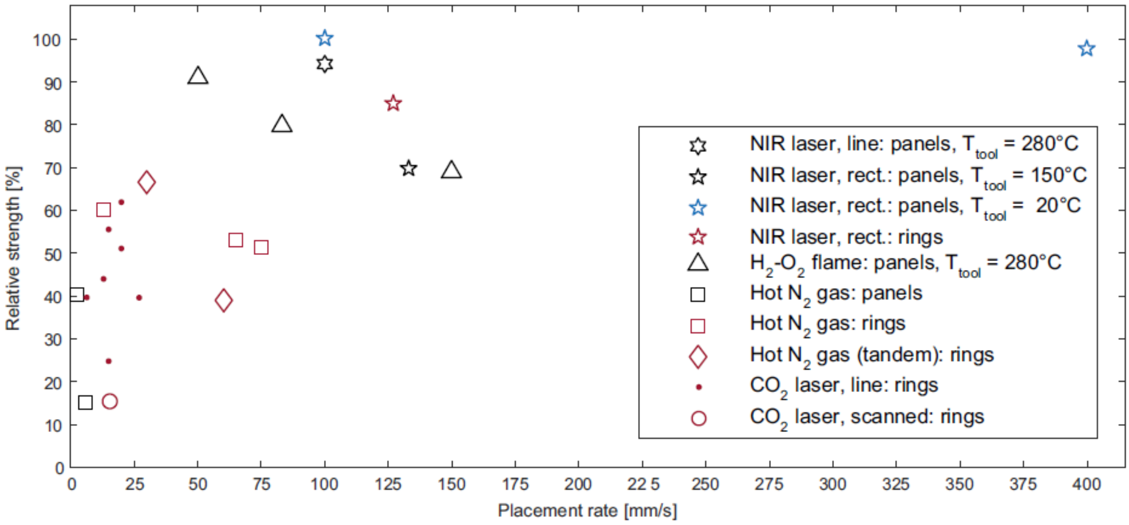

Figure 7 : Relative Interlaminar shear strength as a function of placement rate

Comer et al. [39] conducted a study in which they compared the C/PEEK properties obtained by LATP to the autoclave reference. The differences that were highlighted were attributed to a lower quality in terms of voids of the LATP panels and to a matrix of a more amorphous nature.

These results show that this type of process has not reached its full maturity yet, even though it has been available for more than 20 years. However, an alternative manufacturing process, thermo-compression moulding is well controlled nowadays and is usually taken as a reference compared to other processes.

3.2.Thermo-compression (TC)

The thermo-compression process is used to produce high performance composites and is widely used in industry. In this process, both heat and pressure are used to produce the composite part. Prepreg plies are stacked together at the chosen orientation inside a mould.

The mould is then heated up to the desired temperature (for semi-crystalline polymers, above the melting temperature) and the pressure is applied. The main advantage of this process is that it is highly reproducible. As for every process, optimum process parameters have to be determined and these depend on the chosen material. The effect of heating temperature [40] on the mechanical properties has been reported several times in the literature as well as the effect of cooling rate [41], [42] and holding pressure [43]. This is a very interesting process to investigate such effects in order to obtain the reference mechanical properties and it will be used subsequently in the present study.

4. Residual stresses

Also, during the manufacturing stage of carbon reinforced thermoplastic composites, residual stresses are created and these can have a significant effect on the mechanical properties that may exceed the strain required to initiate damage, especially when the thickness becomes large [44]. The next section will present a short literature review on the formation of residual stresses and experimental techniques for their determination.

4.1.Formation of residual stresses

Residual stresses are introduced in composite materials during manufacture and these are formed at three different scales. These can be formed at the microscopic scale (fiber and matrix scale), mesoscopic scale (lamina, ply to ply) and the macroscopic scale (laminate, structure scale), as shown schematically in Figure 8.

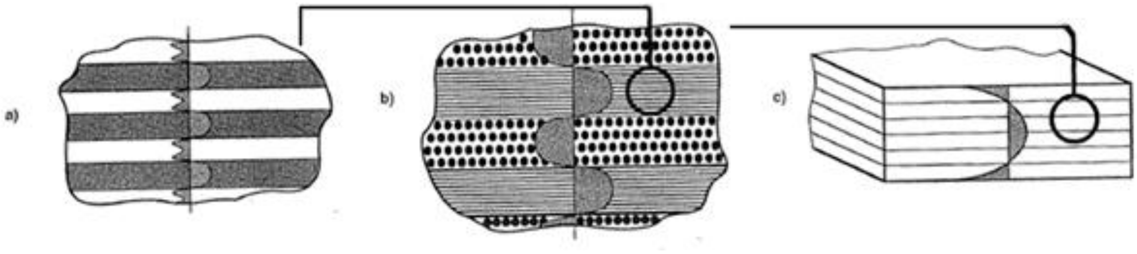

Figure 8 : Different scales (a) Microscopic (b) Mesoscopic (c) Macroscopic [45]

At the microscopic scale, thermal residual stresses arise from the heterogeneity (mismatch) in coefficients of thermal expansion (CTE) between the fibres and the matrix [46]. The shrinkage of the matrix is usually significantly higher than the shrinkage of the fibres, so residual stresses are created between them. Carbon fibres possess a highly anisotropic thermal expansion behaviour. The shrinkage is much higher in the radial direction than in the longitudinal one, making the residual stresses higher [47]. The difference in CTE in radial and longitudinal directions is even greater because the CTE respectively is positive and negative in these directions, Table 2.

Table 2 : Coefficients of thermal expansion of AS4 fibers [48]

Material		CTE (°K^{-1})
AS4 fibres	Longitudinal direction	-0.22.10^{-6}
	Radial direction	10-20.10^{-6}

The morphology of the matrix plays a very important role in the formation of residual stresses. Amorphous and semi-crystalline polymers have very different shrinkages, with those of semi-crystalline polymers being significantly higher. Indeed, for thermosets and amorphous thermoplastics, residual stresses are mainly due to the shrinkage induced by the transition between the rubbery and glassy state, i.e. at the glass transition temperature. Due to their semicrystalline morphology, several thermoplastics combine both the glass transition and crystallization shrinkages during manufacture (Figure 9), which is one factor that significantly increases the residual stresses found in some thermoplastic composites. Another factor responsible for the high level of residual stresses in thermoplastics comes from the high temperature at which the thermoplastic laminate is manufactured, therefore resulting in a high differential temperature. Indeed, the larger the temperature differential during cooling the higher the residual stresses.

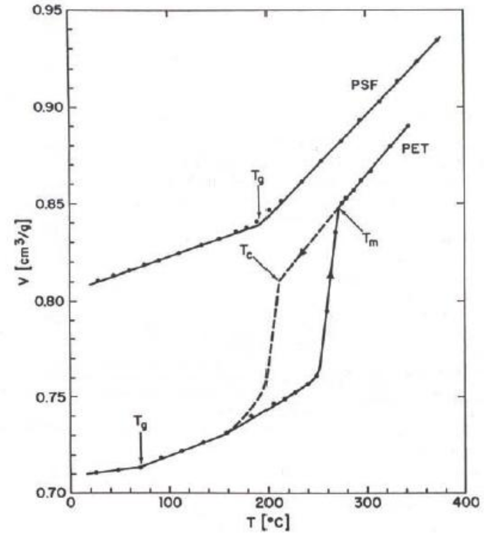

Figure 9 : Specific volume of polysulfone (PSF, amorphous) and polyethyleneterephtalate (PET, semi-crystalline) as a function of temperature at atmospheric pressure [49]

At the mesoscopic scale, i.e. at the ply level, the thermal residual stresses arise from the difference in coefficients of thermal expansion between the different plies, i.e. dependent on their orientation. For instance, in the case of cross-ply $[0/90]_s$ composites, the 0° plies impose a constraint on the 90° plies because of the different coefficient of thermal expansion of the plies (α_1 different from α_2). The residual stresses from this anisotropy are usually called interlaminar residual stresses. Therefore, residual stresses can either be of tensile (90° plies) or compressive (0° plies) nature. When these interlaminar stresses become too important, a bending moment is induced that can create a significant curvature of the composite. Also, when the interlaminar stresses are found to be higher than the transverse tensile strength of the composite, cracks is the 90° ply can be observed, and these can lead to delamination.

At the macroscopic scale (laminate scale), residual stresses can arise due to thermal gradients through the thickness of the composite, e.g. skin-core heterogeneities. A laminate usually experiences a slower cooling rate at the centre of the laminate. This implies that the surface of the laminate solidifies before the centre. Therefore, when the surface shrinks at a certain level rate and the centre does not, residual stresses are created. In the case of thermoplastics, if the laminate experiences different cooling rates through the thickness, there will be a gradient of crystallinity through the thickness that can also be the cause of macroscopic residual stresses.

4.2.Experimental techniques for their determination

Different methods are used for the determination of residual stresses, either destructive or non-destructive. Some of these methods were originally used for metals. It is important to note that in most studies, it is the residual strains that are measured and not directly residual stresses. Residual strains are measured according to different techniques and are then transformed into residual stresses through the elastic coefficients.

Destructive methods include the hole drilling method [50], [51] typically used in metals but also the first ply failure test [52], [53], the compliance method [54], [55] and the Layer Removal Methods [45], [56]. The latter has been used to study the effect of through-thickness crystallinity profiles on the residual stresses found in C/PEEK and C/PET unidirectional laminates. These are respectively shown in Figure 10.a and Figure 10.b.

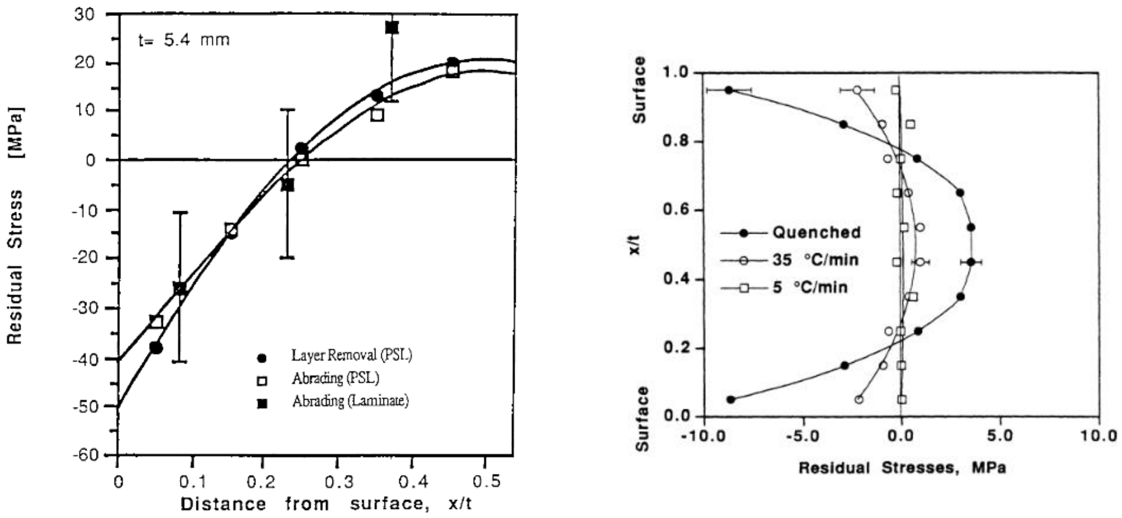

Figure 10 : (a) Though thickness residual stresses induced by through thickness gradient in crystallinity for C/PEEK [45] (b) Effect of cooling rate on the through thickness residual stresses in C/PET unidirectional laminates [56]

Non-destructive techniques include the use of embedded measurement systems such as strain gauges [57] or fibre optic sensors [58]–[61], X-ray diffraction [62], [63], the cure referencing method [64] and the measurement of out-of-plane deformation in asymmetric laminates [65]–[70].

Although considerable work has been done concerning the determination of residual stresses in laminates such as C/PEEK, no work has been reported yet concerning the residual stresses found in C/PA6 laminates. This will be discussed further in Chapter 6.

5. Mechanics of composite materials – Complexity of compression testing

The use of composite materials for deep-sea applications requires a thorough understanding of the behaviour of these materials under hydrostatic pressure. Nevertheless, the ability to predict the implosion pressures of such materials and under such loadings (biaxial compression) is not an easy task, as demonstrated by the World Wide Failure Exercise [13]. This compared various predictions based on different failure criteria with experimental data, and revealed a very poor correlation for biaxial compression. There are various possible reasons for this but one clear area of uncertainty is the testing procedures to identify the compression input data for the models.

The mechanical behaviour of composite materials has been extensively explored in the literature and is globally well understood, especially in the case of tension testing where mechanical behaviour is well predicted. However, the behaviour of composite materials subjected to compression loadings still requires further work. Many studies have shown that the compression strengths are typically 50-70% of the tensile strength [71]–[73] [74]. This large difference has been and is still the source of overdesigned structures, i.e. heavier structures. The main problem comes from the determination of the compression strength itself. It is indeed difficult to measure accurate compression values independent of the test fixture and specimen design, so it is common to obtain failures that are far from the ultimate compression strength of the composite.

5.1.Different compression tests

Many test methods have been developed over the years. Hart et al [75] conducted round robin tests within seven laboratories, each using their own test methods and found significantly different results for the same batch of materials. These differences arose from three main aspects: the test method itself, the specimen preparation and the operator’s experience in compression testing. Over the years, several test methods have been standardised. These can be divided into three groups: Shear loading [76], [77], end loading [78] and combined shear and end loading methods [79], as shown in Figure 11.

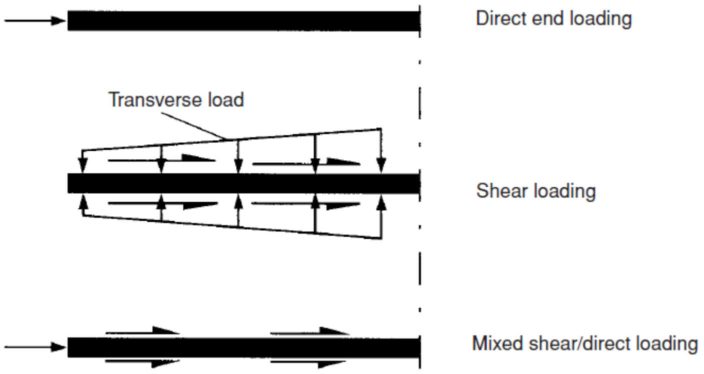

Figure 11 : Different loadings found in compression testing

Other non standardised tests have also been proposed such as the ICSTM (Imperial College of Science, Technology and Medicine) test fixture [80], [81]. In general, stress concentrations can arise when unsupported sections are short, while buckling may occur when the latter is too long. These can both lead to premature failures. The type of end tab (material, orientation, tapered/non tapered) and the tab-bonding technique also have a non negligible effect on the compressive strength [81], [82]. Moreover, a large scatter in the strain at failure can be observed within the same batch of materials [83]. A comparative study of the different tests that exist and between thermoset and thermoplastic composite compression strengths can be found in [84].

An alternative approach is to use flexural tests. These include three point bending [85], four point bending [76], [86], [87], pure bending tests [17] and compression/bending tests [21]–[24]. These tests can be used to monitor the side of the specimen that is subjected to compression. For the first two, the stress concentrations found at the loading points can be critical, even though some fixtures have limited their effect [87]. However, in one version of a pure bending test, a compressive load is applied to a pin supported specimen of rectangular cross section. A bending moment M is induced once the Euler load is reached, thus creating a buckling instability. This test uses a simple fixture, gives reliable results and is also an interesting transition between a material and a structural test. Also, it has been observed that bending tests result in the same type of compressive failure as uniaxial compression tests, especially for thermoplastic composites [92]. This test will be examined in more detail in Chapter 4.

5.2. Compression failure mechanisms

The mechanisms leading to compressive failures for carbon fibre reinforced composites are governed by several parameters such as the glass transition of the material and therefore the temperature at which the test is performed [93] and many mechanical properties such as the shear modulus of the matrix [94], [95] and the composite yield shear strength [95], [96].

Most of the time, kinking is the most common failure mode, involving local buckling of a large number of fibres through the specimen width. Kinking is the final stage of microbuckling, induced by the non-linear (plastic) shearing of the matrix. A kink-band example is shown in Figure 12.

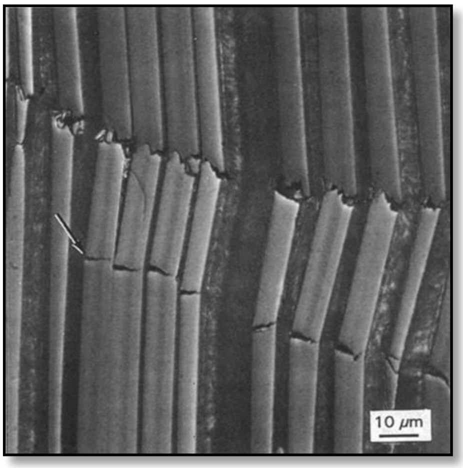

Figure 12 : Kink-band observed in graphite reinforced PEEK composite [97]

Several attempts have been made to rationalise this behaviour and one of the first models, that is most commonly quoted in the community, is the one proposed by Rosen in 1965 [94], several others have been proposed since [96], [98], [99]. Rosen considered that during compressive testing, two buckling modes were possible: one where the matrix shears parallel to the fibres (Figure 13, left) and another where the matrix undergoes extensional strain transverse to the fiber direction (Figure 13, right). However, in the case of advanced composites with high volume fraction of fibres (V_f > 30%), the shear mode governs the compressive strength.

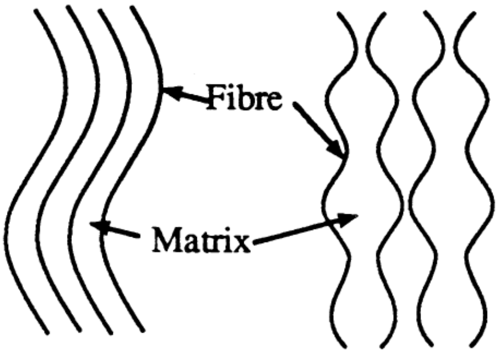

Figure 13 : (left) Shear Mode (right) Extensional mode

Rosen assumed that both fibers and matrix have a perfectly elastic behavior and that the fibers are perfectly aligned initially. It will be explained afterwards why these two assumptions are questionable. Rosen then defined the failure as the compressive stress σ_c, as follows, Eq. 1:

$$\sigma_c = \frac{G_m}{1 - V_f} \approx G_c \qquad \text{Eq. 1}$$

Where G_m is the shear modulus of the matrix and V_f the volumetric fraction of fibres. More precisely, σ_c should be interpreted as G_c, the shear modulus of the composite. However, it was found that this model is very unconservative, with compressive strengths four times higher than the experimental ones. The main problem comes from the fact that kinking is mostly due to the plasticity of the matrix coupled with the misalignments found in the composite, and the latter are not taken into account in Rosen's model.

6. Long term behaviour of composite materials in a marine environment

Any polymer that is immersed in water or exposed to a wet environment will absorb water, and this can drastically change its mechanical properties. Water penetrates the surface of the polymer and as time passes by, more and more water will penetrate the material until equilibrium is reached (in most cases).

6.1. Water diffusion kinetics

6.1.1. Fickian Diffusion

The simplest model that exists for the water diffusion of a solvent in a solid material is given by Fick's law which was established in 1855. Fick established this law based on Fourrier's law for heat transfer. The concentration gradient of the solvent is proportional to a flux F and represents Fick's first diffusion law along one direction, Eq. 2.

$$F = -D\frac{\partial c}{\partial x} \qquad \text{Eq. 2}$$

Fick's second law takes into account the time t and states that the diffusion coefficient D is independent of the concentration, Eq. 3.

$$\frac{\partial c}{\partial t} = D\frac{\partial^2 c}{\partial x^2} \qquad \text{Eq. 3}$$

In many polymers, water sorption follows a Fickian behaviour and can be described as follows using a diffusion coefficient D and a mass at saturation M_∞ [100], Eq. 4.

$$\frac{M(t)}{M_\infty} = 1 - \frac{8}{\pi^2}\sum_i \frac{1}{(2i+1)^2} exp\left(-\frac{D(2i+1)^2\pi^2 t}{h^2}\right) \qquad \text{Eq. 4}$$

Where h is the sample thickness in mm and t the immersion time in s.

The diffusion coefficient can be calculated from the initial linear part of the sorption curve where $\frac{M(t)}{M_\infty} \leq 0.5$, Eq. 5.

$$D = \frac{\pi}{16}.\frac{h^2}{t}\left(\frac{M(t)}{M_\infty}\right)^2 \qquad \text{Eq. 5}$$

A typical Fickian behaviour is shown in Figure 14.

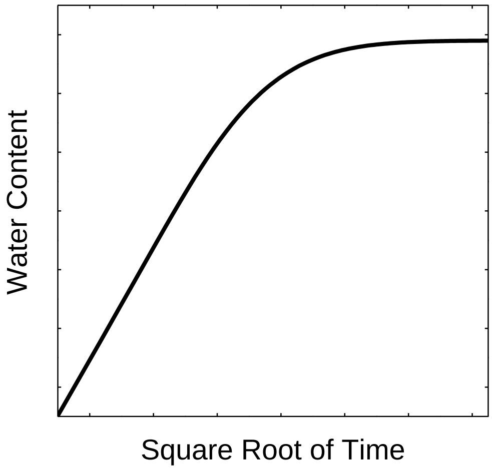

Figure 14 : Example of a Fickian water absorption

Temperature has a significant effect on the water diffusion. The lower the temperature the slower the water diffusion.

6.1.2. Non Fickian diffusion

Even though the Fickian diffusion is very common, other diffusion kinetics are possible, depending on the material and aging conditions used. Figure 15 shows alternative types of behaviour.

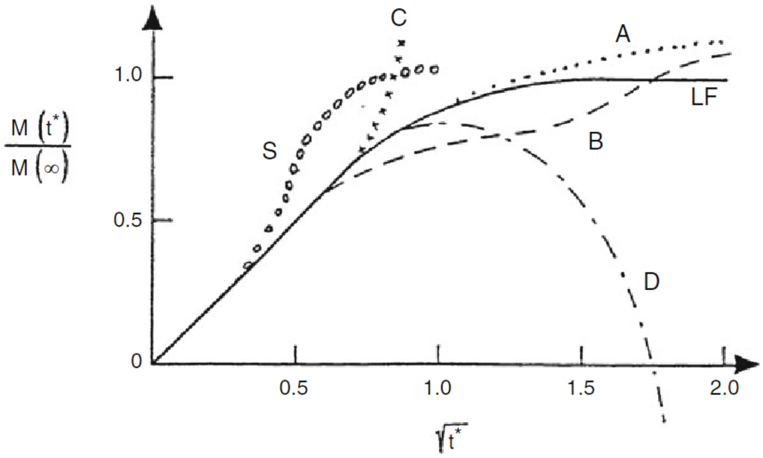

Figure 15 : Different water diffusion kinetics [101]

The curve noted (LF) represents the Linear Fickian behaviour which was presented earlier. The curve noted (A) corresponds to a continuous increase of water content and is usually linked to the Langmuir water diffusion model. The curve (B) corresponds to a “Dual Fick” mechanism in which two different Fickian kinetics can take place at the same time. The curve (C) is associated with a rapid increase of the water diffusion that can be linked to a degradation of the material (damage). The curve (D) corresponds to a decrease of the water content and can be associated with a degradation of the polymer due to hydrolysis or oxidation for instance. The last curve (S), represents a sigmoidal diffusion during which an acceleration of the water diffusion is observed until it reaches an equilibrium. This can correspond to a change in the material’s behaviour during water absorption.

6.2. Consequences of water absorption

Water absorption in polymers is known to have significant effects on their properties. Two different degradation phenomena can take place, either reversible or irreversible. The former is associated with swelling and induces a plasticisation of the polymer. This can be responsible for a drop in the glass transition temperature of the polymer [101], [102], and swelling may introduce internal stresses [103], [104]. Irreversible degradations can be due to oxidation or hydrolysis. In the case of composite materials, water can also cause a degradation of the fibre/matrix interface [105], [106] that will affect the mechanical properties.

7. Conclusion on the literature review

This brief introduction indicates that there is already a large literature on thermoplastic composites. However, with regards to the specific subject of this study (long term behaviour of thick carbon/polyamide composites for underwater use), there are areas where information is scarce or even completely absent.

Concerning the manufacturing conditions and residual stresses, very little work is found in the literature concerning the processing of carbon/polyamide 6 composite parts by LATP. Therefore, additional work is needed in this area.

The effect of processing conditions on the microstructure has been extensively explored in the literature concerning neat PA6 polymers and reinforced PA6s. However, no work has been found in the literature concerning the microstructure of continuous carbon fibre reinforced PA6 composites, which will be one of the original contributions of this work.

Concerning the compression behaviour of thermoplastic composite materials, a significant amount of work is available in the literature concerning C/PEEK laminates.

However, results concerning other thermoplastics such as C/PA6 are rarer. Therefore, another aim of the present study is to compare the compression properties of the low-cost C/PA6 to C/PEEK.

The influence of water aging on the mechanical properties of composite materials is a subject that has attracted much interest, more particularly concerning thermoset composites. Thermoplastic polymers are supposed to absorb much less water than their thermoset counterpart, which is one of the main advantages of these materials. However, this is not the case for PA6 which absorbs a significant amount and this is known to have major effects on the mechanical properties. Therefore, work is still needed in this area.

Finally, the response of composite cylinders under hydrostatic pressure is a subject that has attracted much interest but very few results are found in the literature, especially concerning thermoplastic composites. Some work is available concerning C/PEEK but no work has been found relative to C/PA6.

All these topics will be developed in more detail in the following chapters.

Chapter 2

Materials and Methods

This Chapter describes all the materials and methods that were used in this study. First, the different materials (prepregs and neat polymers) are presented as well as the two manufacturing processes (Thermo-compression and Laser Assisted Tape Placement). Second, the aging conditions are described followed by the different mechanical characterisations (tension, compression) that were performed. Third, the physicochemical characterisation techniques are presented followed by the imaging techniques that were used. Finally, the pressure vessels are presented as well as the residual strain investigation techniques.

1. Materials

In this part the different materials used during this study are presented. This project is mainly focused on composite materials, and different carbon fibre reinforced prepregs have been used. However, to understand in detail the behaviour of the matrix itself, neat polymers have also been studied in parallel, to investigate the water diffusion.

1.1.Composite prepregs

The main material of interest here is a C/PA6 pre-impregnated tape from Celanese® (reference: CFR-TP PA6 CF60-01). It has a fibre volume fraction of 48% and a thickness of 190 µm (information given by the supplier). No information is provided by the supplier related to the type of fibre or about the polymer grade. The second material, taken as a reference is a carbon-Polyetheretherketone (C/PEEK) composite supplied by Toho Tenax® (reference: -E TPUD PEEK-HTS45). The fibre volume fraction is 60% and the tape thickness is 140 µm (information given by the supplier). The fibre is a HTS45 12K carbon reinforcement from Tenax® and the PEEK matrix is a medium viscosity PEEK matrix from Evonic industries (Vestakeep® 2000). Over the past 30 years, many studies have focused on C/PEEK for structural applications (such as aircraft structures). However, using such a material for the targeted underwater applications is difficult, the latter is 10 times more expensive than the C/PA6 counterpart. Therefore, C/PA6 was chosen here as a low-cost solution. It may be noted that the choice of C/PA6 was not arbitrary. A preliminary study was conducted at the start of the PhD and compared the mechanical properties of C/PA6 and C/PA12 in the dry and saturated states. This will be summarised at the end of this Chapter.

1.2.Neat polymers

A neat polyamide 6 matrix supplied by Goodfellow was also studied and has a density of 1.13 $g.cm^{-3}$. It was used to characterise the water diffusion in neat Polyamide 6 specimens.

It was received in the form of 2mm thick panels processed by compression moulding. Polymer films of 70µm thickness were obtained from the latter with a Leica RM2245 microtome. Both thicknesses were used in this study. Polydispersity index and number average molar mass (M_n) were measured by SEC and their values are respectively 2.5 and 48.1 kg/mol with a degree of crystallinity χ of 38% (measured by DSC).

1.3. Reference material

The different thermoplastic composite cylinders that were manufactured were compared to the carbon/epoxy cylinder that is currently used at Ifremer for deep sea applications. It is a commercial wet filament wound carbon/epoxy cylinder. It is made of HTS45 fibres and a proprietary epoxy matrix. It has a fibre volume fraction of 60% and is wound at ±55° along the tube axis.

2. Processing of composite materials

2.1. Thermo-Compression (TC)

Composite panels were manufactured by hot compression moulding. It should be noted that two different hot press systems were used, one located in Brest (from DK technologies) and one located in Knoxville (from Carver and used for the investigation of residual stresses, Chapter 6). These are presented in Figure 16.

(a) (b)

Figure 16 : Hot press used in (a) Brest, DK technologies (b) Knoxville, Carver

The C/PA6 panels were manufactured at 230°C with a pressure of 5 bar. The C/PEEK panels were manufactured at 420°C with a pressure of 10bar. For both cycles, the cooling rate was chosen to be 20°C/min. The manufacturing cycles are presented in Figure 17.a and Figure 17.b. It should be noted that all C/PA6 plies were conditioned at 0% humidity (40°C) until the weight stabilized to ensure that each ply was free of water before processing. Most of the panels that were manufactured were made of 16 plies (about 2 mm). Several panels with different sequences were manufactured: unidirectional $[0]_{16}$, $[\pm 45]_{4s}$ for C/PA6 and C/PEEK and $[\pm 15]_{4s}$, $[\pm 35]_{4s}$, $[\pm 55]_{4s}$, $[0/90_2]_6$, $[0_2/90]_6$, $[0_2/90_2]$, $[0_4/90_4]$, $[0_8/90_8]$ for C/PA6 only.

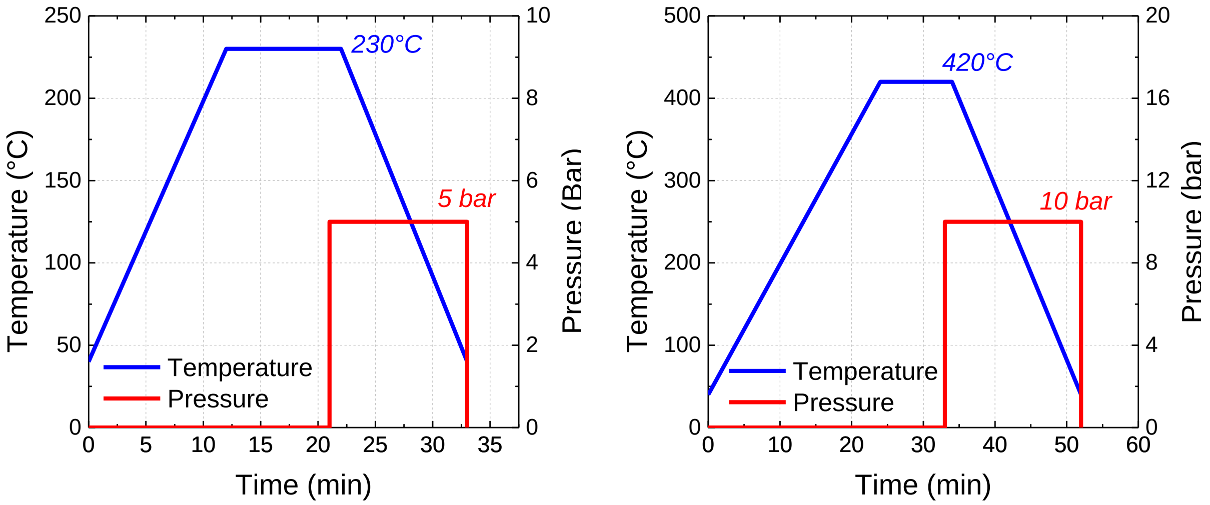

(a) (b)

Figure 17 : Cycle used for the manufacture of (a) C/PA6 and (b) C/PEEK panels

2.2.Laser Assisted Tape Placement

Throughout this project, several composite cylinders, rings and panels were manufactured by Laser Assisted Tape Placement at the dedicated facility at the CETIM in Nantes. A Laser Assisted Tape Placement head is attached to a Kuka robot arm. presented in Figure 18.

To manufacture the different composite cylinders, two mandrels with two different diameters were used (120 and 100mm). One mandrel of 200mm diameter was also used to manufacture composite rings. Finally, a flat mandrel was used to produce composite panels manufactured by LATP.

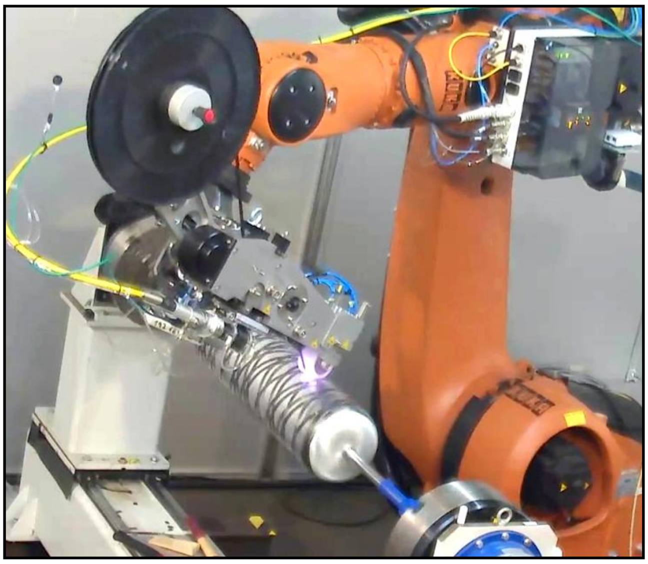

Figure 18 : Laser Assisted Tape Placement machine at the CETIM manufacturing facility

3. Aging conditions

3.1.Sea water tanks

The water absorption was determined from the weight change measurements of square samples (50 x 50 x 2) mm^3 at different temperatures, ranging from 15°C to 60°C for PA6 and at 80°C for PEEK (below the dry T_g of each matrix). The different samples have been immersed in natural renewed sea water from Brest Estuary. The mass gain was followed by periodic weighing of the different specimens on a Sartorius LA310 S balance having a precision of 0.1 mg. Before each measurement in immersion, the water on the surface of the specimen was wiped off with a paper towel. For each measurement, three samples were used at each time. The water content, M(t) in wt.% of a sample is defined as follows, Eq. 6:

$$M(t) = \frac{m(t) - m_0}{m_0}.100 \qquad \text{Eq. 6}$$

Where m(t) is the mass of the sample at a time t and m_0 the initial mass of the sample.

The relative mass ratio w_{H_2O} and the relative volume ratio v_{H_2O} are used to take into account the degree of crystallinity χ (respectively presented in Eq. 7 and Eq. 8). ρ_a and ρ_w are respectively the densities of the polymer and water.

$$w_{H_2O} = \frac{M(t)}{M(t) + (1-\chi).W_0} \quad \text{Eq. 7}$$

$$v_{H_2O} = \frac{w_{H_2O}\rho_a}{w_{H_2O}\rho_a + (1-w_{H_2O})\rho_w} \quad \text{Eq. 8}$$

Prior to water exposure, all the samples were conditioned at 0% relative humidity at 40°C until their weight stabilized. The sea water aging tanks are presented in Figure 19.

Figure 19 : Sea water aging tanks at Ifremer

It may be noted that deionised water was also used in some cases to investigate the water absorption. Aging tests were performed at Ifremer in a water bath at 25°C but also in Knoxville at 21°C.

3.2.Dynamic Vapour Sorption (DVS)

Dynamic Vapour Sorption (DVS) measurements were performed on Q5000 SA equipment from TA Instruments. The weight change of a 70 µm polymer film within a humidity chamber (ranging from 0 to 0.9 water activity) was followed using a microbalance of 0.1 µg resolution at various temperatures (from 15 to 80°C). Again, for each condition, three samples were used.

3.3.Humidity chambers

Controlled humidity chambers were used to investigate the effect of water content at saturation on the overall properties of a 2mm thick specimen. Different humidities were chosen: 0, 33, 63 and 75% relative humidities (RH). Saturated salt solutions were used to obtain these humidities: Magnesium chloride for 33%RH, ammonium nitrate for 63%RH and sodium chloride for 75% RH. Greenspan [107] has shown that these solutions could be used to reach the given humidity levels. To do so, all the salt solutions were prepared at 50°C. For each solution, the given salt was slowly added until the salt no longer dissolved in the solution. It should be noted that for each solution of interest, the relative humidity was checked periodically (twice a week) throughout the aging process. These solutions were placed inside desiccators inside an oven maintained at 40°C (±0.5°C).

Saturated salt solutions were used in Knoxville as well, at 21°C with three different humidities (0, 33 and 75% RH).

Concerning the neat PA6, the samples were fully saturated in a thermo-hygrometric chamber (Servathin B204 3235) at different water activities at 80°C for 48 hours.

3.4. Water diffusion under hydrostatic pressure

Water absorption tests under hydrostatic pressure were performed in a pressure vessel at a pressure of 500 bar. These were then compared to a 1 bar reference test performed at 40°C. The experimental setup is displayed in Figure 20.

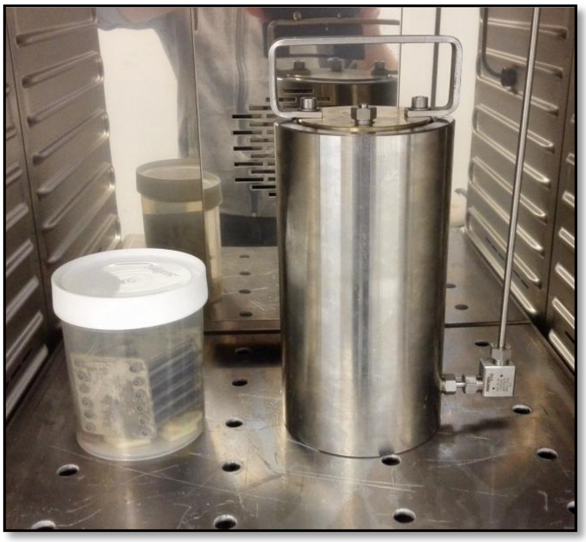

Figure 20 : (Left) 1 bar reference (Right) Test performed at 500 bar inside 40°C oven

4. Physicochemical characterisation

4.1.Differential Scanning Calorimetry (DSC)

The degrees of crystallinity X_c were checked using DSC (Differential Scanning Calorimetry) on Q200 equipment from TA Instrument at a heating rate of 10°C/min from the ambient temperature to 300°C for PA6 and 400°C for PEEK. However, the degree of crystallinity in thermoplastic composite materials is also dependent on the fibre weight fraction W_f, Eq. 9:

$$X_c = \frac{\Delta H_f}{\Delta \mathrm{H}_\mathrm{f}^0 \times (1 - \mathrm{W}_\mathrm{f})} \times 100 \qquad \text{Eq. 9}$$

where ΔH_f is the enthalpy of fusion of the polymer and ΔH_f^0 the theoretical enthalpy of fusion for a 100% crystalline material (taken to be 188 J/g for PA6 [108], 130 J/g for PEEK [108]).

4.2.Thermogravimetric Analysis (TGA)

TGA analyses were conducted on SDT Q600 equipment from Texas Instruments in order to determine the fibre weight fraction W_{fibre} in each laminate that was manufactured. To do so, the sample was heated to 600°C (temperature above the degradation temperature of both polyamide 6 and PEEK matrices) at 20°C per minute under nitrogen (N_2). This temperature was then held for 120 minutes to make sure that all the matrix was burnt off.

4.3.Pycnometer

Densities (ρ) were determined with a gas pycnometer. The purpose of this measurement is to determine the fibre volume fraction V_f of a given composite using Eq. 10:

$$V_f = \frac{W_f \rho_c}{\rho_f} \qquad \text{Eq. 10}$$

Where ρ_c and ρ_f are respectively the densities of the composite and the fibre.

4.4.Dynamic Mechanical Analysis (DMA)

Dynamic mechanical analyses were performed on DMA^+ 150N equipment from Metravib to obtain the glass transition temperatures of the neat polymer and the composite. The latter was taken as the tan δ peak. Measurements were made in tensile mode on unidirectional samples of dimensions (30 x 15 x 2) mm^3 tested under transverse tension for composite specimens at 2°C/min over the temperature range from -100°C to 150°C for the carbon-Polyamide 6 laminates and neat PA6 and 25°C to 250°C for the carbon/PEEK samples. The frequency was 10Hz and the dynamic strain amplitude was 2.10^{-4}. Water evaporation during DMA tests can be neglected here due to the short testing time compared to evaporation time.

5. Imaging techniques

Imaging techniques are powerful methods that serve many purposes across the physical sciences. The results that are obtained mainly depend on the incoming “wave” that is used (e.g. light, electrons, ultrasound, X-Rays, etc.).

5.1. Scanning Electron Microscope (SEM)

SEMs are usually used to observe the surface of a specimen at a very high magnification and resolution. In this case, all samples were coated with platinum to ensure a good reflection of the high-energy electrons on the specimen. In this way, failure surfaces were investigated.

5.2. Optical microscopy

The quality in terms of voids of the different panels that were manufactured was checked using optical microscopy (polished sections) on a LEICA DM ILM microscope. The void contents were determined using the software *ImageJ* from a mean of 30 images for each composite panel, according to AFNOR NF T 57-109. Polished sections for C/PA6 and

C/PEEK manufactured by thermocompression are respectively shown in Figure 21.a and Figure 21.b.

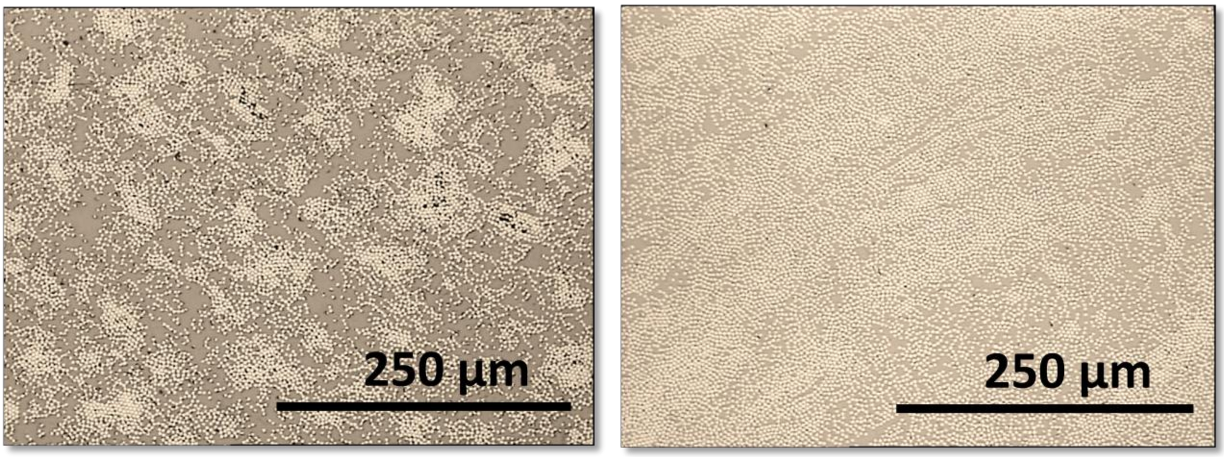

(a) (b)

Figure 21 : Polished sections of unidirectional (a) C/PA6 and (b) C/PEEK specimens

5.3. X-Ray Tomography

X-Ray tomography is a very powerful method to investigate the void content throughout the volume of a composite material at a high resolution (9 µm in this case). These tests were conducted at the Ecole Centrale de Nantes on a Xradia tomograph.

5.4. Ultrasonic C-scan

In order to check the overall quality of a given cylinder, ultrasound scanning is very useful because the imaging techniques presented previously only concern very small specimens (a few tens of millimetres). With ultrasonic C-scan, the through thickness attenuation contained inside an entire cylinder can be investigated. However, the results that are obtained are only qualitative and not quantitative, unlike the other methods presented earlier. A Sofratest ultrasonic inspection system was used to measure through thickness attenuation using 2 MHz focused transducers by placing the cylinder on a rotating table in a water tank.

5.5.Polarised microscope

A polarised microscope was used to observe the crystalline regions found in neat PA6 cooled at different cooling rates. These were observed on thin polished sections using an Axio Scope A.1 polarised microscope from Zeiss.

6. Mechanical characterisation

6.1.Composite panels

6.1.1. Specimen preparation

After processing, each panel was end-tabbed and then cut with a water cooled diamond disc to the chosen dimension (precision of ± 0.5mm). The end tabs are $[\pm 45]_3$ glass/epoxy laminates manufactured by hand lay-up. These tabs were tapered to reduce stress concentrations. These were bonded to the different laminates with a *Loctite 406* glue after a *Loctite 770* surface treatment, specifically developed for thermoplastic materials. The tabs have a length of 50mm and a thickness of 2mm. At least four specimens were tested for each condition and the results are averaged. The modulus values were determined in the range from 0.1 to 0.3% strain. All mechanical tests were performed in a relative humidity and temperature controlled laboratory (50±5% RH, 21±2°C).

6.1.2. Quasi-static mechanical tests

6.1.2.1. Tension

Tensile tests in the longitudinal and transverse direction were performed according to ASTM D 3039 on an Instron testing machine. The moduli were obtained using an extensometer of 50mm gauge length. The dimensions of the specimens were (250 x 25 x 2) mm^3. To obtain the Poisson's ratio ν_{12}, bi-axial strain gauges of 10mm gauge length were bonded to the specimen. The latter were also used for the determination of the shear modulus G_{12} on ± 45° specimens according to ASTM D 3518. The dimensions were (200 x 20 x 2) mm^3**.** Shear strength was taken to be the stress at 2% shear strain. The cross head speed was 2 mm/min for tensile and shear tests.

6.1.2.2. Compression

Initially, a standard test method, ISO 14 126 was used for the compression test. Tests were performed at 1 mm/min. The specimen dimensions were (110 x 10 x 2) mm^3. However, as will be shown later in Chapter 4, strength values from this test were quite low so a second non-standard pin-ended buckling test was subsequently used to evaluate water effects, Figure 22. These tests were performed at 10 mm/min in order for test times to be similar for the two tests (and limit water evaporation in subsequent tests after aging). Strain gauges were bonded at the centre of the compressive and tension sides of the specimen to measure strain (gauge length is 10mm). The specimen dimensions are (250 x 25 x 2) mm^3.

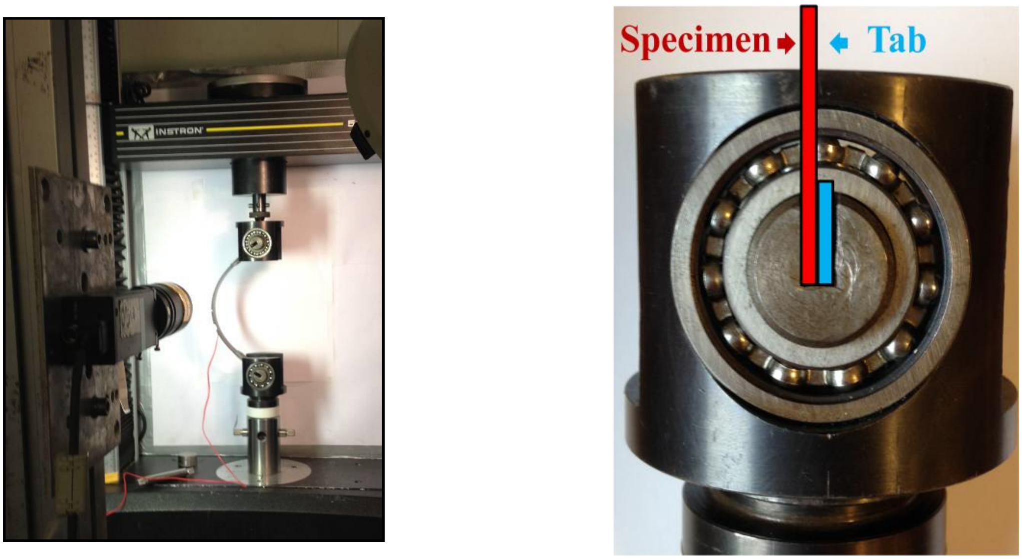

(a) (b)

Figure 22 : (a) Pin-ended buckling test fixture (b) Detail of fixture showing eccentricity of the specimen in the fixture

In the post-buckling stage, the maximum bending moment M in N.mm is defined by Eq. 11:

$$M = P.\delta \tag{Eq. 11}$$

where P is the applied load in N and δ the lateral deflection at mid-span in mm. The latter is recorded by a digital camera throughout the test as shown in Figure 22.a. The maximum bending stress σ_b at the centre of the specimen and the compressive stress due to the pure axial load σ_c define Eq. 12.

$$\sigma = \sigma_b + \sigma_c = \frac{6.P.\delta}{b.h^2} + \frac{P}{b.h} \tag{Eq. 12}$$

Where b and h are respectively the width and thickness of the specimen in mm. As for the tensile modulus, the compressive modulus was then determined in the 0.1-0.3 % strain range.

This equation is a simplified expression, based on a number of assumptions such as identical tensile and compressive behaviour and a linear response. The consequences of these assumptions will be discussed in Chapter 4. However, it should be noted that there are fundamental differences between pin-ended buckling and standard compression tests. The former is a flexural test which introduces a strong strain gradient while the latter should provide a constant strain across the test section. It has been shown that the presence of a strain gradient results in higher compressive strain at failure [109], [110]. This has been attributed to less highly loaded fibres below the compressed specimen surface, which provide support to limit fibre micro-buckling. As a result it is not possible to compare results from the pin-ended buckling test directly with those from pure compression tests.

6.1.2.3. Four point bending

Flexural tests were performed according to ASTM D790 at a cross head speed of 6mm/min. Specimens dimensions were 150 x 25 x 2 mm^3.

6.1.2.4. Double Cantilever Beam (DCB) – Mode I

DCB tests were conducted at 1mm/min following ASTM D5528 standard and aluminium tab blocks were bonded on the different specimens using Loctite 406 glue. The specimen dimensions are 150 x 20 x 3 mm^3 and a 10µm thick aluminium film was inserted at the mid-plane of the specimens to obtain a 40mm long precrack. Then, the toughness G_{IC} was measured using the three different techniques stated in the standard, i.e., the modified Beam Theory (MBT), the Compliance Calibration (CC) and the modified Compliance Calibration (MCC) methods.

6.2. Composite cylinders

6.2.1. Cylinder instrumentation

Strain gauges were bonded around the perimeter at the centre of the cylinder, as shown in Figure 23. Using this number of strain gauges allows the determination of whether the cylinder implodes due to buckling or due to material failure.

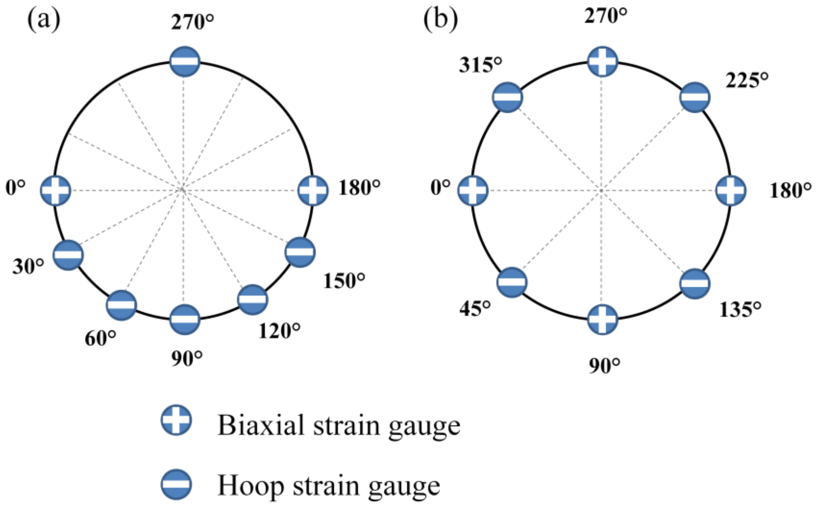

Figure 23 : Strain gauge configurations used for the composite cylinders

Also, for each implosion test, end covers were bonded to the cylinder extremities in order to protect the ends and provide a suitable surface to seal the end plates Figure 24.a. Then, the strain gauges have to be protected from water and connected to the recording system. The cylinder is then ready to test, Figure 24.b. It may be noted that each end fixture is specifically designed for a given cylinder.

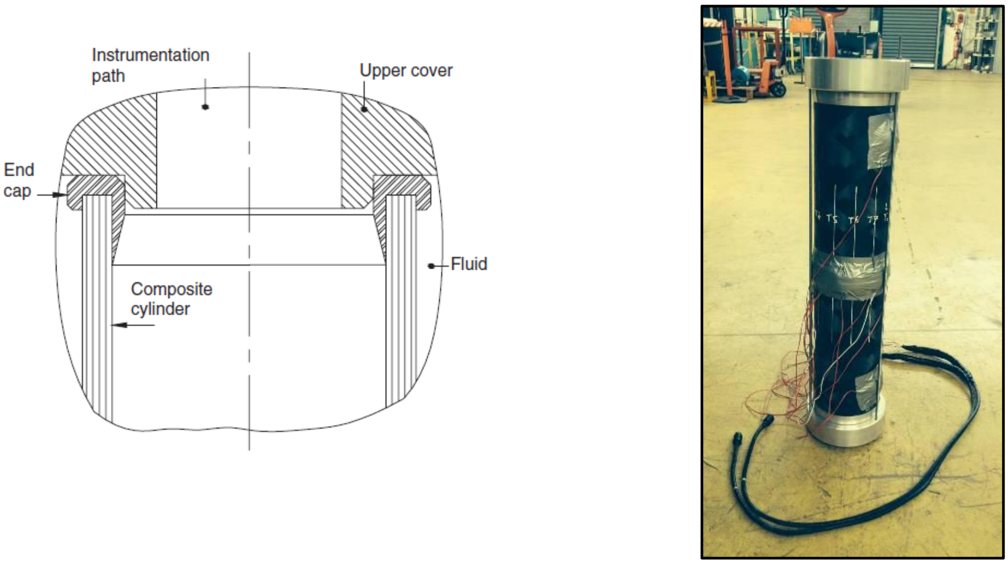

(a)

(b)

Figure 24 : (a) Experimental end fixtures for implosion tests (b) Cylinder ready for implosion test

6.2.2. Axial Compression

Prior to each implosion test, an axial compression test was performed to measure the axial elastic properties (E_z and $\nu_{z\theta}$) and check the response of all the strain gauges, as seen on Figure 25. The cylinder was subjected to a small axial strain, around 1000 microstrains. The tube was rotated to ensure that loading was uniform and an average was then calculated. It should be noted that due to the large cross-section this test required an axial load of several tonnes.

Figure 25: Axial compression test

6.2.3. Radial Compression

The hoop properties (E_θ and $\nu_{\theta z}$) were determined using a radial compression between two plates, Figure 26. These tests were performed at 2mm/min. Biaxial strain gauges of 10mm gauge length were bonded on the outer side of the composite ring. Results from these tests (Load-Strains curves) are then compared with the Abaqus predictions performed by the CETIM.

Figure 26: Radial compression test

6.2.4. Implosion test

All cylinders were tested to implosion in a 2400 bar pressure vessel with continuous recording of pressure, temperature and strain gauge measurements. The pressure was increased at 12 bar/min until failure. The implosion test facilities are presented in Figure 27.

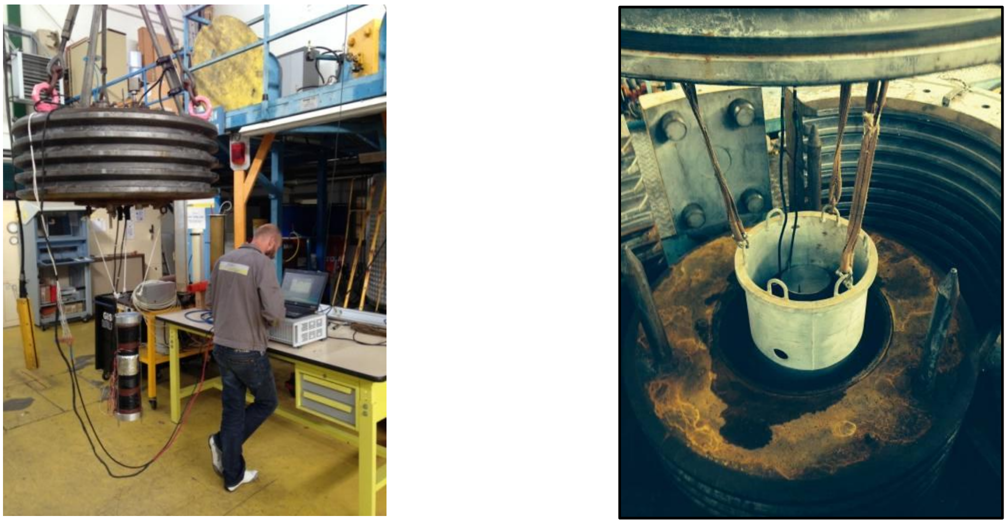

(a) (b)

Figure 27: (a) Cylinder ready for implosion and recording systems connected to the strain gauges (b) Cylinder being lowered in the pressure vessel

7. Measurement of residual strains and stresses

7.1. Fibre optic sensor

The evolution of microstrains during composite manufacture and water intake relaxation were evaluated using a novel in-situ fibre optic system. Unidirectional carbon fibre-polyamide 6 composites were produced using compression moulding with an imbedded fibre optic for strain measurement.

7.1.1. Fibre sensing technique

With Luna’s sensing methodology strain measurements are achieved without the use of gratings by measuring the low amplitude signal of reflected light referred to as Rayleigh backscatter. These small amplitude reflections are an inherent phenomenon in glass fibres as a result of refractive index fluctuations naturally formed during the fibre’s manufacturing process. The Rayleigh backscatter is a random but static signal, making the scatter pattern unique for every individual fibre. Luna's interrogators utilise this scatter “fingerprint” to measure a shift in the fibre between its reference state and externally stimulated state. This shift is calibrated to strain, resulting in strain measurements continuously along the entire length of the fibre optic cable with very high spatial density [111].

Optical Frequency Domain Reflectometry (OFDR) is an interferometric method used to measure the phase and amplitude of reflected light [112], [113]. A diagram of a basic OFDR network is shown in Figure 28 below. Light from a Tunable Laser Source (TLS) is swept linearly through a specified range of frequencies and split, through a coupler, between the reference and measurement arms of the interferometer. In the measurement path, light going through a circulator is reflected from the sensor and recombined with the light from the reference path. The Polarisation Controller (PC) in the reference path helps ensure that light is split evenly between its two orthogonal polarisation states as the combined signal passes through the Polarisation Beam Splitter (PBS) and into the two detectors labelled S and P. A Fourier transform of the signal at the detectors results in the phase and amplitude of the signal as a function of length (or delay) along the sensor, i.e. the Rayleigh scatter fingerprint.

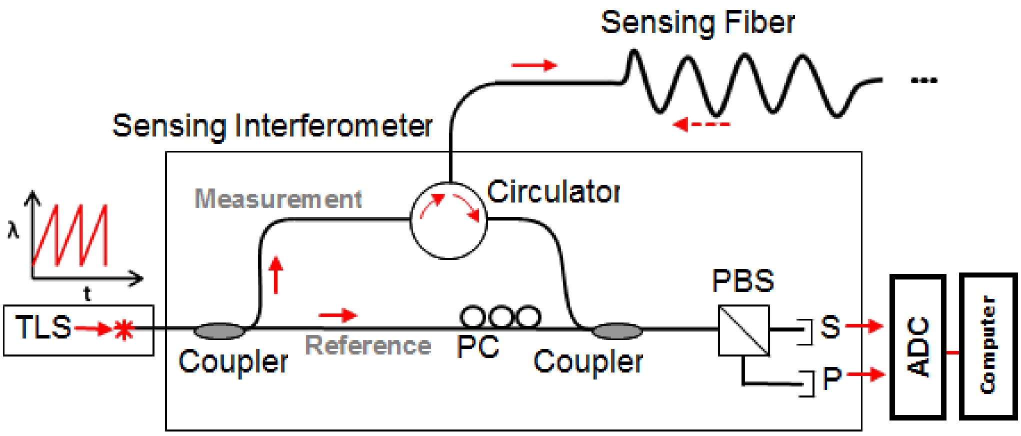

Figure 28 : Basic OFDR optical network

Figure 29 depicts the steps taken to calculate strain from the Rayleigh scatter signature. The spectral content of the sensor is recorded and compared between its reference and measurement state. Figure 29.a shows the Rayleigh scatter signature as a function of length down the optical fibre where the sensor's signal in a measurement (i.e. externally stimulated) state is compared to its baseline state. The data is windowed at a particular location along the scatter trace. This window, typically on the order of a few millimetres, is referred to as the gage length of the strain measurement. The signal's spectral content, shown in Figure 29.b, is obtained through an inverse Fourier transform of the data within the gage. Figure 29.c shows two peaks as the result of a cross correlation between the spectra of the baseline and measurement signals. The shift between these two peaks is referred to as the spectral shift and is converted to strain using an empirically determined calibration coefficient (i.e. gauge factor) [111]. This sequence is repeated along the sensor length, forming a distributed measurement.

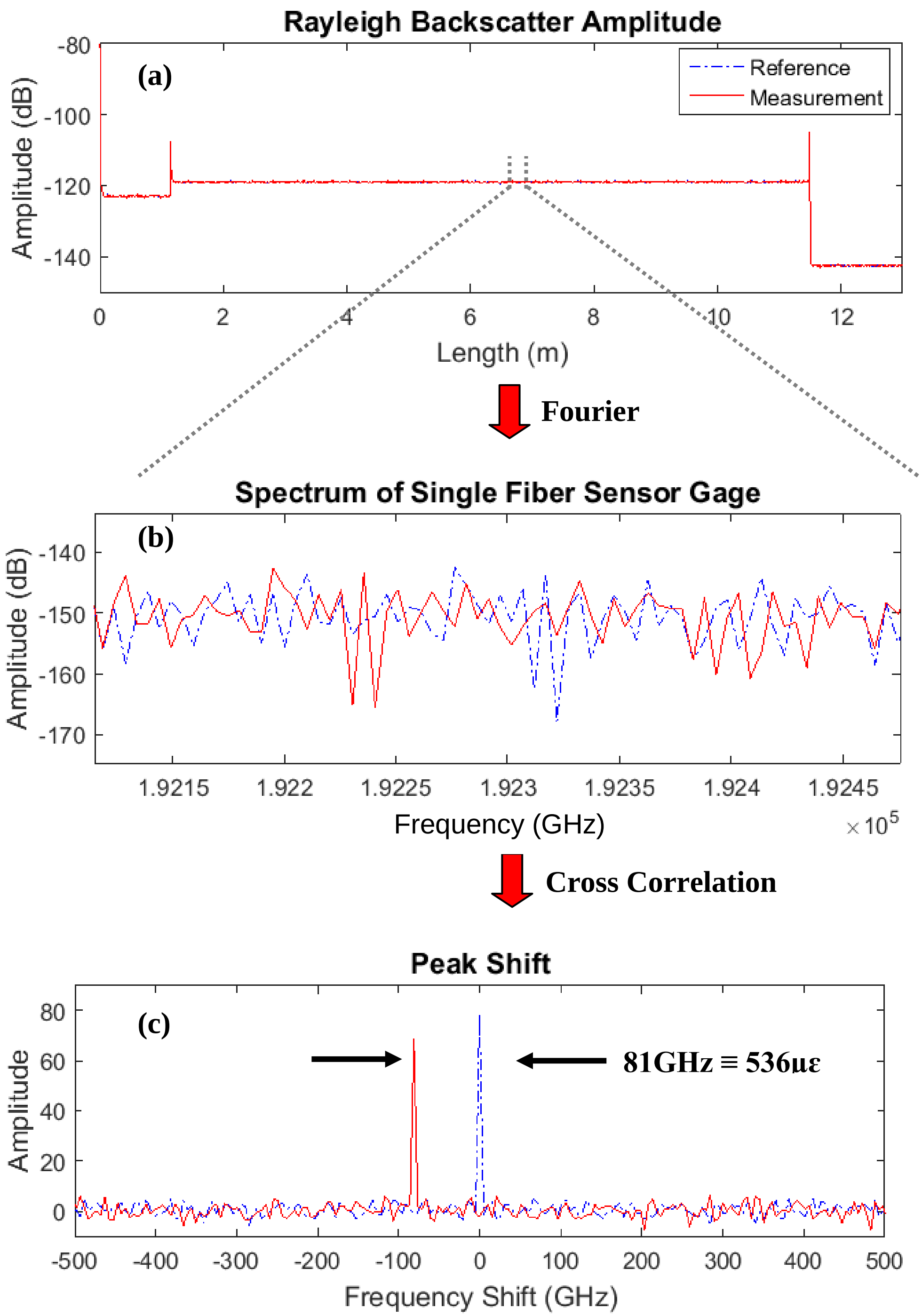

Figure 29 : Steps to obtain a frequency shift calculation from a Rayleigh scatter measurement. (a) Rayleigh scatter is measured along the length of an optical fibre in a reference (unstrained) and measurement (strained) state. (b) A Fourier Transform is applied to a section (i.e. gauge

length) of the Rayleigh scatter traces to obtain a spectrum from the defined gauge length. (c) Cross correlation of the two spectrums results in a peak shift between the reference and measurement traces. This frequency shift can be converted to strain or temperature using a calibration coefficient.

7.1.2. Data acquisition system and fibre layout

The optical distributed sensor interrogator used in this experiment was the ODISI-B model from LUNA Technologies. The ODISI-B is unique in its ability to continuously monitor the sample without user interaction. In addition, it has a sensing range of 20m from 23.8 to 250 Hz acquisition rates. The resolution of this system is ± 5 $\mu\varepsilon$ and ± 0.4 °C [114].

The fibre optic from the ODISI-B was placed in the centre of the unidirectional composite laminates between the 8th and 9th plies. In order to obtain data along all the principal directions, a shamrock arrangement was developed and provides information in the 0°, ± 45° and 90° directions, presented in Figure 30.

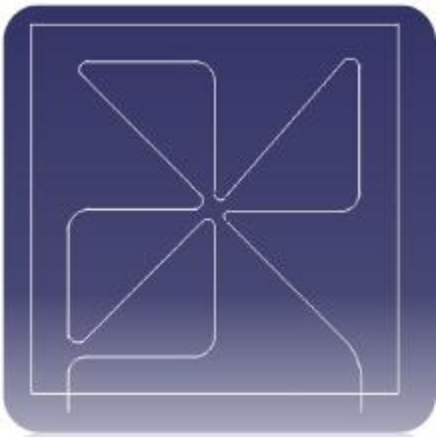

Figure 30 : Fibre configuration at mid panel thickness (between 8th and 9th plies)

This configuration allows us to obtain information along every principal direction as well as across all the surface of the panel (strain gradient). In order to keep this configuration during the entire process, the optic fibre was bonded to the 8th ply using a high temperature epoxy, EPO-TEK® 353ND. It may be noted that only the corners were bonded to the ply, allowing strain monitoring in each direction during processing. A thermocouple was also introduced at the mid-plane of the panels in order to correct the strains only induced by temperature. The ODISI-B fibre optic analyser, Carver press, and the positioning of the fibre on the 8th ply are presented in Figure 31.

(a) (b)

Figure 31 : (a) ODISI Fibre optic sensor and Carver press and (b) Positioning of the fibre optic sensor inside the mould.

7.2.Asymmetric laminates

Asymmetric laminates were produced to investigate the effect of environmental conditions (temperature and humidity) on the relaxation of residual stresses. These are displayed in Figure 32. To do so, the out-of-plane deflections were recorded as a function of aging.

Figure 32 : Asymmetric laminates, from back to front: $[0_2/90_2]$, $[0_4/90_4]$ and $[0_8/90_8]$

The deflection h and the chord length L are measured using a steel ruler with a precision of 0.5mm. The curvature is then defined as follow, Eq. 13.

$$\kappa = \frac{8h}{L^2 + 4h^2} \tag{Eq. 13}$$

For each aging condition, three samples were used and the curvature results were averaged.

7.3. Radial cut method

After manufacture, several composite rings manufactured by LATP were instrumented with strain gauges of 10mm gauge length. These hoop strain gauges were placed both on the inner and outer faces of the composite rings. Then, these composite rings were cut while recording the change in strains using a water cooled diamond disc displayed in Figure 33.

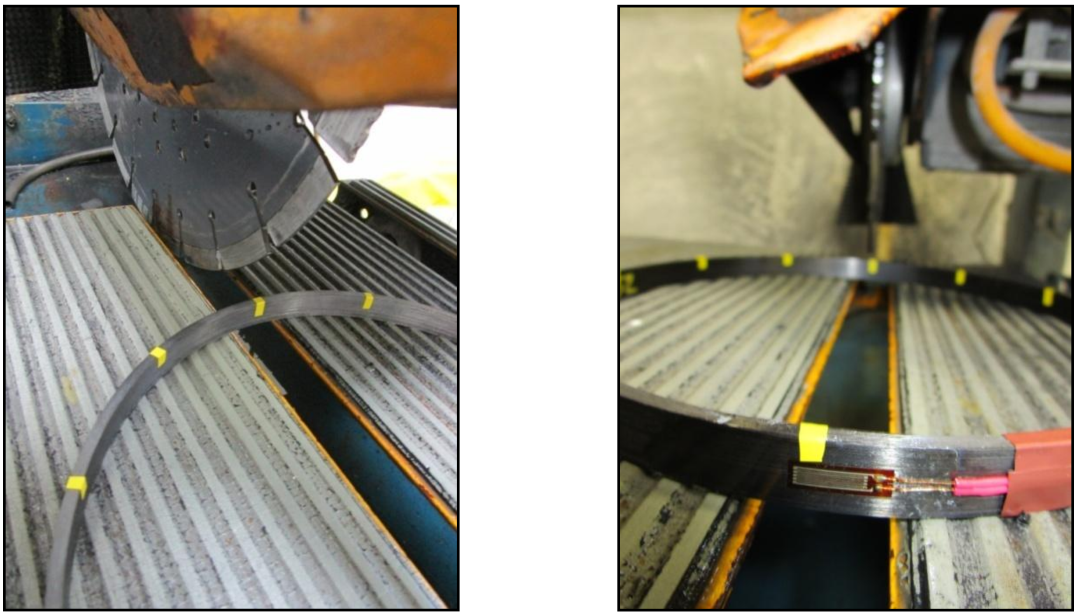

(a) (b)

Figure 33: (a) Composite ring positioned close to the water cooled diamond disc (b) Positioning of the strain gauges relative to the diamond disc

8. Modelling

The 2D model used to model the water diffusion in PA6 was developed using COMSOL Multiphysics 5.1 software. The square geometry considered was of 25mm edge length and 1mm thick with symmetry in all directions in order to simulate a (50 x 50 x 2) mm^3 immersion coupon. A rectangular finite element mesh was used, with 50 elements in each direction, i.e. a mesh size of 0.5 mm by 0.02 mm. Mesh size dependence was examined, and increasing or decreasing mesh size by a factor of 2 gave the same results. The same configuration was used to model the water diffusion in composite materials.

Abaqus software was also used by the CETIM to model the implosion tests performed on the different composite cylinders and to validate the quasi static tests performed on these cylinders.

9. Choice of C/PA6 over C/PA12

At the start of the study, several questions were raised concerning which material should be used. A wide range of polyamides are available in the industry and it was not clear which grade was most suitable. Therefore, a preliminary study was conducted and compared the mechanical properties in the dry and saturated states of C/PA6 and C/PA12 unidirectional laminates produced by thermo-compression. To do so, a mould was made at Ifremer and to produce unidirectional specimens whose dimensions were 250 x 12.7 x 2mm^3. The mould and process parameters used to produce the specimens are respectively presented in Figure 34 and Table 3.

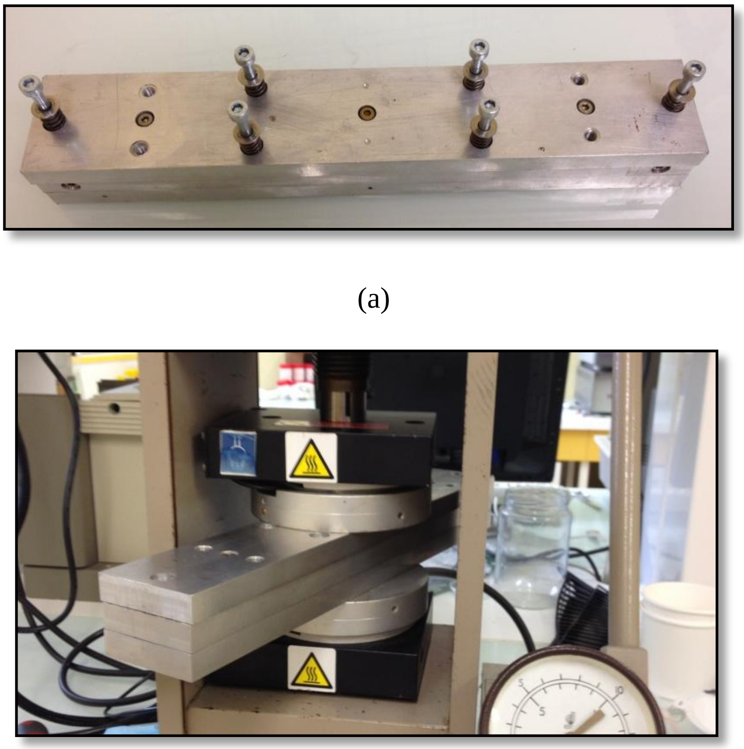

(a)

(b)

Figure 34 : (a) Mould made at Ifremer (b) Mould positioned in the hot press

Table 3 : Process parameters for C/PA6 and C/PA12

Process Parameters	C/PA6	C/PA12
Temperature (°C)	230°C	200
Heating rate (°C/min)	15	15
Holding Time (min)	12	12
Cooling rate (°C/min)	2.5	2.5
Pressure (bar)	2	2

Afterwards, some specimens were immersed in sea water at 40°C until complete saturation. The weight of the specimens was continuously followed during aging. Then, specimens of dimensions 120 x 12.7 x 2 mm^3 were tested under four point bending. The flexural strengths in the dry and saturated states are reported in Figure 35.

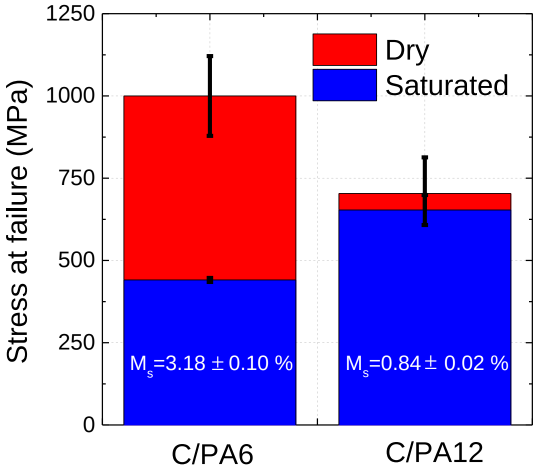

Figure 35 : Four point bending strengths at failure in the dry and saturated states for C/PA6 and C/PA12 unidirectional laminates

These results show that the C/PA6 specimens possess a higher flexural strength at failure than the C/PA12 counterpart in the dry state. However, when fully saturated in sea water, results give the opposite trend and the carbon-polyamide 12 gives the better results.

C/PA6 was retained for the study because of its higher properties in the dry state compared to C/PA12. It was thought that the water diffusion in thick composite 12mm would probably be sufficiently slow not to affect the mechanical properties of the cylinder. However, since the decrease in mechanical properties was much higher than for C/PA12, a specific diffusion model was needed and this hypothesis has to be verified.

Chapter 3

Modelling the water absorption in Polyamide 6 – From the neat matrix to the composite

---

The aim of the following chapter is to present the methodology which allows us to model and predict the water diffusion in a thick composite cylinder immersed in sea water for several years at low temperatures.

First, because of the particular water diffusion behaviour of Polyamide 6 in immersion, a specific diffusion model was developed on the neat PA6 matrix and results were compared to experimental data. Second, the model was adapted for the water diffusion inside a composite material using a homogenisation relationship, and predictions were compared to experimental data to demonstrate the accuracy of the specific model. Finally, the model was used to predict the water diffusion inside a thick cylinder (12mm) immersed for several years at 15°C in sea water.

1. Water absorption in the neat Polyamide 6

1.1. Introduction

The ageing mechanisms in PA are mainly induced by either a reaction of the polymer with oxygen (i.e. oxidation) [115], [116] or interaction with water. The latter has been widely studied in the past, and it has been shown that PA6 absorbs a large amount of water when immersed, up to 10% at 20°C [117]. This behaviour is related to the presence of polar groups (NH) coupled with the formation of clusters at high water activities. The presence of water within the polymer leads to an increase in mobility of the macromolecular chains that is characterised by a decrease in the glass transition temperature (T_g). Lim et al. [118] showed that the T_g decreases from 60°C to –10°C when 10% of water is absorbed. This phenomenon, plasticisation, induces large changes in the mechanical behaviour. For example, Reimschuessel [119] showed that the Young’s Modulus decreases by a factor of 5 when 9% of water is absorbed. Moreover, the presence of water in PA6 can lead to a significant chemical degradation of the polymer. Amide groups react with water through a hydrolysis process [120] when immersed in water at high temperatures and/or for a long duration [121]. The latter leads to chain scissions that induce an embrittlement of the polymer and so lead to a large decrease in the mechanical properties. This irreversible reaction will not be considered in the present study, as exposure times were short enough to avoid this kind of degradation [122].

Despite the fact that the water absorption in PA6 has been widely studied in the literature in terms of mechanisms and consequences, there are still several open questions, and one concerns the modelling of the water diffusion process in the polymer. This modelling stage is absolutely necessary to evaluate the lifetime of thick structural parts. If it is not possible to predict the water diffusion and therefore, the local water content throughout the thickness, it is not possible to predict accurately the loss in mechanical properties induced by water. In some studies, water absorption in PA6 immersed in water has been modelled using Fickian behaviour [123]–[125]. However, this description is clearly not accurate as the Fickian behaviour is not conservative compared to experimental data. Thus, it should not be used when accurate predictions are required. This non-Fickian behaviour is explained by an increase in the water diffusion coefficient with the water content [126], [127] that occurs when the polymer is in the rubbery state [128]. Whereas the origin of the non Fickian behaviour is known, there is no accurate model based on physical considerations to describe the water absorption in PA6 when immersed in water. This is the aim of the following section.

1.2.Results

1.2.1. Water absorption in 2mm thick samples

Immersion of thick specimens (2mm) in water baths is considered here. First, the effect of temperature on the water absorption in sea water was investigated, Figure 36.a. Second, the effect of the medium was examined, Figure 36.b. For both figures, the water content is plotted as a function of the square root of time divided by the sample thickness.

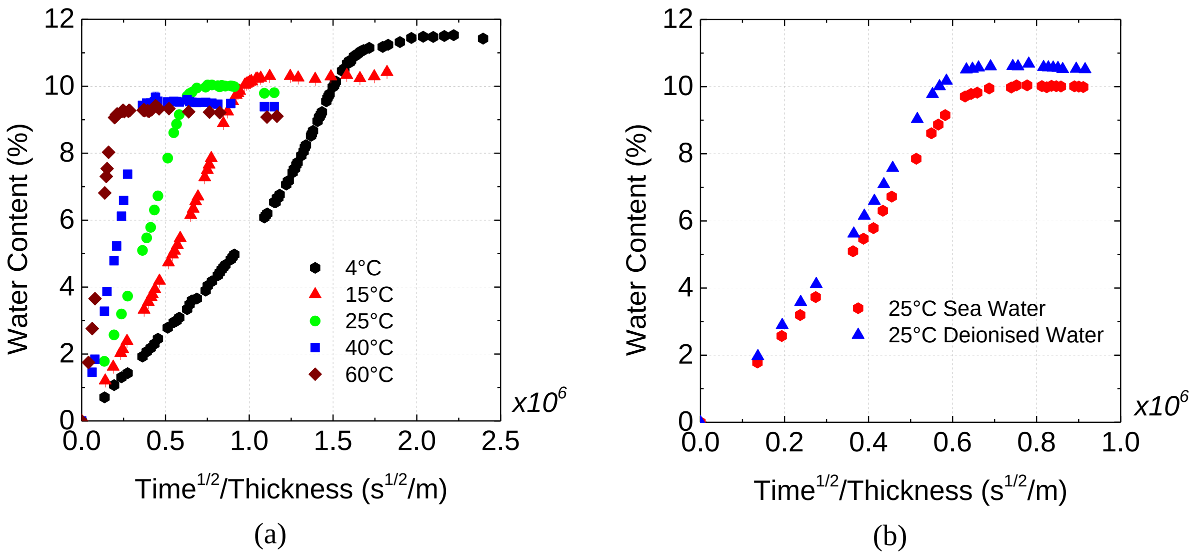

Figure 36 : (a) Water absorption in PA 6 immersed in sea water at several temperature (b) Effect of water activity on 2mm thick specimens at 25°C

Figure 36.a shows that the polymer absorbs a significant amount of water when immersed in sea water, more than 10% at 15°C at saturation. This large water absorption is in accordance with existing results [117] and attributed to the high polarity of NH groups in the polymer. It also appears that the maximal water uptake decreases when the temperature increases due to a negative activation energy of the solubility. Temperature also affects the water absorption kinetics; as expected the higher the temperature, the faster the water diffusion. This behaviour will be discussed in detail later.

Figure 36.b compares the water absorption in two different media: sea and deionised water. It clearly shows that the nature of the water affects both the maximal water uptake and water absorption rate, this can be explained by the fact that water activity in seawater is about 0.98 [129] i.e. lower than in deionised water. However, the overall trend is not affected.

In many polymers, water sorption follows a Fickian behaviour, the water diffusion can be described using a diffusion coefficient D and a mass at saturation M_∞ [100], Eq. 14.

$$\frac{M(t)}{M_\infty} = 1 - \frac{8}{\pi^2}\sum_i \frac{1}{(2i+1)^2} exp\left(-\frac{D(2i+1)^2\pi^2 t}{h^2}\right) \qquad \text{Eq. 14}$$

Where h is the sample thickness in mm and t the immersion time in s.

The diffusion coefficient can be calculated from the initial linear part of the sorption curve where $\frac{M(t)}{M_\infty} \leq 0.5$, Eq. 15.

$$D = \frac{\pi}{16}.\frac{h^2}{t}\left(\frac{M(t)}{M_\infty}\right)^2 \qquad \text{Eq. 15}$$

The diffusion coefficient D and the mass at saturation M_∞ are identified on the experimental water sorption plot of 2mm thick samples immersed at 15°C in sea water. These two values are then used to model a theoretical Fickian diffusion to be compared with the experimental data. Results are presented in Figure 37.

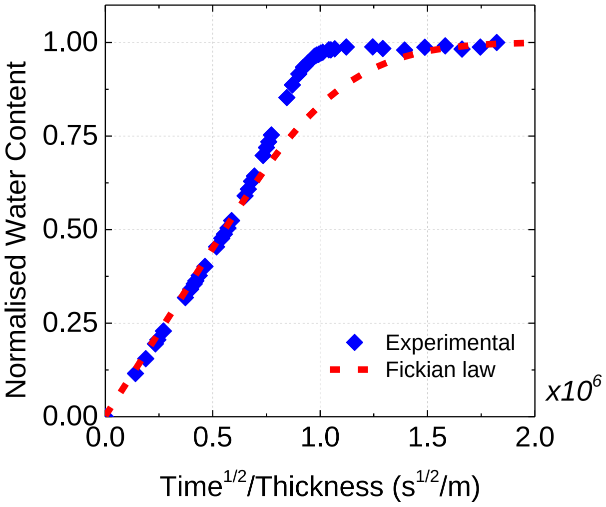

Figure 37 : Comparison between experimental results at 15°C in sea water and a Fickian behaviour with a D equal to $1.6.10^{-13}$ m²/s (identified on the experimental data in the linear part of the sorption curve)

Figure 37 clearly shows that it is not possible to describe the water absorption in these polyamide polymers using the Fickian law. In fact, an increase in water content at the end of the sorption curve is observed compared to the Fickian plot. This behaviour can be explained by an increase in the diffusion coefficient across the thickness of the specimen when the latter is in the rubbery state.

In order to investigate this particular behaviour over a wide range of temperature and water activities, it was chosen to work with polymer films (70µm) using the DVS. The latter is very useful since saturating thick specimens at more than 15 different water activities per temperature would take years.

1.2.2. Water absorption in thin films using DVS

In the DVS, the sample is exposed to an environment at a given water activity and for a certain time until it reaches a plateau. After complete saturation, the water activity is increased by 0.05 and the same cycle is repeated again and again until an activity of a=0.9 is reached. An example of a DVS test conducted at 40°C is presented in Figure 38. Working with a small increase in the water activity allows samples to be obtained in which the water content varies little in the polymer.

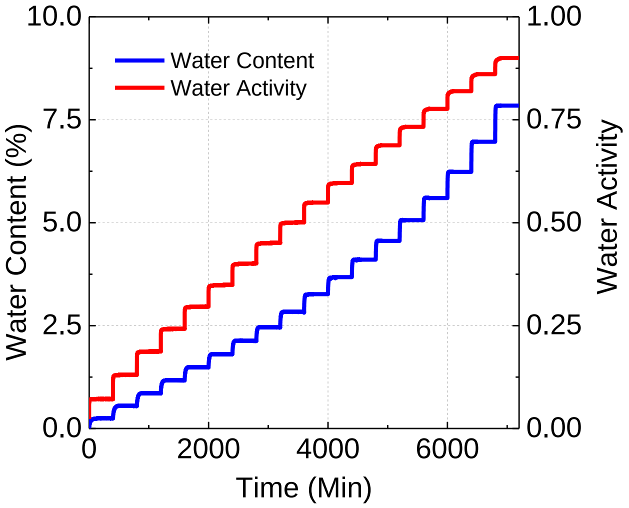

Figure 38 : Typical water absorption at 40°C as a function of water activity

At a=0.9, the polyamide matrix absorbs more than 8% of water (at 40°C). From this test, each condition provides a mass at saturation that is plotted as a function of the water activity in Figure 39.

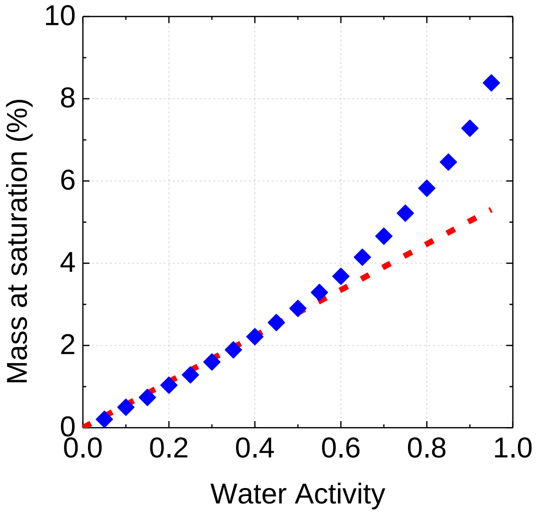

Figure 39 : Changes in the amount of absorbed water as a function of water activity at 25°C

From this figure, it is clear that the water content increases linearly from a=0.05 to approximately a=0.5. Beyond this level, it deviates from linearity, which indicates that Henry's law is no longer verified. The deviation from Henry's behaviour is related to the formation of water clusters in the polymer at high water activities that can be described using a power law. This behaviour has been highlighted in the literature [130], [131]. It is possible to describe the amount of water absorbed in the polymer with Eq. 16 [132] that uses Henry's law in the linear part (at low water activities) and another part that is related to the formation of water clusters in the polymer at high water activities.

$$M_{\infty} = H.a + b.a^{m} \qquad \text{Eq. 16}$$

Where a is the water activity, H, b and m polymer characteristics. Broudin [133] showed that this equation was able to describe the maximal water sorption in Polyamide 6.6. It was shown that H could be represented by a typical Arrhenius law; here, the pre exponential factor H_0 is equal to 0.38 and the activation energy E_a is equal to -7kJ/mol. b and m were found to be respectively equal to 4 and 3 and considered independent of the testing temperature. Now that the maximal water absorption for each humidity step has been considered, it is interesting to focus on the water absorption rate.

For each water sorption at a given water activity, a Fickian diffusion coefficient D was identified from the experimental data and the the Fickian equivalent was plotted at different water activities (0.2, 0.4, 0.6 and 0.8), presented in Figure 40.

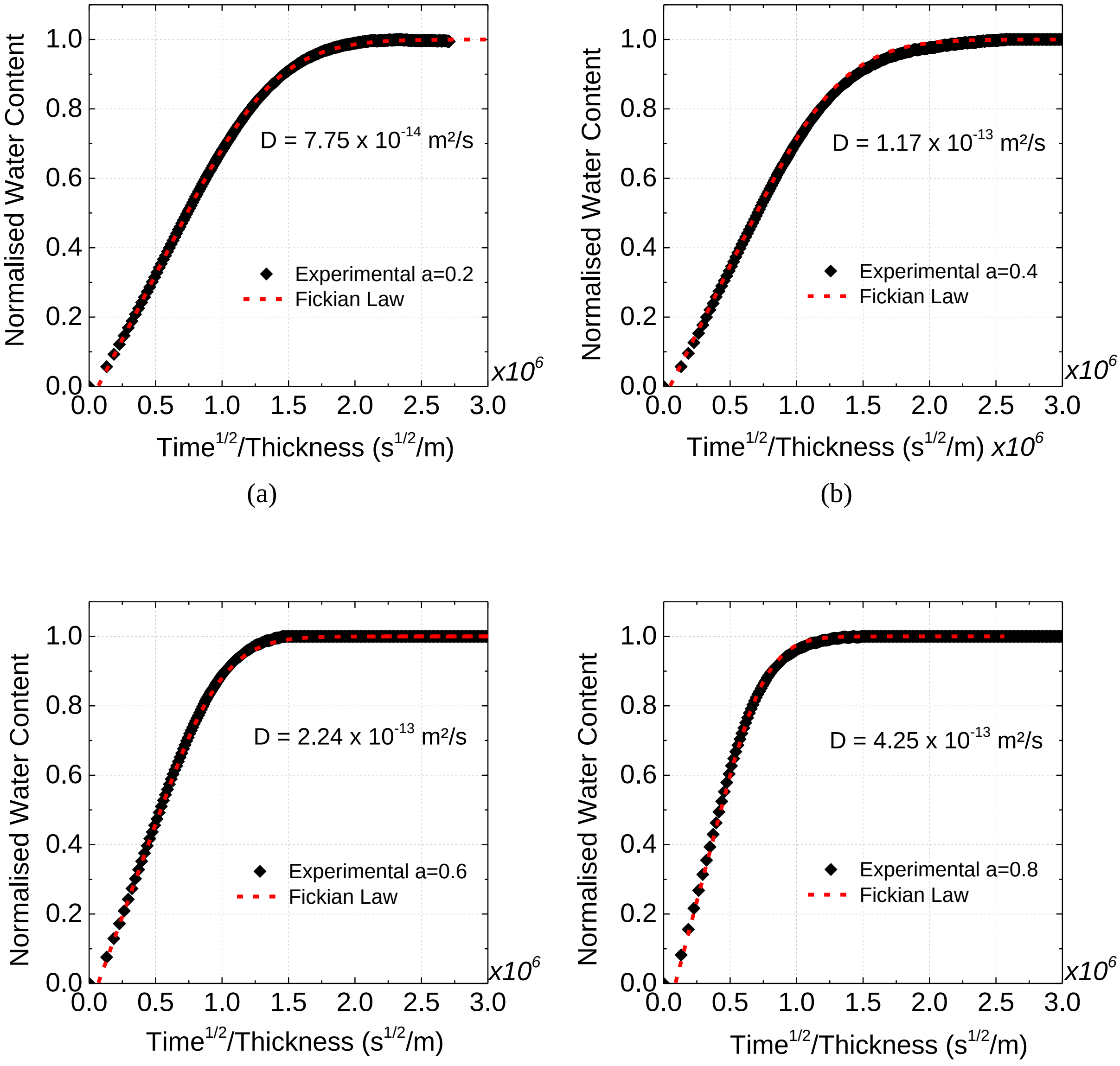

(a) (b)

(c) (d)

Figure 40 : Normalised water absorption at 25°C as a function of water activity (a) a=0.2 (b) a=0.4 (c) a=0.6 (d) a=0.8

Figure 40 shows that in this case, the water absorption can be described based on Fickian behaviour for all the water activities at 25°C. It has to be noted that the results in Figure 40 are not in contradiction with the results in Figure 37. In fact, as noted previously, a non Fickian behaviour is observed when dried thick samples are immersed in water. However, when very slight increases in water are used (DVS), it is possible to model the water uptake using the Fickian law with a given diffusion coefficient that changes with the water content (Figure 40 and Figure 41). The dependence of diffusivity on the water content can be neglected when very slight differences in water contents are considered. However, when large water content differences exist, the diffusion coefficient changes through the thickness and results in an overall non Fickian behaviour.

Showing that the water diffusion follows a Fickian diffusion at every water activity allows the diffusion coefficient D identified for each condition to be plotted as a function of the water activity. An example at 25°C is presented in Figure 41.

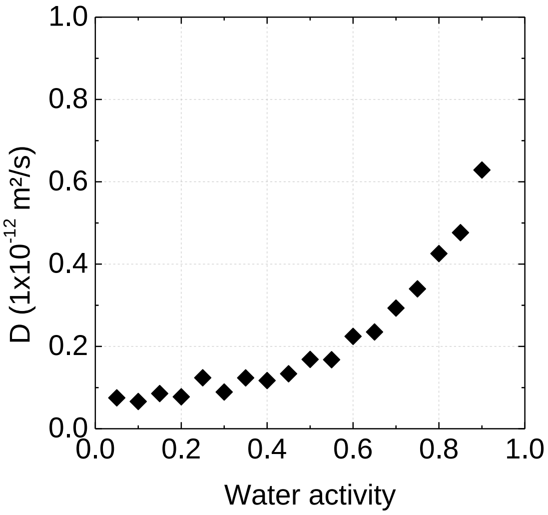

Figure 41 : Change in diffusivity as function of water activity in PA 6 (example at 25°C)

Results from Figure 41 show that the diffusion coefficient is stable (around 1.0.10^{-13} m²/s) at low activities and then increases up to a value of 6.5.10^{-13} m²/s for higher activities.

This behaviour is in agreement with the literature [126], [128], [130] and can be explained by the decrease in the glass transition temperature induced by plasticisation during water absorption. The changes in T_g with water content will be considered in the next section.

It is worth noting however, that some authors, in very recent work, have shown that water diffusivity increase in PA6,6 and PA6,10 can be correlated with the beta relaxation [127] transition in the polymer and this requires study for PA6. Here we will focus on changes in T_g with water content, and these will be considered in the next section.

1.2.3. Changes in T_g with water absorption

It is well known that the water absorption leads to an increase in the chain mobility of the polymer and so to a decrease in the glass transition (T_g). This decrease in T_g has many consequences for both diffusivity and the mechanical properties. Thus, it is necessary to be able to evaluate and describe the T_g changes induced by the presence of water.

Glass transition temperatures values from DMA performed on thick specimens with homogeneous water contents following saturation at different water amounts are presented in Figure 42. It should be remembered that each specimen was saturated at a given water activity for a maximum time of 48 hours. To prevent hydrolysis at this temperature, the samples were tested as soon as saturation was reached. Also, Bernstein [121] showed that a longer time of exposure is needed for hydrolysis to occur.

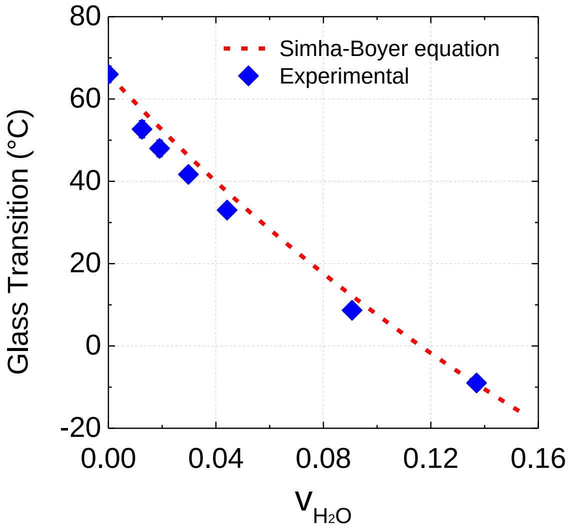

Figure 42 : Changes in T_g with water content measured (points) and predicted (dotted line)

From this result, it is clear that there is a very significant decrease in T_g from 66 ± 1 °C in the dry state to -9 ± 1 °C when the specimen is fully saturated with 9% of water. As water enters the material, the glassy amorphous phase of the polymer goes into the rubbery state because of the increase in chain mobility (plasticisation). This result is in agreement with the literature [119] and can be described using the Simha-Boyer equation, which is a simplified version of the Kelley-Bueche equation [134]. This equation establishes a relationship, based on the free volume theory that relates the decrease in T_g with the water content as described hereafter in Eq. 17 and Eq. 18.

$$\frac{1}{T_g} = \frac{1}{T_{gp}} + Av_{H_{2O}} \qquad \text{Eq. 17}$$

$$A = \frac{1}{T_{gs}} - \frac{1}{T_{gp}} \qquad \text{Eq. 18}$$

Where T_g is the glass transition temperature of the polymer (K), T_{gp} is the polymer glass transition temperature in the dry state (Measured to be 333K by DMA), T_{gs} is the glass transition of solvent (here water) that is taken equal to 110 K [128] and v_{H2O} is the volume fraction of water in the polymer previously described in Eq. 8. The comparison between experimental results (dots) and the Simha-Boyer equation (line) in Figure 42 clearly shows that the decrease in T_g induced by the presence of water can be quite accurately described, which is very useful for modelling.

To conclude on the experimental section, we have shown that Henry's law was not verified here as at high water activities, the formation of clusters is observed. This behaviour can be described using a simple mathematical equation (Eq. 16). In the meantime, using the DVS measurements with small humidity steps, it is possible to show that the water absorption in PA6 follows a Fickian behaviour for all the water activities. This also allows us to determine the diffusion coefficient for all these conditions. It appears that the diffusivity depends strongly on the water activity for a given temperature. At low activities, the diffusion coefficient is constant whereas at high activities, a large increase is observed. This behaviour is explained by the change from the glassy to the rubbery state of the amorphous phase of the PA6. The water absorption leads to a large decrease in T_g that can be accurately described using the simple Simha-Boyer relationship. The description of these changes in water diffusivity with both temperature and water activity will considered in the next section.

1.3.Discussion and modelling

This section aims to propose a new model that describes water absorption in thick polyamide 6 when used in a humid environment and more especially in sea water over a wide range of temperatures.

From the previous results, it is now possible to describe the water content at saturation when a specimen evolves at a given water activity (Eq. 16). Then, it has been shown that from the latter, we can evaluate the T_g for a certain water content (Eq. 17 and Eq. 18). Above a certain water activity, the polymer goes into the rubbery state and we have seen that the behaviour is very different between the glassy and the rubbery state (Figure 39 and Figure

41). The current section will focus on predicting the diffusion coefficient below and above the glass transition of the polymer. First, the prediction of the diffusion coefficient below T_g is made using an Arrhenius equation. Second, the free volume theory is used to describe the behaviour above T_g. Finally, these two laws are combined and used in a model to predict the water diffusion in a thick sample immersed in water at a given temperature and the prediction is compared to experimental data. A schematic representation of the model is presented in Figure 43.

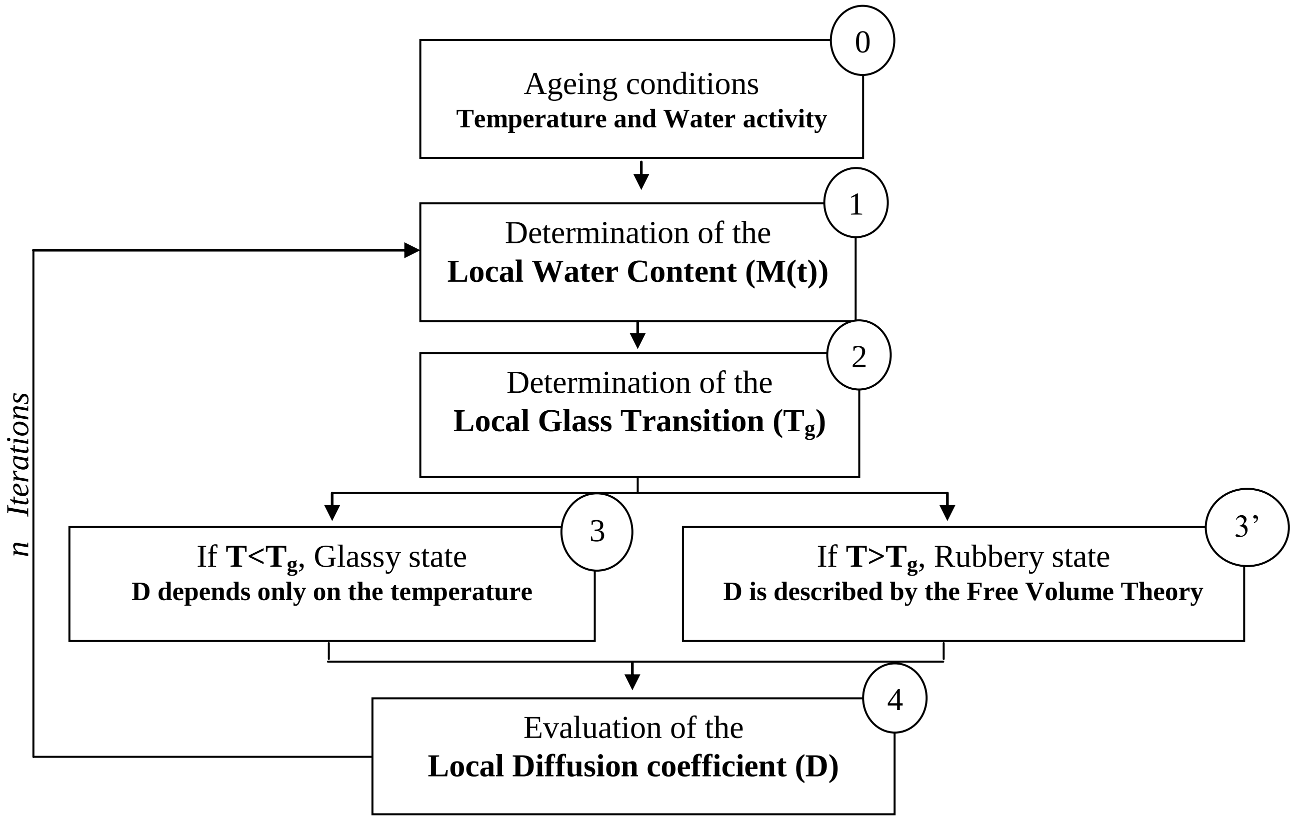

Figure 43 : Schematic representation of the model

The dry specimen is exposed to a given temperature and water activity (0) and water sorption starts. As water enters the polymer, the model is used to calculate the water content at a given position across the thickness of the polymer (1). Then, equation 7 is used to predict the local glass transition of the amorphous phase of the polymer (2). In the case where the predicted glass transition is higher than the test temperature, the diffusion coefficient is calculated using the Arrhenius law because the polymer is in its glassy state (3). However, when the latter is in the rubbery state (3'), i.e. when the glass transition is lower than the test temperature, the model uses the free volume theory to obtain D (4). Then, the model follows an iteration loop for all positions across the thickness and for every immersion time t until complete saturation.

The following sections will present the experimental validations for the calculation of D both below and above T_g.

1.3.1. Behaviour in the glassy state

It was shown in Figure 41 and also in the literature [126], [128] that the water diffusivity does not depend on the water activity when the polymer is in glassy state. However the diffusion coefficient depends on the temperature. This temperature effect can be described using the Arrhenius law (Eq. 19) as shown in Figure 44.

$$D_{(T<T_g)} = D_0 . \exp\left(-\frac{E_a}{RT}\right) \qquad \text{Eq. 19}$$

Where $D_{(T<Tg)}$ is the diffusion coefficient in the glassy state in m²/s, D_0 the pre exponential diffusion coefficient in m²/s, E_a the activation energy in the glassy state, R the gas constant equal to 8.31 $J.mol^{-1}.K^{-1}$ and T the temperature in K.

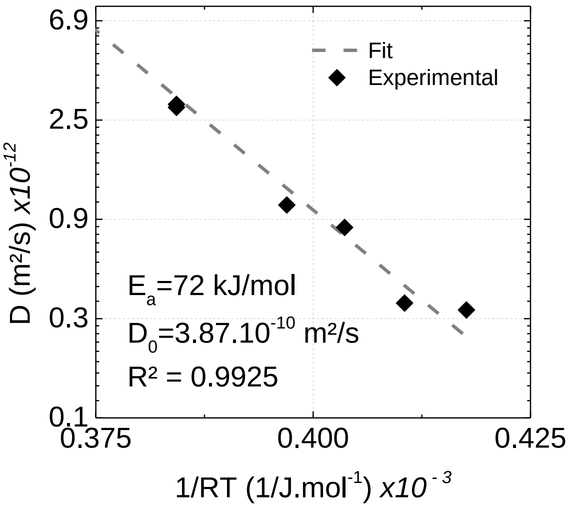

Figure 44 : Measured diffusion coefficient D as a function of 1/RT

The activation energy in the glassy state is 72kJ/mol. For comparaison, Abacha et al. [123] found an activation energy of 54kJ/mol, which lies in the same range. Silva et al. [117] also found comparable values of 64kJ/mol. Therefore, it is now possible to describe the diffusion coefficient below the T_g of the polymer. The next section will focus on the prediction of the diffusion coefficient above the T_g.

1.3.2. Behaviour in the rubbery state

When the polyamide is in the rubbery state, the diffusivity increases strongly with the water activity as shown in Figure 41 and [128]. This section aims to describe the changes in diffusivity with water activity based on the free volume theory that basically considers an increase of the polymer volume due to holes formation when the polymer is above its T_g. The presence of these holes considerably changes the diffusivity of water. In this case, it has been shown by Vrentas [135] that the water diffusion coefficient can be described using the following equations (Eq. 20 and Eq. 21).

$$D_{(T>Tg)} = D_{02}.exp\left(-\frac{E}{RT}\right).\exp\left(-\frac{\gamma.(w_1.\widehat{V_1^*} + \xi.\mathrm{w}_2.\widehat{V_2^*})}{\widehat{V_{FH}}}\right) \qquad \text{Eq. 20}$$

$$\frac{\widehat{V_{FH}}}{\gamma} = \left(\frac{K_{11}}{\gamma}\right).w_1.\left(K_{21} + T + T_{g1}\right) + \left(\frac{K_{12}}{\gamma}\right).w_2\left(K_{22} + T - T_{g2}\right) \qquad \text{Eq. 21}$$

Where $D_{(T>Tg)}$ is the diffusion coefficient above T_g in m²/s, D_{02} is a pre-exponential factor in m²/s, $\hat{V}_1^*$ is the critical local hole free volume required for a molecule of species 1 (water) to jump to a new position, $\hat{V}_2^*$ is the critical local hole free volume per gram of polymer required for the displacement of a jumping unit, w_1 is the mass fraction of component 1 (i.e. water), w_2 is the mass fraction of component 2, ξ is the ratio of the critical molar volume of the solvent jumping unit to the critical molar volume of the polymer jumping unit, γ is an overlap factor (which should be between 0.5 and 1) introduced because the same free volume is available to more than one molecule. E is the energy per mole that a molecule needs to overcome attractive forces holding it to its neighbors. $\hat{V}_{FH}$ is the average hole free volume per gram of mixture and can be calculated with Eq. 21 where K_{11} and K_{21} are free volume parameters for the solvent, here water, and K_{12} and K_{22} are free volume parameters for the polymer, T_{g1} is glass transition temperature of water, T_{g2} is glass transition temperature of polyamide 6.

At the temperatures of the study, the specific hole free volume is relatively small and the diffusion is free volume dominated. Therefore, the energy E in Eq. 20 can be included in the pre exponential factor D_{02} [136]. This leads to Eq. 22 which states that the diffusion above T_g is mainly dominated by free volume effects.

$$D_{(T>Tg)} = D_{02}.\exp\left(-\frac{\gamma.(w_1.\widehat{V_1^*} + \xi.w_2.\widehat{V_2^*})}{\widehat{V_{FH}}}\right) \quad \text{Eq. 22}$$

This equation can now be used to determine the diffusion coefficient above T_g. However, several parameters inside the exponential term still need to be determined. First, the parameters associated with the solvent, which is water here, are presented in Table 4. These values are taken from the literature [137].

Table 4 : Values for water, from [137]

Constant	Value
$\widehat{V_1^*}$	1.071
$\frac{K_{11}}{\gamma}$	$2.18.10^3$
$K_{21} - T_{g1}$	-152.3

Second, the parameters associated with the polymer must be determined as well.

The quantity ξ is defined as follows, Eq. 23:

$$\xi = \frac{V_1^0(0)}{V_2^*(j)} \qquad \text{Eq. 23}$$

Where $V_1^0(0)$ is the molar volume of water and $V_2^*(j)$ is the molar volume of the polymer. To calculate the latter, Hong [137] showed that for a T_g>295K, Eq. 24 can be used.

$$V_2^*(j) = 0.6224.T_g(K) - 86.95 \qquad \text{Eq. 24}$$

In our case, $T_g(K)$ is equal to 333K. The determination of $V_2^*(j)$ allows us to determine several other parameters of interest, Eq. 25:

$$\frac{\gamma.\widehat{V_2^*}}{K_{12}} = 2.303.C_1.C_2 \qquad \text{Eq. 25}$$

The parameter K_{22} is defined in Eq. 26:

$$K_{22} = C_2 \qquad \text{Eq. 26}$$

The parameters C_1 and C_2 are taken from the literature [138] and are summarised in Table 5.

Table 5 : Values for the polymer, from [138]

Constant	Value
C_1	17
C_2	51
$\widehat{V_2^*}$	0,935

Once all the parameters in the exponential term of Eq. 22 are obtained, it is possible to plot in Figure 45 the diffusion coefficient of the polymer at a given temperature above T_g as a function of the exponential term.

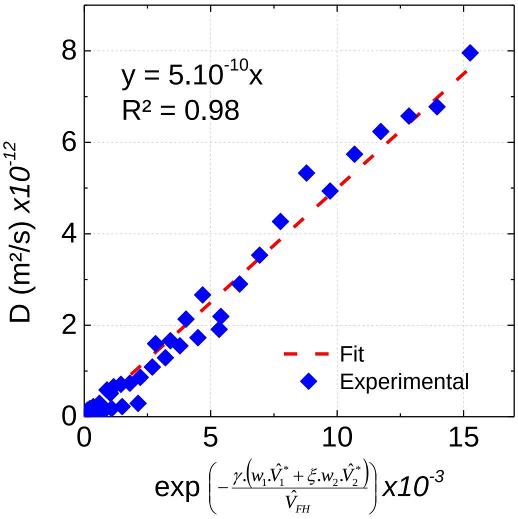

Figure 45 : Experimental D as a function of the term in the exponential

Figure 45 shows that the diffusion coefficient above T_g (whatever the testing temperature) as a function of the exponential in the rubbery state can be represented by a linear relationship. Therefore, the diffusion in polyamide 6 can be described using the free volume theory with a D_{02} value of 5.10^{-10} m²/s.

Let us now compare the experimental values of D with the different expressions presented earlier (above and below T_g). The results are presented in Figure 46.

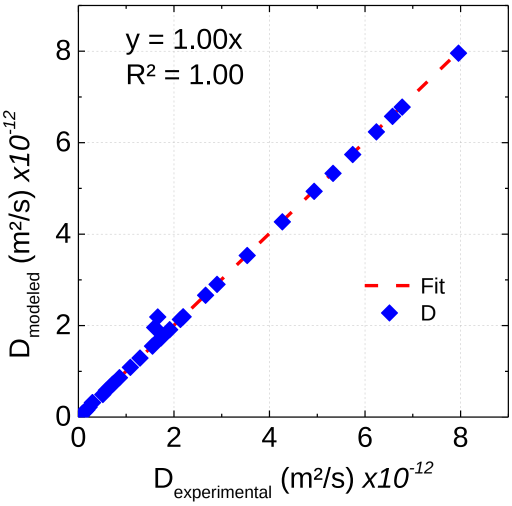

Figure 46 : Predicted diffusion coefficient as a function of the measured D.

Figure 46 shows that the free volume theory can be used to describe the evolution of T_g and D during water absorption. Therefore, now that all the expressions required to model the water absorption have been validated (maximal water absorption, glass transition, diffusion coefficient), it can be used to predict the diffusion in a thick specimen at a given temperature.

1.3.3. Comparison modelling/experiments

As a reminder, the model presented schematically in Figure 43 describes the diffusion behaviour for all positions across the thickness and for every immersion time until complete saturation for a given medium and a given temperature.

Results from the model are presented in Figure 47 together with the experimental data. For each figure, the water content inside a specimen at a given temperature is plotted as a function of the square root of time divided by the sample thickness. The Fickian law identified on the experimental data is presented as well to show the improved accuracy of the specific model.

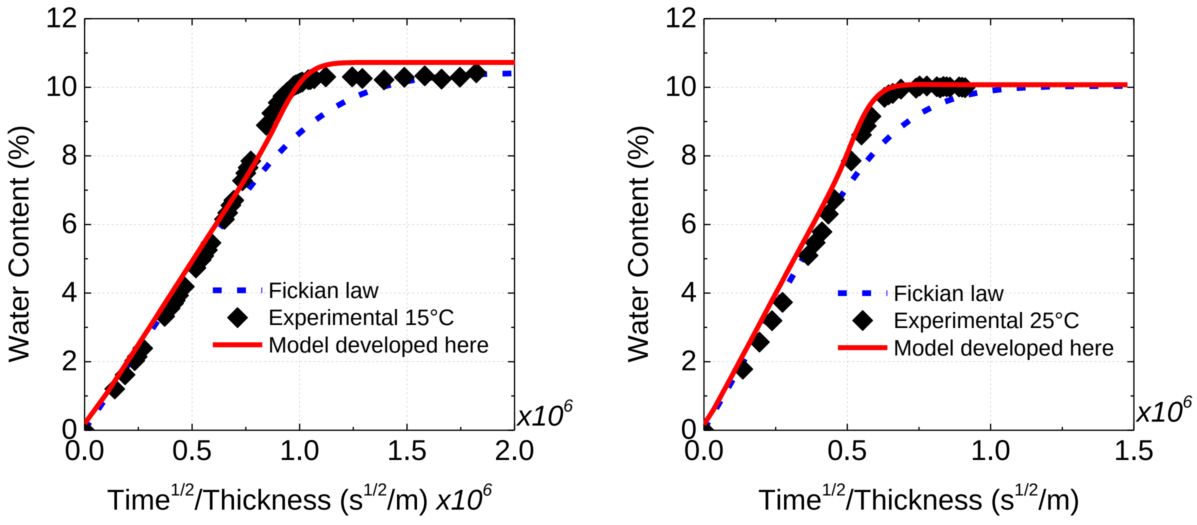

(a)

(b)

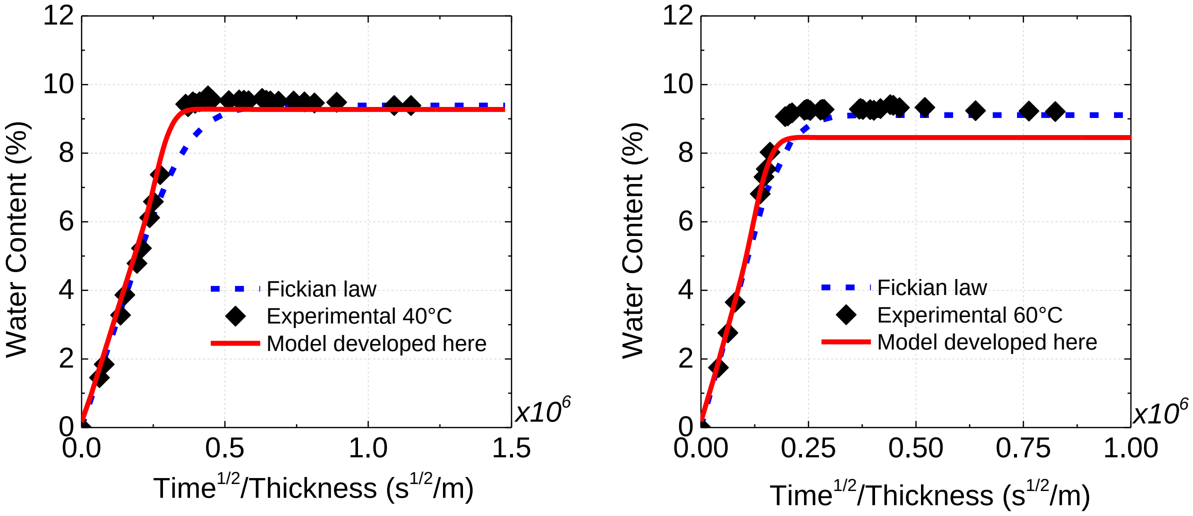

(c) (d)

Figure 47 : Comparison between experimental results obtained on thick samples immersed in sea water and the specific model developed in this study as well as the Fickian equivalent for (a) 15°C (b) 25°C (c) 40°C (d) 60°C

The results show a good agreement between the specific model and the experimental data and are much closer than the Fickian modelling. The model can describe accurately the change of slope (acceleration in water diffusion rate). It should be noted that the Fickian law that is presented in all these figures comes from an identification of the experimental data. The diffusion coefficient D is identified in the linear part of the curve and the mass at saturation is taken as the maximal water absorption. This is not the case for the specific model where each property is predicted based on the temperature and water activity of interest, providing an accurate description of the water content at saturation in the range from 15 to 40°C.

The water absorption in the amorphous phase of polyamide 6 follows a complex behaviour. The large water absorption induced by the presence of polar groups leads to an important plasticisation (decrease of more than 70°C in T_g). The latter increases the chain mobility inside the amorphous phase of the polymer and decreases the glass transition temperature. When the T_g decreases to a value lower than the test temperature, the polymer changes into the rubbery state, which increases the specific volume of the polymer. This increase in volume is attributed to the formation of holes that increase the diffusivity. Moreover, at high activities, the water uptake results in the formation of clusters that increase even more the maximal water absorption at a given water activity (deviation from Henry's law). We have seen that all these complex behaviours have been accurately described one by one leading to a prediction of the water diffusion in a thick specimen (2mm) exposed to a given temperature in the range from 15 to 40°C.

However, some limits for this model can be noted. For instance, Figure 47.d shows a slight difference concerning the water content at saturation compared to the experimental data at 60°C. The maximal water absorption is associated with the formation of clusters during water absorption, as presented in Eq. 16. In this study, b and m were taken to be material parameters independent of the temperature, which might not be valid over a wider range of temperature, more especially at temperatures below 15°C.

1.4. Conclusion

Water absorption in polyamide has been considered in this section. The aim was to be able to model the water diffusion in thick specimens immersed in sea water. First, it has been shown that when PA6 is immersed either in seawater or in deionised water, it is not possible to model the water uptake using a simple Fickian behaviour. This is explained by the fact that the water diffusivity is not constant with the water content. Therefore, DVS measurements have been performed with small humidity steps (5%) in order to characterise with accuracy both the water content and the water diffusion coefficient. Results were described with mathematical equations related to physical processes (cluster formation, free volume theory) in order to propose a new model. This new model considers first the local water content in the polymer that depends on the surrounding environment. From this local water content, it is possible to evaluate the T_g. Then, two cases are possible; if the polymer is in the glassy state ($T<T_g$), the diffusion coefficient D only depends on the temperature and can be described using an Arrhenius law. However, if the polymer is in the rubbery state ($T>T_g$), D depends on both the temperature and the water content. It has been shown that this behaviour can be accurately described with the free volume theory.

This new specific model has been used to predict with precision the water absorption in a thick specimen immersed in sea water at different temperatures. Results show a good agreement between the model and the experimental data. However, the main goal of the current chapter is to model the water diffusion in a thick composite cylinder immersed in sea water at low temperatures. This is the aim of the next section.

2. Water absorption in Carbon-Polyamide 6 laminates

The model that was just presented will now be adapted for the water diffusion process inside a given composite material.

2.1.Differences found in the water uptake at saturation

First, the water uptake measurements conducted on specimens of the neat, commercial PA6 and on matrix in the composite immersed in sea water at different temperatures showed unexpected results. In fact, the water contents at saturation inside the commercial PA6 and in the PA6 matrix from the composite showed significant differences, the composite matrix values are lower than the ones obtained in the commercial polyamide. Results are presented in Figure 48.

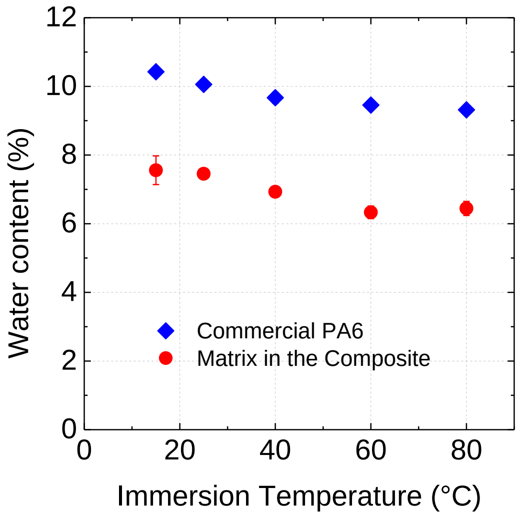

Figure 48 : Water contents at saturation in the commercial polyamide 6 and in the matrix alone

Results show that for each immersion condition, the water uptake in the neat PA6 is significantly higher (30%) than the value for the matrix in the composite. It should be noted that the water uptake in the composite has been calculated to only account for the diffusion in the matrix. One might expect that the water uptake inside the composite material would be higher than in the commercial PA6 since voids and fibre/matrix interface regions could be filled as well, but this is not the case here. The nature of this difference is not clearly identified. Thermo gravimetric analyses conducted under nitrogen flow did not reveal the presence of additional fillers. No differences were also found concerning the degrees of crystallinity. The only difference that was found was related to the molecular mass and polydispersity index, 2.5 and 48.1kJ/mol for the commercial PA6 and 2.8 and 23.7 kJ/mol for the composite, respectively. In order to reduce the viscosity to be able to impregnate the fibres the PA6 grade has been modified, compared to the commercial polymer. However, no work has been found in the literature describing an effect of the molecular mass on the water diffusion. Therefore, the nature of this difference is not clearly understood but will have to be taken into account when modelling the water diffusion in the composite.

2.2. Results

Even though the water contents at saturation are different, we have to make sure that both matrices behave similarly, i.e., that the evolution of the water content as a function of the activity does not follow Henry's law and that the diffusion coefficients are different below and above T_g.

2.2.1. Deviation from Henry's law

As in the previous section, a DVS test was performed on one ply of prepreg (175µm) in order to characterise the water diffusion as a function of the water activity at 40°C, Figure 49. The latter is compared to the test conducted under the same conditions on the commercial PA6.

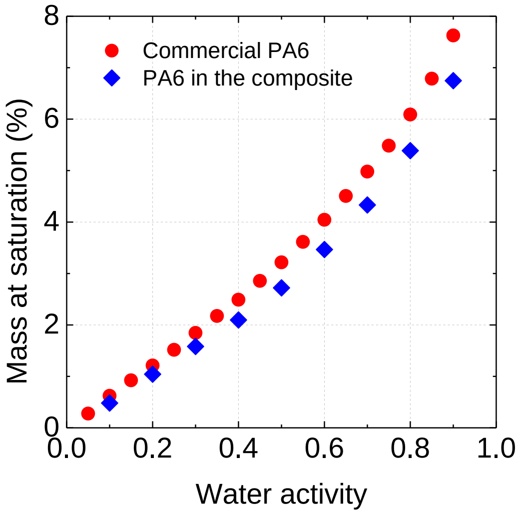

Figure 49 : Changes in the amount of absorbed water as a function of the water activity for the neat commercial Polyamide 6 and the matrix of the composite at 40°C

This figure highlights two main conclusions. First, the results are in accordance with the previous ones in Figure 48, i.e. the water diffusion in the matrix of the composite is lower than for the neat PA6. Second, it is clear that the evolution of the water content as a function of the activity does not follow Henry’s law. Therefore, as for the neat PA6, clustering occurs at high activities and this behaviour can be described using Eq. 16.

2.2.2. Increase in diffusion coefficient at high activities

For each water activity at which the test was conducted, a Fickian behaviour was identified, as was done earlier for the neat PA6, which allows us to plot the diffusion coefficient D as a function of the water activity, Figure 50.

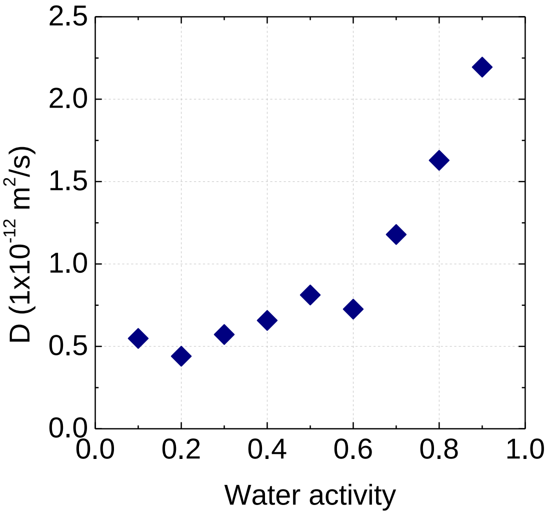

Figure 50 : Changes in diffusivity as a function of the water activity in the matrix of the composite (at 40°C)

Results in Figure 50 show that the diffusion coefficient is relatively stable at low activities (around 7.5.10^{-13} m²/s) and then increases up to a value above 2.0.10^{-12} m²/s for high activities. This result is in accordance with results for the commercial polyamide 6 and is related to the plasticisation behaviour occurring during water absorption in polyamide 6. Let us now verify if the drop in glass transition temperature can be described accurately as for the neat PA6. Composite specimens saturated at different humidity conditions (0, 33%, 63%, 75% and in immersion) were tested by DMA. Results are presented in Figure 51 and are compared to the Simha-Boyer equation and the experimental results from the commercial PA6.

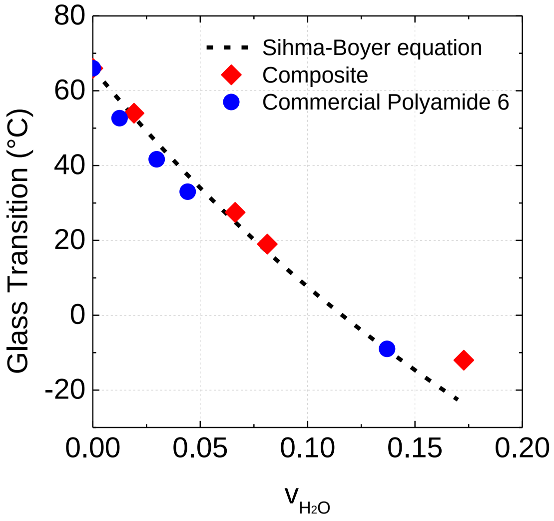

Figure 51 : Changes in Tg with water content in the neat commercial polyamide 6 and the composite - Comparison with the prediction

Results from Figure 51 show that a very similar trend is observed for both materials. The glass transition temperature decreases from 66°C to a negative value. However, a slight deviation is observed for the composite at the highest water volume fraction (v_{H2O}) when compared to the neat PA6 and the Simha Boyer equation. At low water activities, the difference in water content between the neat PA6 and the composite is lower than at high activities, as seen on Figure 49. However, the difference is much higher at high activities, which might explain this slight deviation from the Simha-Boyer equation for the composite.

This section has allowed us to show that the two matrix polymers (commercial and from the composite) behave in a similar manner, and that the laws used for the commercial PA6 can be re-used to model the water diffusion behaviour in the composite. As for the neat PA6, the behaviour of the diffusion coefficient below T_g can be described using an Arrhenius equation. Also, the diffusion coefficient above T_g can be described using the free volume theory.

2.3.Discussion and Modelling

Unidirectional composite materials are considered to be transversely isotropic. In the case of water diffusion in unidirectional composite materials, we will consider two diffusion coefficients D_1 and D_2 corresponding respectively to longitudinal and transversal diffusion. Based on the work of Kondo and Taki [139], the diffusion coefficient along the fibres (direction 1) is taken as the diffusion coefficient of the matrix D_{matrix}, Eq. 27. Then, because of the transverse isotropy, the directions 2 and 3 (through-thickness) are considered equal,Eq. 28.

$$D_1 = D_{matrix} \quad \text{Eq. 27}$$

$$D_2 = D_3 \quad \text{Eq. 28}$$

A schematic representation is presented in Figure 52.

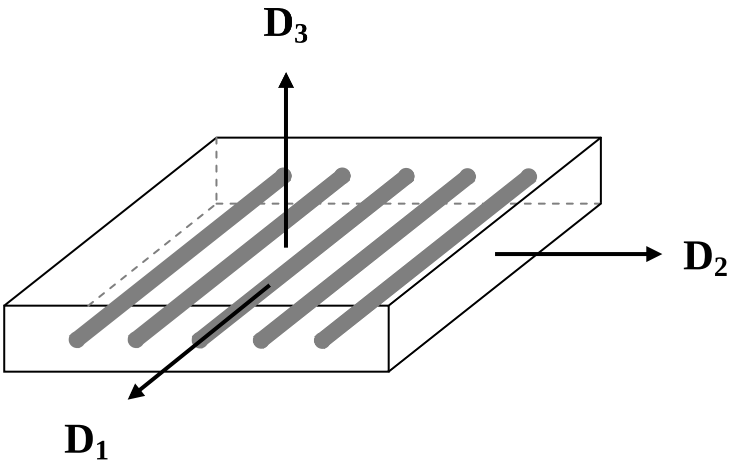

Figure 52 : Schematic representation of the diffusion coefficients used along and perpendicular to the fibre direction

Although the diffusion coefficient along the fibre direction D_1 is most often taken as that of the resin, the transverse diffusion coefficient is much more controversial. Most studies consider that the transverse diffusion coefficient D_2 corresponds to the diffusion coefficient of the resin times a factor that we will call α which has a value lying between 0 and 1, Eq. 29.

$$D_2 = \alpha . D_{matrix} \qquad \text{Eq. 29}$$

The following table (Table 6) resumes the different values of α for a fibre volume fraction of 0.48 (from TGA) according to several equations found in the literature [140].

Table 6 : Homogenisation relations with V_f=0.48

[Reference]	**Transverse diffusion coefficients**	**D_2 calculated with V_f=0.48**
Halpin Tsaï	$D_2 = D_r\left(\frac{1-V_f}{1+V_f}\right)$	$D_2 \simeq 0.351\, D_r$ with ζ=2
Shen-Springer	$D_2 = D_r\left(1-2\sqrt{\frac{V_f}{\pi}}\right)$	$D_2 \simeq 0.218\, D_r$
Springer Tsaï	$D_2 = D_r\left(\frac{1-2\sqrt{\frac{V_f}{\pi}}}{1-V_f}\right)$	$D_2 \simeq 0.419\, D_r$
Shirrel-Halpin	$D_2 = D_r\left(\frac{1}{1+V_f}\right)$	$D_2 \simeq 0.675\, D_r$
Rayleigh	$D_2 = D_r\frac{1-V_f-0.3058V_f^4}{(1+V_f-0.3058V_f^4)(1-V_f)}$	$D_2 \simeq 0.179\, D_r$

Now, in order to investigate which equation best suits the experimental data, the model calculated the water diffusion for every value of α, following the scheme shown in Figure 52. The results for each equation are presented in Figure 53 and are compared to the experimental data at 40°C. It can be noted that since differences in water contents between the neat PA6 and the composite are observed, the model will not be able to predict accurately the water content at saturation when immersed in water. Therefore, the results presented in Figure 53 concern the normalised water content as a function of the square root of time divided by the sample thickness.

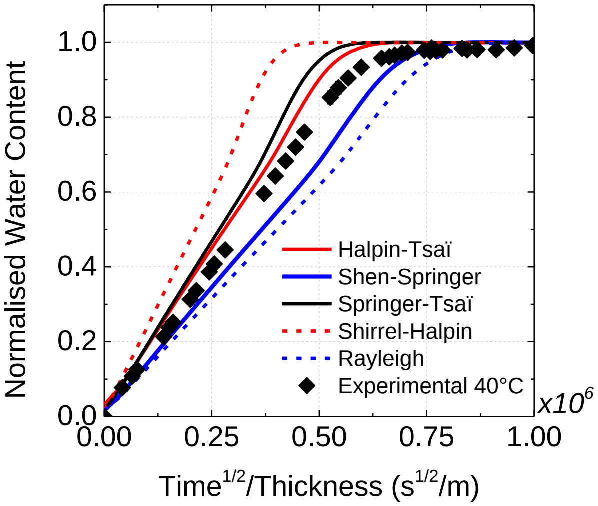

Figure 53**:** Comparison of the transverse coefficient of diffusion obtained using the equations described in Table 6

Results from Figure 53 show that no value of α from the literature corresponds closely to the experimental data. However, the closest one is that of the Halpin-Tsaï equation with a value of α of 0.351. This value is calculated for ζ=2, which usually corresponds to hexagonal packing, which is the case here (high fibre volume fraction). Other calculations were performed in order to fit as closely as possible the experimental data. It was found that a value of α of 0.3 fits the experimental data at several temperatures with good accuracy, as presented in Figure 54.

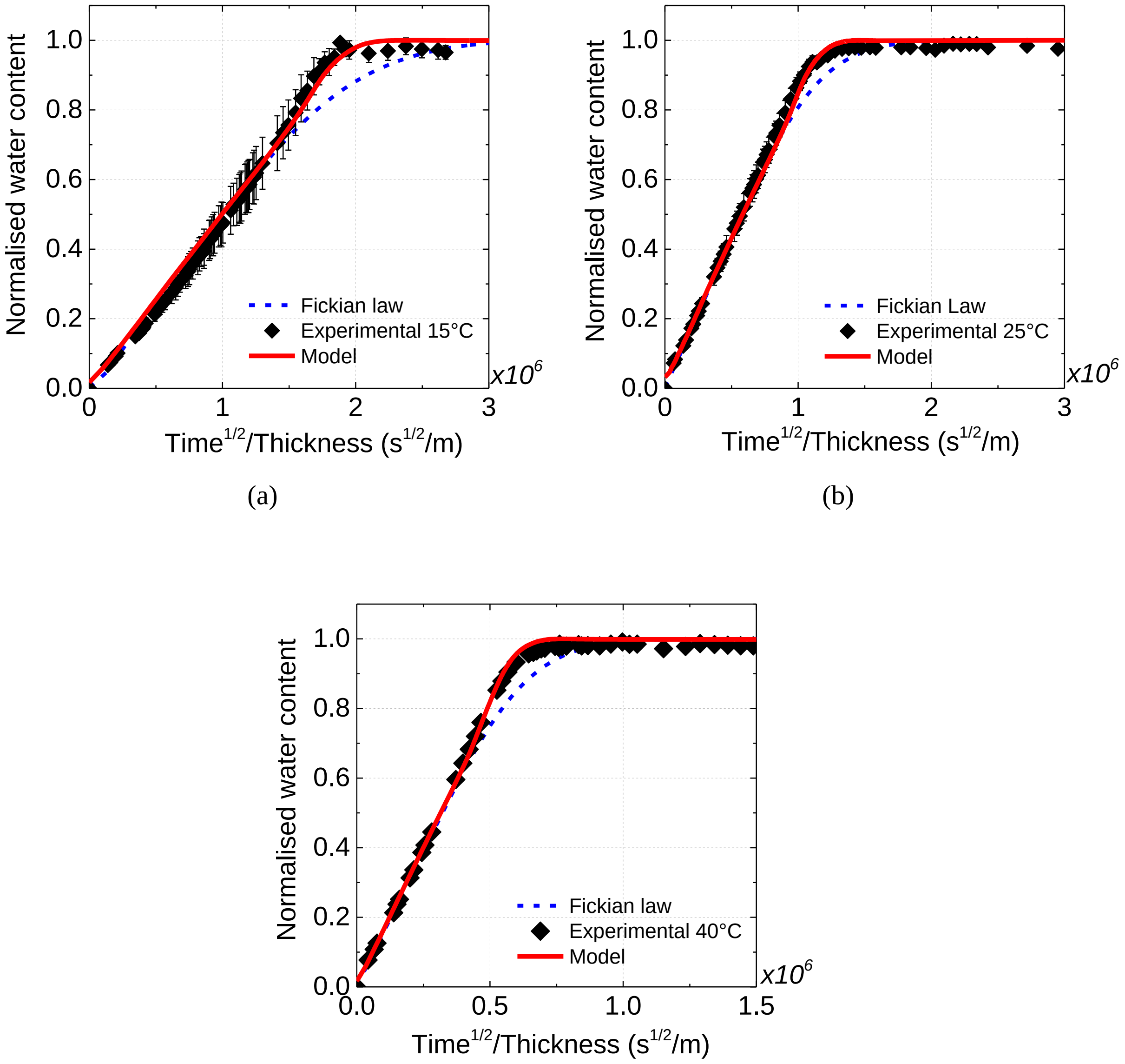

(a)

(b)

(c)

Figure 54 : Comparison between experimental results obtained on thick samples (2mm) immersed in sea water and the specific model developed in this study for a value of α of 0.3 as well as the Fickian equivalent for (a) 15°C (b) 25°C (c) 40°C

The results show a good agreement between the specific model and the experimental data and are much closer than the Fickian modelling. The model can accurately describe the change of slope (acceleration in water diffusion rate).

3. Prediction of the water absorption in a thick composite cylinder immersed at 15°C

The final aim of the following chapter is to predict the water distributions at several immersion times in a thick cylinder (12mm) immersed under realistic conditions (15°C). Water only diffuses on one side, the interior of the cylinder is dry. The specific model adapted for the composite will be used, but because the latter cannot predict the water content at saturation, the mass at saturation was set as the experimental values obtained on the 2mm thick composite specimens, i.e., 3.1% at 15°C in sea water. The sorption curve obtained for these immersion conditions is presented in Figure 55.

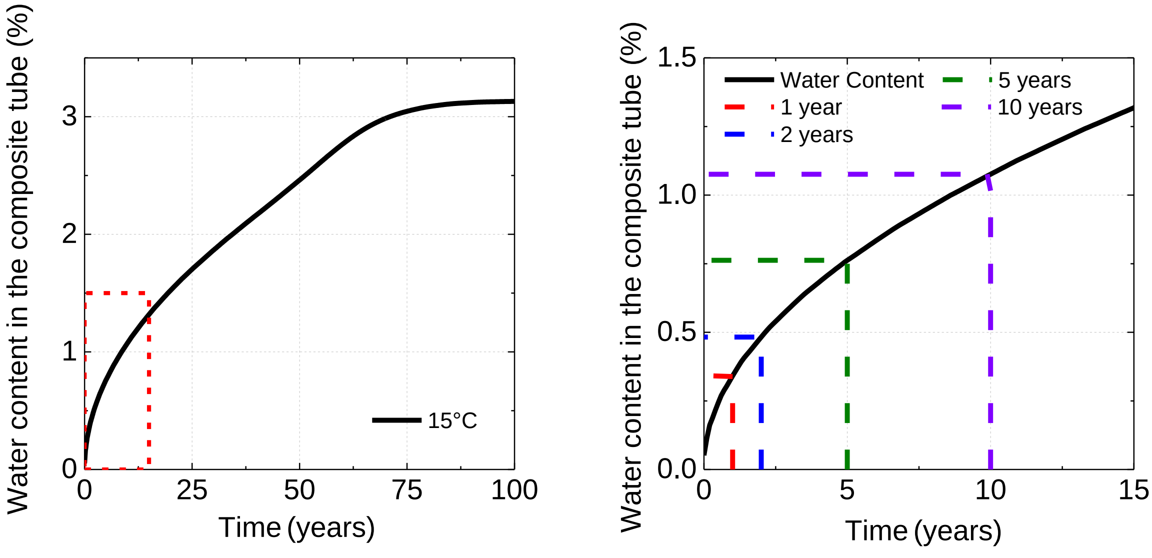

(a) (b)

Figure 55 : (a) Sorption curve modelled at 15°C until complete saturation (b) Water content in the cylinder for the first 15 years

Figure 55.a shows the content in the cylinder as a function of immersion time. It can be seen that the cylinder is completely saturated after 100 years of immersion under these conditions. In Figure 55.b, the water contents in the cylinder at several immersion times are presented (1, 2, 5 and 10 years). The oceanographic profilers are designed to have a lifetime of 2 years. After 2 years of immersion, the water content inside the cylinder is approximately

0.5%, which would suggest that under these immersion conditions, water might not be an issue. However, even if the overall water content in the cylinder is 0.5% after two years, the water distributions inside the cylinder at several times are of particular interest. Results are presented in Figure 56.

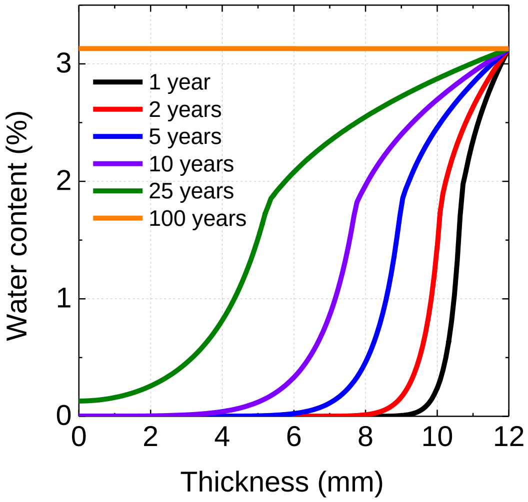

Figure 56 : Water distributions through the thickness of the thick cylinder (12mm) at different immersion times and immersed in sea water at 15°C

This figure shows the water profiles through the thickness of the cylinder for different immersion times (1, 2, 5, 10, 25 and 100 years). After two years, we can see that only 3mm of the total thickness of the cylinder is affected by water, which confirms that any effect of water will be limited. In addition, when the profiler is immersed at deep depth (< 2000 meters), the temperature of the ocean is close to 4°C, which suggests the water diffusion will be even slower in these conditions. It may be noted that water diffusion studies at 4°C were not performed because the DVS machine is not capable of maintaining a given humidity level at this low temperature. In addition, this modelling represents the worst case scenario for the cylinder as an external coating will generally be applied to protect the cylinder.

However, several researchers have shown that high hydrostatic pressures can greatly affect the water diffusion process. Humeau et al. [141] recently showed that the water diffusion was slower for a glass-epoxy laminate immersed in water at 500 bar. Therefore, since the cylinder will be immersed at deep depths and under high hydrostatic pressures, it is important to take into account this parameter. To do so, C/PA6 specimens were immersed at 40°C at 500 bar and at 1 bar to compare the two water diffusion processes. Results are presented in Figure 57.

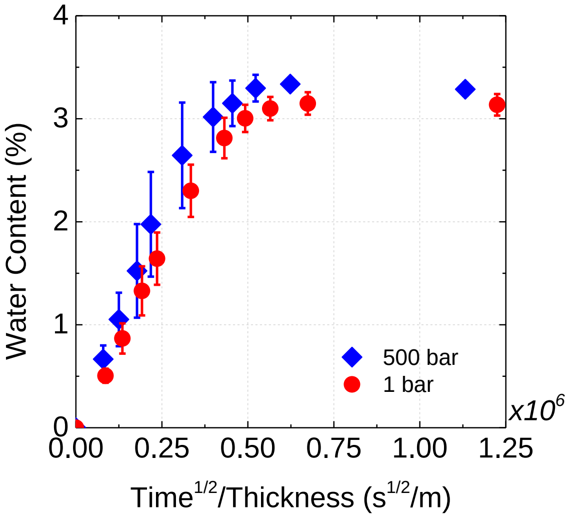

Figure 57 : Effect of hydrostatic pressure on the water diffusion

These first results show that pressure does not have a large effect, as both sorption curves are within one standard deviation. However, the standard deviation observed on the specimens exposed to 500 bar is much higher than for those exposed at 1 bar, which might suggest that some other phenomenon is occurring. Therefore, a more detailed study needs to be performed to clarify this effect, using samples immersed at different humidity conditions and pressures.

To conclude, it has been shown that the water diffusion process in thick C/PA6 cylinders immersed in sea water for two years is slow enough to avoid high amounts of water within the cylinder. However, in order to quantify the effect of this water on the overall response of the cylinder, a study is now required in order to quantify the effect of water on the mechanical properties.

4. Conclusion

Water absorption in polyamide 6 has been considered in this chapter. The aim was to be able to model the water diffusion in a thick composite cylinder immersed in sea water at 15°C. Because of the particular water diffusion process that occurs in PA6 immersed in water, it was chosen to work first on the neat PA6. It has been shown that the water uptake cannot be modelled using Fick's equations. This is explained by an increase in the diffusivity with the water content when the matrix is in the rubbery state. Two cases were identified; one below T_g where the diffusivity can be accurately described using an Arrhenius equation and one above T_g when the diffusivity can be described using the free volume theory. These two cases were then implemented in a model in order to predict the water diffusion at different temperatures. Results show a very good agreement with the experimental data and the predictions are significantly better than those based on Fickian behaviour.

Then this model developed on the neat matrix was adapted to account for the water diffusion in a composite material. Using homogenisation relations, it has been shown that considering a longitudinal diffusion coefficient equal to that of the neat resin and a transverse diffusion coefficient equal to 0.3 times that of the resin, it was possible to describe the water absorption in thick composite materials at several temperatures. Again, the predictions showed much better results than the Fickian model.

Finally, this new model adapted for the composite has been used to predict the water diffusion in more realistic immersion conditions for an oceanographic profiler, i.e., immersion at temperatures equal or below 15°C for several years with a thick cylinder (12mm). Results showed that after two years of immersion, the overall water content throughout the thickness of the cylinder is equal to 0.5% by weight and that only 3mm of the total thickness are affected by water. This result suggests that water ingress may not be the main issue under these conditions. However, to understand the real effect of water aging on the lifetime of a cylinder immersed in such conditions, it is essential to evaluate the change in mechanical properties as a function of the water content, which will be the aim of the next chapter.

Chapter 4

Effect of water on the mechanical behaviour of Carbon/PA6 composites

---

The aim of the following chapter is to be able to quantify the effect of water diffusion on the implosion pressure of a thick cylinder immersed in sea water for several years at low temperatures (from 4 to 15°C).

First, the mechanical properties in tension and compression were determined as a function of water content until complete saturation was reached. As water enters the composite, a significant reduction in the laminate properties is observed. An empirical relationship that links matrix-dominated properties to water content is presented and can be used for modelling. Second, the behaviour of cylinders made of C/PA6 subjected to hydrostatic pressures was investigated, first in the un-aged state then taking account of aging, simple buckling and strength criteria.

1. Effect of water and humidity aging on the tensile and compressive properties

1.1. Introduction

Since the overall aim of the current work is to model water diffusion (see Chapter 3) and its effect on the mechanical properties of thick C/PA6 composite cylinders immersed in sea water for deep sea applications (high hydrostatic pressures and low temperatures ranging from 4 to 15°C), it is essential to focus our work on the evolution of mechanical properties with water content. To provide the data for such a model, several properties are needed. Unidirectional composite materials are usually considered to be transversely isotropic. For such materials, five elastic constants are used to describe the behaviour of composite materials: the longitudinal modulus E_1, the transverse modulus E_2, the Poisson's ratio ν_{12}, the in-plane shear modulus G_{12} and the transverse shear modulus G_{23} (or the Poisson's ratio ν_{23}) [142]. Except for the latter (G_{23}), all these properties have been investigated using tensile tests, as a function of homogeneous amounts of water within the laminate. Delamination properties have also been examined. Moreover, because of the targeted application, tests have also been conducted in compression (hydrostatic pressure). An overview of compression test methods was given in Chapter 1, section 5.1. This chapter will present the tests and discuss the different results.

1.2. Results and discussion

First the water diffusion results are presented, followed by the effect of water diffusion on the glass transition temperature and the mechanical properties (in tension, in plane-shear and compression). It should be noted that such results are rare in the literature, especially over such a wide range of wet conditions. Some studies have used continuous C/PA6 laminates and performed mechanical tests for design purposes [143] but without any aging results. Other studies investigated the effect of aging on the mechanical properties of C/PA6 but without using tests which enable design data to be determined (ILSS, three point bending, etc.) [144], [145]. Also, in the latter, aging was conducted at high temperatures (60 and 80°C) for long exposure times, which is known to cause hydrolysis for polyamides [120], and this not the purpose of the current work. Therefore, the data that are presented here correspond to aging at a lower temperature and provide essential results for the design of composite cylinders immersed in deep waters.

This study only considers the effect of homogeneous amounts of water within the laminate saturated under different wet conditions, in order to directly link the mechanical properties to a given water content.

1.2.1. Saturation of specimens at different water contents

Water conditioning has been performed under different conditions as described in Chapter 2 section 3.3, in order to obtain samples containing different amounts of water. Given the low void contents in these materials, the water ingress is assumed to concern only the matrix. In Figure 58.a and Figure 58.b, the water uptake curves for C/PA6 and C/PEEK samples are plotted as a function of the square root of conditioning time divided by the sample thickness. Times to fully saturate the samples ranged from 1 to 5 months.

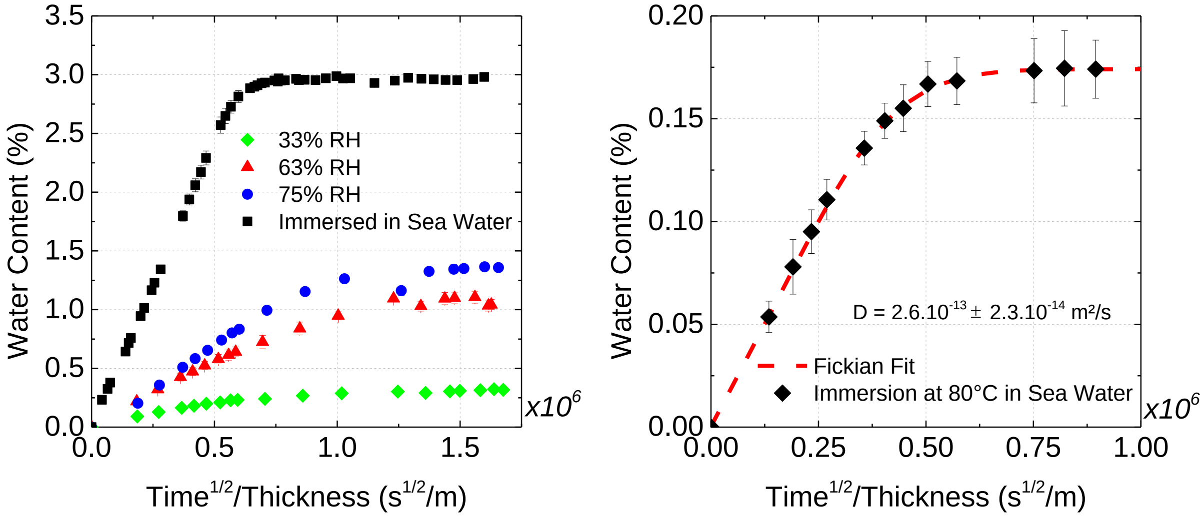

(a) (b)

Figure 58 : Water uptake curves for (a) Carbon/Polyamide 6 specimens conditioned at 33, 63 and 75% RH and immersed in sea water, all at 40°C. And (b) Carbon/PEEK specimens immersed in sea water at 80°C

It was shown in Chapter 3 that the water diffusion process in C/PA6 laminate cannot be described using Fick's equation. However, it is possible to describe the water diffusion using Fick's equation for the C/PEEK laminates, as shown in Figure 58.b. Then, the mass at saturation obtained for each exposure condition is presented in Table 7.

Table 7 : Mass at saturation

Material	**Conditioning**	**M_∞ (%)**	**Temperature (°C)**
Carbon-Polyamide 6	33% Humidity	0.31 ± 0.01	40
	63% Humidity	1.11 ± 0.04	
	75% Humidity	1.36 ± 0.02	
	Sea Water	3.01 ± 0.01	
Carbon-PEEK	Sea Water	0.17 ± 0.01	80

Results from water absorption show that the C/PA6 specimens absorb a much higher amount of water than the C/PEEK. The C/PA6 specimens immersed in sea water absorb 3 % of water by weight during aging compared to 0.17 % for the C/PEEK. Also, the saturation weights increase for the C/PA6 specimens conditioned at increasing humidity levels.

1.2.2. Effect of water on the glass transition temperature

Results from dynamic mechanical analyses (DMA) conducted on the composite specimens with homogeneous water distributions following saturation under different humidity conditions were presented in the previous Chapter and are shown again in Figure 59. The DMA plot in the dry state for C/PA6 is also presented in Figure 59.b.

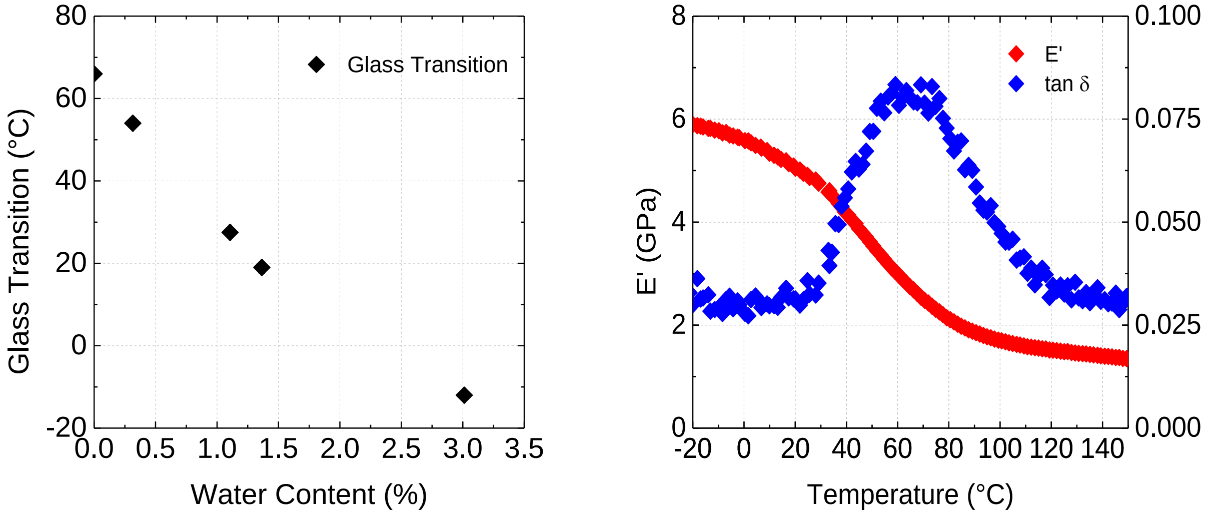

(a) (b)

Figure 59 : Decrease in glass transition temperature for C/PA6 specimens saturated under different humidity conditions (b) DMA plot in the dry state for C/PA6, transverse tension

From this result, it is clear that there is a very significant decrease in T_g from 66 ± 1 °C in the dry state to -12 ± 1 °C when the specimen is fully saturated with water, and we could expect a strong effect on the mechanical properties, especially when the glass transition becomes lower than the test temperature (21°C). This decrease in T_g results in a significant loss in stiffness and an increase in the strain failure for neat PA6 [146]. The question that is now of interest is whether the same trend is observed for composite materials tested in different directions.

It should be noted that the same analyses were performed on the PEEK specimens before and after sea water aging. No significant differences in T_g were observed (177 ± 2°C before aging and 174 ± 3°C when saturated).

1.2.3. Tensile properties

This section will present results from tensile tests performed on specimens with no water profiles (homogeneous amounts of water) after saturation in different environments. These results are essential for design purposes and will be used as a baseline. The strain gauges needed for each test were bonded one by one immediately before testing. The test was then conducted within 30 minutes to minimise evaporation of water.

1.2.3.1. Effect of water on the tensile properties

First, tests were conducted with tensile loading along the fibre direction in order to obtain the longitudinal modulus E_1 and Poisson's ratio ν_{12}. Examples of stress-strain results are presented in Figure 60.a and the evolution of the Poisson's ratio with water aging is shown in Figure 60.b.

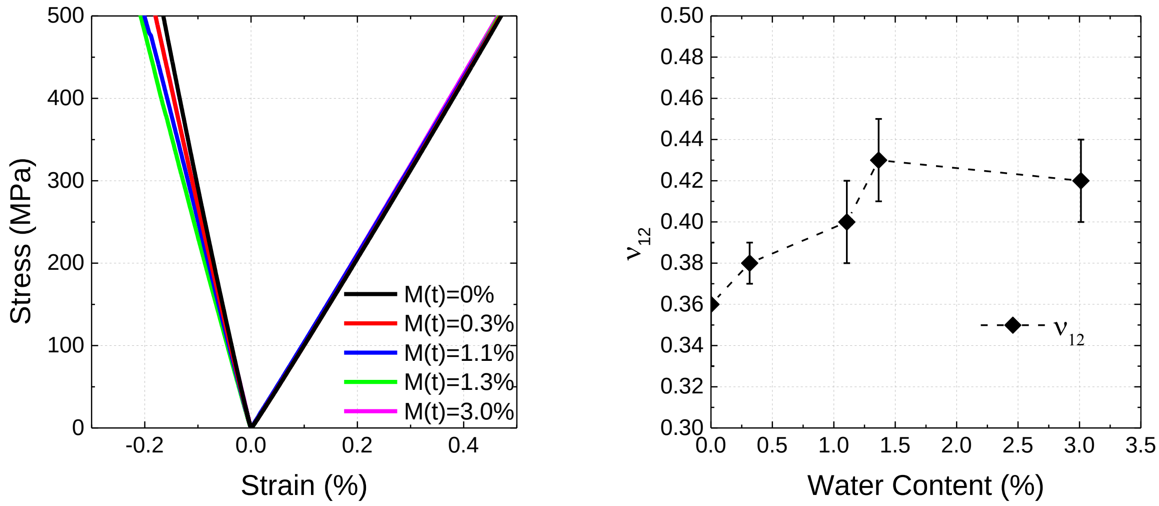

(a) (b)

Figure 60 : Effect of water on (a) the longitudinal and transverse strains under tensile loading (b) Poisson's ratio ν_{12} for C/PA6 specimens

No differences concerning the longitudinal modulus are observed, the modulus shows a mean value of 106 GPa. This result is not very surprising as the behaviour of unidirectional composite materials tested along the fibre direction is highly fibre dominated. It should be noted that no longitudinal tensile stresses at failure are presented in this work. The stress at failure in the dry state was found to be 1808 ± 132 MPa with a typical fibre pullout failure mode. However, the failure modes observed for the specimens saturated in wet conditions were not valid because of an end tab debonding problem. When the tabbed specimens were aged inside the desiccators and water tanks, the quality of the bond between the end tabs and the composite decreased and invalid (premature) failure modes were observed. It can be noted that despite this problem, all stresses at the end of tests of wet samples were found to be higher than 1000 MPa.

The results concerning the changes in the Poisson's ratio as a function of water content are quite different to those for the longitudinal modulus. The Poisson's ratio increases from 0.36 to values higher than 0.4 for water contents higher than 1% and then seems to stabilize,

Figure 60.b. The opposite trend is observed for the shear properties obtained on ± 45° laminates, Figure 61.

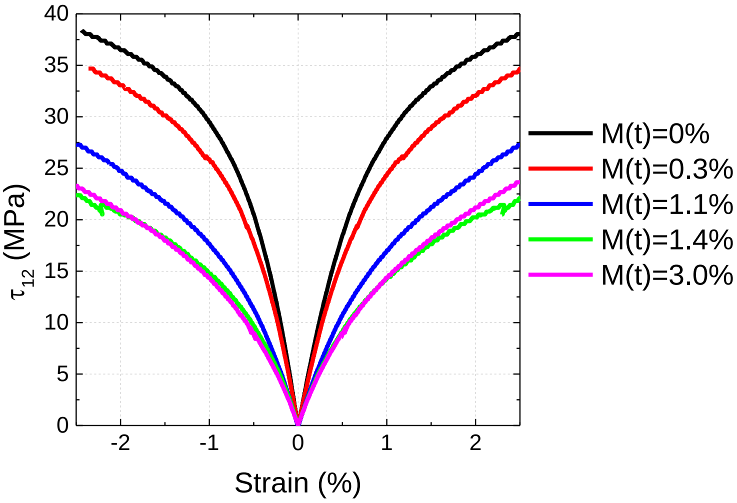

Figure 61 : Influence of water uptake on shear stress versus ±45° strain plots

First, the shear modulus decreases from 2.4 GPa to 1.3 GPa and appears to reach a plateau for water contents above 1%. Second, the same trend is observed for the shear strength with a τ_{12} decreasing from 37 MPa to 22 MPa from 0 to 1% in water content and then stabilising beyond 1%. In a similar way to the results for Poisson's ratio, it seems that a change in the behaviour is observed for water contents higher than 1%. As highlighted in Chapter 2, the shear strength τ_{12} is taken as the stress at 2% strain since no failure occurred during the test, even in the dry state. After a certain strain and because of the high ductility of the nylon matrix, the fibres tend to realign themselves during the test, which means that the test is not suitable for measuring the shear strength.

The third type of test is transverse tensile on unidirectional laminates as a function of water content. Examples of stress-strain plots are presented in Figure 62.

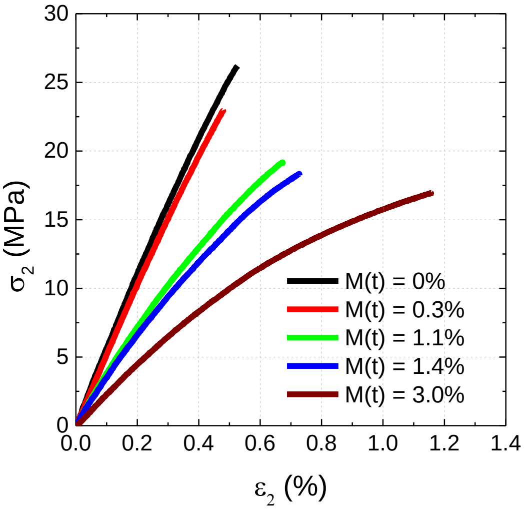

Figure 62 : Transverse tensile (90° to fibres) test curves for C/PA6 specimens saturated under different humidity conditions

These curves clearly indicate that there is a decrease in both stiffness and strength as a function of water content, and an increase in the strain at failure. This result is very similar to what is usually observed on neat PA6 [146] as transverse tensile tests are matrix dominated. Tensile strengths for unreinforced PA6 depend on grades and manufacturing conditions but values cited are around 80 MPa in the dry state [147].

It may be noted that the transverse tensile strength at failure is very low (even in the dry state) compared to the C/PEEK counterpart that is used as a reference (25 ± 2 MPa for C/PA6 and 83 ± 8 MPa for C/PEEK). The failure modes observed on these two materials are presented in Figure 63.

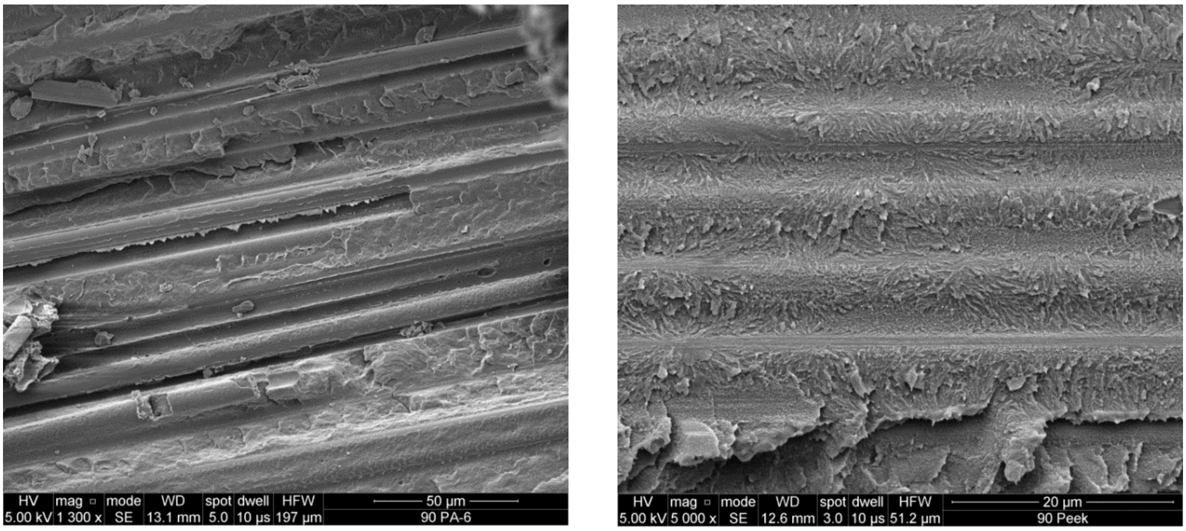

(a) **(b)**

Figure 63 : SEM pictures for transverse tensile test fracture surfaces (a) C-PA6, adhesive failure and (b) C-PEEK cohesive failure

It is clear that these two failure modes are very different from one another. In the case of C-PA6 on Figure 63.a, the failure occurs close to the interface, indicating that the failure is adhesive and responsible for the low strength obtained compared to neat PA6. This also indicates that the sizing that is used is not adapted for this material. However, a strong interface is observed on Figure 63.b where the failure occurs within the matrix of the C-PEEK laminate. Therefore, the failure is cohesive and is responsible for the high strength at failure for the C-PEEK laminate compared to C/PA6.

Finally, concerning the aging behaviour of C/PEEK laminates subjected to tensile tests, several authors showed that the mechanical properties are not affected by sea water when the specimens are fully saturated [148], unlike for C/PA6 as observed above.

1.2.4. Compressive properties

For the underwater applications of interest here it is the compression behaviour which is of particular interest.

1.2.4.1. Un-aged compressive properties

First, the pin-ended bucking test results are compared to those from a standard compression test (ISO 14126, Method 2) on specimens taken from the same C/PA6 panel The results obtained are shown in Table 8.

Table 8 : Results from compression tests, C/PA6

Test Method	σ_{1comp} (MPa)	ε_{1comp} (%)	E_{1comp} (GPa)
Pin-ended Buckling	1385 ± 101	1.53 ± 0.10	89.7 ± 1.9
Uniaxial compression	513 ± 67	0.57 ± 0.17	91.2 ± 1.1

While stiffness values are very similar, within experimental scatter, it is clear that the strengths obtained from these tests are highly dependent on the test fixture. There is a ratio of around 3 between the compressive strength values for these two tests. It can also be noted that the compressive modulus is lower than the tensile modulus, approximately 80% of the latter.

However, despite these differences in strengths, the failure modes remained the same. Compression failures modes are mostly characterised by kink banding failures [97], which were observed for the two different tests performed here, as presented in Figure 64.

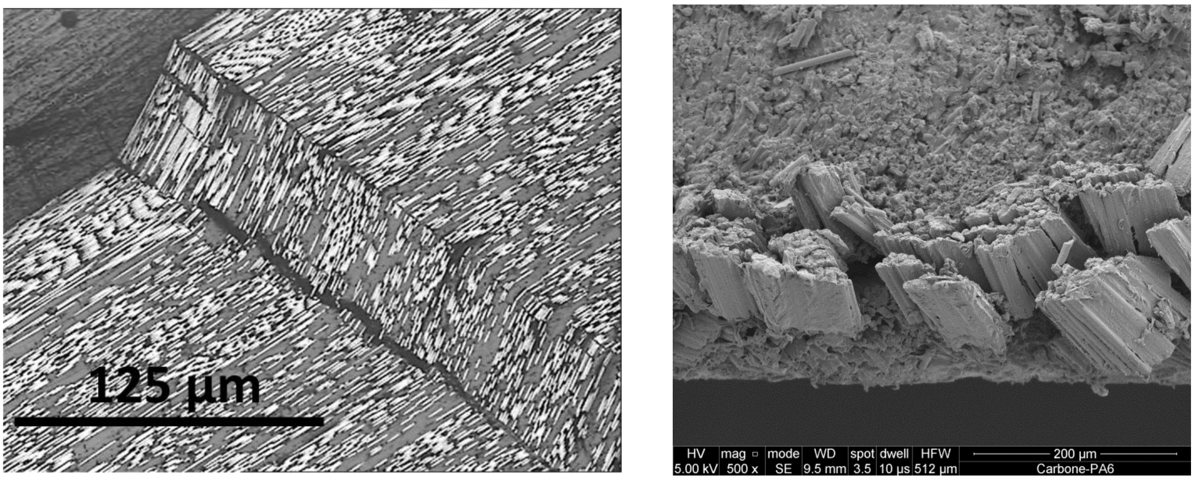

(a)

(b)

Figure 64 : Failure modes observed for the two compression tests (a) Optical microscopy for the standard test (b) SEM for the Pin-ended buckling test

There has been some discussion of the analysis of the pin-ended buckling test in published papers. While compressive strain to failure is measured directly, stresses are usually determined using Eq. 12. An example of the results from strain gauges bonded on each side of a C/PA6 specimen is shown below as a plot of the applied bending moment, Figure 65, versus strain measured both on the tension and compression sides.

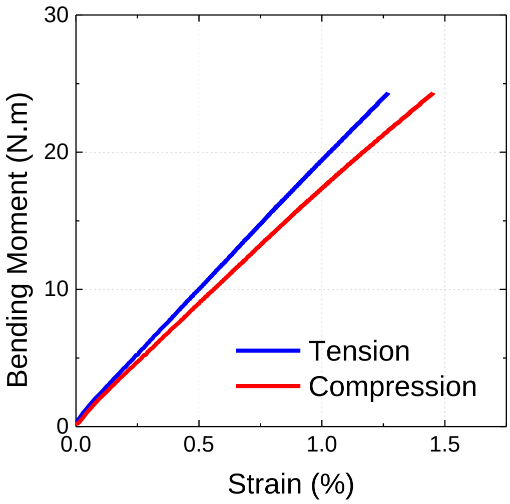

Figure 65 : Pin-ended buckling test performed on C/PA6 specimen, bending moment versus strains on both specimen faces

The results show the presence of a strain gradient through the specimen thickness and the more non-linear response in compression at high strain. The tensile and compressive strains at failure are 1.27 and -1.45% respectively here, leading to a strain gradient of 1.36%/mm. The compressive strain at failure for C/PA6 is slightly lower than values given by Wisnom and Atkinson for carbon/epoxy at a similar strain gradient in [110]. From these results, we can see that there is a 14% difference between the absolute tensile and compressive strains at failure. Eq. 12 can be used to obtain a compressive stress at failure but it is based on analysis of a beam with identical tension and compression behaviour. The increasing difference in modulus values will affect the position of the neutral axis and hence the calculation of the stresses. An estimation of the effect of the non-linear compressive behaviour can be made using the method proposed by Montagnier and Hochard. [83] and Wisnom et al. [89] based on fitting the stress versus strain plots in pure tension (Eq. 30) and compression tests (Eq. 31):

$$\sigma_{tension} = E_{tension}\,(1+\alpha\varepsilon)\varepsilon \qquad \text{Eq. 30}$$

$$\sigma_{compression} = E_{compression}\,(1+\beta\varepsilon)\varepsilon \qquad \text{Eq. 31}$$

Where α and β are respectively the non linear parameters in tension and compression. The values of α and β were identified on the experimental data and are respectively equal to 4.8 and 18. It is worth noting that Eq. 31 is based on an identification of compressive tests at low strains (0.5% compared to 1.5% in pin-ended buckling tests). As stated by Wisnom [90] on C/epoxy specimens, it is thought that Eq. 31 can be used at higher strains. The modulus values were taken as the mean modulus value for pure tension and compression tests in the dry state and are respectively equal to 105 GPa and 91.2 GPa. Results from identification are shown in Figure 66.

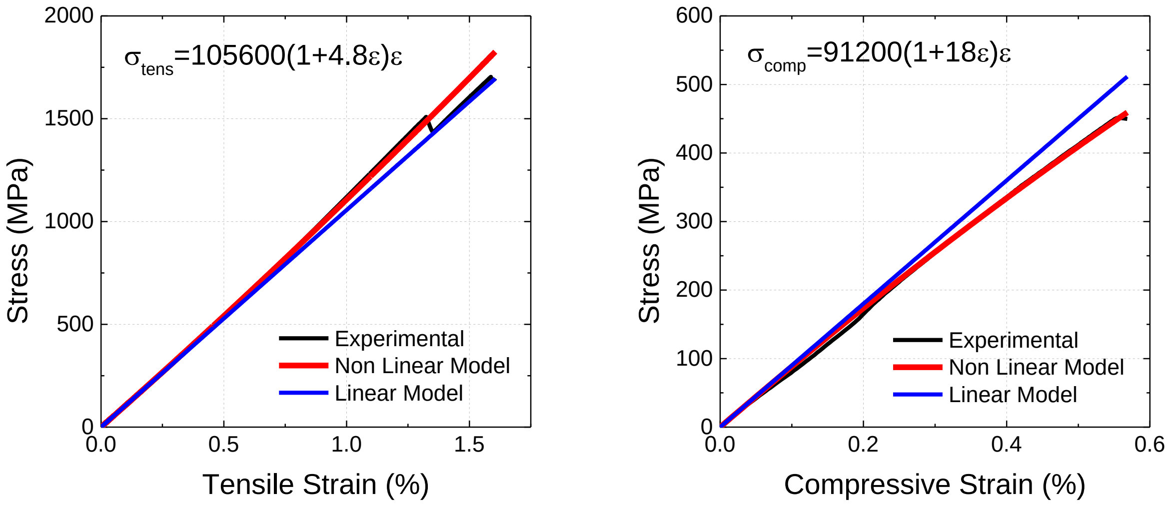

(a) (b)

Figure 66 : Identification of (a) α parameter on tensile tests and (b) β parameter in uniaxial compression tests

For the pin-ended buckling test, Eq. 31 is coupled with the experimental compressive strain measurements to calculate the compressive stress. This leads to a compressive stress of around 70% of the value calculated using Eq. 12, as shown in Figure 67.

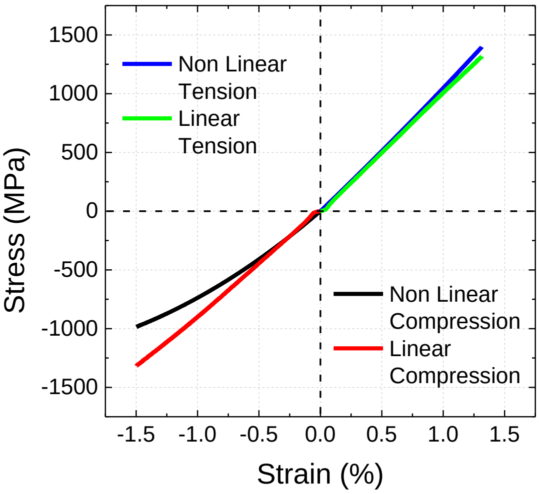

Figure 67 : Differences between linear and non linear behavior in both tension and compression

A more detailed stress analysis could be performed numerically, but here the test is simply used to evaluate how moisture affects compressive strains and estimated stresses at failure, so the latter will be referred to as “apparent compressive strength”.

The high compression stresses at failure (higher than 1000 MPa) for the C/PA6 confirm that the latter is a suitable candidate for underwater applications. Similar tests (pin-ended buckling) were carried out on unidirectional C/PEEK laminates, and yielded apparent compression strength of 1645 ± 29 MPa. Even though the results are a little higher for the C/PEEK counterpart, the fibre volume fraction is also higher by 12%.

These two compression tests are clearly different, the stress states across the specimen sections are not the same and the debate on which test is most appropriate remains open. Wisnom has suggested that the non linear behaviour of unidirectional composites and shear stresses contribute to lower strengths in a pin ended buckling test [89]. However, the non-linear behaviour of carbon fibres is observed in both tension and compression and not always taken into account in modelling. In the remainder of the work presented here the pin-ended buckling test was retained for practical reasons: first, it allowed exactly the same specimen geometry to be used for the tension and compression tests. (The standard compression test dimensions are smaller, so aging times would need to be adjusted to reach the same saturation level). Second, the test specimen is simpler to prepare, as only one strain gauge is needed on the compression side (two are required for the standard test).

1.2.4.2. Effect of water on the compressive properties

The pin-ended buckling test was used to investigate the effect of water aging on the compressive properties. First, pin-ended buckling tests were performed on C/PEEK specimens before and after saturation in sea water at 80°C (approximately 2 months' aging), in order to provide a reference value. The results are presented in Table 9.

Table 9 : C/PEEK before and after aging

Material	σ_{1f} [MPa]	ε_{1f} [%]	E_1 [GPa]
C/PEEK	1645 ± 29	1.37 ± 0.03	117.5 ± 4.5
Aged at 80°C in sea water	1783 ± 245	1.41 ± 0.20	121.4 ± 3.2

It is clear that for the C/PEEK composite the apparent compressive strength at failure and the modulus are not sensitive to aging. However, the results are quite different for C/PA6. The aging conditions are exactly the same as for the tensile tests. Examples of apparent stress-strain plots are presented in Figure 68.

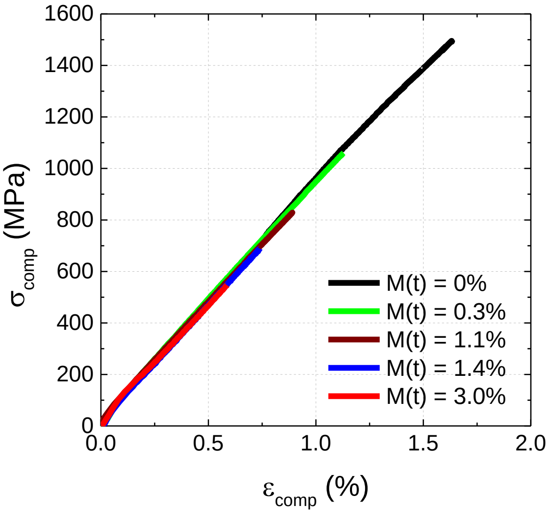

Figure 68 : Apparent compression stress-strain plots for C/PA6 specimens tested with the pin-ended buckling test fixture under several saturated aging conditions

These plots show that there is a large decrease in the failure strain when the specimen is tested with higher uniform water contents. The apparent stress at failure and the value corrected for non-linearity are respectively divided by 3 and 2 between the dry and the sea water saturated specimens. However, the effect on the modulus is very limited. Figure 69 presents the apparent and corrected compression strengths obtained as a function of water content.

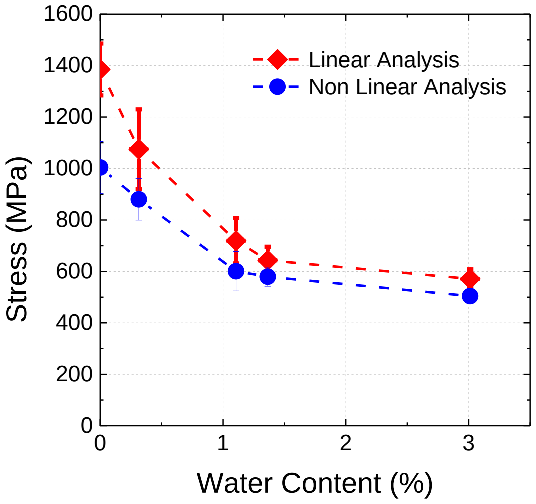

Figure 69: Apparent and corrected compressive strength as a function of water content, using Eq. 12 and Eq. 31

This figure highlights the fact that the compressive strength decreases by approximately 50% when water content increases from 0 to 1%. Above this water level, the compressive strength only further decreases by 10% until saturation. It is interesting to note that the difference between the apparent and the corrected compressive strengths are lower at increasing water levels. In Figure 68, we have seen that the stiffness in the range from 0.1 to 0.3% of the C/PA6 did not evolve with aging. At increasing water levels, the strain at failure is lower. Therefore, since the non linearity depends on the strain level, its effect is much lower at lower strains.

The failure modes of the specimens subjected to different humidity conditions and tested in compression were very different. The dry specimens and those aged at 33% humidity broke in a very brittle manner (the specimen separated suddenly in two pieces) unlike those aged at 75% humidity and immersed in sea water, which failed in a very ductile manner with a wrinkle appearing. Concerning the specimens aged at 63% humidity, four out of five samples broke in a ductile manner and one in a brittle manner. It should be noted that Fukuda [88] associated this failure mode to compressive failures. The two different failure modes observed are shown in Figure 70.

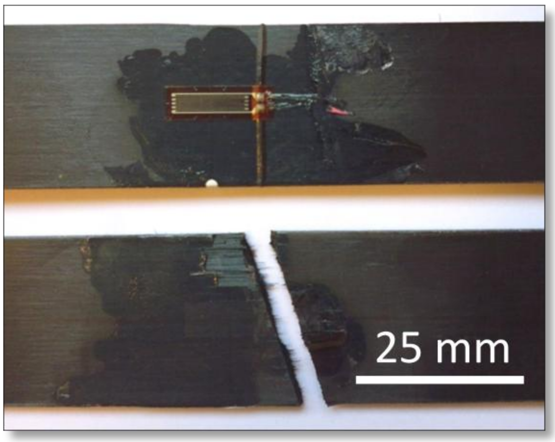

Figure 70 : Upper image: ductile failure mode of a specimen saturated in sea water. Lower image: brittle failure mode for a dry specimen

The desorption process was also investigated, to determine whether the properties were reversible. To do this, several samples were immersed until saturation and were then dried until they reached their initial dry mass. Afterwards, these same samples were tested in compression (pin ended buckling test). Results are shown in Table 10.

Table 10 : Effect of desorption on the compressive properties

	σ_{1f} (MPa)	ε_{1f} (%)	E_1 (GPa)
Dry	1385 ± 101	1.53 ± 0.10	89.7 ± 1.9
Saturated in sea water	571 ± 37	0.62 ± 0.03	82.1 ± 4.8
Saturated then dried	1190 ± 61	1.26 ± 0.03	90.3 ± 2.4

The apparent compressive strength properties are mostly recovered after the desorption process, suggesting that plasticisation is the main aging mechanism, even though they are not fully reversible. The mean strength loss is around 15% after aging and re-drying, but the modulus returns to its initial dry value. The differences found in compressive strength may be due to a permanent decrease in interface quality after aging, though experimental variation is also significant. Moreover, as stated earlier, the compressive strength is known to depend on the matrix shear modulus. Therefore, a lower compressive strength could also be caused by a lower shear modulus after aging. Unfortunately, such tests after aging have not been performed as the neat matrix polymer was not available.

Additionally, all the values for tension, compressive, shear properties and glass transition temperatures in the dry and water saturated states are grouped in Table 11.

Table 11 : Values of tension, compressive and shear properties and glass transition temperatures in the dry and water saturated states with associated coefficients of variation

*PC:Pure Compression **PeB : Pin-ended Buckling

M(t)		0	0.31 ± 3%	1.11 ± 4%	1.36 ± 2%	3.01 ± 1%
T_g (°C)		66 ±4%	54 ±7%	28 ±5%	19 ±3%	-12±3%
$E_{1tension}$ (GPa)		105 ±5%	106 ±3%	105 ±2%	106 ±2%	111 ±2%
$\sigma_{1tension}$ (MPa)		1808 ±7%	/	/	/	/
ν_{12}		0.36 ±8%	0.38 ±3%	0.40 ±5%	0.43 ±5%	0.42 ±5%
G_{12} (GPa)		2.4 ±4%	2.1 ±10%	1.3 ±8%	1.3 ±8%	1.2 ±8%
τ_{12} (MPa)		37 ±4%	33 ±2%	23 ±5%	21 ±3%	21 ±4%
E_2 (GPa)		5,8 ±9%	5,5 ±6%	4,0 ±6%	3,5 ±4%	2,3 ±4%
σ_2 (MPa)		25 ±8%	27 ±9%	21 ±5%	19 ±5%	17 ±3%
$E_{1\,comp}$ (GPa)	**PC***	91,2 ±1%	/	/	/	/
	PeB**	89,7 ±2%	89,9 ±6%	89,6 ±1%	83,9 ±8%	82,1 ±6%
$\varepsilon_{1\,comp}$ (%)	**PC***	0,57 ±30%	/	/	/	/
	PeB**	1,53 ±7%	1,24 ±14%	0,79 ±13%	0,73 ±7%	0,62 ±5%
σ_{1comp} (MPa)	**PC***	513 ±13%	/	/	/	/
	Apparent PeB**	1385 ±7%	1075 ±14%	719 ±12%	643 ±8%	571 ±6%
	Corrected PeB**	1004 ±10%	880 ±9%	601 ±13%	580 ±6%	504 ±4%

1.2.5. Out-of-plane properties

1.2.5.1. Interlaminar Shear Strength (ILSS)

Interlaminar shear strength tests were conducted following ASTM D2344 on dry unidirectional specimens but no valid delamination occurred during the test. Instead, crushing occurred below the loading points. Due to the ductile nature of the matrix, the specimen tends to plasticise instead of delaminating. Therefore, since the test was not valid for the dry specimens, no tests after aging were conducted. To conclude, this test is not suitable for this type of material as Botelho et al. concluded previously [149].

1.2.5.2. Double Cantilever Beam (DCB) – Mode I

One often-cited advantage of thermoplastic composites is their increased ductility that leads to higher toughness values [150]. Therefore, DCB tests were performed, as described in Chapter 2 section 6.1.2.4, first on dry unidirectional specimens and then on specimens saturated in sea water at 40°C. A typical R curve that is obtained from these tests is presented in Figure 71.

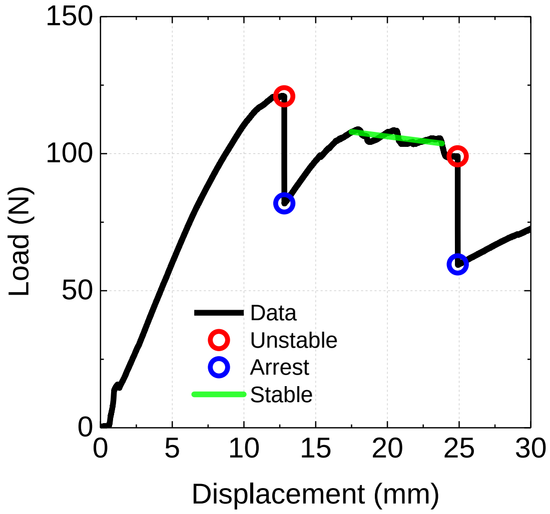

Figure 71 : Mode I load-displacement plot (R curve) obtained for a dry unidirectional specimen

First, it is clear that the R curve for this material is quite different to the ones usually observed in C/Epoxy laminates. The crack propagation is quite unstable here. Therefore, a careful data treatment procedure has to be followed. To do so, three different toughness values are suggested, as presented by Davies et al. for Glass/PA6,6 laminates in [151]:

- Unstable G_{IC} values corresponding to the onset of instability
- Arrest values corresponding to the crack length after an unstable jump, and
- Stable propagation values when some stable propagation is observed

The results obtained from these tests are presented in Figure 72 (MCC method) and the values for each calculation method are shown in Table 12.

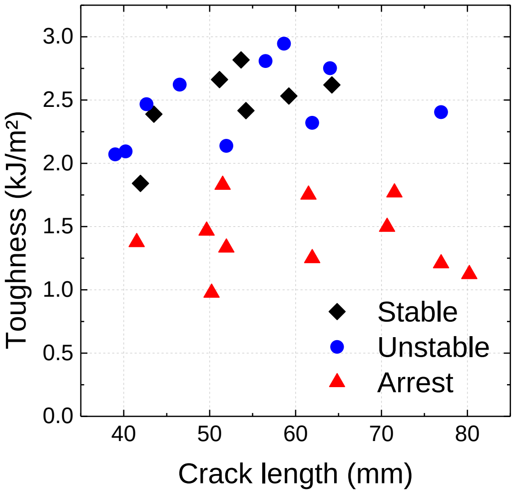

Figure 72 : Mode I toughness calculated using the Modified Compliance Calibration method

Table 12 : Toughness values obtained from DCB tests

Calculation Method	G_{IC} (kJ/m²)		
	MBT	CC	MCC
Stable	2.9 ± 0.2	2.5 ± 0.2	2.5 ± 0.3
Unstable	2.7 ± 0.3	2.4 ± 0.3	2.5 ± 0.3
Arrest	1.6 ± 0.3	1.4 ± 0.2	1.4 ± 0.3

These results show that the fracture toughness values that are obtained for Unstable and Stable conditions lie around 2.5kJ/m², which confirms that thermoplastic composites possess higher delamination resistance than their thermoset counterparts. Moreover, even the Arrest toughness values are found to be higher than 1kJ/m². These values are very similar to the values Davies et al. obtained on Glass/PA6.6 laminates with unstable and stable values around 2kJ/m² and arrest values around 1kJ/m² [151]. In comparison, for most C-Epoxy laminates, the fracture toughness lies between 0.3 and 0.6 kJ/m² [106], [150] and for C/PEEK around 2kJ/m² [40], [150]. It may also be noted that the amount of unstable crack propagation can be reduced by reducing the test speed as Davies et al. showed in [151].

Then, the specimens saturated in sea water at 40°C were tested. However, one major problem occurred during these tests, which is shown in Figure 73.

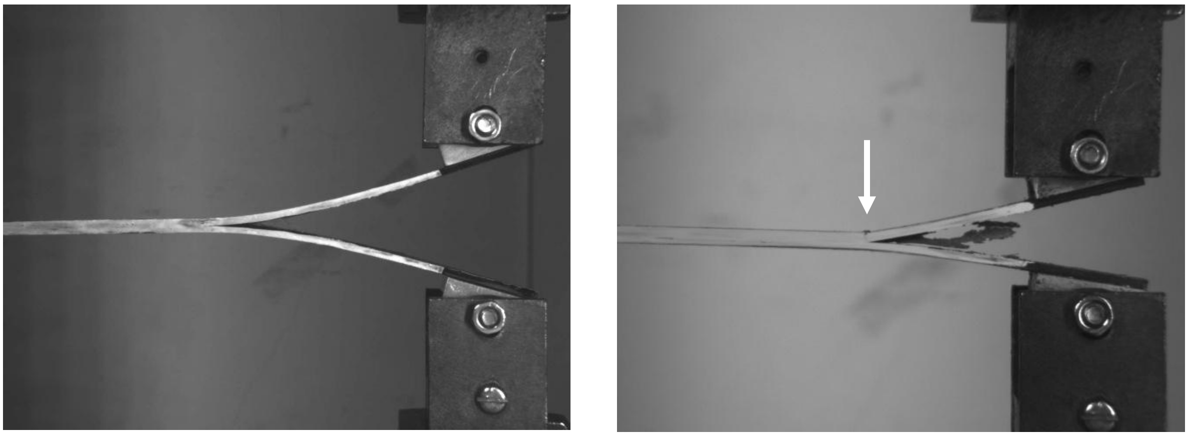

(a) (b)

Figure 73 : (a) DCB test performed on (a) a dry specimen (b) saturated specimen

Contrary to the tests conducted on the dry specimens, Figure 73.a, no propagation was observed for saturated specimens, Figure 73.b. As we observed earlier, the tensile and compressive properties decrease as water enters the composite. Here, a compressive failure occurs on the upper part of the DCB specimen due to the decrease in flexural properties. Therefore, no toughness values could be calculated for specimens fully saturated in sea water. In order to be able to measure this property, the dimensions of the specimens would need to be adjusted, for instance, increasing the thickness of the specimens. However, as the thickness increases, the aging time needs to be adjusted and results in much longer exposure times. Nevertheless, we would expect an increase in toughness as water enters the material as Davies et al. highlighted in [151].

1.2.6. T_g related behaviour

Most of the results presented earlier seem to follow a common trend, i.e. the property of interest changes quickly initially until the water content reaches 1%, then for water contents higher than 1%, the property of interest tends to stabilize. As indicated in Chapter 1, the compressive behaviour depends on the matrix response, so one might expect a similar change in all matrix-dependent properties as water enters the composite. In order to investigate this, the matrix dependent wet properties have been normalised (shear modulus, shear strength, transverse tensile strength, transverse tensile modulus and apparent compressive strength). These are all plotted as a function of the saturated water content, in Figure 74.

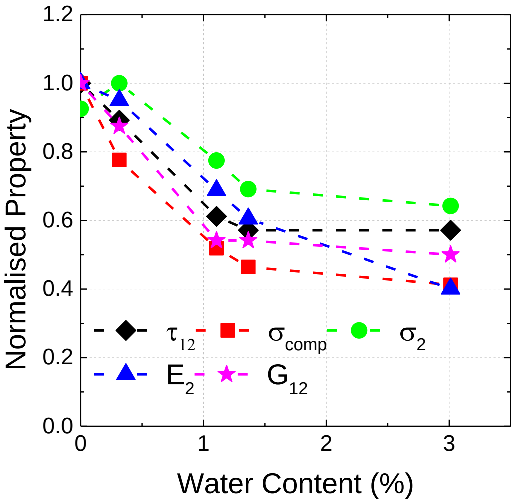

Figure 74 : Normalised properties as a function of the water content for C/PA6

This figure suggests that all the properties are governed by the same behaviour. Two trends are observed. First, the properties decrease by approximately 45% from 0 to 1% water content and then decrease by a further 10% until complete saturation. Two different slopes are identified. This is a very useful result, as it enables all matrix dominated composite properties to be expressed to a first approximation by two simple equations for each property of interest, Eq. 32 and Eq. 33. These can be expressed as follows:

$$\text{For } M(t) < 1\%, Normalised\,property = C_1 \times M(t) + 1 \qquad \text{Eq. 32}$$

$$\text{For } M(t) > 1\%, Normalised\,property = C_2 \qquad \text{Eq. 33}$$

For each property, those two constants are shown in Table 13.

Table 13 : Constants C_1 and C_2 for each property of interest

	C_1	C_2
τ_{12}	-0.3503	0.5849
σ_{comp}	-0.4554	0.4652
σ_2	-0.1884	0.7026
E_2	-0.2732	0.5644
G_{12}	-0.4131	0.5277

These can be used directly in the design process in combination with the diffusion equations to simply establish local properties as a function of local water content. Given the magnitude of the changes, for C/PA6 composites taking account of water ingress is essential (while for C/PEEK this effect may be neglected). It should be noted that the two equations that were just suggested are only valid for tests conducted at 21°C. For the application of interest, the temperature ranges from 4 to 15°C and this has to be taken into account.

It was also shown above that the compression failure modes changed during aging. Below 1% water content, the failures were brittle and after 1%, these were ductile. This indicates that there is a change in mechanism at approximately 1% water content. The glass transition temperatures were determined as a function of water content and were found to decrease from 66°C in the dry state to -12°C when the material was fully saturated in water. This is a well-known effect for PA6 but is an exceptionally large change in a fibre reinforced composite. When tests are performed at 21°C on a specimen fully saturated in water, the test is being conducted above the glass transition temperature of the matrix. Therefore, the matrix exhibits a rubbery, ductile behaviour. On the contrary, a test conducted at 21°C on a dry specimen is performed below the glass transition temperature of the polymer, in the glassy state, and the composite exhibits a brittle behaviour. An alternative representation of the normalized properties is as a function of (T-T_g) with T being the temperature at which the test was conducted, Figure 75. This parameter allows us to determine whether a test is being performed below or above the glass transition temperature of a specimen saturated in a certain environment.

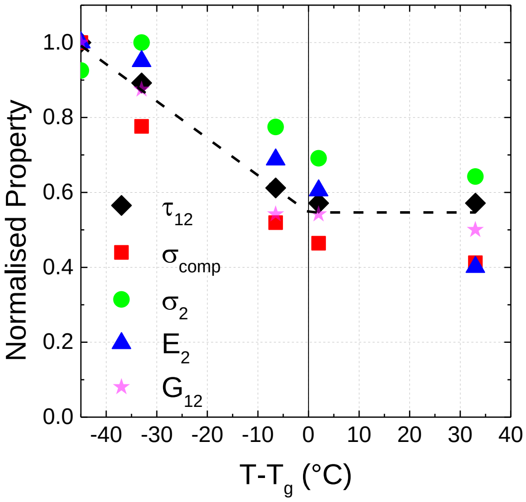

Figure 75 : Normalised property plotted as a function of a T_g-T

The last two figures reveal an equivalence between glass transition temperature and water content. Then, the transverse modulus has been determined here as a function of temperature by DMA. The latter was then plotted as a function of T-T_g in Figure 76, together with the transverse modulus measured on specimens saturated at different conditions.

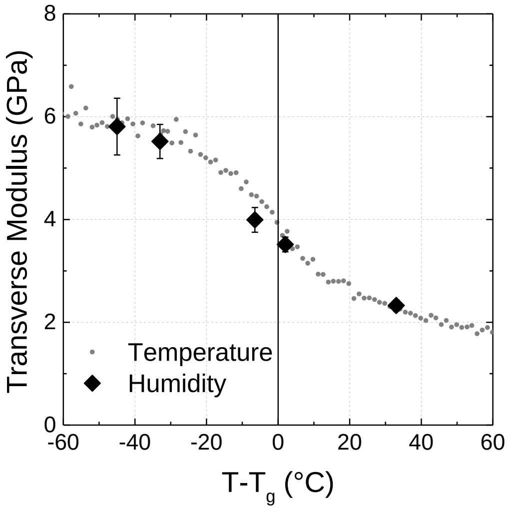

Figure 76 : Transverse modulus as a function of T_g-T for tests conducted in temperature (DMA) and in wet conditions

It is clear that a good agreement exists between these two results. Therefore, it seems that the matrix dominated properties of C/PA6 laminates are governed by the same parameter, which is the difference between the test temperature and the glass transition temperature. This provides a powerful tool to predict composite behaviour over a wide range of conditions. Finally, it was shown in Figure 60.b that the Poisson's ratio increased with water content and stabilized for water contents above 1%, i.e. when the T_g drops below the testing temperature. A similar trend was observed previously for tests at different temperatures [152], [153]. This increase in Poisson's ratio was associated with the transition to a more rubbery behaviour as water enters and T_g drops. Rubbers are usually considered to be materials which show no volume change during elastic deformation with a Poisson's ratio close to 0.5 [138]. A higher Poisson's ratio is therefore obtained when the glass transition is far lower than the test temperature.

1.3. Conclusion

This section presents a unique set of data relating the tensile and compressive properties of C/PA6 to water content. Water has a very negative effect on the matrix dominated mechanical properties of these composites, which are reduced by over 50%. This loss in properties has been linked to the large decrease in the glass transition temperature (from 66°C in the dry state to -12°C when fully saturated with sea water). An empirical relationship between the mechanical properties and the water content and the $T\text{-}T_g$ parameter has been proposed, which can be used to account for environmental changes in matrix-dominated properties. The results were compared to a C/PEEK reference material, for which water saturation had no effect on the mechanical properties.

This section has considered tests on specimens containing homogenous amounts of water. However, the overall aim of the project is to be able to model the water diffusion in thick C/PA6 cylinders and its effect on the mechanical properties (implosion pressure). This will be discussed in the next section of this chapter.

2. Effect of sea water aging on the implosion pressure of thick composite tubes subjected to hydrostatic pressures

2.1. Introduction

Now that we have developed a specific water diffusion model and coupled the effect of water content to several mechanical properties, it is possible to use these data to investigate the effect of water on the implosion pressure of a thick cylinder (12mm) immersed in sea water at 15°C. However, the ability to predict the implosion pressures of composite materials under such loadings (bi-axial compression) is not an easy task. There are two possible failure modes, buckling and material compression failure; the former is dominated by geometric imperfections while the latter is strongly dependent on defects such as misaligned fibres, porosities and other material imperfections. Indeed, the results of the World Wide Failure Exercise [154] showed that none of the commonly-used failure criteria was capable of predicting failure for this loading case. Therefore, the aim of the following section is to use simple tools to help us understand how water could limit the use of thick carbon/PA6 cylinders immersed in sea water using simple analytical formulae, rather than trying to propose new failure criteria.

First, the implosion pressures are studied in the un-aged state using simple buckling and strength predictions as a function of the thickness to diameter ratio. Then, the effect of water is considered using the properties presented in the previous section.

2.2.Results and discussion

2.2.1. Implosion pressure of thick cylinders in the un-aged state

To begin with, it should be noted that the predictions considered in this section only concern cylinders wound at ± 55° with dimensions similar to the existing carbon/epoxy profiler used at Ifremer, i.e. with a thickness of 12mm and an internal diameter of 120mm.

Then, since the properties that were determined in the previous section were only measured along the principal directions, it is of primary interest to be able to predict the properties as a function of a given laminate angle. To do so, several laminates were manufactured by press forming at different angles (±15°, ±35° and ±55°) and tested under tension loading. The results were then compared to the theoretical values determined with laminate theory using the properties obtained along the principal directions. Results are presented for C/PA6 in Figure 77.

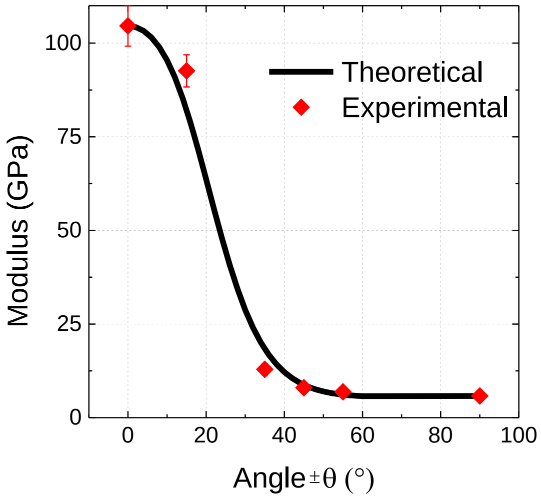

Figure 77 : Experimental and theoretical predictions of the modulus as a function of laminate angle

It can be observed from these results that the properties that were measured coincide reasonably well with the prediction, differences can be related to experimental variability. Therefore, in this case of press-formed composites, the stiffness properties can be predicted accurately when manufacturing carbon/polyamide 6 laminates. Now, these can be used to predict the implosion pressure of a thick cylinder.

Two different formulae are used to predict the implosion pressure P_c. The first one considers the buckling of an infinitely long cylinder in which the hoop modulus governs the buckling pressure, Eq. 34 [1].

$$P_c = (n^2 - 1)\left(\frac{D_y}{r_0 r_m^2}\right) \qquad \text{Eq. 34}$$

With D_y the hoop flexural rigidity presented in Eq. 35, n the buckling mode equal to 2 in most cases, r_0 the outer radius and r_m the mean radius of the cylinder.

$$D_y = \frac{t^3}{12} . \frac{E_\theta}{1 - (\nu_{z\theta} . \nu_{\theta z})} \qquad \text{Eq. 35}$$

The second formula that is used considers a simple maximum hoop stress criterion (material failure) and is presented in Eq. 36.

$$P_c = \sigma_{\theta\theta} \cdot \frac{t}{r} \qquad \text{Eq. 36}$$

Where $\sigma_{\theta\theta}$ is the hoop stress. The hoop stress criterion that was chosen was taken as the stress at failure of ± 35° laminates tested in tension and was measured to be equal to 288 ± 36 MPa. Indeed, a cylinder wound at ± 55° in the longitudinal direction has a hoop angle of ± 35°.

These two equations Eq. 34 and Eq. 36 were then used to calculate the implosion pressure of a given cylinder wound at ± 55° as a function of the thickness to diameter ratio. Results are presented in Figure 78. The longitudinal and hoop modulus as well as the Poisson's coefficient values needed in Eq. 35 were calculated using *MicMac* software using the un-aged tension properties.

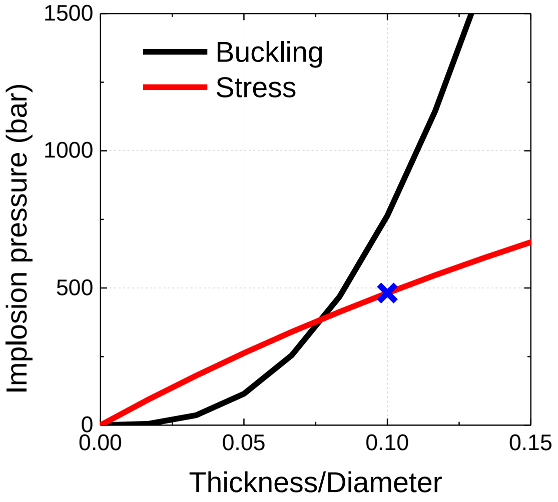

Figure 78 : Implosion pressure versus the thickness/diameter ratio – Simple buckling and strength predictions

This result suggests that for cylinders wound at ± 55°, when the thickness to diameter ratio becomes higher than 0.075, the n=2 buckling mode is suppressed and that material failure dominates afterwards. For cylinders such as the profilers used at Ifremer with a thickness of 12 mm and a diameter of 120 mm, represented as the blue cross on Figure 78, the failure would occur at an implosion pressure close to 500 bar and material failure would be the predominant failure mode.

2.2.2. Effect of water on the implosion pressure of thick cylinders

Now that the implosion pressure in the un-aged state has been investigated, let us focus on the effect of water on the latter. To do so, the wet properties measured in the first section of this chapter are used to determine the moduli and Poisson's coefficients along the ± 35° and ± 55° directions using *MicMac* software again. The different values are summarised in Table 14.

Table 14 : Modulus and Poisson's coefficients calculated for the ± 55 and ± 35° at several water contents

Water content (%)	± 55°		± 35°	
	E_z (GPa)	$\nu_{z\theta}$	E_θ (GPa)	$\nu_{\theta z}$
0	6.1	0.46	18.4	1.39
0.31 (0.01)	5.5	0.47	16.9	1.43
1.11 (0.04)	3.6	0.48	11.9	1.59
1.36 (0.02)	3.5	0.48	11.6	1.61
3.01 (0.01)	2.9	0.47	10.5	1.68

First, we can see that as the water content increases, the modulus decreases, as was observed for all matrix dominated properties in the first section of this chapter. Second, the Poisson's coefficient increases in a very similar manner to the previous section. Then, these data are used to predict the implosion pressure using the simple buckling criterion, Figure 79. The calculation was made using a thickness of 12 mm and an inner diameter of 120 mm.

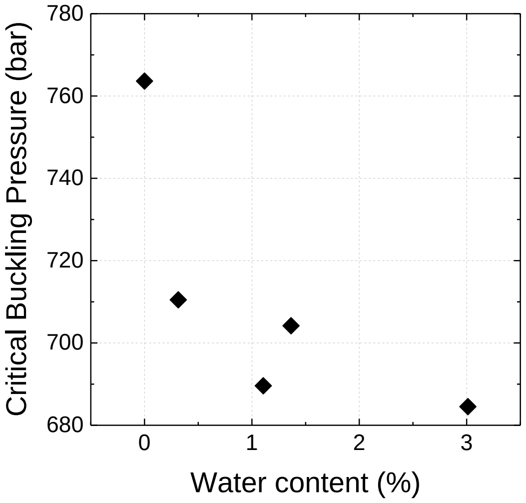

Figure 79 : Effect of water content on the Implosion pressure using the buckling criterion

From this figure, we can see that there is a small decrease in the implosion pressure of approximately 100 bar (10 %) between the un-aged and the fully saturated state. It can be noted that if we do not take into account the change in Poisson's coefficients with water aging, the implosion pressure drops down to 401 bar, i.e. almost half of the initial implosion pressure in the un-aged state. Therefore, the in-plane properties are essential when working with this type of materials.

However, it was shown in Figure 78 that for such dimensions (t=12mm and D=120mm), the predominant failure mode in the unaged state would be material failure and not buckling. Therefore, similar calculations were conducted based on Eq. 36 and taking into account the effect of water. To investigate the latter, the evolution in properties shown in Table 13 was coupled with the dry tensile strength at failure of ± 35° laminates (288 ± 36 MPa). Since the behaviour of ± 35° laminates is mostly governed by shear (close to ± 45°), the constants C_1 and C_2 were taken as those corresponding to τ_{12}. To a first approximation, this assumption appears reasonable. Results from these calculations are presented in Figure 80.

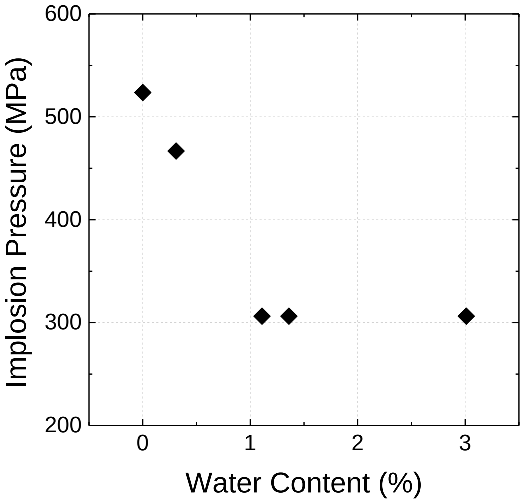

Figure 80 : Effect of water on Implosion pressure using the maximum hoop strength criterion

We can see that as the water content increases, the implosion pressure drops down from 523 bar to values close to 300 bar. Contrary to the results found using the buckling criterion, in this case, the decrease in implosion pressure is much more important (42%), meaning that water has a non negligible effect on the implosion pressure when the water content in the composite is higher than 1%.

Moreover, it was shown earlier that as water enters the composite, plasticization occurs and results in a non linear response. This aspect is not taken into account in these simple equations. A much more complex model would be needed to take into account this parameter.

The aim of the current chapter is to be able to investigate the effect of water on the implosion pressure of a thick cylinder immersed in sea water at 15°C. The predictions relating the water content to the implosion pressure were conducted assuming a homogeneous water profile through the thickness of the cylinder. However, it was shown at the end of the previous chapter that for short immersion times at 15°C, the cylinder was not fully saturated. Therefore, if one were to predict the implosion pressure in such conditions, it would be necessary to take into account the water profile throughout the thickness as well as the evolution in local properties that is induced. To address this question with accuracy, finite element modelling is necessary but this is not the aim of the current work. However, it is possible to obtain the local evolution of the mechanical properties as a function of water through the thickness of the cylinder for all the properties presented in Table 13. As an example, the water profile obtained after one year of immersion presented at the end of the previous chapter has been coupled with the evolution in transverse modulus with water content, Figure 81.

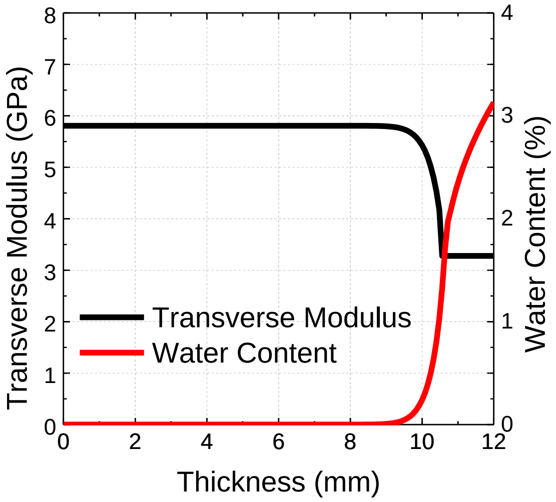

Figure 81 : Evolution of the transverse through the thickness of a 12mm thick cylinder immersed in sea water at 15°C for 1 year – Thickness plotted from inner wall (0mm) to outer wall (12mm)

Using the same approach for all the properties, it is possible to implement them in a predictive model. In our case, for simplification purposes, we can see that after 1 year of immersion, approximately 2mm of the total thickness is affected by water. Let us now consider that these 2mm do not have any mechanical contribution, which is a conservative assumption. If we consider a cylinder of 10 mm (12mm minus the 2mm affected by water) with a diameter of 120mm subjected to hydrostatic pressures, the predictions give us an implosion pressure of 468 bar using the buckling criterion and 412 bar using the strength criterion, i.e. a decrease in implosion pressure of respectively 39% and 21%.

3. Conclusion

The effect of water on the mechanical properties has been considered in this chapter. The aim was to be able to quantify the effect of water diffusion of the implosion pressure of a thick cylinder immersed in sea water for several years at low temperatures. To do so, the mechanical properties in tension and compression were determined as a function of homogeneous water contents through the thickness of the specimens. A unique set of data relating the tensile and compressive properties of C/PA6 to water content was presented. It was shown that water has a very negative effect on the matrix dominated mechanical properties of these composites that are reduced by over 50%. This loss in properties has been linked to the large decrease in the glass transition temperature (from 66°C in the dry state to -12°C when fully saturated with sea water). An empirical relationship between the mechanical properties and the water content and the T-Tg parameter has been proposed, which can be used to account for environmental changes in matrix-dominated properties. The results were compared to a C/PEEK reference, for which water saturation had no effect on the mechanical properties.

Then, these properties were used to investigate the implosion pressures of thick infinitely long cylinders in the un-aged and aged state using simple buckling and strength criteria. It was shown that for a cylinder in the un-aged state and with a thickness and diameter of respectively 12 and 120mm, the failure mode would be material failure rather than buckling. In this condition the failure would occur above 500 bar, which suggests that it is theoretically possible to use this material for underwater applications. Then, the effect of aging was considered and it was shown in Chapter 3 that for short immersion times at 15°C, the cylinder would be not fully saturated and that after 1 year of immersion, only 2mm of the total thickness would be affected by water. If we consider that these 2mm do not make any mechanical contribution, which is a strong but conservative assumption, the implosion pressure would drop to 412 bar using the strength criterion, showing that the decrease in implosion resistance is quite limited (21%).

Finally, the criteria that were used in this chapter assumed linear elastic responses of the material, which is not the case either for the un-aged (non linear response of carbon fibres in tension and compression) or the aged state (plasticisation of the matrix). A finite element model could be used to couple the water diffusion model presented in Chapter 3 and the results presented in Chapter 4. Nevertheless, this is not the purpose of the present work. However, results have shown that for cylinders immersed at low temperature and for short immersion times, water is not the main issue. Now that the effect of water (both the water diffusion and its effect on the mechanical properties) has been considered in Chapters 3 and 4, particular emphasis will be put on the effect of processing conditions on the mechanical properties and microstructure of C-PA6 laminates.

Chapter 5

Effect of processing conditions on the microstructure and mechanical properties

The aim of the current chapter is to study the effect of processing conditions on both the microstructure and mechanical properties of C/PA6 composite components.

First, the effect of cooling rate on the degree of crystallinity was investigated and emphasis was placed on the crystallization kinetics in neat and reinforced PA6. Second, several panels were manufactured by thermo-compression at different cooling rates in order to study the effect of crystallinity on the mechanical properties. Finally, composite panels and rings were manufactured by Laser Assisted Tape Placement and an extensive study was conducted in order to investigate the effects of processing conditions on the degree of crystallinity and mechanical properties. These were compared to those obtained for composites manufactured by thermo-compression.

1. Effect of cooling rate on the crystallization behaviour

1.1. Modelling the crystallization kinetics in neat and reinforced PA6

1.1.1. Introduction

Thermoplastic polymers and more especially semi-crystalline polymers have very specific properties. Contrary to their thermoset counterparts, semi-crystalline polymers possess a melting temperature (T_m) that allows them to be processed several times, which makes recycling possible. Also, these types of polymers are able to crystallize upon cooling allowing a degree of crystallinity X_c to be measured, see Chapter 1, section 2. The following section will focus on the degrees of crystallinity obtained at different cooling rates and on the crystallization kinetics in neat and reinforced PA6 upon cooling. For the latter, several models have been used and compared in order to describe accurately the crystallization kinetics.

1.1.2. Results and discussion

1.1.2.1. Effect of cooling rate on the crystallization temperature, degree of crystallinity and spherulite size

Differential Scanning Calorimetry (DSC) was applied to investigate the non isothermal crystallization behaviour of neat and reinforced PA6. First, the matrix contained within the prepreg was extracted after a press forming process and analysed. Then, the C/PA6 pre-impregnated tapes were used to study the effect of fibres on the crystallization behaviour.

The two materials (neat PA6 and C/PA6) were tested in the DSC at a heating ramp of 10°C/min from 25°C to 300°C and this temperature was held for 5 minutes to make sure that the matrix was completely melted. Then, different cooling rates were used (2, 5, 10, 20 and 50°C) in order to investigate the effect of cooling rate on the crystallinity. The heat flow curves obtained upon cooling from these tests are presented in Figure 82.a for the neat PA6 and in Figure 82.b for the C/PA6. For each cooling rate condition, three samples were tested to check reproducibility.

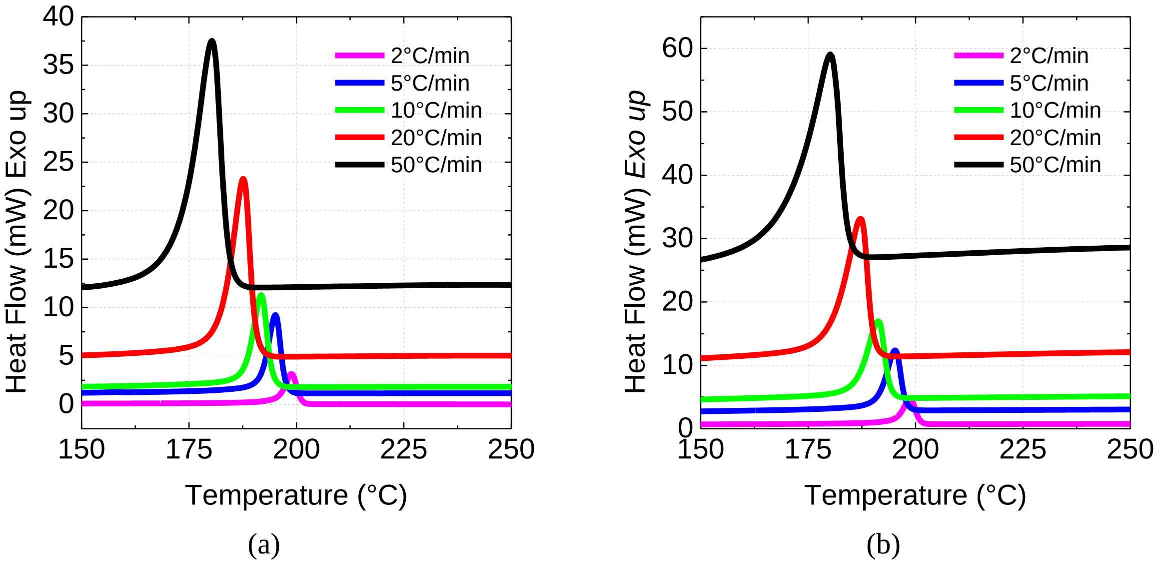

Figure 82 : Effect of cooling rate on (a) Neat PA6 (b) C/PA6

We can see that the crystallization peak temperature (T_c) decreases with increasing cooling rate. For the neat PA6, it decreases from 198 ± 1°C at 2°C/min to 181 ± 1°C at 50°C/min. Very similar results are obtained with the C/PA6 (from 199 ± 1°C at 2°C/min to 180 ± 1°C/min at 50°C/min). This result also shows that the fillers, i.e. the carbon fibres do not have a significant effect on the crystallization temperature. We can also observe that as the cooling rate increases, the crystallization peaks are broader. This is related to the fact the nucleation and crystal growth are highly dependent on the temperature. Figure 83 shows the crystallization times as a function of the cooling rate.

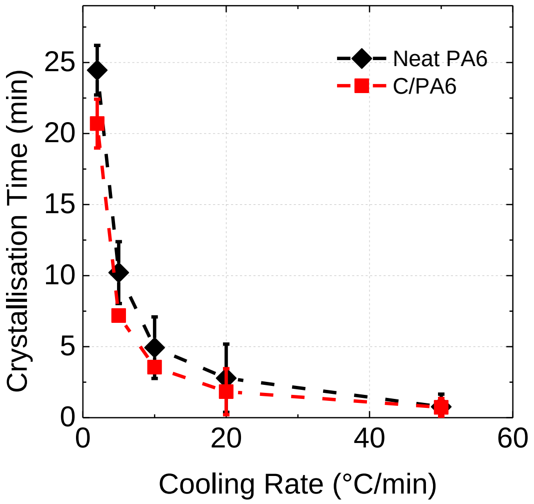

Figure 83 : Effect of cooling rate on the crystallization time

We can see that again, the fibres do not have a strong effect on the crystallization times. The crystallization times are slightly longer for the neat PA6 but some measurements are within the standard deviations. However, a shorter crystallization time obtained for a specimen with fillers is logical as fibres create more nucleation sites [28].

Then, the degrees of crystallinity obtained at different cooling rates are presented in Figure 84. It should be noted that these were measured during a second heating ramp at 10°C/min after the crystallization stage, the usual procedure in published studies. Figure 84.a shows the evolution of the degree of crystallinity as a function of cooling rate for the neat PA6 extracted from the pre-impregnated tapes but also the commercial PA6 presented in Chapter 3 for comparison purposes. Then, Figure 84.b presents the degrees of crystallinity obtained at different cooling rates for the neat PA6 and the C/PA6 tapes.

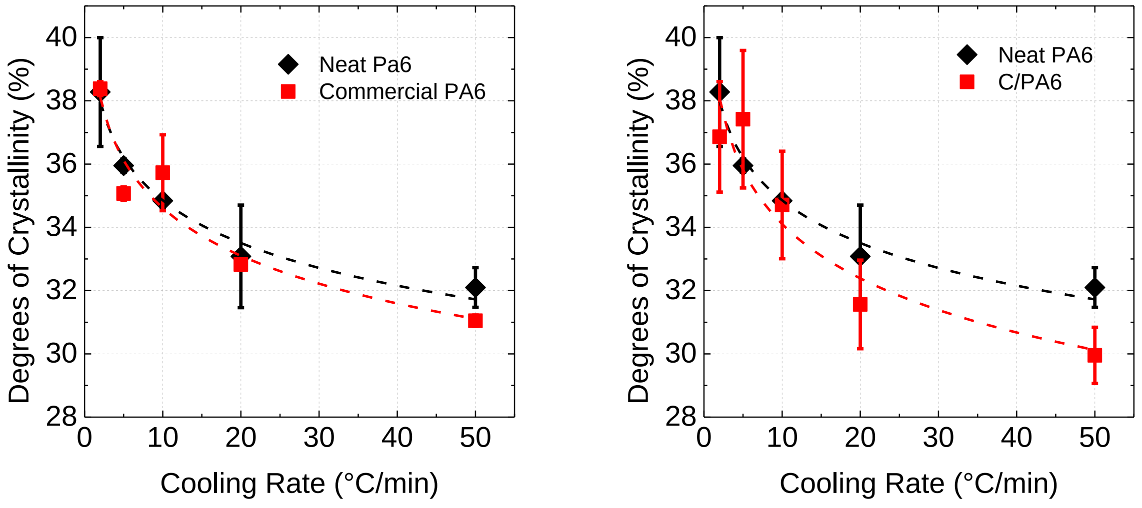

(a)

(b)

Figure 84 : Effect of cooling rate on the degree of crystallinity (a) Neat and commercial PA6 (b) Neat and C/PA6

Figure 84.a shows that the two PA6s behave similarly in terms of degrees of crystallinity. The degrees of crystallinity decrease from approximately 38% at 2°C/min to values around 32% at 50°C/min. Results are quite similar for the C/PA6 tapes as these decrease from 37% to 30%, i.e., slightly lower than for the neat PA6.

Therefore, the drops in degrees of crystallinity are not significant (around 6-7%) and would suggest that this effect is quite limited. It also confirms that the commercial PA6 used in Chapter 3 to predict the water diffusion in the composite is pertinent.

However, degree of crystallinity is a global indicator of the amount of crystalline material present; it provides no information on the microstructure, which can vary considerably at a given value of cooling rate.

Several samples were therefore prepared in order to observe the evolution of the microstructure (spherulite shapes and sizes) as a function of the cooling rate, using the commercial PA6. We have shown that the two matrix polymers (neat and commercial PA6) behave similarly in terms of degree of crystallinity. It is assumed here that the crystallites (shape and size) also behave similarly. Results obtained from the polarised microscope are shown in Figure 85.

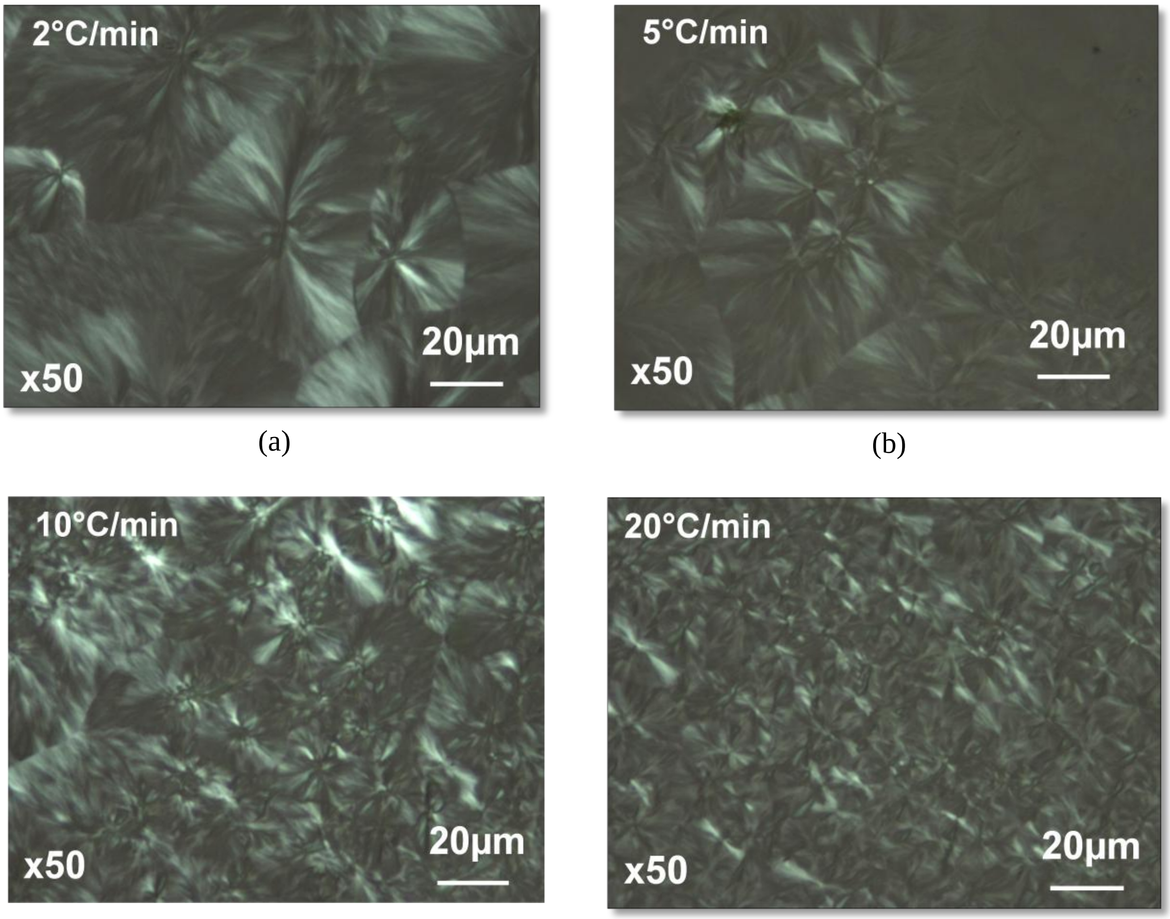

(a) (b)

(c) (d)

Figure 85 : Effect of cooling rate on the spherulite size and shape

It can be seen that the spherulite size decreases from 30-40 µm at 2°C/min to 10-20 µm at 20°C/min, which confirms that smaller spherulites are obtained for higher cooling rates. Several attempts were made to try and observe these spherulites as well as transcrystallinity in the composite, using the same thin film light transmission method. However, experimental problems were encountered as the film thickness required is similar to fibre dimensions, and did not allow us to observe this.

Now that we have investigated the crystallization behaviour of neat and reinforced PA6, we will focus on the crystallization kinetics and the associated models.

1.1.2.2. Modelling the non-isothermal crystallization kinetics

In this section, several models are used and compared to the experimental data.

- Avrami's equation [155]

Avrami's equation has been used many times in the literature to describe the crystallization kinetics of polymers. However, it only considers isothermal crystallization, which is not the purpose of the current work. Mandelkern [156] slightly modified Avrami's equation and considered that only the primary stage of non isothermal crystallization could be described with Avrami's equation. The following equation is obtained, Eq. 37.

$$1 - X_c(t) = \exp(-Z_t t^n) \quad \text{Eq. 37}$$

Where $X_c(t)$ is the relative crystallinity at time t, Z_t the crystallization rate constant and n the Avrami exponent. The parameters Z_t and n can be determined by using the previous equation in the double logarithmic form, Eq. 38.

$$\log\left[-\ln\left(1 - X_c(t)\right)\right] = n \log\, t + \log Z_t \quad \text{Eq. 38}$$

Plots of log[-ln(1-Xc(t))] versus log t are presented in Figure 86.a for the Neat PA6 and in Figure 86.b for the C/PA6.

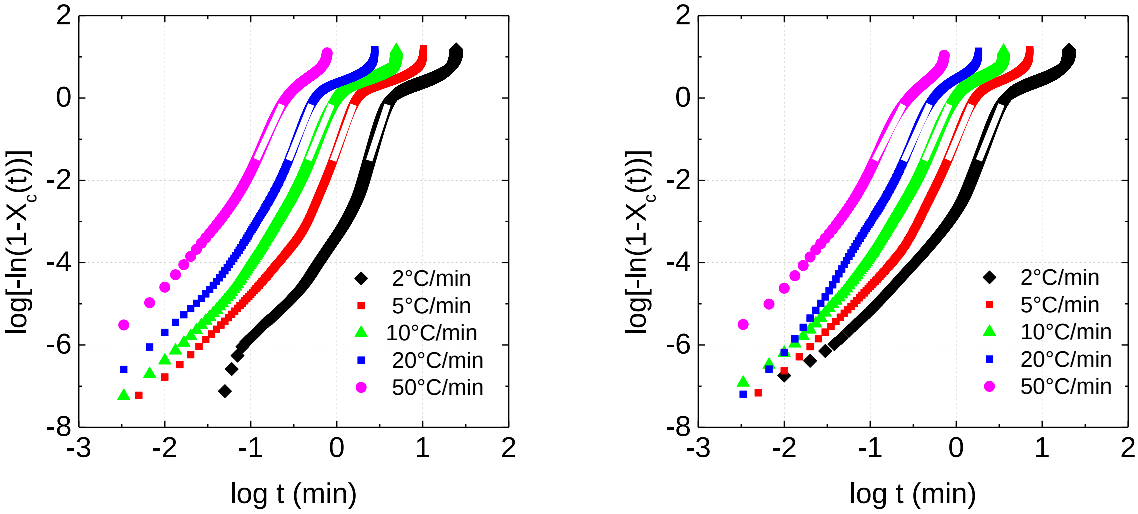

(a) (b)

Figure 86 : Avrami plots for (a) Neat PA6 (b) C/PA6

For both materials, we can see that the curves obtained are not linear. However, as stated by Mandelkern [156], only the primary stage of the crystallization can be represented using Avrami's equation. Therefore, it was chosen to work only in the linear part of the plots from $3\%<X_c(t)<50\%$, represented by the white lines for each cooling rate in Figure 86. From the slope n and intercept Z_c, we are able to determine the two parameters for each cooling rate of interest. However, as Avrami's equation is related to isothermal crystallization, Z_t should be modified to account for the rate of non-isothermal crystallization, Z_c, Eq. 39.

$$\log Z_c = \frac{\log Z_t}{\phi} \qquad \text{Eq. 39}$$

Where ϕ is the cooling rate. The different values for n and Z_c are presented in Table 15 for the neat and reinforced PA6 at different cooling rates.

Table 15 : Avrami coefficients and Z_c measured in the range from $3\%<X_c(t)<50\%$

Material	Cooling rate (°C/min)	n	Z_c x10^3 (min/°C)
Neat PA6	2	6.38	0.06
	5	5.68	10.64
	10	5.03	143.19
	20	5.21	1247.01
	50	4.52	10651.97
C/PA6	2	5.18	0.65
	5	4.96	18.96
	10	4.74	165.39
	20	4.61	945.30
	50	4.06	4298.63

These values of n (n>4) would suggest that the crystallization behaviour that occurs in both the neat and reinforced PA6 is complex because usual values are in the range from 2 to 3. However, it was shown in Figure 85 that the crystallites shapes and sizes are not so complex. Therefore, it was decided to identify the n and Z_c values for crystallization rates between $0\%<X_c(t)<1\%$. This range corresponds to the values located at the bottom left of Figure 86.a and Figure 86.b. Results are presented in Table 16.

Table 16 : Avrami coeffcients and Z_c measured between in the range from $0\%<X_c(t)<1\%$

Material	Cooling rate (°C/min)	n	Z_c x10^3 (min/°C)
Neat PA6	2	3.01	0.28
	5	2.65	1.87
	10	2.89	11.17
	20	2.77	20.37
	50	2.55	71.24
C/PA6	2	2.43	0.94
	5	2.70	3.53
	10	2.81	13.92
	20	3.18	33.86
	50	2.57	75.32

After this second data treatment, the Avrami coefficients are much closer to what is usually observed for semi-crystalline polymers. The n values lie between 2 and 3 and would suggest that the crystallization is sporadic and spherical, as corresponding to the the spherulite geometry observed on Figure 85. However, this result has to be used very carefully as this n value is strongly dependent on the data treatment. In several studies, the linear plots that are used to determine n are not defined using a parameter between two crystallization rates (i.e. 0 to 1% or 3 to 50%). To conclude, Avrami's equation is not sufficient to fully describe to non-isothermal crystallization in both neat and reinforced PA6.

- Ozawa [157]

Ozawa's theory is used in the case of non-isothermal crystallization at a constant cooling rate ϕ and assumes that the crystallisates grow as spherulites with a constant radial growth. The theory is presented hereafter, Eq. 40.

$$1-X_c(T)=\exp\left[-\frac{K(T)}{|\phi|^m}\right] \qquad \text{Eq. 40}$$

Where m is the Ozawa exponent and K(T) the crystallization rate constant. As for the Avrami theory, the double logarithmic form (Eq. 41) is used to determine m and K(T) by plotting the log[-ln(1-X_c(T))] as a function of ϕ at given temperature during the crystallization stage, Figure 87.

$$\log[-\ln(1-X_c(T))] = \log K(T) - m \, log \, \phi \qquad \text{Eq. 41}$$

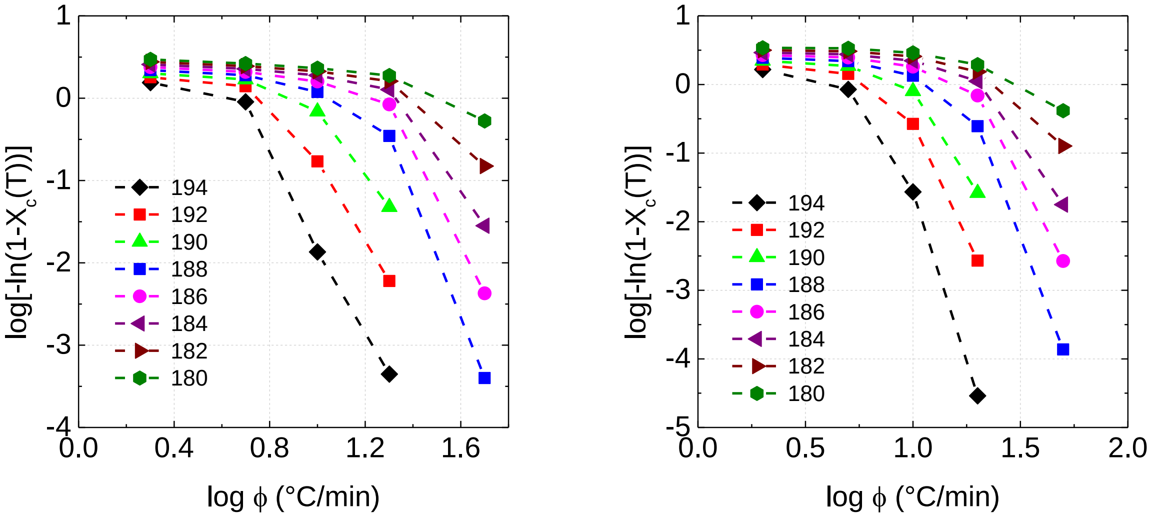

(a) (b)

Figure 87 : Ozawa plots for (a) Neat PA6 (b) C/PA6

These two figures show that for both neat and reinforced PA6, Ozawa's theory cannot be used to describe the crystallization kinetics in a simple manner. The plots at different temperatures are not linear during the crystallization stage.

- Mo's theory– Combined Avrami and Ozawa theory [158]

Since the two theories presented above were not able to fully describe the crystallization kinetics, Mo suggested combining Avrami and Ozawa's theories. Since the degree of crystallinity is related to the cooling rate (Ozawa) but also to the crystallization time t (Avrami), a relationship that links these two aspects can be used to describe the non-isothermal crystallization, which is presented in Eq. 42 and Eq. 43.

$$\log Z_t + n \log t = \log K(T) - m \log \phi \qquad \text{Eq. 42}$$

$$\log \phi = \log F(T) - b \log t \qquad \text{Eq. 43}$$

Where

$$F(T) = \left[\frac{K(T)}{Z_t}\right]^{\frac{1}{m}} \qquad \text{Eq. 44}$$

F(T) refers to the cooling rate at a given time t for a certain degree of crystallization. b is the ratio between Avrami and Ozawa exponents.

Following Mo’s method, plotting the log ϕ against the log t for a given degree of crystallization would allow us to fully describe the crystallization kinetics in neat and reinforced PA6. The results are presented in Figure 88.

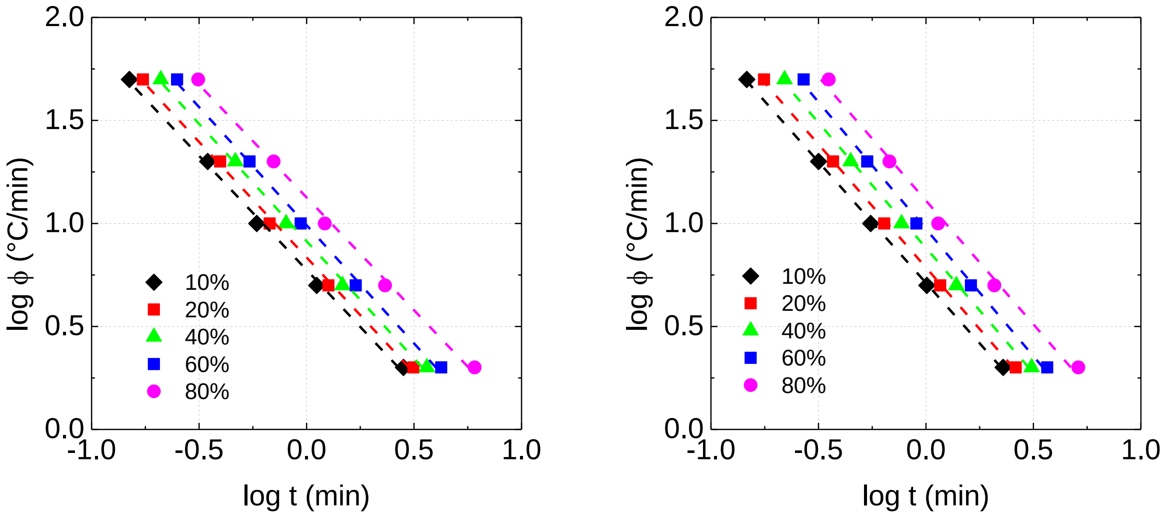

Figure 88 : Combined Avrami/Ozawa plots of log ϕ vs. log t for non isothermal crystallization: (a) Pure PA6 (b) PA6/CF

It can be observed that for both neat and reinforced PA6s, using Mo’s method to describe the crystallization kinetics provides a linear plot for every degree of crystallization. From these plots, the parameters b and F(T) are identified and presented in Table 17.

Table 17 : Combined Avrami/Ozawa parameters

Material	X (%)	b	F(T)	R²
Pure PA6	10	1,1074	5,95	0,9978
	20	1,1211	6,84	0,9981
	40	1,1392	8,21	0,9983
	60	1,1471	9,80	0,9978
	80	1,095	13,37	0,9972
PA6/CF	10	1,1751	5,15	0,9996
	20	1,1957	6,11	0,9994
	40	1,2164	7,61	0,999
	60	1,2337	9,38	0,9981
	80	1,2019	12,92	0,9942

These results show that the values of F(T) increase for both materials, indicating that a lower crystallization rate is needed to reach the given degree of crystallinity at a time t. Very few differences are found between the neat and reinforced PA6. To conclude, Mo’s method can be used to fully describe the crystallization kinetics in both the neat and reinforced PA6 and shows that the effect of carbon fibres on the crystallization kinetics is quite limited.

1.1.3. Conclusion

The effect of cooling rate on the crystallization behaviour of neat PA6 and C/PA6 has been considered in this section. First, the degree of crystallinity was investigated as a function of cooling rate. It was found that the latter decreases from 38% at 2°C/min to values around 32% at 50°C/min for the neat PA6. Results are quite similar for the C/PA6 tapes for which a decrease from 37% to 30% is measured. The crystallization temperatures were also found to decrease as the cooling rate increases. Then, different theories were applied to try and describe accurately the crystallization kinetics in both the neat and the C/PA6. It was found that Mo’s theory gave the closest representation and allowed us to fully describe the kinetics.

Now that the crystallization kinetics have been investigated, we will focus on the effects of crystallinity (and indirectly the cooling rate) on the mechanical properties of C/PA6 laminates.

2. Mechanical properties of composite panels manufactured at different cooling rates

2.1. Introduction

The effects of crystallinity on mechanical properties have been studied several times in the literature for both neat polymers [26], [27], [159] and composite materials [41], [159]–[161]. High degrees of crystallinity usually lead to higher modulus and lower toughness values. The through-thickness crystallinity can also affect the residual stresses [162]. Moreover, crystal structure has an effect on the water uptake at saturation as shown in Chapter 3. Indeed, the higher the degree of crystallinity, the lower the water uptake.

The aim of the following section is to investigate the effects of crystallinity on the mechanical properties of C/PA6 laminates manufactured by thermo-compression at different cooling rates.

2.2. Results and discussion

In this study, three unidirectional panels were manufactured at three different cooling rates (1, 5 and 20°C/min) on the same hot press used to manufacture the samples presented in Chapter 4. Due to the hot press capacity, it was not possible to manufacture panels at higher cooling rates. First, the degrees of crystallinity (measured by DSC) obtained from these three manufacturing conditions are presented in Figure 89 and compared those obtained on the pre-impregnated tapes cooled at different cooling rates.

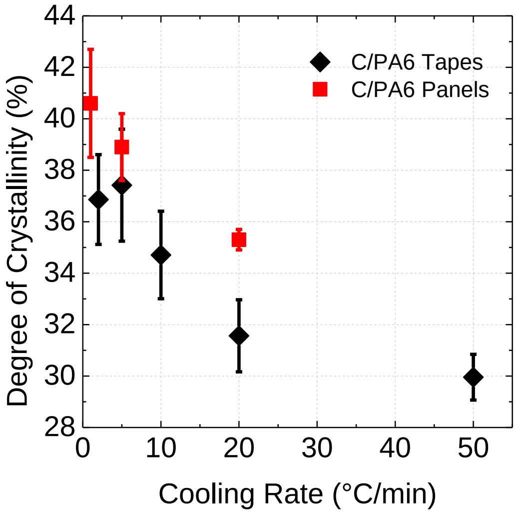

Figure 89 : Evolution of the degrees of crystallinity vs cooling rate for C/PA6 tapes and panels

Results show that the degrees of crystallinity obtained as a function of the cooling rate within the panels are different and decrease from 40.5% at 1°C/min down to 35% at 20°C/min. It is also clear that the degrees of crystallinity obtained for the composite panels are higher than for the pre-impregnated tapes. However, the composite panels are much thicker (2mm compared to 160µm for the tapes) and the cooling rate for the panels is taken as that of the mould. Therefore, a slower cooling rate occurs at the heart of the panel and leads to higher degrees of crystallinity.

Now that we have been able to manufacture several panels containing different amounts of crystallinity, let us investigate if these differences have an effect on the transverse tensile strength. This test was chosen as it gives information on the matrix and the interface strength. Results are presented in Figure 90.

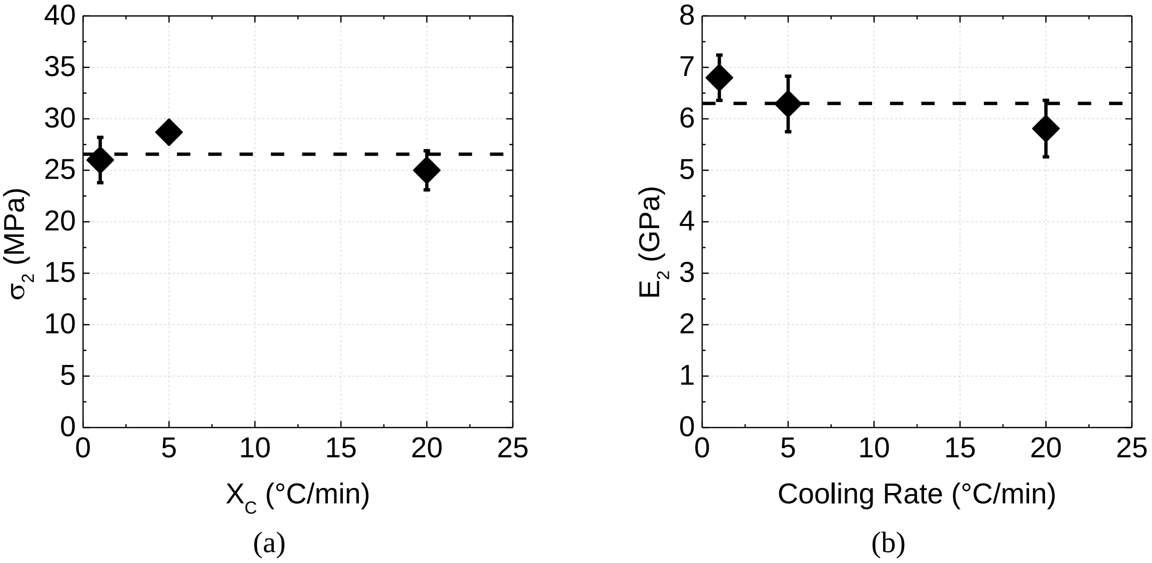

(a) (b)

Figure 90 : Effect of cooling rate on the mechanical properties (a) Transverse tensile strength and (b) Transverse modulus

The differences that are found in terms of mechanical properties (modulus and strength) are quite small. This can be explained by the relatively small difference in degrees of crystallinity (around 5%) within these panels. Therefore, it seems that the matrix is not very sensitive to the cooling rate in this range of cooling rates. Also, it has been shown in Chapter 4 that the interface in such laminates is not very strong (σ_2=25MPa in the dry state). Due to this low initial interface strength, the effect of other parameters such as the degree of crystallinity might be very limited.

It would be interesting to perform DCB tests at different degrees of crystallinity as several researchers have shown that it can have a significant influence in other thermoplastic composites [42], [160].

2.3.Conclusion

In this section, particular emphasis was placed on the effect of degree of crystallinity on the transverse tensile strength. Unidirectional composite panels were manufactured at different cooling rates to obtain panels with different degrees of crystallinity. Results from transverse tensile tests performed on these specimens did not show a clear influence of the degree of crystallinity on the mechanical properties although one might be expected over a wider range of cooling rates.

The next section will focus on the effects of manufacturing process on the mechanical properties of C/PA6 composites manufactured by Laser Assisted Tape Placement (LATP). The results obtained from mechanical tests performed on these composites will then be compared to the thermo-compression reference presented in Chapter 4.

3. Mechanical properties of composite panels and rings manufactured by Laser Assisted Tape Placement

3.1. Introduction

Over the last two decades, Automated Tape Placement (ATP) attracted considerable interest for automotive and aerospace applications, as it allows the production of high performance and complex composite parts at high productivity rates. Most ATP processes that are used nowadays tend to process thermoset composites [29] and result in very interesting performances close to those of autoclave composites [32] but still require a long curing stage, which is not the case for thermoplastic composites. However, it has proved difficult to obtain similar results on thermoplastic composites [39]. For the latter, processes such as thermo-compression allow the processing of a given laminate using three main parameters (heating temperature, cooling rate and pressure) that can be closely controlled. Several additional parameters are to be taken account with thermoplastic ATP processes such as the laser angle, the tape back tension, the manufacturing speed, the mandrel temperature, etc. Additionally, parameters related to the hardware itself (heat source, roller type), material aspects (fibre distribution through the tape thickness, roughness, void content) and composite structure (side connections between tapes: gaps, overlaps) have also proved to have a significant influence.

Comer et al. [39] conducted a study in which they compared the C/PEEK properties obtained by LATP to the autoclave reference. The differences that were highlighted were attributed to a lower quality in terms of voids of the LATP panels and to a matrix of a more amorphous nature. Results concerning other thermoplastic composite materials are rarer and mostly concern C/PA6 laminates. One study was recently presented at the ICCM20 conference by Namani et al. [163] which reported flexural strengths of about 60% of the autoclave reference using a hot gas ATP process.

The aim of the following section is to highlight and identify the differences that may arise using C/PA6 tapes manufactured by LATP compared to thermo-compression. These will serve as a baseline for the following chapters. To do so, several composite panels and rings were manufactured using LATP. Their quality in terms of voids was checked first as well as their degrees of crystallinity. Then, several mechanical tests were performed (tension, flexure, radial compression). Emphasis was placed on compression and flexural tests as these are known to be very sensitive to defects such as fibre misalignments and voids. These will then be compared to the thermo-compression results presented in Chapter 4.

3.2.Processing conditions

The processing conditions for the unidirectional composite panels and circumferential rings are presented in Table 18. It may be noted that the composite panels were manufactured on a flat mandrel. The composite parts that were obtained (panels and rings) are shown in

Figure 91. The composite panel dimensions were 500 x 300 x 2 mm^3 and the composite rings were 12.7mm thick, i.e., the width of one tape (half an inch) and have an inner diameter of 200mm.

Table 18 : Processing parameters used to manufacture the composite panels and rings using LATP

	Panels	Rings
Lay up	$[0]_{16}$	$[0]_{16, 32, 64, 96}$
T° (°C)	260	280
Speed (m/min)	15	7
Roller pressure (bar)	2	3
Mandrel	Flat Mandrel	Ø200mm

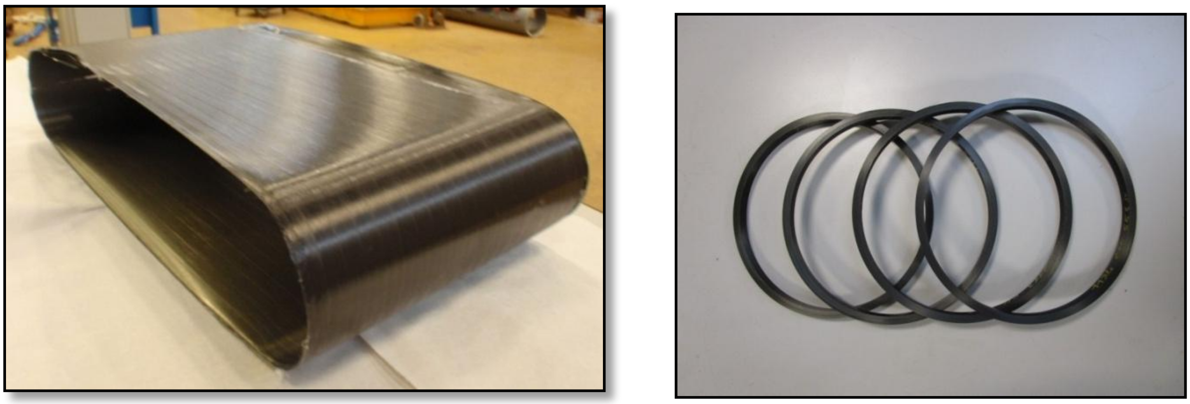

(a) (b)

Figure 91 : Composite parts manufactured by LATP (a) Composite panels (b) Rings

First, the process parameters for the composite panels and rings are different as these were not manufactured at the same time. The panels were manufactured just after the LATP machine was received, i.e. at the beginning of the study and therefore with less experience on the machine. The rings were then manufactured two years and a half after installation of the machine, which explains the differences observed in process parameters as these were optimised over time. The two mandrels that were used were at ambient temperature at the beginning of the process.

Moreover, we can see that the heating temperatures (260-280°C) for LATP are quite different from the one that was used for panels manufactured by thermo-compression (230°C). Processing C/PA6 composite parts with LATP is relatively difficult at a temperature of 230°C as the viscosity of the matrix at this temperature is too high to achieve a proper intimate contact between the tapes. To solve this problem, the temperature is increased to obtain a matrix with a much lower viscosity. Also, the pressures (2-3 bar) are different from the one used for thermo-compression.

3.3.Results and discussion

3.3.1. Quality control

The quality in terms of consolidation (voids) of the different panels and rings that were manufactured was checked using optical microscopy (polished sections) and is presented in Figure 92.a and Figure 92.b respectively. Concerning the composite rings, it may be noted that the study was mainly focused on thick rings (t=13mm), as these would be the ones having the most voids.

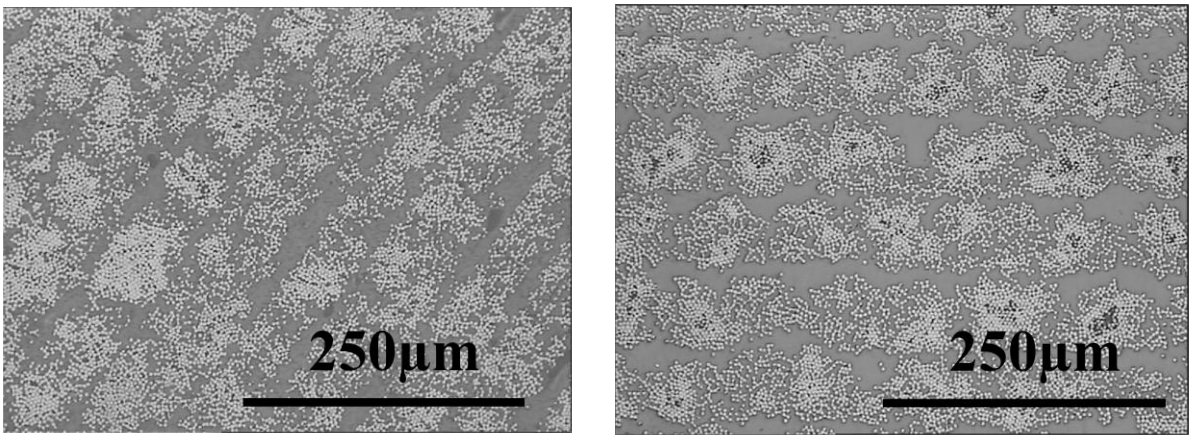

(a) (b)

Figure 92 : Quality control of composites manufactured by LATP (a) Composite panels, 2 mm thick (b) Composite rings, 13mm thick

From these polished sections, the void contents were obtained for the composite panels and rings and were found to be respectively 1.2 ± 0.9% and 2.0 ± 0.6%.These values are slightly higher than the ones obtained with thermo-compression (0.9 ± 0.2%). However, these void contents values are still relatively low compared to what can be obtained with thick filament wound carbon/epoxy laminates (more than 5%).

3.3.2. Degrees of crystallinity

It is known that the cooling rates obtained with LATP are much faster than those found in thermo-compression. For instance, in the case of C/PEEK composites manufactured by LATP, Comer [39] reported cooling rates values above 400°C/min, which is much higher than the range over which the crystallization model was applied in the previous section. However, it was not possible to study the effect of such a high cooling rate using DSC. It is therefore essential to verify the degrees of crystallinity obtained in the composite panels and rings that were manufactured.

In the case of the LATP composite panels, the degree of crystallinity was 35.9 ± 1.3%, which is very similar to those obtained with thermo-compression (35.3 ± 0.4%). This result is not surprising as the cooling rate used in thermo-compression (20°C/min) was adjusted in order to reach comparable crystallinity degrees. Even if we reported that the degree of crystallinity had no effect on the mechanical properties, it is still important to obtain similar microstructures when comparing two different processes. Moreover, it may be noted that for the composite panels manufactured by LATP, we did not report a through thickness crystallinity gradient. However, for the thick composite rings (13mm), a through thickness gradient was observed. As was presented in Chapter 2, each DSC measurement that is conducted gives us an enthalpy value that is a function of the fibre weight content. The thick composite rings were cut into 12 parts through the thickness and were then tested in the DSC. However, since the cutting stage might induce damage and variations in local fibre weight contents, each DSC sample was then heated in a TGA under a nitrogen flow to burn off the resin. The through thickness fibre weight content results are shown in Figure 93.a and the through thickness degrees of crystallinity in Figure 93.b.

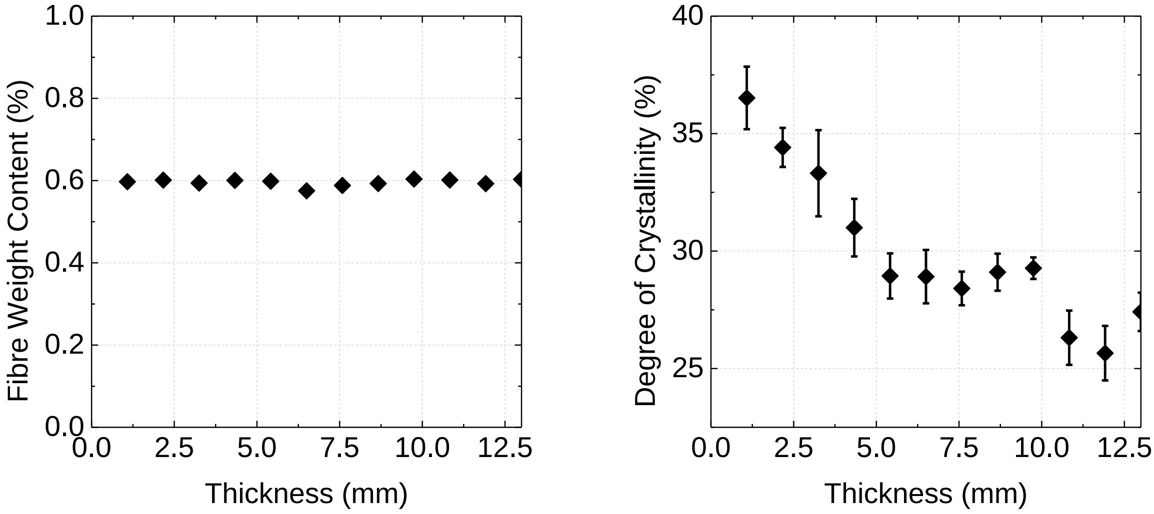

(a) (b)

Figure 93 : LATP 13mm ring, through the thickness (a) Fibre weight content (b) Degrees of crystallinity – Inner wall at 0mm thickness

Results from through thickness fibre weight content measurements show that there is no variation through the thickness of the composite rings. It may be noted that no standard deviation are presented here, as only one TGA was conducted for each point through the thickness. The fact that there is no variation through the thickness was expected since the fibre weight content depends on the composition of the original tape (already checked in Chapter 2), so it was not necessary to conduct repeatability tests. Therefore, the fibre weight content was fixed at 60% for all the DSC measurements that were performed. However, three DSC tests were conducted for each through thickness localisation, resulting in 36 DSC tests (12 per ring). The results from Figure 93.b show that there is a decrease of more that 10% in the degree of crystallinity between the face in contact with the mandrel (X_c=36%) during the process and the outside surface (X_c=26%). Therefore, this result shows that a mean cooling rate value cannot be used to model the crystallization behaviour in this process. Modelling such a behaviour is complex as each tape that is laid is reheated several times during each tape placement pass and one needs to know if these are reheated above or below the melting/crystallization temperature. Local thermal measurements are needed throughout the process to develop such a model and this should be developed in the future.

Then, it may be noted that the lower degree of crystallinity obtained here (26%) is lower than the one obtained on pre-impregnated tapes cooled at 50°C/min (30%) presented in the first section of this chapter. This result suggests that higher cooling rates occur in LATP processes, as highlighted by Comer [39]. Therefore, it would be very interesting to obtain thermal measurements throughout the process and to conduct additional DSC tests on composite tapes cooled at cooling rates higher than 50°C/min. However, the degree of crystallinity of 26% suggests the cooling rate is probably above 100°C/min if we extrapolate the results shown in Figure 84.b.

However, the main result highlighted here is that a significant crystallinity gradient is obtained when manufacturing thick composite parts using this process. These through thickness variations may lead to detrimental residual stresses [162].

Now that we have investigated the microstructure of the composite panels and rings, let us focus on the mechanical properties of these composite parts.

3.3.3. Mechanical properties

In this section, results from several mechanical tests including radial compression on the composite rings, and tensile and flexural tests on the composite panels will be described. In the literature, in order the verify the mechanical performance of composite parts manufactured by LATP, researchers tend to focus on interlaminar shear strength, as this test gives information on the bonding quality of the different tapes. However, as highlighted in Chapter 4, it is not possible to perform such tests on C/PA6 as this material tends to plasticise instead of delaminating. That is why this type of test was not used here.

3.3.3.1. Radial Compression tests

Diametrical compression tests were performed following the method presented in Chapter 2 on composite rings of different thicknesses (from 2 to 12 mm). It may be noted that no stresses at failure are presented here as only the stiffness was studied because these rings were then be cut in order to obtain the hoop residual strains (described in the next chapter). Therefore, the aim of the current section is to study if we are able to describe the stiffness evolution (load-strain curve) as a function of the ring thickness evolution. Hoop strain gauges were positioned on each composite ring, both on the outer and inner diameter.

The circumferential modulus E_θ can be determined analytically from the three equations presented hereafter, Eq. 45, Eq. 46, Eq. 47. These have been used in [164] and are originally derived from Roark [165].

$$E_\theta = \left[\frac{\pi r}{4A} + \frac{r^3}{I}\left(\frac{\pi}{4} - \frac{2}{\pi}\right)\right] S \qquad \text{Eq. 45}$$

Where r is the average radius of the cylinder, I the moment of inertia and S the slope of the force-displacement curve. Then, r and A are defined as follows:

$$r = \frac{r_{out} + r_{in}}{2} \qquad \text{Eq. 46}$$

$$A = \frac{(r_{out} - r_{in})}{2} . h \qquad \text{Eq. 47}$$

Where r_{out} and r_{int} are respectively the outer and inner diameter, A is the area of the cross section under bending and h the thickness of the cylinder.

Table 19 : Apparent modulus values measured for composite rings of different thicknesses

Lay Up	Thickness (mm)	E_θ (GPa)
$[0]_{16}$	2	79 ± 2
$[0]_{32}$	4	86 ± 5
$[0]_{64}$	8	68 ± 13
$[0]_{96}$	12	61 ± 5

These results show that there is a decrease in compression modulus when the thickness of the rings is increased. The modulus value that is measured for the $[0]_{32}$ rings is close to the one measured using the pin-ended buckling and pure compression tests on unidirectional specimens manufactured by thermo-compression in Chapter 4. However, these modulus values are to be taken carefully as the method used to measure the modulus was developed for isotropic materials, as described in ISO 9969. There is no correction for transverse shear. Therefore, the modulus values presented can be considered as apparent modulus values.

A study was performed in the past on glass/epoxy composites of different thicknesses (from 4.3 mm to 15 mm) [166] and compared finite element modulus values to the analytical ones and showed that the analytical modulus prediction was valid for thin thicknesses (1.4% difference between the finite element analysis and the analytical prediction). However, for significant thicknesses (15mm) a deviation of 13.8% was found between the FE analysis and the analytical prediction because of transverse shear effects.

Here, the anisotropic nature of carbon fibre composites will accentuate the influence of thickness and the decrease in modulus values that is observed id probably due to the fact that no through thickness properties are taken into account. Therefore, in order to investigate the real effect of thickness on the stiffness, a specific finite element model was needed.

These finite element calculations were performed by the CETIM using the elastic properties ($E_{1compression}$, E_2, G_{12}, ν_{12}, etc.) obtained in Chapter 4 on composites processed by thermo-compression. If the load-strain response obtained using the finite element calculations correlates well with the experimental data, this means that we are able to describe the stiffness evolution as a function of the ring thickness.

Results from radial compression tests (load-strain) curves were then compared to the finite element calculations (presented in Appendix I) and results showed it is possible to describe the stiffness evolution for all the thicknesses of interest (from 2 to 12mm) [167]. Therefore, this finite element method can be used later to study the stiffness of composite rings manufactured by LATP at different sequences.

The results presented afterwards only concern composite panels manufactured by LATP.

3.3.3.2. Tensile tests

Concerning the composite panels, tensile tests were first conducted along the fibre direction under the same conditions (specimens of 250 x 25 x 2 mm^3 tested at 2mm/min until failure) to those manufactured by thermo-compression. Modulus and stresses at failure are given in Table 20 as well as the thermo-compression reference values.

Table 20 : Results from tensile tests performed on unidirectional specimens manufactured by LATP and Thermo-Compression

	E (GPa)	$\sigma_{failure}$ (MPa)
Laser Assisted Tape Placement	110 ± 2	819 ± 62
Thermo-Compression	105 ± 5	1808 ± 132

Modulus results indicate lower variation for the specimens manufactured by LATP as the fibres are almost perfectly aligned compared to those manufactured by thermo-compression. In the case of thermo-compression, due to the low viscosity of the matrix and combined with the high pressure that is applied (5bar), the fibres and matrix tend to flow out of the mould and result in less perfectly aligned fibres, as shown by X-ray tomography results presented in Figure 94.

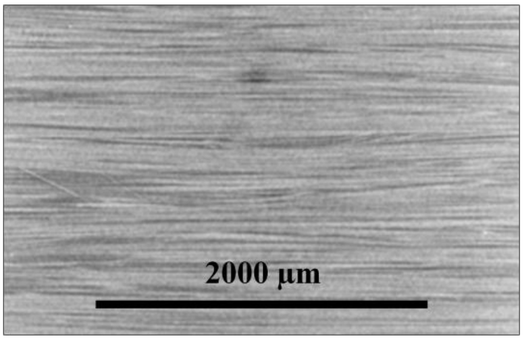

Figure 94 : Fibre misalignment observed via X-Ray tomography on the specimens manufactured by thermo-compression (voxel: 3.96µm)

However, results concerning the longitudinal tensile strength show significant differences between the specimens manufactured by LATP (819 ± 62 MPa) and thermo-compression (1808 ± 132 MPa). The strength at failure is divided by two. This result is very surprising as the properties along the fibre direction are mostly fibre dominated. However, the failure modes are completely different and will allow us to understand why these values are so low. These LATP specimens are shown in Figure 95.

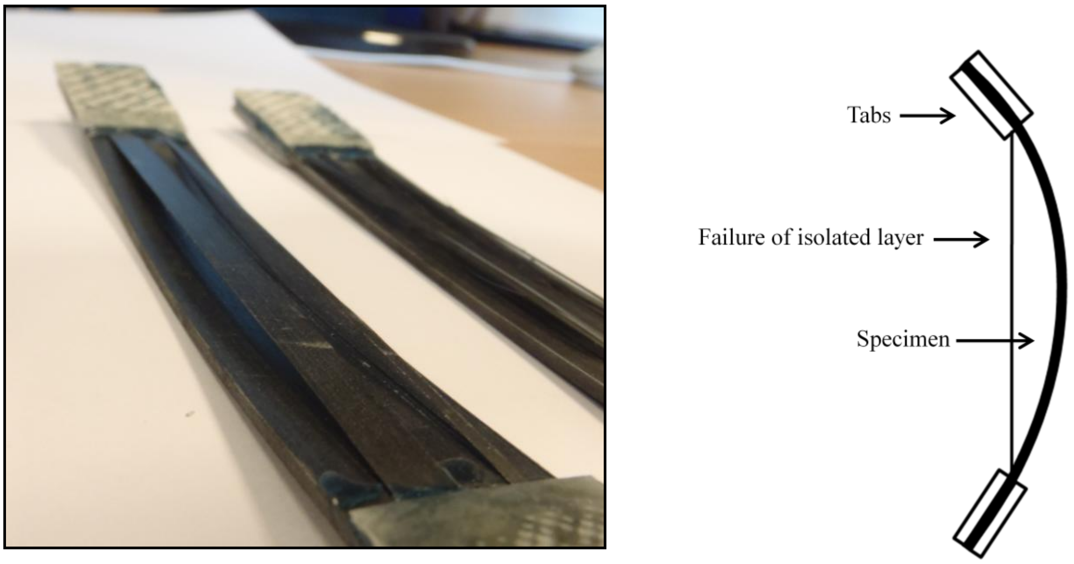

Figure 95 : Residual strains observed on unidirectional specimens manufactured by LATP after failure

In the case of specimens manufactured by thermo-compression, the failure was characterised by a typical fibre pull-out mode and resulted in high stresses at failure. However, concerning the specimens manufactured by LATP, the failure occurred very early due to an isolated layer on one side of the specimen that failed and initiated failure. Then, when the specimens were then removed from the test machine, they started to bend, as seen in Figure 95. It should be noted that this type of failure is not associated with a tab debonding problem. In the literature, Daniel [168] observed similar failure modes on hybrid (carbon/glass/epoxy) laminates tested under tension. Because of the different fibre properties, the glass fibres failed first and this resulted in very similar failure modes to those observed here. Therefore, it would seem that the two faces of our specimens manufactured by LATP are not subjected to the same stress levels. These differences might be can used by the presence of high residual stresses created by the process itself. These will be discussed later.

3.3.3.3. Flexural tests

Then, flexural tests (four point bending and pin-ended buckling compression tests) were conducted and results were compared to the reference values obtained from similar specimens manufactured by thermo-compression. Results are presented in Table 21.

Table 21 : Results from flexural tests conducted on unidirectional specimens manufactured by LATP compared to Thermo-Compression

Manufacturing process	$\sigma_{failure}$ (MPa) [LATP]	$\sigma_{failure}$ (MPa) [Thermo-compression]	Reduction
Four point bending	542 ± 43	961 ± 56	44%
Pin-ended Buckling	778 ± 36	1385 ± 101	46%

As for the results concerning the longitudinal tensile strength, the stresses at failure obtained from flexural tests conducted on the specimens manufactured by LATP are much lower than those obtained with thermo-compression. It may be noted that Namani et al. [163] observed similar reductions (40%) in mechanical properties when testing C/PA6 with the same fibre volume contents (50%) manufactured by LATP and autoclave under three point bending tests. Also, we have shown earlier that the void contents and the degrees of crystallinity were very similar for the two processes, so these would not explain the 45% mean strength reduction in mechanical properties observed here. Additionally, it is shown here that the pin-ended buckling test allows higher stresses at failure to be achieved than the four point bending test. This is due to the fact that below the loading points in four point bending tests, high stress concentrations are found which initiate premature failure.

The results from the tensile tests suggested that the two faces of the specimens were not subjected to the same initial stress levels. Therefore, this might induce differences in mechanical properties on the two sides of the specimens. Flexural tests are known to produce a stress gradient through the thickness of the specimens as was highlighted in Chapter 4. In many cases, in these tests, the failure occurs on the compression side of the specimens since the compression properties are lower than the tensile ones along the fibre direction. Therefore, it was decided to perform the same flexural tests but inversing the loading direction so that the two faces of the specimens are tested under compression.

In one case, the face that was in contact with the mandrel (named M) during the process is subjected to compression and is tested until failure. In the second case, the face that was not in contact with the mandrel (named O for outside) is subjected to compression loading until failure. Four point bending and pin-ended buckling tests were performed in these conditions. Therefore, four different configurations were tested. The results are now presented in Table 22.

Table 22 : Results from flexural tests conducted on unidirectional specimens on which each face of the specimen was subjected to compression loadings. * NUPF: No Upper Ply Failure on the Mandrel side

	Four Point Bending		Pin-ended Buckling	
Face subjected to compression	O	M	O	M
$\sigma_{failure}$ (MPa)	542 ± 43	550 ± 36	778 ± 36	750 ± 26
First upper ply failures (MPa)	NUPF*	268 ± 34	NUPF*	517 ± 15
E (GPa)	/	/	89 ± 4	85 ± 5
Failure mode	Compression Face O	Compression Face M	Compression Face O	Delamination Face M Tension Face O

Results for the bending stress at failure in the two configurations show very similar values, around 550MPa for the four point bending tests and 750 MPa for the pin-ended buckling tests. However, the behaviour during testing was quite different. When the face M was subjected to compression, delamination on the compression side occurred as shown in Figure 96 for the two different flexural tests, which was not observed when the face O was subjected to compression. These delaminations were reported in Table 22 as the “upper ply failures”.

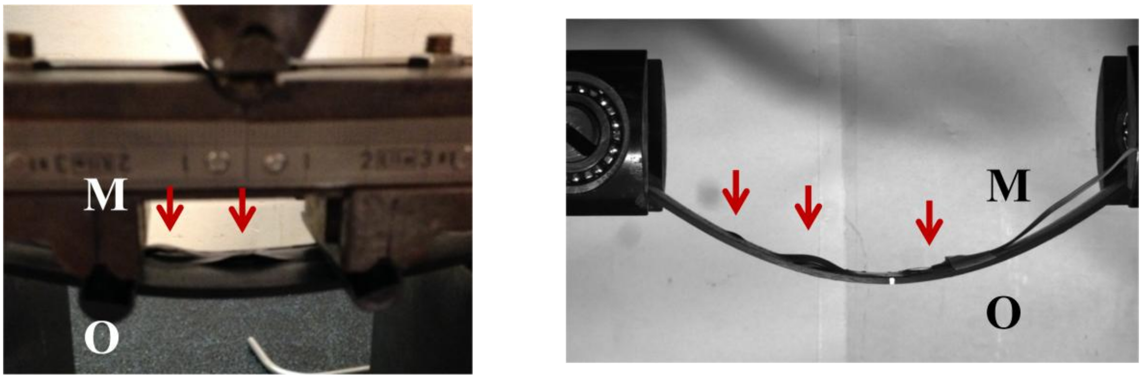

(a)

(b)

Figure 96 : Upper ply failures observed during flexural tests in which the mandrel face is subjected to compression for (a) pin-ended buckling and (b) four point bending

For the pin-ended buckling tests, the failure modes were completely different in the two configurations. It may be noted that for each testing condition, three specimens were tested and that the failure modes were exactly the same within each batch. These different failure modes are shown in Figure 97.

Figure 97 : Different failure modes observed on unidirectional specimens tests under pin-ended buckling tested on the two sides (left) Face O subjected to compression and (right) Face M subjected to compression

In one case, when the face O was subjected to compression, the failure occurred on the compression side and a ductile type failure, previously identified in Chapter 4 for specimens fully saturated with water occurred. In the other case, when the face M was subjected to compression, delamination occurred first on the face M but did not have an effect on the structural integrity of the specimen and the test continued until a brittle type failure occurred. Therefore, these tests show that the LATP process has a significant effect on the composite behaviour as the properties are different on the two sides. In the case where the face M is subjected to compression, delamination occurs. These differences might come from different initial stress levels on the sides of the specimens induced by the process itself. One characteristic of the LATP process is that a tape tension is used to wind the composite. Further discussion on the effects of fibre tension is presented hereafter.

3.3.4. Effect of process parameters on the residual stresses

Fibre tension or fibre pre-stressing is known to have an effect on the mechanical properties and residual stresses. For instance, Krishnamurthy [169] showed that in unidirectional carbon/epoxy composites, the transverse compressive residual strains could be reduced with fibre pre-stress. However, he also showed that above a certain pre-stress level, the compressive residual stresses could become positive. Therefore, an optimum pre-stress level has to be determined. Several studies conducted by Motahhari and Cameron on glass/epoxy laminates considered the effect of fibre pre-stressing on the mechanical properties. They showed that fibre pre-stressing increased the impact strength by 33% and that it had an effect on the failure modes. The higher the fibre pre-stress, the more splitting failure occurred [170]. They also increased the flexural strength and modulus by 33% with fibre pre-stress in another study [171]. Concerning thermoplastic composites, Zhao and

Cameron [172] conducted similar studies on glass/PP composites and also obtained increased flexural strength and modulus with fibre pre-stress. They showed that after an optimum fibre pre-stress level, the properties stabilized. Therefore, fibre pre-stressing has a non negligible effect on the mechanical properties.

However, these studies considered uniform pre-stress levels through the thickness of the specimens, which is not the case in our study as the two faces of the specimens are not subjected to the same stress levels. Moreover, the manufacturing processes are different. The behaviours observed in this section showed unexpected results and suggest that an optimisation stage is required to increase the mechanical properties along the fibre direction of these composites manufactured by LATP.

In order to explain this phenomenon, Lu [173] conducted a theoretical and experimental study on the effect of fibre tension profiles during manufacture on the residual stresses found in thermoplastic composite tubes (G/PP and C/PEEK). Results showed that lower residual stresses (divided by two) were obtained when increasing the fibre tension during the process compared to a constant fibre tension. When a thermoplastic composite tape is laid, stress relaxation may occur due to the viscoelastic nature of the thermoplastic matrix [174] and may reduce the fibre pre-stress introduced. Considering a constant tape tension during the process, as more and more tapes are laid, through the thickness differences in relaxation occur during the process as the viscoelastic behaviour is time dependent. Therefore, a high residual stress gradient is obtained through the thickness. However, if we increase the tape tension during the process, it compensates the time dependent relaxation and induces lower residual stresses profiles. This also means that if one were able to control this tape tension parameter, it might be possible to adjust it for specific applications, and take advantage of it, i.e. for cylinders subjected to internal or external pressures.

In our case, the tape tension throughout the process was constant and resulted in high residual stresses, as shown in Figure 98.

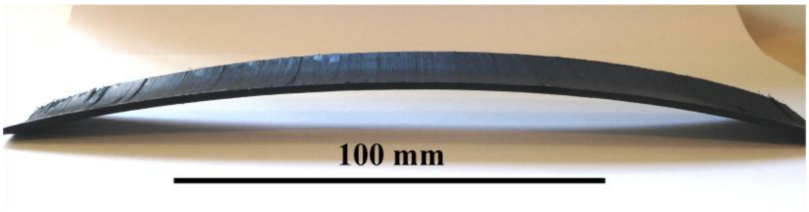

Figure 98 : Residual strains observed on the composite panel manufactured by LATP after cutting

It is clear from this figure that the specimens obtained from LATP are not flat and that the residual stresses cannot be neglected. Polyamides are known to be highly viscolelastic materials [175], [176] and this could greatly affect the residual stresses. From the curvature that is identified on this specimen, it possible to calculate the residual strain using the formula presented by Qureshi [34], Eq. 48.

$$\varepsilon_r = \frac{2t}{2\rho} \qquad \text{Eq. } 48$$

Where t is the thickness of the laminate and ρ the radius of curvature. The residual strain was estimated to be equal to 0.38%. The transverse tensile strain at failure obtained on specimens tested under tension was 0.5%. Therefore, this shows that the residual strain in the laminate could greatly reduce its strength.

Since the composite panels manufactured by LATP were not flat, the flexural strengths at failure that were presented may not be accurate. The method used to calculate the bending strength considers flat beams, which is not the case here. It would be interesting to conduct a study on the effect of curvature on the flexural properties in order to quantify this effect.

To conclude, controlling the fibre tension and its effect is an important challenge, when working with thick thermoplastic composites, which, when coupled to through thickness crystallinity differences, must clearly be considered when designing with these materials.

4. Conclusion

The effect of processing conditions was investigated in this chapter. First, emphasis was placed on the effect of cooling rate on the degree of crystallinity. It was found that the latter decreased by 10% when decreasing the cooling rate from 2°C/min to 50°C/min. Then, several models were used in order to accurately describe the non-isothermal crystallization kinetics in neat and reinforced PA6. Results showed that Mo’s theory could be used to accurately describe the kinetics.

Then, several panels were manufactured by thermo-compression at different cooling rates. Panels containing different degrees of crystallinity were obtained and transverse tensile tests were conducted in order to quantify the effect of crystallinity on the mechanical properties. It was found that the latter had no effect on the mechanical properties for cooling rates ranging from 1 to 20°C/min.

Finally, several composite panels and rings were manufactured by Laser Assisted Tape Placement. The induced microstructure was investigated and showed that the composite parts obtained had a very low void content. For thick composite rings a crystallinity gradient was observed through the thickness because of the non uniform cooling rate occurring in such processes. Then, several mechanical tests were performed which revealed a much lower strength than the composite panels manufactured by thermo-compression. These differences were not associated with differences in microstructure. However, it was found that in the case of composite panels manufactured by LATP, the two faces of the specimens were not initially subjected to the same loadings. The difference was associated with a significant residual stress level induced by the process itself.

Therefore, the work presented in the next chapter is mainly focused on the development and the effect of environmental conditions on the residual stresses.

Chapter 6

Build up of residual stresses during manufacture and relaxation induced by water ingress

---

The aim of the current chapter is to investigate the residual stresses that are created during processing of thermoplastic matrix composites as well as the effect of environmental conditions (temperature and humidity).

First, a novel strain measurement technique has been used to study the residual strain development during the processing of unidirectional C/PA6 panels by thermocompression. The effect of temperature and water ingress on the residual strain relaxation has been investigated. This has allowed us to monitor the residual strains during the entire lifetime of the composite panel. Then, asymmetric laminates were manufactured by thermocompression and an extensive experimental study was performed to study the effect of both temperature and water aging on the residual stresses. Finally, the residual strains found in composite *rings of different thicknesses (from 2 to 12mm) manufactured by Laser Assisted Tape Placement were measured and discussed.*

It should be noted that most of the work presented in this Chapter was conducted at The University of Tennessee in Knoxville, USA and is the result of a strong collaboration with Professor Dayakar Penumadu and Nathan Meek.

1. Monitoring residual strains using integrated continuous fibre optic sensing

1.1. Introduction

Carbon fibres possess highly anisotropic thermal behaviours such as high shrinkage in the radial direction relative to the longitudinal direction. This difference in shrinkage, combined with the mismatch in the coefficient of thermal expansion (CTE) of the matrix, results in the development of unavoidable residual stresses [177].

Understanding the causes of residual stress formation and their effect on the mechanical properties are of great importance. They are formed during cooling from the melt or cure temperature down to the service temperature. Larger temperature differentials lead to higher residual stresses. Various past studies in the published literature have employed the use of non destructive [64], [178] and destructive testing [51], [179] to evaluate the presence and magnitude of residual stresses found in composite materials.

Over the past few years, composite materials have started replacing metal parts in several industries such as in aviation, automotive, and offshore applications. These materials are particularly of interest in offshore applications because of their corrosion resistance and strength-to-weight ratio. Unfortunately, composite materials are known to be sensitive to delamination failure mechanisms, which have a significant impact on the lifetime of composite parts especially in corrosive environments such as seawater. To maximize their use in high stress environments, it is essential to optimize manufacturing processes to reduce residual strains induced during production and to have the ability to monitor stresses and/or strains during the use of the composite in service. Traditionally strain measurements are made with strain gauges. Strain gauges have been used for many years to measure strains during mechanical testing on material specimens and structures, however, they have significant drawbacks. They are highly sensitive to placement on orthotropic materials which can lead to errors in data collection depending on the user [180]. In addition, strain gauges only offer measurement at a single location and therefore, for entire part mapping, several strain gauges are required. The use and implementation of strain gauges is also quite laborious and cumbersome due to cabling especially if more than one is required. Industries have begun switching to digital image correlation (DIC) for on-specimen mapping or the use of embedded fibre optics to measure strain [181].

Fibre optic cables have been utilised for strain and temperature monitoring for several decades but have seen a rise in application in recent years [182]. Traditional fibre optic sensing techniques employ Fibre Bragg Gratings (FBG) to measure at a single or a series of discrete point sensors engraved along the length of an optical fibre. Optic fibres offer the advantage of multiple points of measurement instead of a single point, which can lead to entire part monitoring or mapping. Regarding composite materials these sensors can be imbedded inside laminated parts and monitor internal strain. This technology has been applied to thermoplastic and thermoset composites to measure internal strains during manufacture and for structural health monitoring [183]–[185].

The unique approach described here, termed High Definition Fiber Optic Sensing (HD-FOS), avoids the need to etch individual gratings into a fibre, providing a truly distributed measurement continuously along the optical fibre. This allows the sensors to be manufactured from relatively inexpensive telecommunication grade optical fibre composed of a germanium doped fused silica core, a fused silica cladding, and an outer polyimide coating. Sensors are lightweight, flexible, and minimally invasive, making them ideal for embedding in composite materials during manufacturing. Other properties of optical fibre, such as immunity to RF/EMI (Radio Frequency/ElectroMagnetic Interference) and excellent fatigue lifetime, make them adaptable for use in many other strain and temperature sensing applications. Sensors can be tens of meters long with sensing points reported approximately every 1mm along the entire cable. Significant work has been completed in adapting this HD-FOS technology for thermoset composite materials [186]–[192], however, little work has been performed to date on the implementation into thermoplastic composite material manufacture or structural health monitoring.

This study presents the use of fibre optics to measure the internal strains that develop during manufacture of a thermoplastic matrix composite by compression moulding and subsequent monitoring of residual strains during water ingress. This technique demonstrates the measurement of internal stress/strain during the entire composite life-cycle using a single fibre optic system.

1.2.Results

1.2.1. Accuracy of the fibre optic system – Correlation with DIC

Before manufacturing applying embedded fibre optic sensor during the manufacturing of a composite panel, the accuracy of the fibre optic sensor was checked. To do so, a simple tension test (five load-unload cycles) was conducted. A fibre optic sensor (LUNA fibre) was bonded on one side an unidirectional specimen (shown on Figure 99). The strains obtained were then compared to the strain values obtained on the other side of the specimen using DIC.

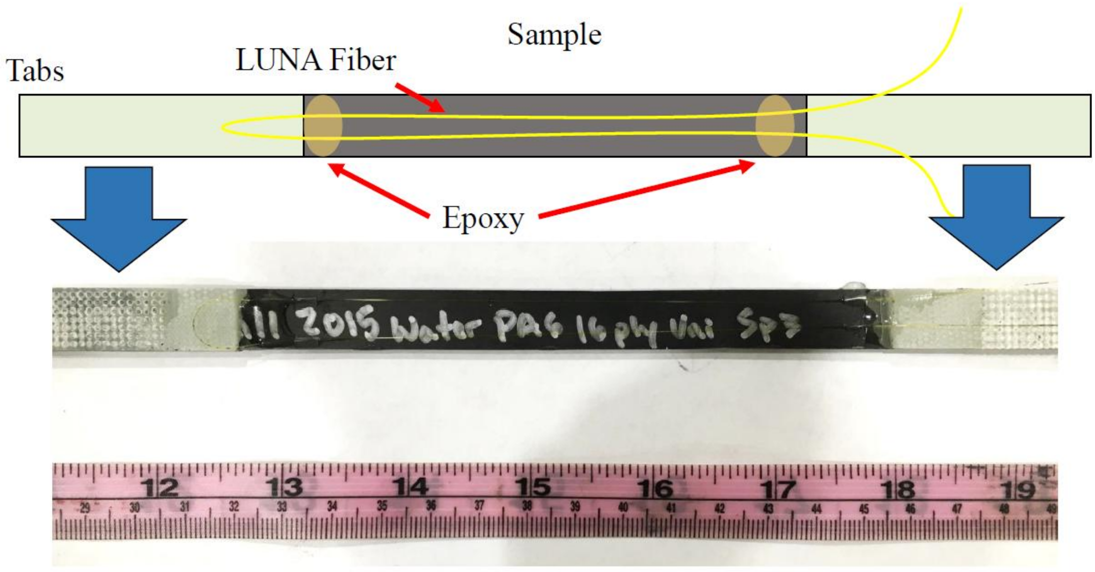

Figure 99 : Fibre optic sensor bonded to the unidirectional C/PA6 specimen

The evolution of strain as a function of time is presented in Figure 100.

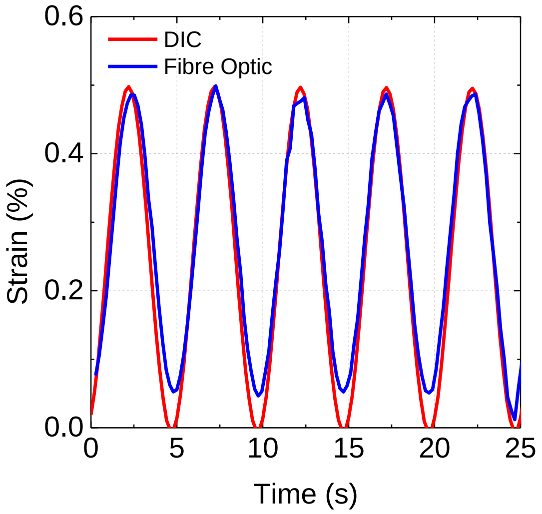

Figure 100 : Cycling tests comparing fibre optic sensor and DIC

These results show that the embedded fibre sensor provides correct data compared to traditional surface measurements during a controlled tensile loading, however, there is a small mismatch when the cyclic loading nears 0% strain. The cycling test also shows that the fibre is also accurate when investigating the fatigue life, but that is not the purpose of the current work. These results show that the strains experienced by the fibre optic sensor are very similar to those obtained with the DIC measurements, except at low strain values. Therefore, these fibre optic sensors can now be used to follow the build up of residual strains during the processing of thermoplastic composite panels.

1.2.2. Data treatment

Unidirectional composite panels were manufactured by hot compression moulding. The C/PA6 panels were manufactured at 230°C with a pressure of 5 bar, as presented earlier in Figure 17.a. A Carver 4531 press was utilized to manufacture the composite panels. Temperature profiles were monitored using external thermocouples. Three panels were manufactured following this cycle, two panels with water cooling (50°C/min) and one panel with air cooling (15°C/min).

However, for each panel that was manufactured, the entire fibre raw data analysis was complicated due to noisy data from the bend regions in the fibre optic, Figure 101.a. At each corner in the fibre optic layup, the microstrain was significantly higher relative to adjacent sections indicating that compression in the corners was causing spikes in the data. Therefore data from these sections were removed, so that they would not affect the data analysis for the 0, 45 and 90° sections, Figure 101.b.

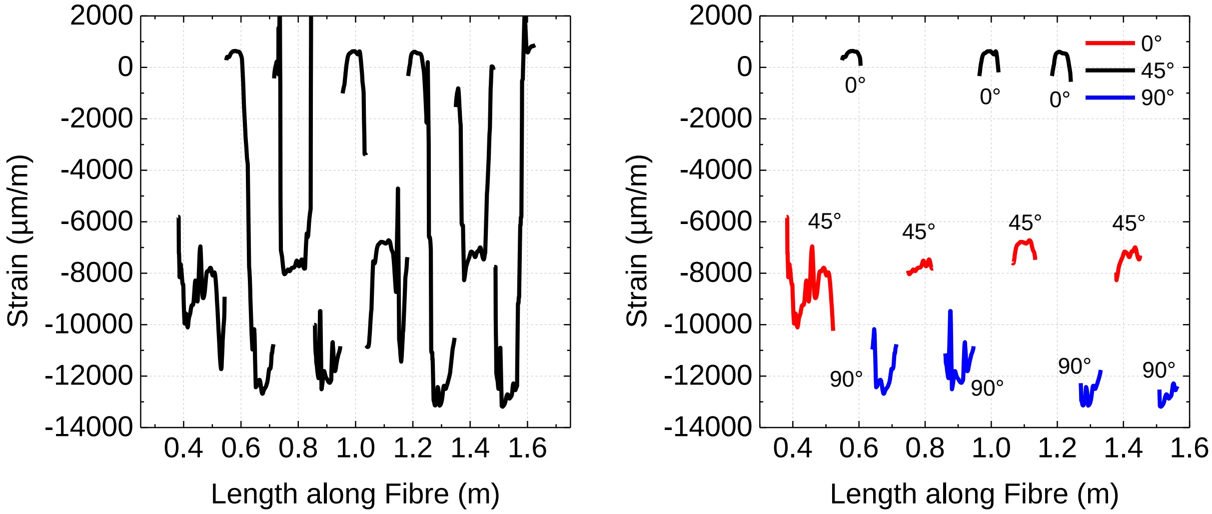

(a) (b)

Figure 101 : Fibre optic data along the length of the fibre (a) Raw Data (b) Data after removing the corners values

This data treatment allowed us to define each segment at 0, 45 and 90° along the length of each optical fibre that was used to monitor the residual strains during processing.

1.3.Discussion

1.3.1.1. Evolution of residual strains along different directions

As stated earlier, three different unidirectional panels were manufactured. Here, an example of the evolution of strain during processing is presented in Figure 102 for the first unidirectional panel that was manufactured. Results concern the strains along the fibre direction (0°) and transverse to the fibre direction (90°). Several regions corresponding to different stages during the process are identified (numbered from 1 to 6) and explained afterwards.

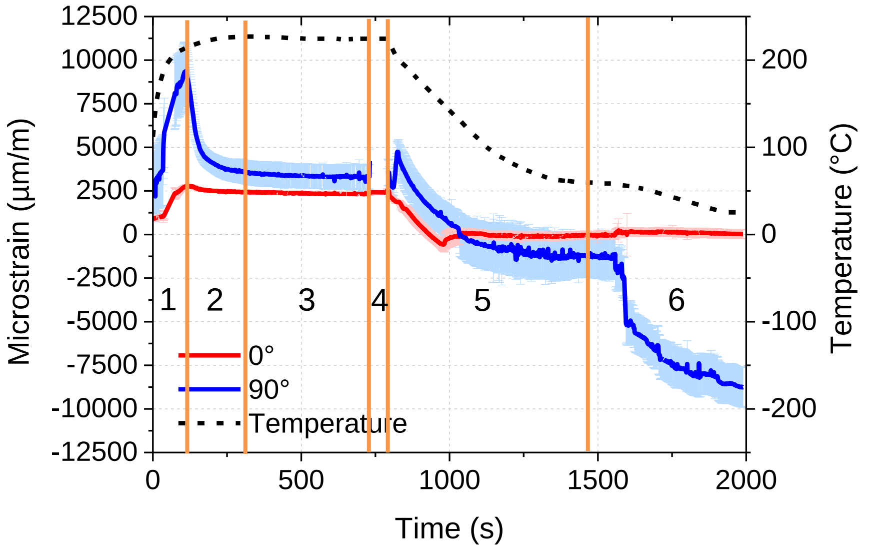

Figure 102 : Evolution of strain during processing

In Region 1, the mould is heating up to the desired temperature (230°C). It can be seen that the strains are increasing both in the longitudinal and transverse direction. Concerning the longitudinal direction, the increase in strains is only due to the increase in temperature. For each increment in temperature (each degree), the fibre is expected to see approximately 10 microstrains. Therefore, for 230°C, the fibre is supposed to see approximately 2100 microstrains (ambient temperature, 25°C°), which is the case here. In the transverse direction, the strains are much higher because the matrix is not melted yet and the fibre is bonded to the 8th ply using an epoxy resin. Therefore, this significant increase in transverse strains is only due to the transverse coefficient of thermal expansion.

In the second region, the mould is now at the desired temperature (230°C), which is above the melting temperature of the polyamide 6 matrix. Therefore, the polyamide 6 matrix starts to melt until it reaches equilibrium when the polyamide 6 matrix is completely melted. This behaviour is seen for strains in the transverse direction (blue curve) but also slightly observed in the longitudinal direction (red curve). In this stage, because the matrix is melted, no mechanical strain is transferred to the fibre optic.

In the third stage, the polyamide 6 matrix is now completely melted. The remaining strains observed in the transverse direction are above 2300 microstrains (strains due to temperature in the longitudinal direction). Therefore, these strains are not only due to temperature. Also, along the length of each 90° (and 45°) fibre, a strain gradient is observed from the edge to the centre of the panel and this is responsible for the standard deviation observed here.

In the fourth stage, the pressure (5bar) is now applied and results in a slight increase in strains. It can be seen that some measurements are missing during this stage.

Once the pressure has been applied, the cooling stage begins (region 5) and the strains start to decrease along with the temperature. Around 150°C, the solidification occurs and the residual strains start to develop. It is worth noting that these residual strains are negative because of the thermal contraction upon cooling occurring in the fibre and matrix.

Finally, the sixth and last region corresponds to the end of the cycle where the panel is removed from the mould. This stage can be divided into three sub regions that are presented in Figure 103.

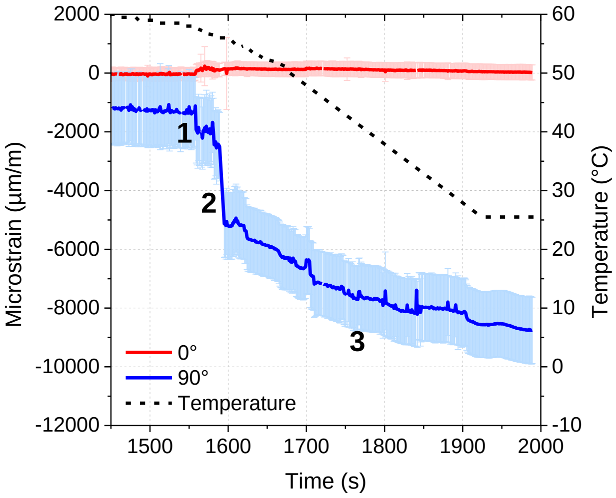

Figure 103 : Final stage of the process – Removing the panel from the mould and induced residual strain development

The first sub stage corresponds to the pressure release inside the press, and results in a slight increase in residual strains (slightly less than 1000 microstrains). The second one, corresponding to the demoulding stage (when the panel is extracted from the mould), results in a much higher increase in residual strains (3000 microstrains). The last stage corresponds to the evolution of strains when the panel has been completely removed from the mould. It is interesting to note that the residual strains are still developing inside the panel but these are mainly due to the decrease in temperature that is observed. Once the temperature stabilizes, the residual strains stabilize. The increase in residual strains for this last stage is approximately 4000 microstrains.

For the three panels that were manufactured, the different stages were identified as well as the residual strains along several directions and the associated standard deviation. For each panel, the final residual strains in the 0, 45 and 90° direction are now given in Table 23. It is worth noting that the strain evolution presented in Figure 102 and Figure 103 account for both the mechanical strains and the strains induced by temperature only. However, at the end of the process, since the panel is back at ambient temperature, no correction is needed.

Table 23 : Residual strains after moulding obtained from different unidirectional panels manufactured with fibre optic sensors

Panel N°	**0° strain (µm/m)**	**45° strain (µm/m)**	**90° strain (µm/m)**
Panel 1	21 ± 259	-5915 ± 1560	-8758 ± 1130
Panel 2	1 ± 138	-7892 ± 3886	-10281 ± 1191
Panel 3	444 ± 243	-7859 ± 839	-12141 ± 728
Mean	155 ± 250	-7222 ± 1132	-10393 ± 1694

These results show that the residual strains are strongly dependent on the fibre optic orientation relative to the carbon fibres. Along the 0° direction, almost no residual strains are observed at the end of the process. In the case of unidirectional carbon fibre reinforced composites, the longitudinal coefficient of thermal expansion is usually considered negligible, which is in accordance with the results presented here. However, concerning the other two orientations (45 and 90°), higher levels of residual strains are observed.

The mean residual strain value along the 90° direction for the three panels is approximately 1%, which is higher than the transverse failure strain of such laminates and this value seems quite significant. However, it should be noted that two out of three panels were cracked after removing them from the mould, indicating high levels of residual stresses were generated. In a similar study, Mulle et al. [59] monitored the residual strain development in glass/polypropylene unidirectional laminates using Fibre Bragg Gratings. They obtained residual strain values at the end of the process in the transverse direction close to 0.5%, which was also higher than the transverse failure strain of such laminates.

Also, it is interesting to note that for the three panels, most of the residual strains, approximately 80% of the total, developed after the demoulding stage. Therefore, the type of mould and the extent to which it blocks ply movement will play an important role in the residual strain development, as highlighted several times in the literature [178].

In this section, we have shown that significant levels of residual strains were identified along the transverse direction and that the nature of this high value is not clearly identified. Usually, the residual strain development is predicted from the crystallization temperature down to the service temperature using a simple thermo-mechanical relationship that links the coefficient of thermal expansion α to the temperature differential ΔT, Eq. 49.

$$\varepsilon = \alpha . \Delta T \qquad \text{Eq. 49}$$

The next section will focus on the effect of environmental conditions (temperature and humidity) on the residual strain relaxation. First, the effect of temperature is considered and allows us to study the strain relaxation due to temperature only. This also allows us to determine the transverse CTE of the panel. In this way, the residual strain prediction can be made and compared to the experimental residual strain. Then, the effect of water ingress and the induced strain relaxation is investigated. It is worth noting that no previous studies on residual strain relaxation due to water ingress using embedded sensors have not been found in the literature concerning thermoplastic composites, even though some results exist for thermosets [193].

1.3.2. Environmental effects on the relaxation of residual strains

1.3.2.1. Effect of temperature

In this section, the effect of temperature on residual strain is investigated by performing strain measurements at different temperatures. The tests were conducted on Panel 1 and the results obtained at presented in Figure 104 and only concern the strains along the transverse direction. Also, the results presented here take into account the correction of strain induced by temperature only (approximately 10 microstrains per degree Celsius).

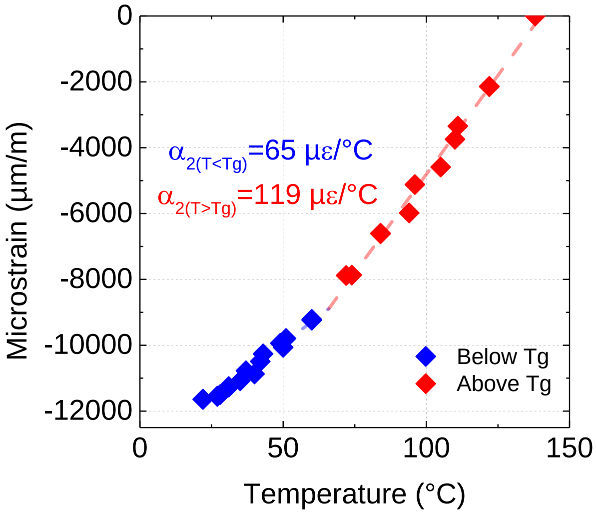

Figure 104 : Residual strain relaxation with temperature and measurement of the transverse CTE

First these results allow us to show that the 10 000 microstrains obtained at the end of the process can be totally relaxed by increasing the temperature. Then, two different slopes are identified, corresponding to the transverse coefficient of thermal expansion below and above the glass transition temperature. It should be noted that the intercept corresponds to the dry value of T_g measured by DMA (tan δ peak) around 66°C.

In the previous section, the residual strain development after demoulding was associated with the associated decrease in temperature (approximately 4000 microstrains). At this stage, the temperature of the panel was 55°C (Figure 103). However, considering the transverse CTE below T_g and the temperature differential (from 55°C down to 25°C), the induced residual strain should be around 2000 microstrains using Eq. 49. Therefore, only half of the residual strain is due to the temperature differential and the residual strains in the unidirectional panels cannot be predicted using a simple thermomechanical law. Similar conclusions were found by Mulle et al. [59] for glass/polypropylene panels.

Now that the effect of temperature has been investigated, we will focus on the effect of water on the relaxation of residual strains.

1.3.2.2. Effect of water ingress

Panel 3 was immersed in deionised water at 40°C. The weight of the panel was recorded periodically during immersion until it reached complete saturation. The changes in residual strains induced by water aging along the different directions (0, 90 and 45°) are presented in Figure 105 and plotted as a function of the square root of time divided by the panel thickness. It should be noted that the effect of water on the fibre optic alone has not been studied; however, it is thought that it is not sensitive.

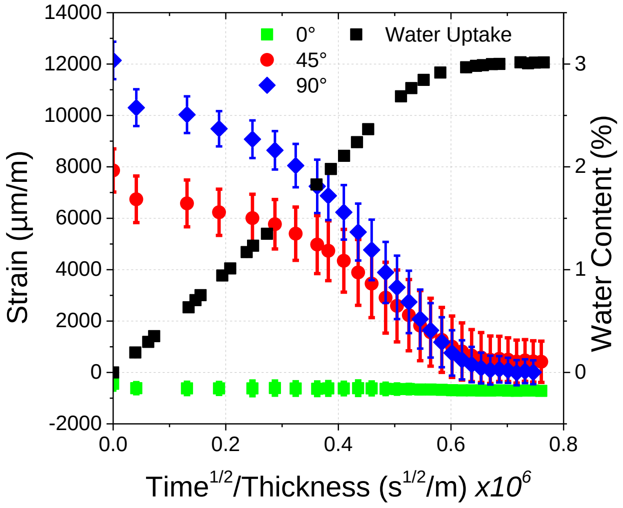

Figure 105 : Relaxation of residual strains induced by water ingress

These results show that when the panel reaches full saturation, the residual strains along the 45 and 90° directions are completely removed. Along the 0° direction, no evolution in residual strains is observed, carbon fibres are insensitive to water.

It may be noted that immediately after immersion, the residual strains along the 90 and 45° directions decreased slightly (by almost 2000µstrains along the 90° direction). This decrease is related to the increase in temperature from 25°C (ambient temperature) to the water temperature (40°C) as seen in Figure 104.

Contrary to the temperature measurements, it is not possible to determine the coefficient of moisture expansion from this result. To measure the latter, one would need to fully saturate panels at different levels of humidity. However, such a study would be very long, as saturating a 2mm thick panel at a certain level of humidity would take more than 5 months.

1.4. Conclusion

In this section, the development of residual strains has been monitored using a novel strain measurement technique applied during the processing of unidirectional C/PA6 panels. The original layout (shamrock shape) allowed the measurement of strain along all the principal directions during processing (0, ±45 and 90°). The fibre optic sensor has proved to be sensitive to all the changes occurring during the process. Results showed that very low residual strains are obtained along the fibre direction and that high levels of residual strains are obtained in the transverse direction. This is an important finding, as it suggests that processing conditions must be optimized to limit the development of these strains.

Then, environmental conditions have been shown to have a major effect on the residual strains. First, it was possible to totally relax the residual strains by increasing the temperature. Second, it was shown that when a panel immersed in water reaches full saturation, a complete residual strain relaxation is also observed. These results represent a unique set of data as similar results have not been found in the published literature for thermoplastic composites.

All these aspects showed that it is possible to use optical fibre sensors to monitor both the residual strains induced by processing and also the strain relaxation induced by environmental conditions. The magnitude of the effects indicated that it was important to study them in more detail, so a second more global technique was then applied, using asymmetric laminates.

2. Effect of environmental conditions on the residual stresses found in asymmetric laminates

2.1.Introduction

One simple technique that is commonly used to investigate the development of residual stresses is the curvature development in asymmetric laminates [0/90] [178]. Due to the thermal anisotropy between these two fibre directions, a bending moment is created upon cooling because the 0° plies impose a constraint on the 90° plies. The overall laminate curvature results from the induced residual stresses in these laminates. Various studies have examined the degree of curvature during cooling in thermoset composites [65]–[67], [194], [195] and in C/PEEK laminates [53], however, only a few studies have been published concerning other thermoplastic composites. Two studies were conducted on C/PEI [196] and C/PES [195] laminates but asymmetric C/PA6 laminates have received little attention to date.

There are environmental factors that affect residual stresses or strains in composite materials such as final service temperature and water uptake or aging. The lower the service temperature, the higher the residual stresses and vice-versa [53], [196]. Therefore several researchers have investigated this effect, principally to determine the stress free temperature, i.e. the temperature at which residual stresses start to develop [65].

There has been less emphasis placed on the effect of water aging on the residual stresses and therefore little information is presently available. Most of the work reported concerns carbon/epoxy laminates [68]–[70], [194], however, we have found no results for the effect of water aging on the residual stresses in thermoplastic composites.

Investigating asymmetric laminates and the effects of environmental conditions is of particular interest here, because an asymmetric lay-up will be used in the next chapter for manufacturing thick composite cylinders $[0/90_2]$.

This section discusses the effect of environmental conditions on the residual stresses found in C/PA6 asymmetric laminates. The effect of temperature is evaluated and the stress free temperature T_{SF} was determined. In addition, the effect of water absorption and desorption processes were investigated. Three different asymmetric laminates, $[0_2/90_2]$, $[0_4/90_4]$ and $[0_8/90_8]$ will be discussed with associated thicknesses of 0.5, 1 and 2mm, respectively.

2.2.Results and discussion

The effect of temperature on the curvature present in asymmetric laminates was investigated on 1mm thick coupons. Following this, the effect of water was studied in detail on laminates with thicknesses of 0.5, 1 and 2 mm conditioned at 21°C.

2.2.1. Effect of temperature

The aim of this first section is to determine the stress free temperature (T_{SF}), i.e. the temperature at which the residual stresses and strains start to build-up in the laminate. To measure this, three 1mm thick asymmetric coupons were placed in an oven and the curvature measurements were performed at several temperatures until the specimen were flat. Curvature measurements were made through a glass window and the evolution of curvature as a function of temperature is presented in Figure 106.

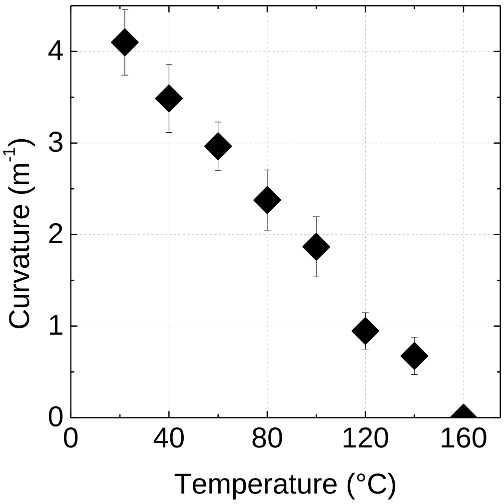

Figure 106 : Evolution of curvature with temperature

These results show that the decrease in curvature is linear with temperature and the stress free temperature is found to be 160 ± 0.5°C. It is interesting to note that this value does not correspond to the value of T_g (66°C in the dry state) but rather to the crystallization onset temperature, as highlighted previously by Jeronimidis [53] in the case of C/PEEK asymmetric laminates. In the present study, the T_{SF} value corresponds to the crystallization temperature presented in Chapter 5 for a cooling rate of 50°C/min, which corresponds with the manufacturing cycle. This temperature can then be used to predict the levels of curvature present in asymmetric laminates.

In addition to elevated temperature measurements, others were conducted below the ambient temperature and these resulted in an increase in composite curvature, indicating the presence of higher residual stresses. This finding indicates that for a composite cylinder immersed in water at low temperatures (between 4°C to 15°C), higher residual stresses would exist and may lead to damage development.

2.2.2. Effect of water

2.2.2.1. Effect of homogeneous water contents on the relaxation

To further investigate the environmental effects on residual stresses in composite materials, water absorption is considered. To evaluate water absorption, 1 mm thick asymmetric coupons were aged under different conditions: 33%, 75% humidity and immersed in deionised water at 21°C until complete saturation. The sorption curves are presented in Figure 107. Time periods to fully saturate the laminate samples ranged from 1 to 9 months.

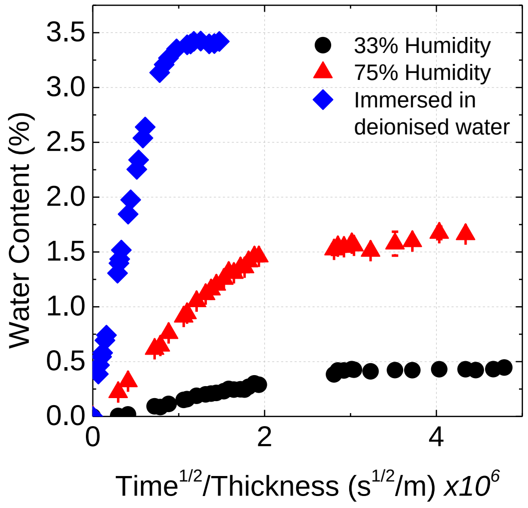

Figure 107 : Water uptake curves for specimens conditioned at 33%, 75% and immersed in deionised water

Results from water absorption show that the asymmetric C/PA6 specimens saturated under different conditions absorb different amounts of water, as information in Chapter 3 indicated. From this conclusion, it is clear that the time needed to fully saturate the different specimens depends on the water activity as the diffusion is much faster when the specimen is immersed in water compared to high humidity conditions.

As previously stated, several authors have shown that water absorption in asymmetric laminates can relax residual stresses [68]–[70]. Therefore we would expect a drop in curvature as the water content increases. The curvatures obtained as a function of water contents at saturation are presented in Figure 108.

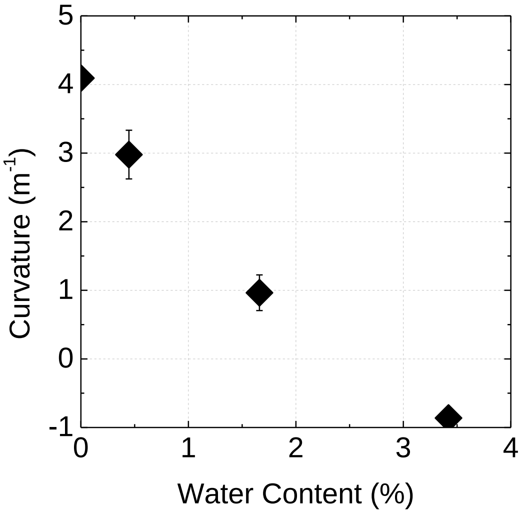

Figure 108 : Evolution of curvature with homogeneous water contents

These results show that the curvature decreases from 4.1 m^{-1} to -0.9 m^{-1}. Regarding the relaxation induced by the increase in temperature, results from curvature and water absorption demonstrate that it is possible to fully relax these residual stresses existing in these asymmetric laminates.

From curvature and water content measurements, it is possible to determine a stress free water content M_{SF} (around 3% water content) that can be used in modelling composite behaviour. Concerning the reverse curvature (negative) when the specimens are fully saturated, it may be noted that Gigliotti [65] observed similar reverse curvatures in asymmetric thermoset composites when testing the laminate slightly above their stress free temperature. Hence, the mass at saturation slightly exceeds the stress free water content and can therefore induce a slight reverse curvature.

This section considered the effect of homogeneous water contents inside the asymmetric laminates saturated in different wet conditions and demonstrated that complete relaxation of residual stresses is possible through water absorption.

The relaxation of stresses with increasing water uptake is quite interesting because information in Chapter 4 indicated that the mechanical properties decreased with increasing the water content. However, since residual stresses can be fully relaxed with water ingress, the residual stress relaxation could limit the effect of water on the mechanical properties. The next section will study the effects of water on the curvature during the sorption and desorption processes.

2.2.2.2. Sorption and desorption

The effect of homogeneous water contents inside the asymmetric laminates was considered in the previous section. Now, the effect of through thickness water profiles in both sorption and desorption will be examined for specimens of different thicknesses.

In order to shorten the time needed to fully saturate and dry the different specimens, series of sorption and desorption were first conducted on the 0.5mm thick asymmetric laminates. The results from these sorption and desorption tests are presented in Figure 109. The water content as well as the induced curvature is plotted as a function of time.

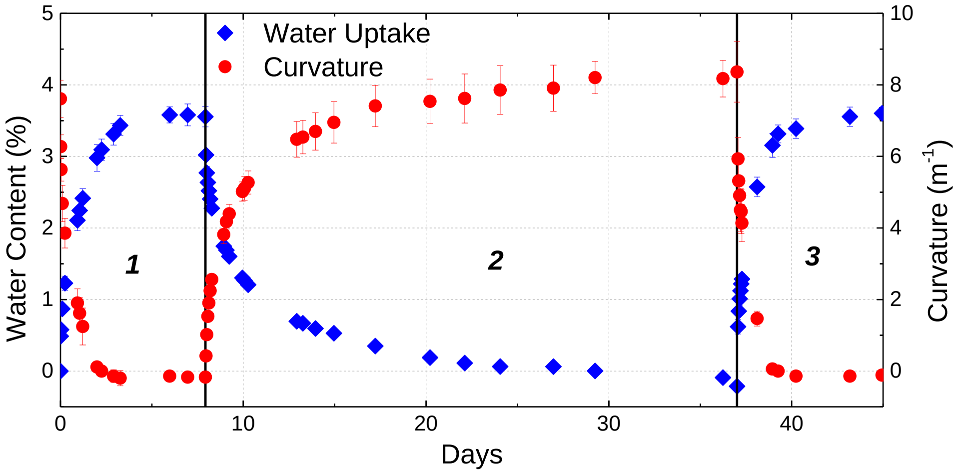

Figure 109 : Evolution of curvature and water uptake over time (1) First sorption (2) Desorption and (3) Second sorption

These results show that as the water content increases during the first sorption, the curvature decreases and drops down to zero when the coupon reaches full saturation. Then, the desorption process starts and the opposite trend is observed. As the water content decreases, the curvature increases again up to the initial dry curvature (around 8 m^{-1}). Finally, a second sorption was performed and the specimen reaches the same mass at saturation as during the first sorption (around 3.4 %). It is also obvious that the desorption process is much slower than the sorption process.

It is interesting to note that these phenomena are fully reversible, though the behaviour is quite different during sorption and desorption as the latter is much longer than the sorption process.

The evolution of curvature as a function of water content is now plotted in Figure 110 for both the sorption and desorption process for all three thicknesses of interest.

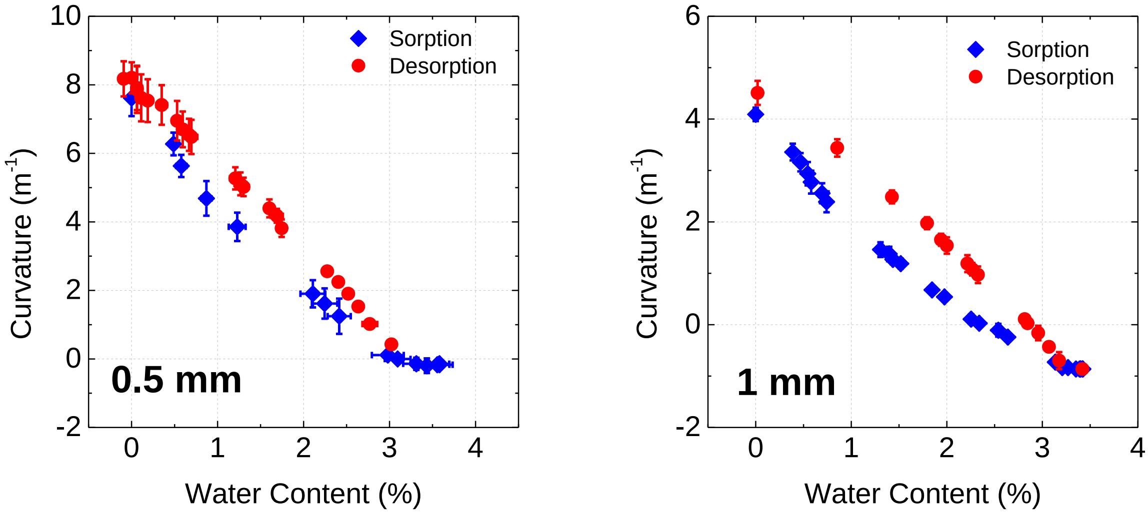

(a)

(b)

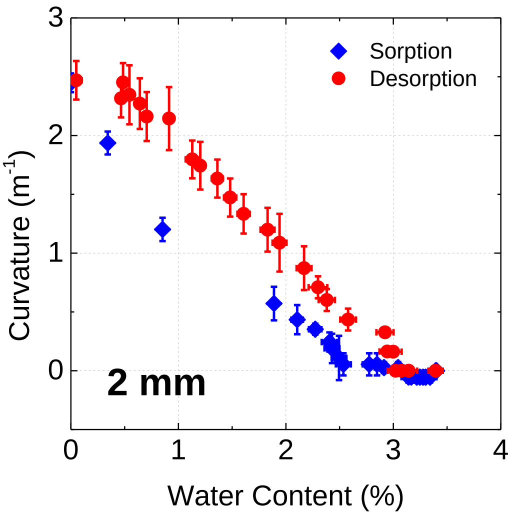

(c)

Figure 110 : Evolution of curvature with water content for sorption and desorption for (a) 0.5mm thick specimens (b) 1mm thick specimens and (c) 2mm thick specimens

For these three results, it is clear that a hysteresis is observed when conducting sorption and desorption tests. The changes in curvature as a function of water content for sorption and desorption are different. Therefore, modelling this behaviour is difficult because one needs to account for through thickness water profiles within the specimens. However, it is worth noting that for all these asymmetric laminates of different thicknesses the sorption and desorption processes are fully reversible.

2.2.2.3. Effect of residual stresses on the water diffusion

Once all the water uptake measurements had been performed on these asymmetric laminates, the model developed in Chapter 3 was used to try and describe the water uptake. However, the water diffusion in the asymmetric laminates was much faster than the prediction, even though the water content at saturation was similar. First, these differences were associated with specimens of different dimensions. For the asymmetric laminates, long specimens were used (220 x 20 x 1 mm^3) and for the unidirectional reference specimens, square specimens (50 x 50 x 2 mm^3) were used. Also, we were comparing tests conducted in Knoxville (asymmetric) and tests conducted at Ifremer (unidirectional).

Therefore, it was decided to re-conduct three new water absorption tests at Ifremer at the same temperature (21°C) with the same long and asymmetric specimens, square asymmetric laminates (50 x 50 x 1 mm^3) and square unidirectional specimens (50 x 50 x 1mm^3). In this way, the same thickness was used for all the tests. This allows us to study both the effect of specimen dimension on the water diffusion in asymmetric laminates and, the effect of layup (asymmetric and unidirectional) could also be investigated using the same specimen dimensions. The results from these water absorption tests are presented in Figure 111.

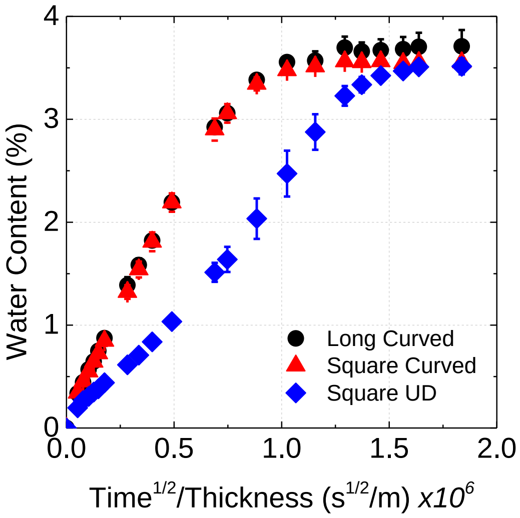

Figure 111 : Comparison of water diffusion of curved asymmetric specimens to the unidirectional reference values

The results from these absorption tests are quite surprising as the water diffusion in the asymmetric laminates is much faster than in the unidirectional reference. It should be emphasised that these were manufactured from the same prepreg material and the same fibre volume fraction of 48%.

First, it is clear that for the three tests, the weights at saturation are similar. Therefore, the differences in water diffusion that are observed are not associated with the presence of additional voids that may change the diffusion but would also affect the mass at saturation. Moreover, the standard deviation in all these tests is quite low.

For the unidirectional specimens, the behaviour described in Chapter 3 is clearly identified. At low water contents, the polymer is in the glassy state and once the polymer is in the rubbery state, an increase in diffusivity is observed. However, this behaviour is not observed on the asymmetric laminates. This result is quite surprising as these tests were performed in exactly the same conditions. Therefore, it seems that residual stresses have a strong effect on the water diffusion kinetics and that the model developed in Chapter 3 cannot be used to model the water diffusion in asymmetric composite parts. This suggests that it is essential to include stress-diffusion coupling in any prediction of the long term behaviour of multi-directional laminates of these materials. Various authors have indicated the importance of coupling (Weitsman [101], Jacquemin [103], [104], Fahmy [197], etc.) but is a complex area requiring the integration of damage mechanisms. This is being studied in another PhD study (C.Humeau).

This conclusion adds another difficulty because as stated in the introduction, particular emphasis in the next chapter will be placed on the mechanical behaviour of asymmetric [0/90$_2$] composite cylinders under high hydrostatic pressures. Therefore, the prediction of the water diffusion profiles in thick composite cylinders presented in Chapter 3 after two years of immersion may not be valid and could be very unconservative. Because of the results presented in Figure 111, it would seem that the water diffusion would be significantly faster than the prediction if similar residual stresses develop during LATP manufacture of cylinders. Therefore, additional work is needed to adjust the model to a particular lay-up, either symmetric or asymmetric. To do so, it would be interesting to conduct similar sorption tests on symmetric and asymmetric laminates with different off-axis orientations at different immersion temperatures, to compare them to the unidirectional reference.

2.3. Conclusion

In this section, the use of asymmetric laminates has allowed us to investigate the effect of environmental conditions on the residual stresses. First, the effect of temperature was considered and the stress free temperature was determined which can be used for predictions purposes. This temperature was found to be equal to 160 ± 0.5°C and corresponds to the crystallization temperature for a cooling rate of 50°C/min. Several measurements were also conducted at temperatures lower than the ambient temperature and showed that higher levels of residual stresses are obtained. Therefore, a composite cylinder immersed at temperatures ranging from 4 to 15°C would have higher residual stresses that could induce additional damages.

Then, the effect of water aging was considered, first on specimens containing homogeneous water profiles. It was shown that the residual stresses (curvature) could be totally relaxed with water ingress. Therefore, a stress free water content was suggested. Next, the desorption process was investigated and it was shown that the residual stress relaxation induced by water is totally reversible and can therefore be predicted. However, it was shown that the behaviours during sorption and desorption were very different (hysteresis) and this adds a certain difficulty to the prediction. Finally, it was shown that the water diffusion process in asymmetric laminates was much faster than the unidirectional reference, even though they saturated at exactly the same water content. Therefore, it is not possible to use the simple model developed in Chapter 3, because the latter does not take into account the change in diffusion induced by the asymmetry. Studies elsewhere are examining how to develop more complex models including stress-diffusion-damage development coupling.

From a practical point of view it is important to examine the transition from samples produced by plate moulding, to cylindrical specimens manufactured by tape laying. The next section will present the evolution in residual strains measured in unidirectional composite rings of different thicknesses manufactured by LATP.

3. Residual strains in composite rings manufactured by LATP

3.1. Introduction

Manufacturing thick composite cylinders is not an easy task. As the thickness increases, the residual stresses tend to be of a higher magnitude and several studies have shown that they can result in significant delamination through the thickness of the cylinder [44]. However, by optimising the process parameters, it is possible to lower the residual stresses found in the cylinder. For instance, Lu et al. [173] have shown that the tape tension profile during the process has a significant effect on the residual stresses in G/PP and C/PEEK unidirectional composite rings. Moreover, using the same materials (G/PP and C/PEEK), Schlottermüller et al. [198] obtained lower residual stresses when heating the mandrel to temperatures close to the crystallization temperature ($T=0.9T_c$). To optimise the different parameters, one measurement technique is commonly used to characterise the cylinder, the radial cut method. The procedure is to cut the cylinder and to record the strains that are relieved during cutting, usually by strain gauges. This method has been extensively used for thermoset [55], [199]–[201] but also for thermoplastic composites [173].

We have shown earlier in Chapter 5 that high levels of residual stresses were found in flat composite panels manufactured by Laser Assisted Tape Placement and that these might be associated with the tape tension used in the process. The aim of the current section is to investigate the evolution of residual stresses and strains with increasing the thickness of composite rings manufactured with LATP.

3.2.Results and discussion

This section describes a simple method to investigate the residual strains found in composite rings manufactured by Laser Assisted Tape Placement. To do so, strain gauges were bonded on each side of the composite rings and the residual strains were relieved by cutting radially, as shown earlier in Figure 33. The composite rings of interest were first presented in Chapter 5 and are of different thicknesses from 2 to 12mm.

The results from these radial cuts are presented in Figure 112.a for the strains at the inner surface and in Figure 112.b for the strains at the outer surface. It may be noted that all these composite rings tended to close themselves after the cutting stage.

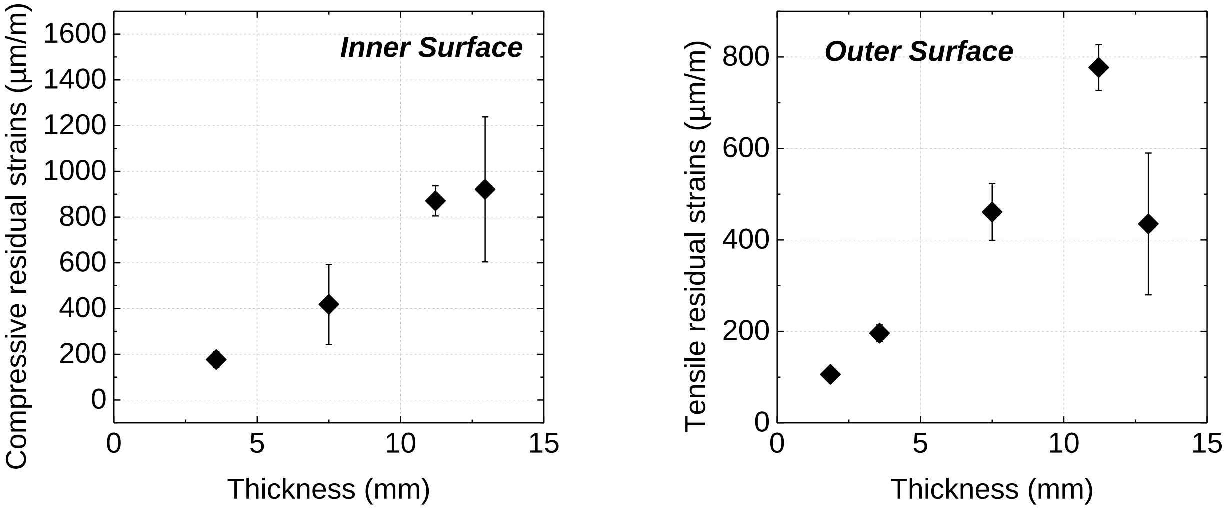

(a) (b)

Figure 112 : Evolution of (a) compressive and (b) tensile residual strains with ring thickness, LATP rings, unidirectional

These results show that when the thickness of the composite rings increases, the residual strains increase on both sides of the specimen and that the evolution is linear. It is worth noting that these strains almost reach values of 0.1%.

In order to further investigate the residual stresses in composite cylinders, it would be very interesting to conduct similar studies on composite rings manufactured with different lay-up angles, more especially asymmetric sequences.

4. Conclusion

The aim of this chapter was to investigate the residual stresses and strains that are created during processing as well as the effect of environmental conditions (temperature and humidity).

First, the development of residual strains has been monitored using a novel strain measurement technique during the processing of unidirectional C/PA6 panels. The original layout (shamrock shape) allowed the measurement of strain along all the principal directions during processing (0, ±45 and 90°). The fibre optic sensor has proved to be sensitive to the different stages of the compression moulding process. Results showed that very low residual strains were obtained along the fibre direction and that high levels of residual strains were obtained in the transverse direction. The effect of environmental conditions has also been investigated using this new fibre optic sensor. Results have shown that a complete relaxation of residual strains was possible by either increasing the temperature or by saturating the composite with water. These results are quite unique as the sensor is able to monitor the residual strain development during processing as well as in severe environments.

Then, a second approach to residual strain measurement was investigated, by following the curvature in asymmetric laminates and once again the effect of environmental conditions was examined. The effect of temperature was considered and allowed us to determine a stress free temperature of 160 ±0.5°C, which corresponds to the crystallization temperature for a cooling rate of 50°C/min. Several measurements were also conducted at temperatures lower than the ambient temperature and showed that higher levels of residual stresses are obtained, so a composite cylinder immersed at temperatures ranging from 4 to 15°C would have higher residual stresses. Second, the effect of water aging on the curvature was considered on specimens containing homogeneous water profiles. It was shown that the residual stresses (curvature) could be totally relaxed with water ingress, as for the unidirectional panel immersed in water with the fibre optic sensor. Therefore, a stress free water content was defined. In addition, the desorption process was investigated and it was shown that the residual stress relaxation induced by water ingress is totally reversible. However, the behaviour during sorption and desorption was very different (hysteresis). To model this behaviour, a water diffusion model is needed and it was shown that the diffusion model developed in Chapter 3 could not be used. Indeed, the water diffusion in the asymmetric laminates was much faster than in unidirectional C/PA6 specimens, even though they saturated at exactly the same water level. Therefore, further work is needed to adjust the model developed in Chapter 3 to asymmetric laminates.

Finally, the residual strains found in composite rings manufactured by LATP were studied and results have shown that increased levels of residual strains and stresses were obtained for higher thicknesses.

The final chapter will focus on the processing of thick thermoplastic composite cylinders manufactured by Laser Assisted Tape Placement and their mechanical properties. Particular emphasis will be placed on their resistance relative to hydrostatic pressure.

Chapter 7

Thermoplastic Composite Cylinders Manufactured by Laser Assisted Tape Placement

---

The aim of this final Chapter is to investigate the performance of thick thermoplastic composite cylinders manufactured by Laser Assisted Tape Placement subjected to high hydrostatic pressures. To do so, three composite cylinders were studied. The first one corresponds to the C/epoxy reference used today at Ifremer for Deep Sea applications (4500 meters). It was manufactured by wet filament winding at an angle of ± 55° relative to the tube axis. The two other cylinders were both thermoplastic composite cylinders. The first one was laid at ± 55° to compare with the C/epoxy reference. Then, in order to investigate the effect of winding angle, the last thermoplastic cylinder was laid at 0/±88 as this sequence should perform better than the ± 55° angle optimised for internal pressures.

First, the manufacturing parameters used to produce the thermoplastic composite cylinders are presented and the quality in terms in voids was checked for all three cylinders.

Then, mechanical tests were performed to obtain the elastic properties of the cylinders along the axial and hoop directions. Finally, implosion tests were performed on the three cylinders and the associated failure modes are discussed. This last chapter will allow us to compare the performance of thick C/PA6 cylinders subjected to hydrostatic pressures to the C/Epoxy reference.

1. Introduction

The use of composites for pressure hulls of underwater vehicles and submarines has been as ongoing research topic for many years. At Ifremer, these materials have been used since the 1990’s as stated in Chapter 1. However, applications for autonomous ocean profilers only started 5 years ago. To the knowledge of the authors, no results concerning the implosion performance of C/PA6 cylinder manufactured by Laser Assisted Tape Placement have been reported yet in the literature. This is the aim of the following chapter. Results are then compared to the C/Epoxy reference used today at Ifremer.

First, the process parameters used to manufacture the thermoplastic cylinders are presented. Then, the impregnation quality is checked and compared to the C/Epoxy reference. Finally, implosion tests were performed and the results are discussed.

2. Cylinders manufactured by Laser Assisted Tape Placement

Three different composite cylinders have been investigated. First, the C/Epoxy reference was produced by wet filament winding at a sequence of ±55° relative to the tube axis and it has a fibre volume fraction of 0.6. Second, two C/PA6 thermoplastic composite cylinders were manufactured by Laser Assisted Tape Placement at the CETIM composite facility in Nantes, Figure 113. The first was manufactured at ±55° in order to be compared with the C/epoxy reference. Then, for the second thermoplastic cylinder, an optimised sequence was used [0/±88]. It has been shown and stated several times in the literature that this sequence should perform better than the ±55° sequence when subjected to hydrostatic pressure [11], [20]. The fibre volume fraction for the two C/PA6 cylinders is 0.48, as for the composite panels manufactured by thermo-compression.

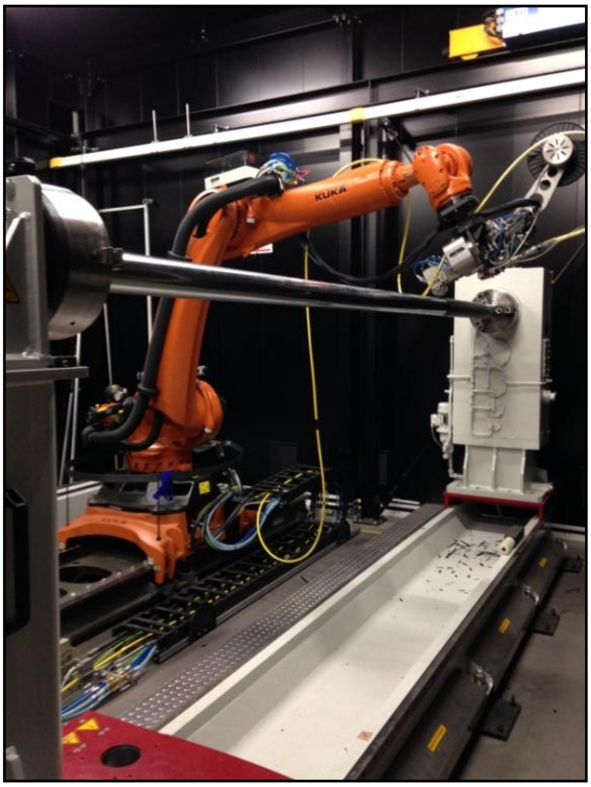

Figure 113 : Cylinder being manufactured by LATP at CETIM composite facility

The dimensions, sequence and geometry of the different composite cylinders are presented in Table 24.

Table 24 : Dimensions and geometry of the cylinders

Tube	Length (mm)	Inner Diameter (mm)	Wall thickness (mm)	Shape
C/Epoxy ±55	600	120	12.7	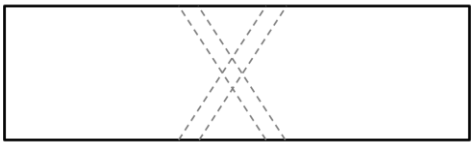
C/PA6 ±55	600	120	9.2	
C/PA6 0/±88	500	100	12.1	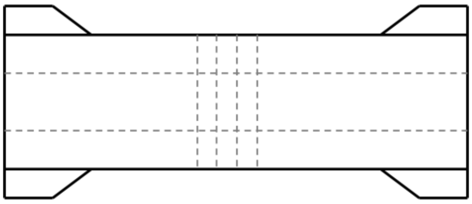

The first two cylinders were manufactured on a mandrel of 120mm diameter and the last one was manufactured using a mandrel of 100mm diameter for reasons that will be explained in section 3.1. It may be noted that the third cylinder, laid at 0/±88, was manufactured with reinforcements at the end of the cylinder to prevent failure at this location. The process parameters used to manufacture the thermoplastic cylinders are shown in Table 25. These were optimised during the PhD study for the two sequences by the CETIM.

Table 25 : Process parameters used for manufacturing thermoplastic composite cylinders

Material	Sequence	Laying speed (m/min)		Temperature (°C)	Roller pressure (bar)
C/PA6	$[\pm 55]_{31}$	18.0		280	2
C/PA6	$[0/\pm 88]_{26}$	± 88°	6.3	280	3
		0°	3.0	300	3

An example of a cylinder manufactured by LATP is presented in Figure 114.

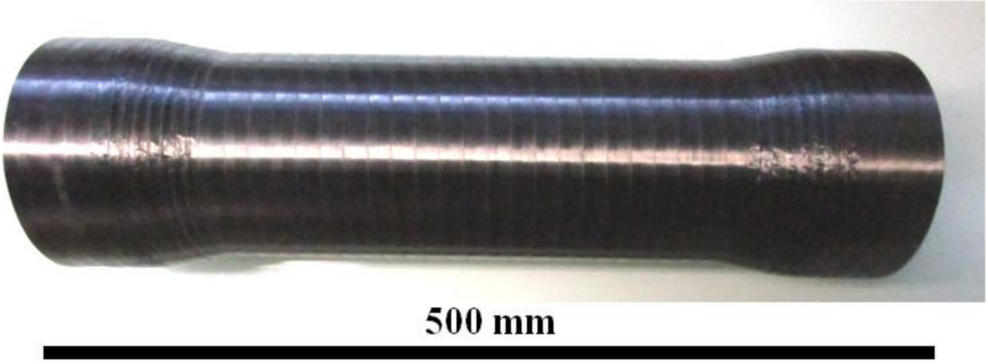

Figure 114 : C/PA6 cylinder laid at 0/±88

3. Results and discussion

3.1. Quality control

All three cylinders were first checked by Ultrasonic C-scan. This technique allows the quality of the entire length of the composite cylinders to be checked. The attenuation levels also provide a rapid indication of the overall quality in terms of voids. C-scan results are presented in Figure 115.

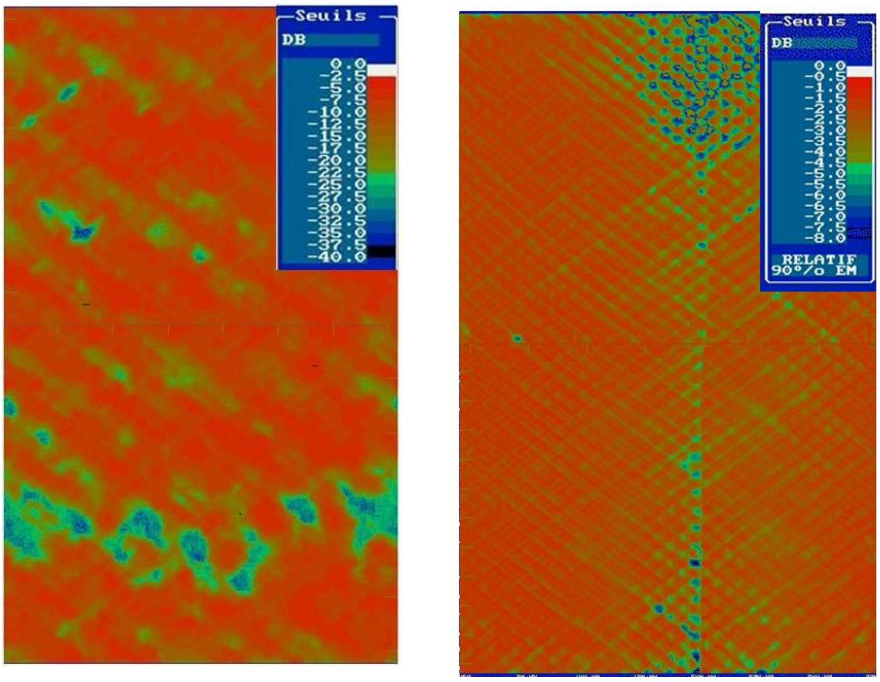

(a) (b)

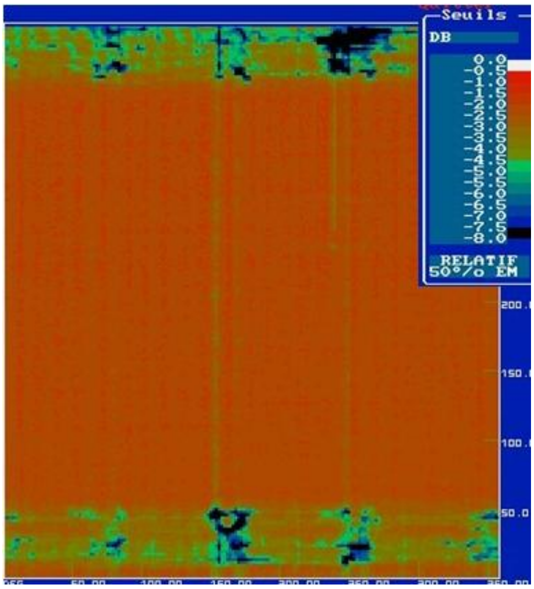

(c)

Figure 115 : (a) C/Epoxy ±55° (b) C/PA6 ±55° (c) C/PA6 0/±88

Based on experience, high levels of through thickness attenuation (over 20dB) usually correspond to the presence of a significant quantity of voids. On the other hand, low levels of attenuation (below 10dB) indicate good cylinder quality. These ultrasonic C-scans highlight two main results. First, it is shown that the C/epoxy cylinder has high localised levels of attenuation, meaning that there are defects at these locations. On the contrary, the two polyamide 6 tubes are of very good quality (the attenuation scale is much smaller, below 8dB). The voids are mostly localised at the end of the two thermoplastic cylinders (in the reinforcements for the one laid at 0/±88). Concerning the ±55° cylinder, one defect is found all along the cylinder at an attenuation value of approximately 5dB. This corresponds to the groove induced by the mandrel, Figure 116. Indeed, the mandrel used to manufacture the C/PA6 composite cylinder at ±55° is a two-shell mandrel that allows easy removal of the cylinder. This results is a shallow defect which may affect the implosion behaviour.

Figure 116 : Groove induced by the two-shell mandrel

These US inspection results show that the thermoplastic composite cylinders that were manufactured at the CETIM composite facility by Laser Assisted Tape Placement are of excellent quality in terms of voids compared to the C/epoxy cylinder processed by wet filament winding. These results were confirmed by X-ray tomography. Results are presented for the two cylinders at ±55° in Figure 117.

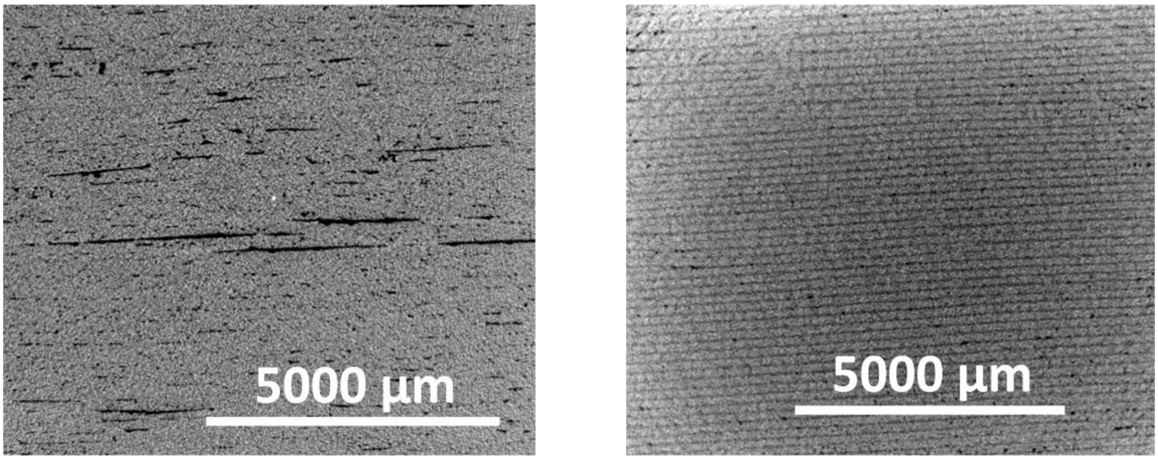

(a) (b)

Figure 117 : X-ray tomography (Voxel: 12µm) performed on the (a) C/Epoxy cylinder and (b) C/PA6 cylinder laid at ±55°

3.2.Elastic properties of the composite cylinders

3.1.1. Axial compression tests

Axial compression tests were performed on all three cylinders to obtain the elastic properties (moduli and Poisson's ratios) along the axial direction of the cylinders. Results from these tests are presented in Table 26 and are compared with the prediction calculated with laminate theory.

Table 26 : Elastic properties measured on each composite cylinder and theoretical prediction calculated using laminate theory

Tube	Sequence	Experimental		Theoretical	
		E_z (GPa)	$\nu_{z\theta}$	E_z (GPa)	$\nu_{z\theta}$
C/Epoxy	$[\pm 55]_{31}$	11.3	0.36	11.7	0.42
C/PA6	$[\pm 55]_{31}$	5.9	0.44	6.1	0.46
C/PA6	$[0/\pm 88]_{26}$	39.8	0.13	39.3	0.03

These results show a good correlation between the experimental and theoretical axial modulus and Poisson's ratio for the different sequences. Therefore, these results can be used later to predict the implosion pressures.

3.1.2. Radial compression tests

Concerning the modulus in the hoop direction, it is not possible from the radial compression test to obtain the modulus directly for thick carbon reinforced composites. As presented in Chapter 5, a finite element calculation stage is needed in which the elastic properties determined by thermo-compression are used ($E_{1compression}$, E_2, G_{12}, ν_{12}, etc.), Chapter 4. Results from the calculations are then compared to the experimental data. If the model fits the experimental results, the stiffness can therefore be predicted, for instance using laminate theory. If not, the stiffness is different from the prediction.

These calculations were performed by the CETIM on the two thermoplastic cylinders and are further discussed in Appendix I. Results showed that an excellent correlation was found between the experimental data and the model for the 0/±88 cylinder. Therefore, the modulus for this sequence can be predicted using laminate theory. However, results concerning the ±55° cylinder did not correlate with the model. Results indicated that the strains at a given load in the experimental test were much higher than those given by the model, indicating a lower stiffness. This result is quite surprising and is associated with the groove induced by the non circular model. This will be discussed later.

The Poisson's ratios were also measured in the hoop direction and results are compared to the laminate theory prediction in Table 27.

Table 27 : Poisson's ratios measured on composite rings and theoretical prediction calculated using laminate theory

Tube	Sequence	Experimental	Theoretical
		$\nu_{\theta z}$	
C/Epoxy	$[\pm 55]_{31}$	1.26	1.19
C/PA6	$[\pm 55]_{31}$	1.47	1.39
C/PA6	$[0/\pm 88]_{26}$	0.04	0.05

These results show a good correlation between the experimental and theoretical hoop Poisson's ratio for the different sequences.

3.3. Implosion tests

Once the quality and the elastic properties of all three cylinders were checked, implosion tests were performed in a hyperbaric chamber at 12 bar/min until failure. It may be noted that the cylinders were partially filled with water to limit the shock wave at implosion that can damage the pressure vessel. A composite cylinder just before implosion in the 2400 bar capacity pressure vessel is shown in Figure 118.

Figure 118 : Instrumented cylinder being lowered into the pressure vessel

As presented in Chapter 2, all these cylinders were instrumented with strain gauges in the hoop and axial direction to determine whether buckling occurred. Also, aluminium end closures were machined respecting each cylinder’s dimensions.

3.3.1. Implosion test on C/epoxy cylinder

The carbon/epoxy reference cylinder imploded at a pressure of 77.2 MPa (772 bar). The strain gauge data along the axial and hoop directions are respectively presented in Figure 119.a and Figure 119.b as a function of applied hydrostatic pressure.

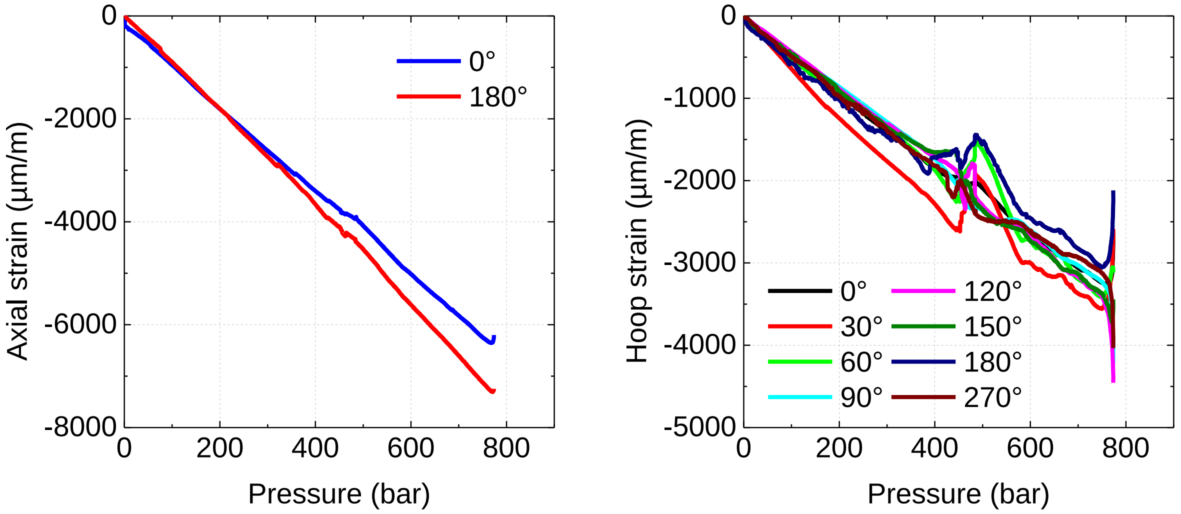

(a) (b)

Figure 119 : Example of (a) axial and (b) hoop strains for the C/epoxy cylinder

The strains at failure in the axial and hoop directions are respectively -7000 microstrains and -3200 microstrains. It is worth noting that a significant drop in hoop compressive strains occurred at approximately 500 bar, however, it had no impact on the structural integrity of the cylinder. In order to identify the failure mode of the composite cylinder (buckling or material failure), the strains were then plotted radially as a function of the hoop angle, presented in Figure 120.

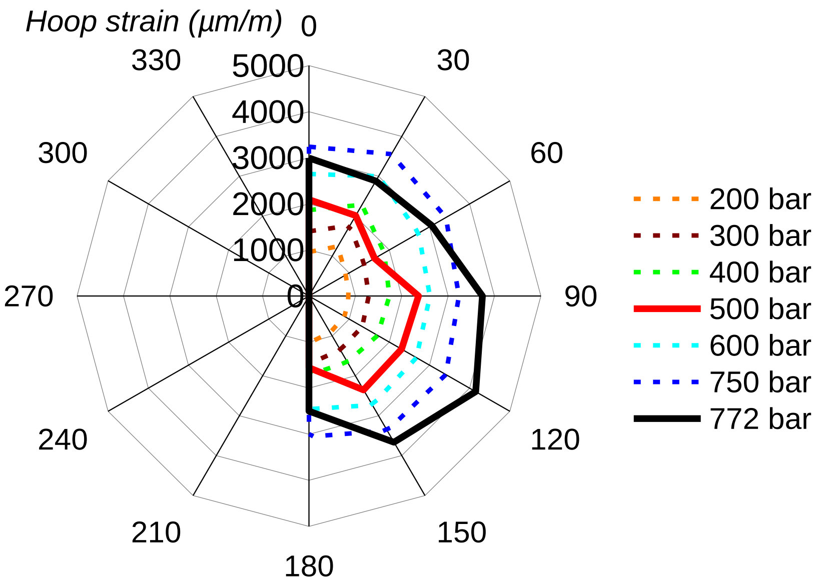

Figure 120 : Radial plot of the hoop strains in the C/Epoxy cylinder

The black plot represents the compressive strain response just before implosion. An elliptical shape is identified before failure, suggesting that the failure mode was overall buckling (mode II) of the C/Epoxy cylinder. These C/epoxy cylinders are used in applications down to 4500 meters (around 450 bars). Therefore, a safety factor of 1.7 is used when working at 450 bars compared to the implosion test pressure. This first implosion test represents the implosion pressure reference that is targeted for the thermoplastic composite cylinders.

3.3.2. Implosion test on the C/PA6 cylinder laid at ±55°

The ±55° C/PA6 cylinder was tested in the pressure vessel and imploded at 209 bar, which is much lower than the C/epoxy reference. The strain responses along the axial and hoop directions are plotted in Figure 121.

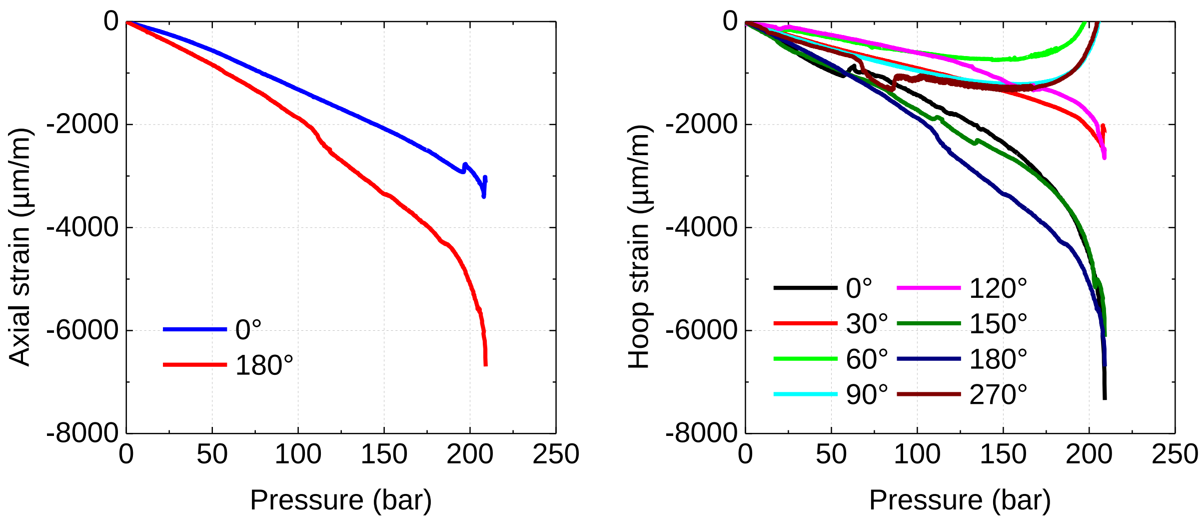

(a) (b)

Figure 121 : Example of (a) axial and (b) hoop strains for the C/PA6 cylinder laid at ±55°

Unlike the strain responses observed on the C/epoxy cylinder, considerable scatter is observed in the axial and hoop directions. The strain gauges all seem to diverge at a pressure slightly above 100 bar and the failure mode appears to be buckling which starts early in the test. The hoop strains are also plotted radially in Figure 122.

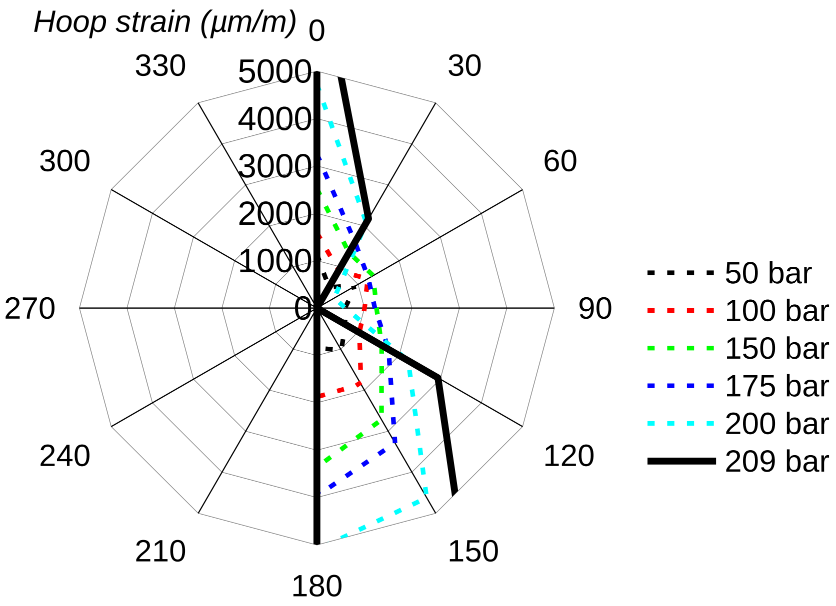

Figure 122 : Radial plot of the hoop strains in the C/PA6 cylinder laid at ±55°

From these plots, it is clear that the strains obtained for the ±55° C/PA6 cylinder are much higher (around 5000 microstrains at 200 bar) than for the C/epoxy counterpart (around 1000 microstrains at 200 bar). Even at low pressures (from 0 to 100 bar), a significant difference in strains is observed between the two cylinders, Figure 123.

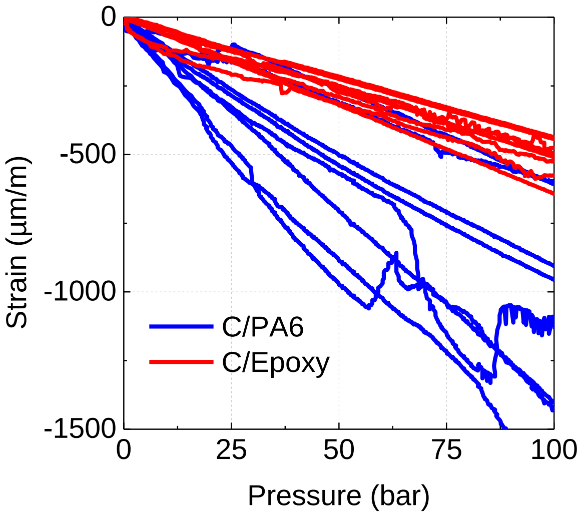

Figure 123 : Hoop strain evolution at low pressures (from 0 to 100 bar) for the C/PA6 and C/epoxy cylinders would at ±55°

Therefore, this might indicate a significant plasticisation of the matrix. It may be noted that the C/PA6 cylinder was slightly thinner than the C/Epoxy and the fibre volume content was slightly lower, however, these differences would not explain such a large difference in the implosion pressure. Several aspects might be responsible. The first one is associated with an early plasticisation of the PA6 matrix as stated earlier. There are almost no fibres in the hoop direction so matrix yielding will lead to failure. The second might be associated with the non circular/elliptical shape of the C/PA6 cylinder. Any circular variability, either circularity or coaxiality, has a strong effect on the critical buckling load [6]. These were measured on both cylinders wound at ±55° and results are presented in Table 28.

Table 28 : Concentricity and coaxiality of the composite cylinders wound at ±55°

	Mean Diameter (mm)	Cylindricity	Coaxiality
C/Epoxy ± 55°	120.30	0.02	0.20
C/PA6 ± 55°	121.34	0.54	0.62

Results show that much higher concentricity and coaxility variations are observed on the thermoplastic cylinder. These variations are related to the mandrel, but may also be affected by creep during manufacture. A third factor may be due to the two-shell mandrel used to manufacture this tube, which induces a significant groove (defect) along the length of the cylinder, as presented in Figure 116.

3.3.3. Implosion on the C/PA6 cylinder laid at 0/±88°

Due to the uncertainty on the last implosion test performed on the cylinder laid at ±55°, concerning both the low implosion pressure and the failure mode, it was decided to perform a new test in which conditions were optimised. Three changes were made: The first change was to modify the sequence to 0/±88 which should perform much better than the ±55 angle in compression. To confirm this, composite panels were manufactured by press forming with two different sequences, [±35] and [0_2/90], corresponding respectively to the hoop sequence for cylinders manufactured at ±55° and 0/±88 along the tube axis. Then, tensile tests to failure were performed on these two sequences. Results are presented in Figure 124.

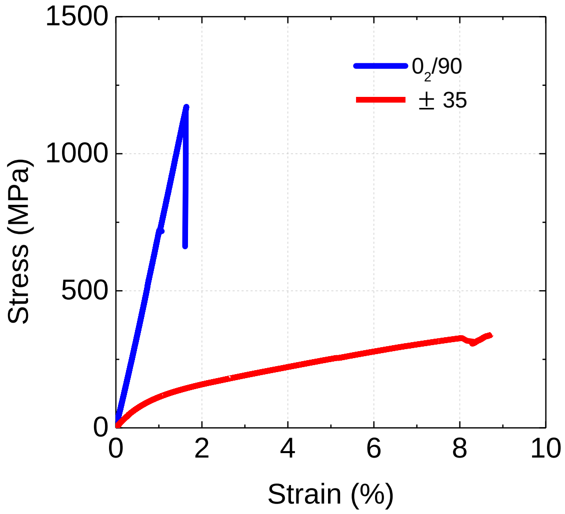

Figure 124 : Stress-strain plots of specimens which sequences at [±35] and [0_2/90]

These stress-strain plots confirm that the [0_2/90] sequence is much stiffer in the hoop direction and behaves in a much less plastic manner than the [±35] sequence, even though this result is not really surprising. However, the strain at failure for the [±35] sequence reaches values close to 9%, which shows that significant plasticisation and fibre reorientation occur, which is not observed for the [0_2/90] sequence. The properties in compression have also been measured, these will be presented and used later. The second change was to use a different mandrel, that allowed us to avoid the groove defect and also improved circularity and coaxiality. The third change was to add overlaid end reinforcements to the tube extremities, in order to limit the risk of end-initiated failure.

Then, the [0/±88] thermoplastic cylinder was tested in the pressure vessel in the same conditions as the other two cylinders. The three cylinders after implosion are presented in Figure 125.

Figure 125 : Cylinders after implosion (left) C/PA6 [0/±88] (middle) C/PA6 [±55] (right) C/Epoxy [±55]

The third cylinder imploded at a pressure of 610 bar, which is much higher than the C/PA6 cylinder laid at [±55]. The axial and hoop strain evolutions as a function of pressure are respectively presented in Figure 126.a and Figure 126.b.

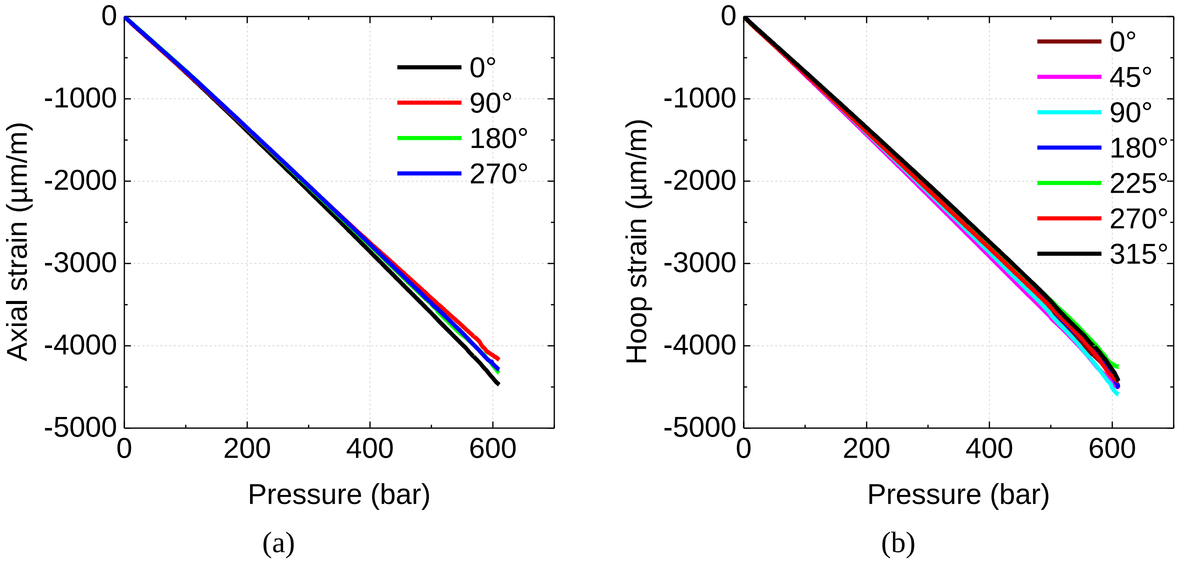

Figure 126 : Example of (a) axial and (b) hoop strains for the C/PA6 cylinder laid at 0/±88

Unlike the other two cylinders strain responses, the plots presented in Figure 126 behave in an almost perfectly linear manner until a sudden failure occurred. This would suggest that material failure occurred rather than buckling, which is confirmed by the radial plot shown in Figure 127 where the evolution of strains is perfectly circular until failure. Also, the failure strains are very similar in the axial and hoop directions, suggesting that the modified stacking sequence is effective. The hoop strains achieved are a little higher than those at failure in the carbon/epoxy cylinder which was slightly thicker.

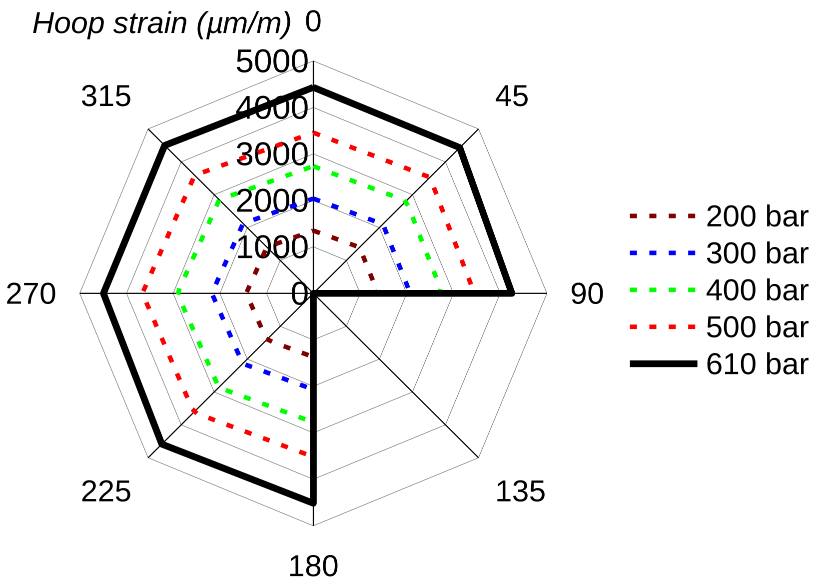

Figure 127 : Radial plot of the hoop strains in the C/PA6 cylinder laid at 0/±88

Even though it is difficult to identify the failure mode based on the cylinder's shape and appearance after implosion, kinkbanding failure was identified at several positions inside the composite cylinder. These are shown in Figure 128.

Figure 128 : Kinkbanding failure observed inside the [0/±88] cylinder

These kinkband failures suggest that material failure was indeed the predominant failure mode in this last implosion test. The next section will compare the analytical and finite element predictions with the experimental implosion results.

3.3.4. Comparison with analytical and finite element predictions

Similarly to the calculations presented in Chapter 4, the buckling and material failure criteria will be used in this section to predict the implosion pressures for the C/PA6 cylinders. These are simple calculations and are based on a number of assumptions but allow us to quickly investigate if the predominant failure would be buckling or material failure. These equations were presented in Chapter 4 but are recalled hereafter, Eq. 34 for buckling using Smith's equation and Eq. 36 for a maximum hoop stress strength criteria:

$$P_c = (n^2 - 1)\left(\frac{D_y}{r_0 r_m^2}\right) \qquad \text{Eq. 34}$$

$$P_c = \sigma_{\theta\theta} \cdot \frac{t}{r} \qquad \text{Eq. 36}$$

Concerning the buckling criteria, laminate theory was used to obtain the elastic properties based on the experimental data presented in Chapter 4. Also, it is worth noting that the equation proposed by Smith considered infinitely long cylinders. In order to account for the length L of the cylinder, Mistry's equation has also been used for comparison purposes, Eq. 50. The lengths of the cylinders that were used for the calculation were respectively 600mm and 300mm for the cylinders laid at ±55° and 0°/±88°.

$$P_c = \frac{0.807 E_\theta}{(1 - \nu_{z\theta}\nu_{\theta z})^{\frac{3}{4}}}\left(\frac{t}{r}\right)^{2.5}\frac{r}{L} \qquad \text{Eq. 50}$$

To measure the compressive properties needed for the calculations, pin-ended buckling tests were performed on the $[0_2/90]$ and on the $[\pm 35]$ specimens. A clear compressive failure was identified on the [0_2/90] specimens (Figure 129.a). Therefore, the compression strength was taken as the one that occurred at failure. However, concerning the [±35], no failure occurred during the test (Figure 129.b) and plasticisation was identified. Similarly to the tensile tests performed on the [±45] specimens, the yield stress was taken at 2% strain for the [±35] specimens.

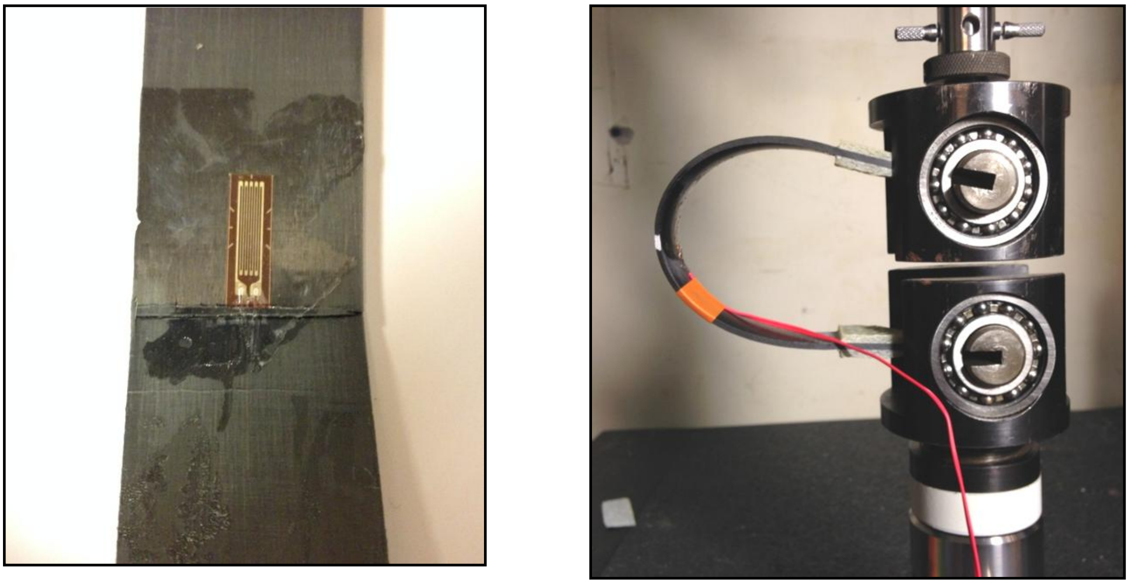

(a) (b)

Figure 129 : (a) Failure observed on the [0_2/90] specimens (b) Pin-ended buckling test performed on [±35] specimens

Results from these pin-ended buckling tests are shown in Table 29.

Table 29 : Apparent compressive strength measured on the [±35] and [0_2/90] C/PA6 specimens tested in compression

Sequence	[±35]	[0_2/90]
Compressive strength (MPa)	122 ± 26	715 ± 17

Results from the calculations are presented in Figure 130 as well as the experimental implosion pressures obtained for the two C/PA6 cylinders.

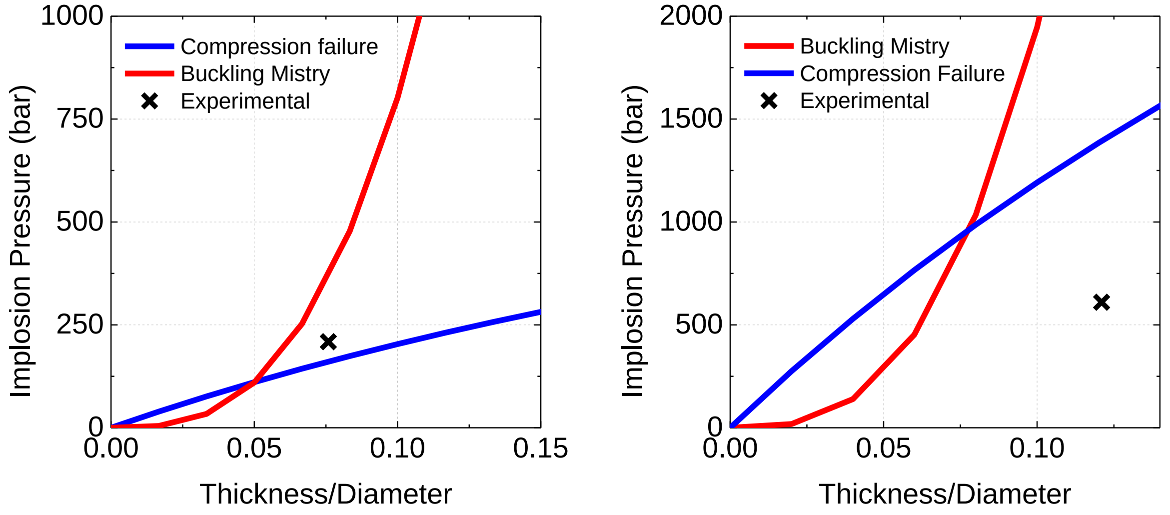

(a) (b)

Figure 130 : Implosion pressure versus the thickness to diameter ratio – Simple buckling (Mistry) and strength prediction compared to the experimental implosion pressures for the C/PA6 cylinders laid at (a) [±55] and (b) |0/±88]

Results presented in Figure 130 show that in both cases, material failure is expected in these implosion tests. However, it was shown earlier that concerning the thermoplastic cylinder laid at ±55°, buckling failure was identified from the strain gauges response during the implosion test. Therefore these predictions are to be taken carefully. Also, these predictions are highly dependent on the compression strength that is used. Concerning the cylinder laid at 0/±88, results show the experimental implosion pressure is quite far from the predicted value (45%). Again, these conclusions have to be taken carefully because these criteria are based on a number of assumptions; these include perfectly circular cylinders, which is not the case for the ±55° C/PA6 cylinder as shown in Table 28.

In order to compare the results from cylinders with different diameters and thicknesses, an apparent hoop stress at implosion is presented for each cylinder in Table 30.

These values allow for the compression plot to pass through the experimental point in Figure 130.

Table 30 : Results from implosion tests performed on the three cylinders

Tube	Sequence	Inner Diameter (mm)	Wall thickness (mm)	t/D	Implosion pressure (bar)	Apparent hoop strength at failure $\sigma_{\theta\theta}$ (MPa)
C/Epoxy	$[\pm 55]_{31}$	120	12.7	0.11	772	365
C/PA6	[±55]	120	9.2	0.08	209	136
C/PA6	$[0/\pm 88]_{26}$	100	12.1	0.12	610	252

It should be kept in mind that for each condition of interest, only one cylinder was tested for implosion. From a reproducibility point of view, it would clearly have been preferable to perform at least three tests per condition; however, manufacturing and testing such cylindrical structures is both expensive and time-consuming. It may be noted that for the C/epoxy cylinders, many other tests have been performed in the past at Ifremer [6]. These included a series on cylinders of the same thickness from the same supplier but of different lengths. These were 1.2 meters long, i.e. the actual length of the profilers used today at Ifremer for deep sea applications. Considering that the implosion of the 600mm long cylinder was due to buckling, it is thought that for a longer cylinder, implosion pressures would be lower. However, this was not the case because those cylinders imploded at 886 and 684 bar [202]. This underlines the fact that in these intermediate thickness-to-diameter ranges, it is very difficult to define a failure criterion, either due to buckling or material failure. The experience from the World Wide Failure Exercise emphasised this conclusion [154].

One additional factor which was noted previously in Chapter 6 is residual strains and stresses, these will be discussed in the next section.

3.3.5. Residual strains

It was discussed in the two previous Chapters that residual stresses are likely to have a significant effect on the composite behaviour. In order to relate those results to the situation in the tubes, radial cut tests were performed on composite rings (15 mm wide) extracted from all three cylinders. This allows the residual strain evolution induced by the release of the bending moment to be measured. The residual strain results are presented in Table 31. Three rings per cylinder were tested, taken from an extra length of the cylinders produced during the same manufacturing operation.

Table 31 : Residual strains in composite rings

Cylinder	Outer strains (µm/m)	Inner strains (µm/m)
C/Epoxy ±55	662 ± 113	-710 ± 123
C/PA6 ±55	216 ± 76	-239 ± 77
C/PA6 0/±88	-82 ± 211	89 ± 237

These results show that the highest level of residual strains is found in the C/Epoxy cylinder, which is quite surprising. Another interesting result is the residual strains obtained for the 0/±88 cylinder. For all radial cuts on the ±55° rings, the released bending moment tended to close the rings onto the saw blade, however, concerning the 0/±88 rings, out of three rings, one opened up and the strains were quite low. The results for each ring from the 0/±88 cylinder are presented in Table 32.

Table 32 : Residual strains measured on the 0/±88 rings

Ring number	1	2	3
Outer strains (µm/m)	73	4	-322
Inner strains (µm/m)	-85	-8	359

These results show that the residual strains in the 0/±88 cylinder are not uniform along the length of the cylinder. Therefore, it is difficult to conclude on their effect but these residual strain values are all quite low. While this effect is related to the fibre orientation, and in particular their hoop orientation, the fact that the strains in the 55° orientation rings are also low suggests that the residual strains in cylinders may not be as detrimental to implosion performance as anticipated from the panel tests.

This clearly requires further study, and the instrumentation of cylinders with optical fibres during manufacture and testing would be one direct method to provide essential data to quantify these effects.

4. Conclusion

The aim of this Chapter was to study the implosion performance of thermoplastic composite cylinders compared to the C/Epoxy reference used today at Ifremer. First, the quality of these cylinders was checked using Ultrasonic C-scan and X-ray tomography. Results from ultrasonic C-scan showed high levels of attenuation (>20dB) in the C/Epoxy cylinder and very low attenuation levels were found in the C/PA6 cylinders (<8dB). These results indicate that the thermoplastic composite cylinders are of much better quality in terms of voids than the thermoset counterpart. These results were also confirmed by X-ray tomography. Then, the elastic properties of the different cylinders were checked and compared to the analytical and finite element predictions (appendix 1) for the thermoplastic cylinders. Results showed a good correlation between the experimental results and the prediction concerning the cylinder laid at 0/±88. However, the hoop modulus for the 55° cylinder did not correlate with the prediction and indicated a lower stiffness than the prediction.

Then, implosion tests were performed on the different cylinders. Results showed the highest implosion pressure for the C/Epoxy reference, at 772 bar. The thermoplastic counterpart laid at ±55° imploded at a much lower pressure, 209 bar. Even though this cylinder was slightly thinner than the C/epoxy cylinder, this would not explain such a high difference. The lower stiffness is probably responsible for this low implosion pressure, which is also associated with the groove induced by the two-shell mandrel. Finally, the sequence was optimised to 0/±88 which provides a much stiffer behaviour than the ±55 angle. This last cylinder imploded at 610 bar, which is much higher than the cylinder laid at ±55°. This value is still lower than the C/Epoxy counterpart but one has to keep in mind that the fibre volume fraction for the thermoplastic cylinders is lower than that of the C/Epoxy (0.48 for C/PA6 and 0.6 for C/Epoxy). Residual strain measurements using the radial cut method also indicated that these were not uniform along the length of the cylinder.

This last implosion test shows that it is indeed possible to use C/PA6 cylinders for underwater applications at depths down to 4000m (with a safety factor of 1.5)., but further study is needed to achieve equivalent performance of the carbon/epoxy cylinders.

Conclusion & Future Work

Although composite materials have been used underwater for many years, those used in a marine environment are almost exclusively thermoset resin-based. Those being developed today for oceanographic profilers are more than 10 mm thick and manufacturing such composite parts is not an easy task because of the high levels of residual stresses and delaminations. Several thermoplastic matrix polymers are potential replacements including PP, PPS, PEEK, PEKK and PA, however, very few results concerning the resistance of thermoplastic cylinders subjected to high hydrostatic pressures can be found in the literature. In addition, few results are available concerning the aging behaviour of such materials in a marine environment and it is not clear how this will limit the use of such materials.

The objective of the study was to manufacture thick thermoplastic composite cylinders by Laser Assisted Tape Placement that can resist high hydrostatic pressures, above 400 bar, and to investigate how water affects the use of such materials.

Most of the studies reported in the literature on the implosion strength of thermoplastic composite materials were focused on high performance composite materials such as C/PEEK and C/PEKK, however, for the application of interest, these are far too expensive compared to the C/Epoxy oceanographic profiler used today at Ifremer. Therefore, low-cost thermoplastic composite materials such as C/PA6 are of particular interest and were selected for the study, however, these are known to be particularly sensitive to water aging. It was thought that the water diffusion in composite 12 mm thick might be sufficiently slow not to affect the mechanical properties of the cylinder greatly but to examine this a water diffusion model and tests were needed.

First, the water diffusion kinetics in neat PA6 and in C/PA6 were investigated over a wide range of conditions. It was shown that the water diffusion in these materials did not follow a Fickian behaviour because of an increase in the diffusivity with water absorption when the material goes from the glassy to the rubbery state. As water penetrates the material, the glass transition temperature T_g drops and this changes greatly the water diffusion kinetics. Two cases were identified; one below T_g where the diffusivity can be accurately described using an Arrhenius equation and one above T_g when the diffusivity can be described using the free volume theory. These two cases were then implemented in an original model in order to predict the water diffusion at different temperatures. Results show a very good agreement with the experimental data and the predictions are significantly better than those based on Fickian behaviour which was very non-conservative, especially at low temperatures (15°C) [203]. This model based on physical considerations was applied to composite materials using homogenisation relationships that were then used to predict the water absorption in the thick (12mm) C/PA6 thermoplastic composite cylinder immersed at 15°C. Predictions showed that water was not the main issue at these temperatures as only 3mm of the outer surface of the cylinder would be affected by water after two years of immersion. This raised the question of the influence of this water on the mechanical properties so this was investigated next.

The evolution of the tensile, compressive and out-of-plane properties of C/PA6 laminates have been evaluated on 2mm thick specimens as a function of water aging over a wide range of wet conditions. This allowed a complete understanding of the behaviour of these materials immersed in water. This study showed that water has a very negative effect on the matrix dominated mechanical properties of these composites that are reduced by over 50%. This loss in properties has been linked to the large decrease in the glass transition temperature (from 66°C in the dry state to -12°C when fully saturated with sea water). An empirical relationship between the mechanical properties and the water content and the $T-T_g$ parameter has been proposed. Coupled with the specific water diffusion model developed earlier, results showed that water diffusion would not be the limiting issue for the mechanical behaviour of 12 mm thick C/PA6 cylinders immersed at 15°C for 2 years.

The next step was to focus on the effect of processing conditions on the crystallization kinetics and mechanical properties of C/PA6. Due to the semi-crystalline nature of PA6, a crystallization model was needed and one was applied to accurately describe the non isothermal kinetics in the PA6 matrix and in the composite. Then, 2 mm thick composite panels were manufactured by press forming at different cooling rates (between 1 and 20°C/min). Tests performed under transverse tension revealed that the evolution in crystallinity in this cooling rate range had no effect on the transverse tensile strength, suggesting that this parameter was not a major issue here. Additionally, composite panels and rings were manufactured by Laser Assisted Tape Placement and mechanical tests were performed to quantify the differences existing between composites manufactured by LATP and press forming. Results showed that lower mechanical properties were obtained when using composites manufactured by LATP and this difference was associated with significantly higher levels of residual stresses induced by processing. A specific study on residual stress measurement in C/PA6 composites was therefore performed, using different techniques, in order to examine this difference.

First, a novel fibre optic sensor was integrated during the processing of C/PA6 panels manufactured by press forming. The evolution of residual strains was continuously monitored during processing and subsequent strain relaxation induced by environmental conditions (temperature and humidity) was successfully followed. Environmental conditions were also studied in details using asymmetric laminates. Results from sorption and desorption tests showed that the relaxation of residual stresses due to environmental conditions was a fully reversible process. However, the specific water diffusion model that was developed earlier was not able to describe the water diffusion process in asymmetric laminates because the water diffusion is much faster than the prediction. This result suggests that residual stresses have a significant effect on the water diffusion process. Finally, the residual strains found in unidirectional composite rings manufactured by Laser Assisted Tape Placement were investigated and it was found that these evolved linearly with increasing the thickness of the composite rings, suggesting that this could have a significant coupling effect for thick composite cylinders manufactured by Laser Assisted Tape Placement.

The last part of the study concerned the performance of thick thermoplastic composite cylinders manufactured by Laser Assisted Tape Placement subjected to high hydrostatic pressures. Results were compared to the C/Epoxy reference cylinder used today at Ifremer. First, results from quality control tests (Ultrasonic C-scan, X-ray Tomography) showed that the thermoplastic composite cylinders were of much better quality in terms of voids than the C/Epoxy, which represents one important improvement. Then, results from implosion tests performed on the thermoplastic and thermoset composite cylinders showed the highest implosion pressure for the C/Epoxy reference at 772 bar. The thermoplastic counterpart laid at the same sequence [±55°] imploded at a much lower pressure (209 bar). This was associated with a significant circularity defect that resulted in an elliptical shape of the cylinder caused by the two-shell mandrel used. This type of defect is known to have a major influence on the bucking strength. Moreover, the lower implosion strength was also associated with the lower matrix dominated properties of the PA6 composites compared to the epoxy. Then, the fibre orientation was subsequently optimised to a much less matrix dominated sequence which should also perform better under hydrostatic pressure, $[0/\pm88]_{26}$ and an improved mandrel was employed. Results from an implosion test on this new sequence were much closer to the C/Epoxy reference as it imploded at 610 bar (albeit for a smaller 100 mm inner diameter). The residual strains found in these thick composite cylinders were also investigated and results were quite surprising as the level of residual strains obtained was much lower for the thermoplastic composite cylinders. However, it was also shown that for the cylinder laid at [0/±88], the residual strains were not uniform along the length of the cylinder, which requires further investigation. Nonetheless, the implosion pressure value obtained for this type of sequence shows that it is indeed possible to use C/PA6 cylinders for underwater applications at depths down to 4000 meters with a safety factor of 1.5.

The results presented in this study are very promising but have raised several other questions that will need to be answered in future work. These can be divided into six sections.

First, it would be particularly interesting to use the specific water diffusion model developed in this study to predict the mechanical property loss induced by water ingress in C/PA6 laminates. It is worth noting that such a study has been successfully performed on the neat PA6 [204] but is yet to be adapted for composite materials. Validation of the model by immersion of sections from thick cylinders has started, but requires very long immersion times.

Second, it was shown that the specific model that was developed here was not able to describe the water absorption in asymmetric laminates. Therefore, future work includes adapting this model to such laminates. However, first, we need to understand why the model cannot be applied. To do so, it would be particularly interesting to perform DVS tests on thin asymmetric laminates over a wide range of temperature and wet conditions, similar to those performed to develop the model in the first place. This would provide improved understanding of which property deviates from those identified in the model (water clustering, value of T_g, evolution of diffusivity) and to correct the model accordingly. It would also be very interesting to quantify stress-diffusion coupling effects for these materials, such studies are being performed in another PhD study (C.Humeau) and are allowing coupled models to be developed [141].

Third, a novel strain measurement technique was successfully used to monitor in-situ the evolution of residual strains during processing in thermoplastic composite panels manufactured by press forming. Therefore, it would be very interesting to adapt this new strain measurement technique to composite parts manufactured by Laser Assisted Tape Placement, in order to understand the differences between the two manufacturing techniques.

Fourth, for each condition of interest, a very limited number of cylinders (only one) was tested for implosion, and reproducibility need to be evaluated. This was not performed during the study because even though C/PA6 is less expensive than C/PEEK, producing, instrumenting and testing 12 mm thick composite cylinders is quite expensive. Therefore, it would be particularly interesting to perform tests on thinner cylinders with similar thickness to diameter ratios. This would allow the quantity of materials used to produce each cylinder to be reduced and would also allow the production of several cylinders for each condition of interest. Also, it was shown that predicting the implosion pressure of such cylinders is not an easy task and the use of mechanical properties determined by press forming may not be the solution. Therefore, performing mechanical tests such as axial and radial compression tests to failure directly on small composite cylinders manufactured by LATP may help to improve implosion predictions. Moreover, the use of even less expensive materials such as Glass/PP and Glass/PA [205] would also allow the production of cylinders with different sequences and thicknesses and would permit a more complete understanding of the LATP process parameters and their influence on the implosion pressure. Such materials have been studied in other work so there is already material and diffusion data available [205].

Another aspect that has not been studied here is the creep behaviour of such cylinders. This may be important for the application of interest, in particular concerning the damage that may develop during use. It may be noted that a PhD on this subject has started at the ENS Cachan together with the CETIM.

One other aspect that would require further work is the effect of impact on the implosion pressure. Many thermoplastic composites possess higher toughness properties than their thermoset counterparts and this suggests that thermoplastic composites would greatly enhance the resistance of structures subjected to impact. However, a previous study performed at Ifremer [20] investigated the residual implosion strength after impact of C/epoxy and C/PEEK cylinders and results showed that the implosion after impact properties actually decreased more rapidly for C/PEEK compared to C/Epoxy, in spite of smaller impact damage zones in the former, suggesting that further work is needed to fully understand how material toughness is transferred to the structure.

There is considerably more work to be performed in order to qualify carbon/polyamide cylinders for deep sea applications, but the first results from this study suggest that they offer great potential. A final aspect, which has not been developed here, is the possibility for recycling. In the context of increasing concerns over environmental impact this will play a larger role in design in the future, and thermoplastic composites offer one solution to reducing waste. Detailed Life Cycle Analysis would help to quantify these benefits.

References

[1] C. S. Smith, “Design of submersible pressure hulls in composite materials,” *Mar. Struct.*, vol. 4, no. 2, pp. 141–182, 1991.

[2] P. Stevenson, D. Graham, and C. Clayson, “The Mechanical Design and Implementation of an Autonomous Submersible,” *Underw. Technol.*, vol. 23, no. 1, pp. 31–41, Jan. 1998.

[3] J. D. Stachiw and B. Frame, “Graphite-Fiber-Reinforced Plastic Pressure Hull Mod 2 for the Advanced Unmanned Search System Vehicle,” Tech. Report 1245, Naval Ocean Systems Center, San Diego, Aug. 1988.

[4] Y. Lemiere, “The evolution of composite materials in submarine structures.,” presented at the La Construction Navale en Composites, Paris (France), 7-9 Dec 1992, 1992.

[5] A. P. Mouritz, E. Gellert, P. Burchill, and K. Challis, “Review of advanced composite structures for naval ships and submarines,” *Compos. Struct.*, vol. 53, no. 1, pp. 21–42, Jul. 2001.

[6] J. Graham-Jones and J. Summerscales, *Marine Applications of Advanced Fibre-reinforced Composites*. Woodhead Publishing, 2015.

[7] J. Starbuck and H. Blake, “Failure of thick composite cylinders subjected to external hydrostatic pressure,” *ASTM 1185*, pp. 159–176.

[8] D. Graham, “Eighth International Conference on Composite Structures, Composite pressure hulls for deep ocean submersibles,” *Compos. Struct.*, vol. 32, no. 1, pp. 331–343, Jan. 1995.

[9] N. G. Tsouvalis, A. A. Zafeiratou, and V. J. Papazoglou, “The effect of geometric imperfections on the buckling behaviour of composite laminated cylinders under external hydrostatic pressure,” *Compos. Part B Eng.*, vol. 34, no. 3, pp. 217–226, Apr. 2003.

[10] P. Davies, D. Choqueuse, L. Riou, P. Warnier, P. Jegou, J. . Rolin, B. Bigourdan, and P. Chauchot, “Matériaux Composites pour véhivule sous marin 6000 mètres. Comptes rendus des dixièmes journées nationales sur les composites (JNC10),” Paris, 1996, vol. 1.

[11] T. Messager, “Buckling of imperfect laminated cylinders under hydrostatic pressure,” *Compos. Struct.*, vol. 53, no. 3, pp. 301–307, Aug. 2001.

[12] T. Messager, M. Pyrz, B. Gineste, and P. Chauchot, “Optimal laminations of thin underwater composite cylindrical vessels,” *Compos. Struct.*, vol. 53, no. Issue 3, pp. 301–307, 2001.

[13] M. J. Hinton, P. D. Soden, and A. S. Kaddour, “Strength of composite laminates under biaxial loads,” *Appl. Compos. Mater.*, vol. 3, no. 3, pp. 151–162, 1996.

[14] P. D. Soden, M. J. Hinton, and A. S. Kaddour, “Biaxial test results for strength and deformation of a range of E-glass and carbon fibre reinforced composite laminates: failure exercise benchmark data,” *Compos. Sci. Technol.*, vol. 62, no. 12–13, pp. 1489–1514, Sep. 2002.

[15] P. D. Soden, A. S. Kaddour, and M. J. Hinton, “Recommendations for designers and researchers resulting from the world-wide failure exercise,” *Compos. Sci. Technol.*, vol. 64, no. 3–4, pp. 589–604, Mar. 2004.

[16] S.-H. Hur, H.-J. Son, J.-H. Kweon, and J.-H. Choi, “Postbuckling of composite cylinders under external hydrostatic pressure,” *Compos. Struct.*, vol. 86, no. 1–3, pp. 114–124, Nov. 2008.

[17] C.-J. Moon, I.-H. Kim, B.-H. Choi, J.-H. Kweon, and J.-H. Choi, “Buckling of filament-wound composite cylinders subjected to hydrostatic pressure for underwater vehicle applications,” *Compos. Struct.*, vol. 92, no. 9, pp. 2241–2251, Aug. 2010.

[18] P. Davies and D. Le Flour, “Long term behaviour of fibre reinforced structures for deep sea applications,” presented at the Proceedings Polymers in Oilfield Engineering, London, 2001, pp. 255–268.

[19] M. B. Gruber, M. A. Lamontia, M. A. Smoot, and V. Peros, “Buckling Performance of Hydrostatic Compression-Loaded 7-Inch Diameter Thermoplastic Composite Monocoque Cylinders,” *J. Thermoplast. Compos. Mater.*, vol. 8, no. 1, pp. 94–108, Jan. 1995.

[20] P. Davies, “Thermoplastic Composite Cylinders for Underwater Applications,” *J. Thermoplast. Compos. Mater.*, vol. 18, no. 5, pp. 417–443, Sep. 2005.

[21] C. Sparks, “Lightweight Composite Production Risers for a Deep Water Tension Leg Platform,” presented at the International Conference on Offshore Mechanics and Artic Engineering, Tokyo, 2986, pp. 86–93.

[22] D. Baldwin, N. Newhouse, and K. Lo, “Composite Production Riser design,” presented at the Proceedings of the Twenty-ninth Annual Offshore Technology Conference, Houston, USA, p. 1997.

[23] Shorbaug, “Significant achievments in composite technology in 2001 - Qualification and testing of Composite tethers and risers for Ultra deep water,” presented at the Deep Offshore Technology, Rio de Janeiro, 2001.

[24] M. Salama, G. Stjern, T. Shorbaug, B. Spencer, and A. T. Echtermeyer, “The First Offshore Field Installation for a Composite Riser Joint,” presented at the Offshore Technology Conference, Houston, USA, 2002.

[25] O. Ochoa, “Composite riser experience and design guidance,” OTRC Final Project Report, 2006.

[26] H. W. Starkweather and R. E. Brooks, “Effect of spherulites on the mechanical properties of nylon 66,” *J. Appl. Polym. Sci.*, vol. 1, no. 2, pp. 236–239, Mar. 1959.

[27] T. J. Bessell, D. Hull, and J. B. Shortall, “The effect of polymerization conditions and crystallinity on the mechanical properties and fracture of spherulitic nylon 6,” *J. Mater. Sci.*, vol. 10, no. 7, pp. 1127–1136, 1975.

[28] A. S. Nielsen and R. Pyrz, “A Raman study into the effect of transcrystallisation on thermal stresses in embedded single fibres,” *J. Mater. Sci.*, vol. 38, no. 3, pp. 597–601, 2003.

[29] D. H.-J. A. Lukaszewicz, C. Ward, and K. D. Potter, “The engineering aspects of automated prepreg layup: History, present and future,” *Compos. Part B Eng.*, vol. 43, no. 3, pp. 997–1009, Apr. 2012.

[30] M. A. Lamontia, M. B. Gruber, J. J. Tierney, J. W. Gillespie Jr, B. J. Jensen, and R. J. Cano, “In situ thermoplastic ATP needs flat tapes and tows with few voids,” in *30th International SAMPE Europe Conference, Paris*, 2009.

[31] M. A. Khan, P. Mitschang, and R. Schledjewski, “Identification of some optimal parameters to achieve higher laminate quality through tape placement process,” *Adv. Polym. Technol.*, vol. 29, no. 2, pp. 98–111, Jul. 2010.

[32] M. Lan, D. Cartié, P. Davies, and C. Baley, “Microstructure and tensile properties of carbon–epoxy laminates produced by automated fibre placement: Influence of a caul plate on the effects of gap and overlap embedded defects,” *Compos. Part Appl. Sci. Manuf.*, vol. 78, pp. 124–134, Nov. 2015.

[33] S. K. Mazumdar, “Automated Manufacturing of Composite Components by Thermoplastic Tape Winding and Filament Winding,” Concordia University, PhD Thesis, Monteral, Canada.

[34] Z. Qureshi, T. Swait, R. Scaife, and H. M. El-Dessouky, “In situ consolidation of thermoplastic prepreg tape using automated tape placement technology: Potential and possibilities,” *Compos. Part B Eng.*, vol. 66, pp. 255–267, Nov. 2014.

[35] W. J. B. Grouve, *Weld strength of laser-assisted tape-placed thermoplastic composites*. University of Twente, PhD thesis, 2012.

[36] C. M. Stokes-Griffin, “A combined Optical-Thermal Model for Laser-Assisted Fibre Placement of Thermoplastic Composite Materials,” The Australian National University, PhD thesis, Canberra, 2015.

[37] R. Pitchumani, J. W. Gillespie, and M. A. Lamontia, “Design and Optimization of a Thermoplastic Tow-Placement Process with In-Situ Consolidation,” *J. Compos. Mater.*, vol. 31, no. 3, pp. 244–275, Jan. 1997.

[38] C. M. Stokes-Griffin and P. Compston, “The effect of processing temperature and placement rate on the short beam strength of carbon fibre–PEEK manufactured using a laser tape placement process,” *Compos. Part Appl. Sci. Manuf.*, vol. 78, pp. 274–283, Nov. 2015.

[39] A. J. Comer, D. Ray, W. O. Obande, D. Jones, J. Lyons, I. Rosca, R. M. O’ Higgins, and M. A. McCarthy, “Mechanical characterisation of carbon fibre–PEEK manufactured by laser-assisted automated-tape-placement and autoclave,” *Compos. Part Appl. Sci. Manuf.*, vol. 69, pp. 10–20, Feb. 2015.

[40] P.-Y. B. Jar, R. Mulone, P. Davies, and H.-H. Kausch, “A study of the effect of forming temperature on the mechanical behaviour of carbon-fibre/peek composites,” *Compos. Sci. Technol.*, vol. 46, no. 1, pp. 7–19, Jan. 1993.

[41] P. Davies, W. J. Cantwell, P.-Y. Jar, H. Richard, D. J. Neville, and H.-H. Kausch, “Cooling rate effects in carbon fiber/PEEK composites,” in *Composite Materials: Fatigue and Fracture (Third Volume)*, ASTM International, 1991.

[42] P. Davies and W. J. Cantwell, “Fracture of glass/polypropylene laminates: influence of cooling rate after moulding,” *Composites*, vol. 25, no. 9, pp. 869–877, 1994.

[43] J. Bernhardsson and R. Shishoo, “Effect of Processing Parameters on Consolidation Quality of GF/PP Commingled Yarn Based Composites,” *J. Thermoplast. Compos. Mater.*, vol. 13, no. 4, pp. 292–313, Jan. 2000.

[44] L. G. Stringer, R. J. Hayman, M. J. Hinton, R. A. Badcock, and M. R. Wisnom, “Curing stresses in thick polymer composite components Part II: Management of residual stresses,” in *Proceedings of ICCM-12 Conference. Paris (France)*, 1999, pp. 1–10.

[45] J.-A. E. Manson and J. C. Seferis, “Process Simulated Laminate (PSL) : A Methodology to Internal Stress Characterization in Advanced Composite Materials,” *J. Compos. Mater.*, vol. 26, no. 3, pp. 405–431, Jan. 1992.

[46] J. A. Nairn and P. Zoller, “Matrix solidification and the resulting residual thermal stresses in composites,” *J. Mater. Sci.*, vol. 20, no. 1, pp. 355–367, 1985.

[47] C. Pradere and C. Sauder, “Transverse and longitudinal coefficient of thermal expansion of carbon fibers at high temperatures (300–2500 K),” *Carbon*, vol. 46, no. 14, pp. 1874–1884, Nov. 2008.

[48] J. . Barnes, “The formation of residual stresses in laminated thermoplastic composites,” *Compos. Sci. Technol.*, vol. 51, pp. 479–494, 1994.

[49] J. A. Nairn and P. Zoller, “The development of residual thermal stresses in amorphous and semicrystalline thermoplastic matrix composites,” *ASTM STP 937*, pp. 328–341, 1987.

[50] O. Sicot, X. L. Gong, A. Cherouat, and J. Lu, “Determination of Residual Stress in Composite Laminates Using the Incremental Hole-drilling Method,” *J. Compos. Mater.*, vol. 37, no. 9, pp. 831–844, Jan. 2003.

[51] O. Sicot, X. L. Gong, A. Cherouat, and J. Lu, “Influence of experimental parameters on determination of residual stress using the incremental hole-drilling method,” *Compos. Sci. Technol.*, vol. 64, no. 2, pp. 171–180, Feb. 2004.

[52] R. Y. Kim and H. T. Hahn, “Effect of Curing Stresses on the First Ply-failure in Composite Laminates,” *J. Compos. Mater.*, vol. 13, no. 1, pp. 2–16, Jan. 1979.

[53] G. Jeronimidis and A. T. Parkyn, “Residual Stresses in Carbon Fibre-Thermoplastic Matrix Laminates,” *J. Compos. Mater.*, vol. 22, no. 5, pp. 401–415, Jan. 1988.

[54] N. Ersoy and O. Vardar, “Measurement of Residual Stresses in Layered Composites by Compliance Method,” *J. Compos. Mater.*, vol. 34, no. 7, pp. 575–598, Jan. 2000.

[55] P. Casari, F. Jacquemin, and P. Davies, “Characterization of residual stresses in wound composite tubes,” *Compos. Part Appl. Sci. Manuf.*, vol. 37, no. 2, pp. 337–343, Feb. 2006.

[56] A. P. Deshpande and J. C. Seferis, “Processing Characteristics in Different Semi-Crystalline Thermoplastic Composites Using Process Simulated Laminate (PSL) Methodology,” *J. Thermoplast. Compos. Mater.*, vol. 9, no. 2, pp. 183–198, Apr. 1996.

[57] W. J. Unger and J. S. Hansen, “The Effect of Thermal Processing on Residual Strain Development in Unidirectional Graphite Fibre Reinforced PEEK,” *J. Compos. Mater.*, vol. 27, no. 1, pp. 59–82, Jan. 1993.

[58] G. Zhou and L. M. Sim, “Damage detection and assessment in fibre-reinforced composite structures with embedded fibre optic sensors-review,” *Smart Mater. Struct.*, vol. 11, no. 6, p. 925, 2002.

[59] M. Mulle, H. Wafai, A. Yudhanto, G. Lubineau, R. Yaldiz, W. Schijve, and N. Verghese, “Process monitoring of glass reinforced polypropylene laminates using fiber Bragg gratings,” *Compos. Sci. Technol.*, vol. 123, pp. 143–150, Feb. 2016.

[60] H. Hernández-Moreno, F. Collombet, B. Douchin, D. Choqueuse, and P. Davies, “Entire Life Time Monitoring of Filament Wound Composite Cylinders Using Bragg Grating Sensors: III. In-Service External Pressure Loading,” *Appl. Compos. Mater.*, vol. 16, no. 3, pp. 135–147, Apr. 2009.

[61] H. Hernández-Moreno, F. Collombet, B. Douchin, D. Choqueuse, P. Davies, and J. L. G. Velázquez, “Entire Life Time Monitoring of Filament Wound Composite Cylinders Using Bragg Grating Sensors: I. Adapted Tooling and Instrumented Specimen,” *Appl. Compos. Mater.*, vol. 16, no. 3, pp. 173–182, May 2009.

[62] B. Benedikt, M. Kumosa, P. K. Predecki, L. Kumosa, M. G. Castelli, and J. K. Sutter, “An analysis of residual thermal stresses in a unidirectional graphite/PMR-15 composite based on X-ray diffraction measurements,” *Compos. Sci. Technol.*, vol. 61, no. 14, pp. 1977–1994, Nov. 2001.

[63] R. Meske and E. Schnack, “Particular adaptation of X-ray diffraction to fiber reinforced composites,” *Mech. Mater.*, vol. 35, no. 1–2, pp. 19–34, Jan. 2003.

[64] P. G. Ifju, X. Niu, B. C. Kilday, S.-C. Liu, and S. M. Ettinger, “Residual strain measurement in composites using the cure-referencing method,” *Exp. Mech.*, vol. 40, no. 1, pp. 22–30, 2000.

[65] M. Gigliotti, M. R. Wisnom, and K. D. Potter, “Development of curvature during the cure of AS4/8552 [0/90] unsymmetric composite plates,” *Compos. Sci. Technol.*, vol. 63, no. 2, pp. 187–197, 2003.

[66] M. Gigliotti, Y. Pannier, M. Minervino, M. C. Lafarie-Frenot, and P. Corigliano, “The effect of a thermo-oxidative environment on the behaviour of multistable [0/90] unsymmetric composite plates,” *Compos. Struct.*, vol. 106, pp. 863–872, Dec. 2013.

[67] M. R. Wisnom, M. Gigliotti, N. Ersoy, M. Campbell, and K. D. Potter, “Mechanisms generating residual stresses and distortion during manufacture of polymer–matrix composite structures,” *Compos. Part Appl. Sci. Manuf.*, vol. 37, no. 4, pp. 522–529, Apr. 2006.

[68] J. Etches, K. Potter, P. Weaver, and I. Bond, “Environmental effects on thermally induced multistability in unsymmetric composite laminates,” *Compos. Part Appl. Sci. Manuf.*, vol. 40, no. 8, pp. 1240–1247, Aug. 2009.

[69] R. Telford, K. B. Katnam, and T. M. Young, “The effect of moisture ingress on through-thickness residual stresses in unsymmetric composite laminates: A combined experimental–numerical analysis,” *Compos. Struct.*, vol. 107, pp. 502–511, Jan. 2014.

[70] J. Borges de Almeida, “Analytical and Experimental Study of the Evolution of Residual Stresses in Composite Materials,” University of Porto, Porto, 2005.

[71] C. Soutis, “Measurement of the Static Compressive Strength of Carbon-Fibre/Epoxy Laminates,” *Composite Science and Technology*, pp. 373–392, 1991.

[72] R. Y. Kim and A. S. Crasto, “Longitudinal compression strength of glass fiber-reinforced composites,” *J. Reinf. Plast. Compos.*, vol. 13, no. 4, pp. 326–338, 1994.

[73] P. Berbinau, C. Soutis, and I. A. Guz, “Compressive failure of 0 unidirectional carbon-fibre-reinforced plastic (CFRP) laminates by fibre microbuckling,” *Compos. Sci. Technol.*, vol. 59, no. 9, pp. 1451–1455, 1999.

[74] R.-R. Effendi, Analyse des mécanismes de dégradation en compression des composites unidirectionnels fibres de carbone-matrice organique et modélisation associée *(PhD thesis, in french).* Toulouse, ENSAE, 1993.

[75] W. Hart, R. Aoki, H. Bookholt, P. T. Curtis, I. Krober, N. Marks, and P. Sigety, “Garteur compression behavior of advanced CFRP,” Workshop on Advanced Composites in Military Aircraft, San Diego CA, Oct. 1991.

[76] ASTM D3410, “Test Method for Compressive Properties of Polymer Matrix Composite Materials with Unsupported Gage Section by Shear Loading,” ASTM International, 2008.

[77] ISO 14126, “Composites plastiques renforcés de fibres - Détermination des caractéristiques en compression dans le plan,” *Norme Eur.*, 1999.

[78] ASTM D695, “Test Method for Compressive Properties of Rigid Plastics,” ASTM International, 2010.

[79] ASTM D6641, “Test Method for Compressive Properties of Polymer Matrix Composite Materials Using a Combined Loading Compression (CLC) Test Fixture,” ASTM International, 2014.

[80] A. J. Barker and V. Balasundaram, “Compression testing of carbon fibre-reinforced plastics exposed to humid environments,” *Composites*, vol. 18, no. 3, 1987.

[81] J. . Haberle and F. L. Matthews, “An improved technique for compression testing of unidirectional fibre-reinforced plastics; development and results,” *Composites*, vol. 25, no. 5, 1994.

[82] E. M. Odom and D. F. Adams, “Failure modes of unidirectional carbon/epoxy composite compression specimens,” *Composites*, vol. 21, no. 4, 1990.

[83] O. Montagnier and C. Hochard, “Compression Characterization of High-modulus Carbon Fibers,” *J. Compos. Mater.*, vol. 39, no. 1, pp. 35–49, Jan. 2005.

[84] M. Arhant, “Rapport d’avancement 2014 - Thermoplastic composites for underwater applications,” 14–149, Dec. 2014.

[85] N. Carbajal and F. Mujika, “Determination of compressive strength of unidirectional composites by three-point bending tests,” *Polym. Test.*, vol. 28, no. 2, pp. 150–156, Apr. 2009.

[86] N. V. De Carvalho, S. T. Pinho, and P. Robinson, “An experimental study of failure initiation and propagation in 2D woven composites under compression,” *Compos. Sci. Technol.*, vol. 71, no. 10, pp. 1316–1325, Jul. 2011.

[87] E. Vittecoq, “Sur le comportement en compression des composites stratifiés carbone-epoxy,” PhD Thesis (in french), Paris 6, Paris, 1991.

[88] H. Fukuda, “A new bending test method of advanced composites,” *Exp. Mech.*, vol. 29, no. 3, pp. 330–335, 1989.

[89] M. R. Wisnom, “On the high compressive strains achieved in bending tests on unidirectional carbon-fibre/epoxy,” *Compos. Sci. Technol.*, vol. 43, no. 3, pp. 229–235, 1992.

[90] M. R. Wisnom, “The effect of specimen size on the bending strength of unidirectional carbon fibre-epoxy,” *Compos. Struct.*, vol. 18, no. 1, pp. 47–63, 1991.

[91] I. Grandsire-Vinçon, “Compression des composites unidirectionnels: Méthode d’essai et approche micromécanique,” PhD thesis (in french) ENS Cachan, 1993.

[92] S. W. Yurgartis and S. S. Sternstein, “A micrographic study of bending failure in five thermoplastic-carbon fibre composite laminates,” *J. Mater. Sci.*, vol. 23, no. 5, pp. 1861–1870, 1988.

[93] J. A. Grape and V. Gupta, “The effect of temperature on the strength and failure mechanisms of a woven carbon/polyimide laminate under compression,” *Mech. Mater.*, vol. 30, no. 3, pp. 165–180, Nov. 1998.

[94] B. W. Rosen, “Mechanics of composite strengthening.” 01-Jan-1965.

[95] R. J. Lee, “Compression strength of aligned carbon fibre-reinforced thermoplastic laminates,” *Composites*, vol. 18, no. 1, pp. 35–39, 1987.

[96] A. S. Argon, “Fracture of Composites,” in *Treatise of materials science and technology*, vol. 1, New York: Academic Press, 1972, pp. 79–114.

[97] J. Lankford, “Compressive failure of fibre-reinforced composites: buckling, kinking, and the role of the interphase,” *J. Mater. Sci.*, vol. 30, no. 17, pp. 4343–4348, Sep. 1995.

[98] B. Budiansky and N. A. Fleck, “Compressive failure of fibre composites,” *J.Mech.Phys.Solids*, vol. 41, no. 1, pp. 183–221, 1993.

[99] B. Budiansky, “Micromechanics,” *Comput. Struct.*, vol. 16, no. 1–4, pp. 3–12, 1983.

[100] J. Crank, *The mathematics of diffusion*, 2d ed. Oxford, [Eng]: Clarendon Press, 1975.

[101] Y. J. Weitsman, *Fluid Effects in Polymers and Polymeric Composites*. Boston, MA: Springer US, 2012.

[102] E. L. McKague, J. D. Reynolds, and J. E. Halkias, “Swelling and glass transition relations for epoxy matrix material in humid environments,” *J. Appl. Polym. Sci.*, vol. 22, no. 6, pp. 1643–1654, Jun. 1978.

[103] T. Peret, A. Clement, S. Freour, and F. Jacquemin, “Numerical transient hygro-elastic analyses of reinforced Fickian and non-Fickian polymers,” *Compos. Struct.*, vol. 116, pp. 395–403, Sep. 2014.

[104] M. Gigliotti, F. Jacquemin, and A. Vautrin, “Assessment of approximate models to evaluate transient and cyclical hygrothermoelastic stress in composite plates,” *Int. J. Solids Struct.*, vol. 44, no. 3–4, pp. 733–759, Feb. 2007.

[105] C.-H. Shen and G. S. Springer, “Effects of Moisture and Temperature on the Tensile Strength of Composite Materials,” *J. Compos. Mater.*, vol. 11, no. 1, pp. 2–16, Jan. 1977.

[106] N. Tual, N. Carrere, P. Davies, T. Bonnemains, and E. Lolive, “Characterization of sea water ageing effects on mechanical properties of carbon/epoxy composites for tidal turbine blades,” *Compos. Part Appl. Sci. Manuf.*, vol. 78, pp. 380–389, Nov. 2015.

[107] L. Greenspan and others, “Humidity fixed points of binary saturated aqueous solutions,” *J. Res. Natl. Bur. Stand.*, vol. 81, no. 1, pp. 89–96, 1977.

[108] J. Mark, *Polymer Data Handbook*. Oxford University Press, 1999.

[109] M. R. Wisnom, J. W. Atkinson, and M. I. Jones, “Reduction in compressive strain to failure with increasing specimen size in pin-ended buckling tests,” *Compos. Sci. Technol.*, vol. 57, no. 9, pp. 1303–1308, Jan. 1997.

[110] M. R. Wisnom and J. W. Atkinson, “Constrained buckling tests show increasing compressive strain to failure with increasing strain gradient,” *Compos. Part Appl. Sci. Manuf.*, vol. 28, no. 11, pp. 959–964, Jan. 1997.

[111] S. T. Kreger, D. K. Gifford, M. E. Froggatt, B. J. Soller, and M. S. Wolfe, “High resolution distributed strain or temperature measurements in single-and multi-mode fiber using swept-wavelength interferometry,” in *Optical Fiber Sensors*, 2006, p. ThE42.

[112] B. Soller, D. Gifford, M. Wolfe, and M. Froggatt, “High resolution optical frequency domain reflectometry for characterization of components and assemblies,” *Opt. Express*, vol. 13, no. 2, pp. 666–674, 2005.

[113] B. J. Soller, M. Wolfe, and M. E. Froggatt, “Polarization resolved measurement of Rayleigh backscatter in fiber-optic components,” *OFC Tech. Dig.*, 2005.

[114] Luna Technologies, “Optical Distributed Sensor Interrogator (Model ODiDI-B) - Data Sheet,” Roanoke, VA, 2014.

[115] O. Okamba-Diogo, E. Richaud, J. Verdu, F. Fernagut, J. Guilment, and B. Fayolle, “Molecular and macromolecular structure changes in polyamide 11 during thermal oxidation,” *Polym. Degrad. Stab.*, vol. 108, pp. 123–132, Oct. 2014.

[116] P. Gijsman, W. Dong, A. Quintana, and M. Celina, “Influence of temperature and stabilization on oxygen diffusion limited oxidation profiles of polyamide 6,” *Polym. Degrad. Stab.*, vol. 130, pp. 83–96, Aug. 2016.

[117] L. Silva, S. Tognana, and W. Salgueiro, “Study of the water absorption and its influence on the Young’s modulus in a commercial polyamide,” *Polym. Test.*, vol. 32, no. 1, pp. 158–164, Feb. 2013.

[118] L.-T. Lim, I. J. Britt, and M. A. Tung, “Sorption and transport of water vapor in nylon 6,6 film,” *J. Appl. Polym. Sci.*, vol. 71, no. 2, pp. 197–206, Jan. 1999.

[119] H. K. Reimschuessel, “Relationships on the effect of water on glass transition temperature and young’s modulus of nylon 6,” *J. Polym. Sci. Polym. Chem. Ed.*, vol. 16, no. 6, pp. 1229–1236, Jun. 1978.

[120] C. El-Mazry, O. Correc, and X. Colin, “A new kinetic model for predicting polyamide 6-6 hydrolysis and its mechanical embrittlement,” *Polym. Degrad. Stab.*, vol. 97, no. 6, pp. 1049–1059, Jun. 2012.

[121] R. Bernstein and K. T. Gillen, “Nylon 6.6 accelerating aging studies: II. Long-term thermal-oxidative and hydrolysis results,” *Polym. Degrad. Stab.*, vol. 95, no. 9, pp. 1471–1479, Sep. 2010.

[122] R. Bernstein, D. K. Derzon, and K. T. Gillen, “Nylon 6.6 accelerated aging studies: thermal–oxidative degradation and its interaction with hydrolysis,” *Polym. Degrad. Stab.*, vol. 88, no. 3, pp. 480–488, Jun. 2005.

[123] N. Abacha, “Diffusion behavior of water in polyamide 6 organoclay nanocomposites,” *Express Polym. Lett.*, vol. 3, no. 4, pp. 245–255, Mar. 2009.

[124] J. Hanspach and F. Pinno, “Concentration dependent diffusion of water in polyamide 6,” *Acta Polym.*, vol. 43, no. 4, pp. 210–213, Aug. 1992.

[125] T. Asada and S. Onogi, “The diffusion coefficient for the nylon 6 and water system,” *J. Colloid Sci.*, vol. 18, no. 8, pp. 784–792, Oct. 1963.

[126] E. Picard, J.-F. Gérard, and E. Espuche, "Water transport properties of polyamide 6 based nanocomposites prepared by melt blending: On the importance of the clay dispersion state on the water transport properties at high water activity," *J. Membr. Sci.*, vol. 313, no. 1–2, pp. 284–295, Apr. 2008.

[127] F.-M. Preda, A. Alegría, A. Bocahut, L.-A. Fillot, D. R. Long, and P. Sotta, "Investigation of Water Diffusion Mechanisms in Relation to Polymer Relaxations in Polyamides," *Macromolecules*, vol. 48, no. 16, pp. 5730–5741, Aug. 2015.

[128] M. Broudin, P. Y. Le Gac, V. Le Saux, C. Champy, G. Robert, P. Charrier, and Y. Marco, "Water diffusivity in PA66: Experimental characterization and modeling based on free volume theory," *Eur. Polym. J.*, vol. 67, pp. 326–334, Jun. 2015.

[129] R. A. Robinson, "The vapour pressure and osmotic equivalence of sea water," *J. Mar. Biol. Assoc. U. K.*, vol. 33, no. 2, pp. 449–455, Jun. 1954.

[130] N. J. W. Reuvers, H. P. Huinink, H. R. Fischer, and O. C. G. Adan, "The influence of ions on water transport in nylon 6 films," *Polymer*, vol. 54, no. 20, pp. 5419–5428, Sep. 2013.

[131] P. Y. Le Gac, G. Roux, P. Davies, B. Fayolle, and J. Verdu, "Water clustering in polychloroprene," *Polymer*, vol. 55, no. 12, pp. 2861–2866, Jun. 2014.

[132] X. Colin and J. Verdu, "Humid Ageing of Organic Matrix Composites," in *Durability of Composites in the Marine Environment*, Springer Netherlands., vol. 208, 2014, pp. 47–114.

[133] M. Broudin, V. Le Saux, P. Y. Le Gac, C. Champy, G. Robert, P. Charrier, and Y. Marco, "Moisture sorption in polyamide 6.6: Experimental investigation and comparison to four physical-based models," *Polym. Test.*, vol. 43, pp. 10–20, May 2015.

[134] F. N. Kelley and F. Bueche, "Viscosity and glass temperature relations for polymer-diluent systems," *J. Polym. Sci.*, vol. 50, no. 154, pp. 549–556, Apr. 1961.

[135] J. S. Vrentas and J. L. Duda, "Diffusion in polymer—solvent systems. I. Reexamination of the free-volume theory," *J. Polym. Sci. Polym. Phys. Ed.*, vol. 15, no. 3, pp. 403–416, 1977.

[136] J. S. Vrentas and J. L. Duda, "Diffusion in polymer–solvent systems. II. A predictive theory for the dependence of diffusion coefficients on temperature, concentration, and molecular weight," *J. Polym. Sci. Polym. Phys. Ed.*, vol. 15, no. 3, pp. 417–439, 1977.

[137] S.-U. Hong, "Prediction of polymer/solvent diffusion behavior using free-volume theory," *Ind. Eng. Chem. Res.*, vol. 34, no. 7, pp. 2536–2544, 1995.

[138] D. W. van Krevelen and K. te Nijenhuis, Properties of Polymers: Their Correlation with Chemical Structure; their Numerical Estimation and Prediction from Additive Group Contributions. Elsevier, 2009.

[139] K. Kondo and T. Taki, "Moisture Diffusivity of Unidirectional Composites," *J. Compos. Mater.*, vol. 16, no. 2, pp. 82–93, Jan. 1982.

[140] H. R. Dana, A. Perronnet, S. Fréour, P. Casari, and F. Jacquemin, "Identification of moisture diffusion parameters in organic matrix composites," *J. Compos. Mater.*, vol. 47, no. 9, pp. 1081–1092, Apr. 2013.

[141] C. Humeau, P. Davies, and F. Jacquemin, "Moisture diffusion under hydrostatic pressure in composites," *Mater. Des.*, vol. 96, pp. 90–98, Apr. 2016.

[142] I. M. Daniel and O. Ishai, *Engineering Mechanics of Composite Materials*. Oxford University Press, 2006.

[143] C. Thomas, "Étude des mécanismes d'endommagement des composites fibres de carbone / matrice polyamide : application à la réalisation de réservoirs de stockage de gaz sous haute pression de type IV," PhD Thesis (in french) École Nationale Supérieure des Mines de Paris, 2011.

[144] R. T. D. Prabhakaran and H. Toftegaard, “Environmental effect on the mechanical properties of commingled-yarn-based carbon fibre/polyamide 6 composites,” *J. Compos. Mater.*, p. 21998313501012, Sep. 2013.

[145] E. C. Botelho and M. C. Rezende, “Evaluation by Free Vibration Method of Moisture Absorption Effects in Polyamide/Carbon Fiber Laminates,” *J. Thermoplast. Compos. Mater.*, vol. 23, no. 2, pp. 207–225, Mar. 2010.

[146] R. Taktak, N. Guermazi, J. Derbeli, and N. Haddar, “Effect of hygrothermal aging on the mechanical properties and ductile fracture of polyamide 6: Experimental and numerical approaches,” *Eng. Fract. Mech.*, vol. 148, pp. 122–133, Nov. 2015.

[147] T. Le Huec, “Etude du comportement du Polyamide 6 en milieu marin (in french),” Plouzané, France, Internship report, 2015.

[148] G. Zhang, R. A. Latour Jr, J. M. Kennedy, H. Del Schutte Jr, and R. J. Friedman, “Long-term compressive property durability of carbon fibre-reinforced polyetheretherketone composite in physiological saline,” *Biomaterials*, vol. 17, no. 8, pp. 781–789, 1996.

[149] E. Botelho, “Mechanical behavior of carbon fiber reinforced polyamide composites,” *Compos. Sci. Technol.*, vol. 63, no. 13, pp. 1843–1855, Oct. 2003.

[150] P. Davies, H. H. Kausch, J. G. Williams, A. J. Kinloch, M. N. Charalambides, A. Pavan, D. R. Moore, R. Prediger, I. Robinson, N. Burgoyne, K. Friedrich, H. Wittich, C. A. Rebelo, A. Torres Marques, F. Ramsteiner, B. Melve, M. Fischer, N. Roux, D. Martin, P. Czarnocki, D. Neville, I. Verpoest, B. Goffaux, R. Lee, K. Walls, N. Trigwell, I. K. Partridge, J. Jaussaud, S. Andersen, Y. Giraud, G. Hale, and G. McGrath, “Round-robin interlaminar fracture testing of carbon-fibre-reinforced epoxy and PEEK composites,” *Compos. Sci. Technol.*, vol. 43, no. 2, pp. 129–136, Jan. 1992.

[151] P. Davies and D. R. Moore, “Glass/nylon-6.6 composites: Delamination resistance testing,” *Compos. Sci. Technol.*, vol. 38, no. 3, pp. 211–227, Jan. 1990.

[152] S. Pandini, “Time and temperature effects on Poisson’s ratio of poly(butylene terephthalate),” *Express Polym. Lett.*, vol. 5, no. 8, pp. 685–697, May 2011.

[153] S. Pandini and A. Pegoretti, “Time, temperature, and strain effects on viscoelastic Poisson’s ratio of epoxy resins,” *Polym. Eng. Sci.*, vol. 48, no. 7, pp. 1434–1441, Jul. 2008.

[154] M. J. Hinton, A. S. Kaddour, and P. D. Soden, Failure Criteria in Fibre Reinforced Polymer Composites: The World-Wide Failure Exercise. Elsevier, 2004.

[155] L. H. Sperling, *Introduction to physical polymer science*. John Wiley & Sons, 2005.

[156] L. Mandelkern and others, *Crystallization of polymers*, vol. 38. McGraw-Hill New York, 1964.

[157] T. Ozawa, “Kinetics of non-isothermal crystallization,” *Polymer*, vol. 12, no. 3, pp. 150–158, Mar. 1971.

[158] Y. Liu and G. Yang, “Non-isothermal crystallization kinetics of polyamide-6/graphite oxide nanocomposites,” *Thermochim. Acta*, vol. 500, no. 1–2, pp. 13–20, Mar. 2010.

[159] S.-L. Gao and J.-K. Kim, “Cooling rate influences in carbon fibre/PEEK composites. Part 1. Crystallinity and interface adhesion,” *Compos. Part Appl. Sci. Manuf.*, vol. 31, no. 6, pp. 517–530, Jun. 2000.

[160] S.-L. Gao and J.-K. Kim, “Cooling rate influences in carbon fibre/PEEK composites. Part II: interlaminar fracture toughness,” *Compos. Part Appl. Sci. Manuf.*, vol. 32, no. 6, pp. 763–774, Jun. 2001.

[161] S.-L. Gao and J.-K. Kim, “Cooling rate influences in carbon fibre/PEEK composites. Part III: impact damage performance,” *Compos. Part Appl. Sci. Manuf.*, vol. 32, no. 6, pp. 775–785, Jun. 2001.

[162] A. P. Deshpande and J. C. Seferis, “Processing Characteristics in Different Semi-Crystalline Thermoplastic Composites Using Process Simulated Laminate (PSL) Methodology,” *J. Thermoplast. Compos. Mater.*, vol. 9, no. 2, pp. 183–198, Jan. 1996.

[163] N. Namani, T. Sato, T. Ikeda, and T. Ishikawa, “Flexural Performance and Process Conditions of Thermoplastic Composite Laminates Processed by Automated Tape Placement,” presented at the ICCM 20, Copenhagen, 2015.

[164] L. A. Torres, K. Ghavami, and J. J. Garcia, “A transversely isotropic law for the determination of the circumferential young’s modulus of bamboo with diametric compression tests,” *Lat. Am. Appl. Res.*, vol. 37, no. 4, pp. 255–260, 2007.

[165] W. Young and R. Budynas, *Roark’s Formulas for Stress and Strain*, 7th ed. McGraw-Hill, 1989.

[166] F. Pierron and P. Davies, “Ring Compression Test for Cylindrical Composite Mechanical Characterization,” presented at the 4th European Conference on Composites: Testing & Standardisation, Lisbon, Portugal, 1998.

[167] C. Briançon, “Résultats de calculs par éléments finis (in french),” Nantes, Internal report (CETIM), Sep. 2016.

[168] I. M. Daniel, “Thermal Deformations and Stresses in Composite Materials,” in *Thermal Stresses in Severe Environments*, D. P. H. Hasselman and R. A. Heller, Eds. Springer US, 1980, pp. 607–628.

[169] S. Krishnamurthy, “Pre-stressed advanced fibre reinforced composites fabrication and mechanical performance,” 2006.

[170] S. Motahhari and J. Cameron, “Impact Strength of Fiber Pre-Stressed Composites,” *J. Reinf. Plast. Compos.*, vol. 17, no. 2, pp. 123–130, Jan. 1998.

[171] S. Motahhari and J. Cameron, “Fibre Prestressed Composites: Improvement of Flexural Properties through Fibre Prestressing,” *J. Reinf. Plast. Compos.*, vol. 18, no. 3, pp. 279–288, Jan. 1999.

[172] J. Zhao and J. Cameron, “Polypropylene matrix composites reinforced with pre-stressed glass fibers,” *Polym. Compos.*, vol. 19, no. 3, pp. 218–224, Jun. 1998.

[173] H. Lu, “Effects of Tape Tension on Residual Stress in Thermoplastic Composite Filament Winding,” *J. Thermoplast. Compos. Mater.*, vol. 18, no. 6, pp. 469–487, Nov. 2005.

[174] J. Colton, J. Muzzy, S. Birger, H. Yang, and L. Norpoth, “Processing parameters for consolidating PEEK/carbon fiber (APC-2) composites,” *Polym. Compos.*, vol. 13, no. 6, pp. 421–426, Dec. 1992.

[175] T. Yoshitomi, K. Nagamatsu, and K. Kosiyama, “On the stress relaxation of nylon 6,” *J. Polym. Sci.*, vol. 27, no. 115, pp. 335–347, Jan. 1958.

[176] N. J. Abbott, “Extension and Relaxation of Nylon Filaments,” *Text. Res. J.*, vol. 21, no. 4, pp. 227–234, Jan. 1951.

[177] J. A. Barnes, “Thermal expansion behaviour of thermoplastic composites,” *J. Mater. Sci.*, vol. 28, no. 18, pp. 4974–4982, Jan. 1993.

[178] P. P. Parlevliet, H. E. N. Bersee, and A. Beukers, “Residual stresses in thermoplastic composites—A study of the literature—Part II: Experimental techniques,” *Compos. Part Appl. Sci. Manuf.*, vol. 38, no. 3, pp. 651–665, Mar. 2007.

[179] M. P. I. M. Eijpe and P. C. Powell, “Residual stress evaluation in composites using a modified layer removal method,” *Compos. Struct.*, vol. 37, no. 3, pp. 335–342, Mar. 1997.

[180] A. Ajovalasit, “Advances in Strain Gauge Measurement on Composite Materials: Strain Measurement on Composite Materials,” *Strain*, vol. 47, no. 4, pp. 313–325, Aug. 2011.

[181] B. Pan, K. Qian, H. Xie, and A. Asundi, “Two-dimensional digital image correlation for in-plane displacement and strain measurement: a review,” *Meas. Sci. Technol.*, vol. 20, no. 6, p. 62001, Jun. 2009.

[182] C.-K. Soh, Y. Yang, and S. Bhalla, Smart materials in structural health monitoring, control and biomechanics. Hangzhou: Zhejiang Univ. Press, 2012.

[183] I. De Baere, G. Luyckx, E. Voet, W. Van Paepegem, and J. Degrieck, “On the feasibility of optical fibre sensors for strain monitoring in thermoplastic composites under fatigue loading conditions,” *Opt. Lasers Eng.*, vol. 47, no. 3, pp. 403–411, 2009.

[184] L. Sorensen, T. Gmür, and J. Botsis, “Residual strain development in an AS4/PPS thermoplastic composite measured using fibre Bragg grating sensors,” *Compos. Part Appl. Sci. Manuf.*, vol. 37, no. 2, pp. 270–281, Feb. 2006.

[185] Ksc. Kuang, R. Kenny, M. P. Whelan, W. J. Cantwell, and P. R. Chalker, “Embedded fibre Bragg grating sensors in advanced composite materials,” *Compos. Sci. Technol.*, vol. 61, no. 10, pp. 1379–1387, 2001.

[186] J. H. L. Grave, M. L. Håheim, and A. T. Echtermeyer, “Measuring changing strain fields in composites with Distributed Fiber-Optic Sensing using the optical backscatter reflectometer,” *Compos. Part B Eng.*, vol. 74, pp. 138–146, Jun. 2015.

[187] S. Uchida, E. Levenberg, and A. Klar, “On-specimen strain measurement with fiber optic distributed sensing,” *Measurement*, vol. 60, pp. 104–113, Jan. 2015.

[188] D. M. Sánchez, M. Gresil, and C. Soutis, “Distributed internal strain measurement during composite manufacturing using optical fibre sensors,” *Compos. Sci. Technol.*, vol. 120, pp. 49–57, Dec. 2015.

[189] J. R. Pedrazzani, S. M. Klute, D. K. Gifford, A. K. Sang, and M. E. Froggatt, “Embedded and surface mounted fiber optic sensors detect manufacturing defects and accumulated damage as a wind turbine blade is cycled to failure,” *Luna Innov. Inc*, 2012.

[190] J. R. Pedrazzani, M. Castellucci, A. K. Sang, M. E. Froggatt, S. M. Klute, and D. K. Gifford, “Fiber Optic Distributed Strain Sensing Used to Investigate the Strain Fields in a Wind Turbine Blade and in a Test Coupon with Open Holes,” in *Proceedings of the 44th International SAMPE Tech. Conf*, 2012, pp. 22–25.

[191] S. M. Klute, A. K. Sang, D. K. Gifford, and M. E. Froggatt, “Appendix H Defect detection during manufacture of composite wind turbine blade with embedded fiber optic distributed strain sensor, *Conference proceedings*, 2013”

[192] S. M. Klute, D. R. Metrey, N. Garg, and N. A. A. Rahim, “In-Situ Structural Health Monitoring of Composite-Overwrapped Pressure Vessels,” *SAMPE J.*, vol. 52, no. 2, pp. 7–17, 2016.

[193] H. Ramezani-Dana, P. Casari, A. Perronnet, S. Fréour, F. Jacquemin, and C. Lupi, “Hygroscopic strain measurement by fibre Bragg gratings sensors in organic matrix composites – Application to monitoring of a composite structure,” *Compos. Part B Eng.*, vol. 58, pp. 76–82, Mar. 2014.

[194] M. Gigliotti, F. Jacquemin, J. Molimard, and A. Vautrin, “Transient and cyclical hygrothermoelastic stress in laminated composite plates: Modelling and experimental assessment,” *Mech. Mater.*, vol. 39, no. 8, pp. 729–745, Aug. 2007.

[195] K. D. Cowley and P. W. R. Beaumont, “The measurement and prediction of residual stresses in carbon-fibre/polymer composites,” *Compos. Sci. Technol.*, vol. 57, no. 11, pp. 1445–1455, Jan. 1997.

[196] L. L. Warnet, On the effect of residual stresses on the transverse cracking in cross-ply carbon-polyetherimide laminates, PhD thesis, University of Twente, 2000.

[197] A. A. Fahmy and J. C. Hurt, “Stress dependence of water diffusion in epoxy resin,” *Polym. Compos.*, vol. 1, no. 2, pp. 77–80, Dec. 1980.

[198] M. Schlottermöller, R. Schledjewski, and P. Mitschang, “Influence of process parameters on residual stress in thermoplastic filament-wound parts,” *Proc. Inst. Mech. Eng. Part J. Mater. Des. Appl.*, vol. 218, no. 2, pp. 157–164, Apr. 2004.

[199] S. K. Ha, H.-T. Kim, and T.-H. Sung, “Measurement and Prediction of Process-induced Residual Strains in Thick Wound Composite Rings,” *J. Compos. Mater.*, vol. 37, no. 14, pp. 1223–1237, Jan. 2003.

[200] S. K. Ha and J. Y. Jeong, “Effects of winding angles on through-thickness properties and residual strains of thick filament wound composite rings,” *Compos. Sci. Technol.*, vol. 65, no. 1, pp. 27–35, Jan. 2005.

[201] G. Aleong and M. Munro, “Evaluation of the Radial-Cut Method for Determining Residual Strains in Firer Composite Rings,” *Exp. Tech.*, vol. 15, no. 1, pp. 55–58, Jan. 1991.

[202] C. Trautmann, “Recherches sur les tubes composites pour les profileurs (Researches on composite tubes for profilers),” Ifremer, Internal report (Ifremer) 12–083, 2012.

[203] M. Arhant, P. Y. Le Gac, M. Le Gall, C. Burtin, C. Briançon, and P. Davies, “Modelling the non fickian water absorption in polyamide 6,” *Polymer Degradation and Stability*, 2016.

[204] P. Y. Le Gac, M. Arhant, M. Le Gall, P. Davies, and C. Burtin, “Prediction of mechanical property loss in polyamide during immersion in sea water,” presented at the VIII International conference on "times of polymers and composites: from Aerospace to Nanotechnology, Naples, Italy, 2016.

[205] H. Obeid, P. Casari, A. Clément, S. Fréour, and F. Jacquemin, “Caractérisation du comportement hygro-mécanique de composites à matrice polyamide renforcée par des fibres de verre (in french),” presented at the JNC19, Lyon, France, 2015.

Appendix I: Finite element calculations performed on composite rings tested under radial compression

A – Introduction

This first Appendix presents the results from finite element calculations performed by Christophe Briançon from the CETIM. Here, emphasis is placed on radial compression tests performed on composite rings.

B - Meshing conditions

A hexahedron finite element mesh was used (type C3D8R), with 7 through thickness elements of 5 mm, Figure I-A.

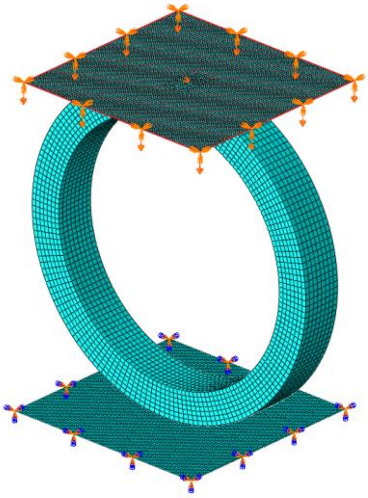

Figure I-A: Mesh used for radial compression calculations

C - Mechanical properties

The mechanical properties used for the finite element calculations are presented in Table I-A. Most of the mechanical properties were measured on composite panels manufactured by thermo-compression, presented in Chapter 4.

Table I-A: Mechanical properties used for finite element calculations (*: property not measured experimentally)

Property	Value
M_f (%)	60
V_f (%)	48
Void Content (%)	2
$E_{1compression}$ (MPa)	89700
E_2 (MPa)	5810
E_3 (MPa)*	5810
ν_{12}	0.36
ν_{13}*	0.36
ν_{23}*	0.4
G_{12} (MPa)	2370
G_{13} (MPa)*	2370
G_{23} (MPa)*	2030

D - Unidirectional rings

The results from the calculations performed on unidirectional composite rings (wound at 90°, diameter=200 mm) of different thicknesses (2, 4, 8 and 12mm) are presented in Figure I-B. These results are compared to the experimental data. A displacement between 0.5 to 6 mm was applied on the different composite rings.

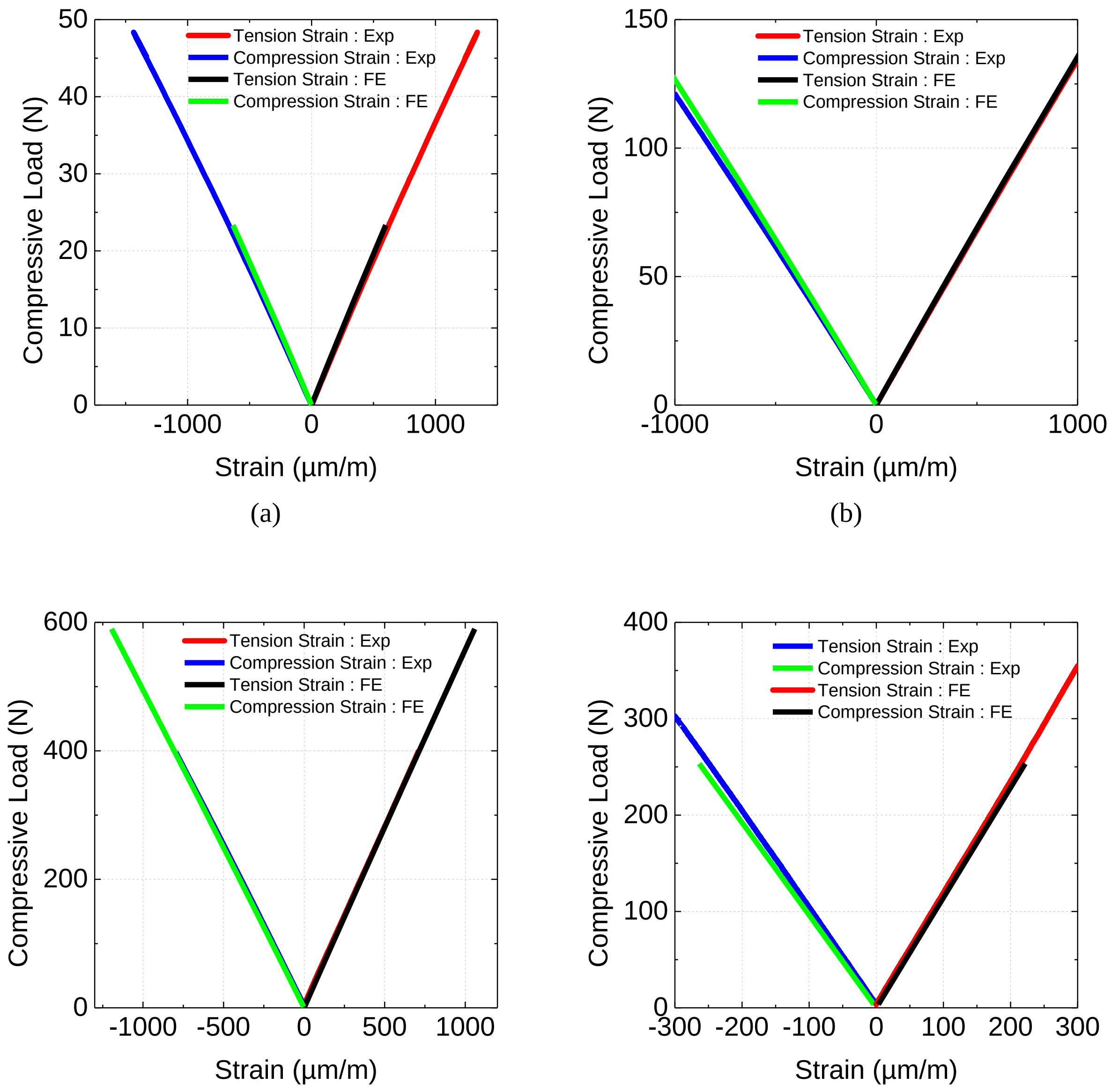

(a) (b)

(c) (d)

Figure I-B: Experimental and finite element calculation (load-strain) results for unidirectional composite rings of different thicknesses tested under radial compression (a) 2 mm (b) 4 mm (c) 8 mm (d) 12 mm

The results shown in Figure I-B show that a good correlation is found between the experimental results and the finite element calculations.

E - Rings from composite tubes

Similar calculations were performed on composite rings extracted from the C/PA6 cylinders tested under hydrostatic pressure (±55° and 0/±88).

First, results concerning the cylinder laid at ±55° (inner diameter of 120mm, thickness 9.1mm) are presented in Figure I-C.a. For these calculations, a displacement of 1 mm was applied on the composite ring.

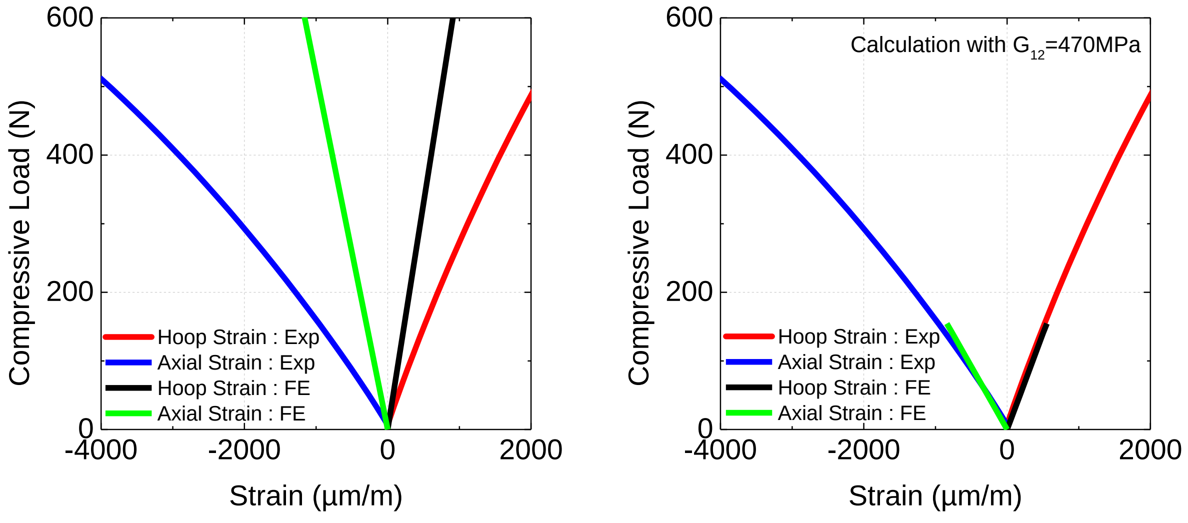

(a) (b)

Figure I-C: (a) Experimental and finite element calculation (load-strain) results for the ±55° composite rings and (b) G_{12} value adjusted to fit the experimental data

The results presented in Figure I-C.a indicate that the strains at a given load in the experimental test were much higher than those given by the model, indicating a lower stiffness. This result is quite surprising and can be associated with the groove induced by the non circular model or due to lower matrix dominated properties. The shear modulus G_{12} was then adjusted to fit the experimental data (Figure I-C.b) and a value of G_{12} of 470MPa was able to describe the strain evolution. It is worth noting that this value of G_{12} is quite low and does not really have any physical meaning. However, it proves that the mechanical properties are lower than those expected for this type of sequence.

The same calculations were performed on rings extracted from the 0/±88 cylinder (inner diameter of 100mm, thickness 12.1mm). A displacement of 2 mm was applied on the different composite rings. Results are presented in Figure I-D.

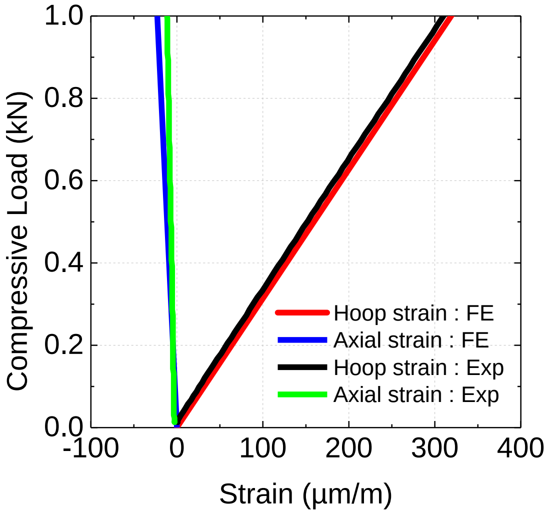

Figure I-D: (a) Experimental and finite element calculation (load-strain) results for the 0/±88 composite rings

Concerning these composite rings, results are in good correlation with the experimental data.

Appendix II: Finite Element Calculations performed on the [0/±88] C/PA6 cylinder

A – Introduction

This second Appendix presents the results from finite element calculations obtained when simulating the response to hydrostatic pressure of the [0/±88] cylinder.

B – Dimensions of the cylinder

The cylinder of interest is the one laid at [0/±88]. The dimensions of the latter are shown in Figure II-A and the dimensions of the end covers are presented in Figure II-B.

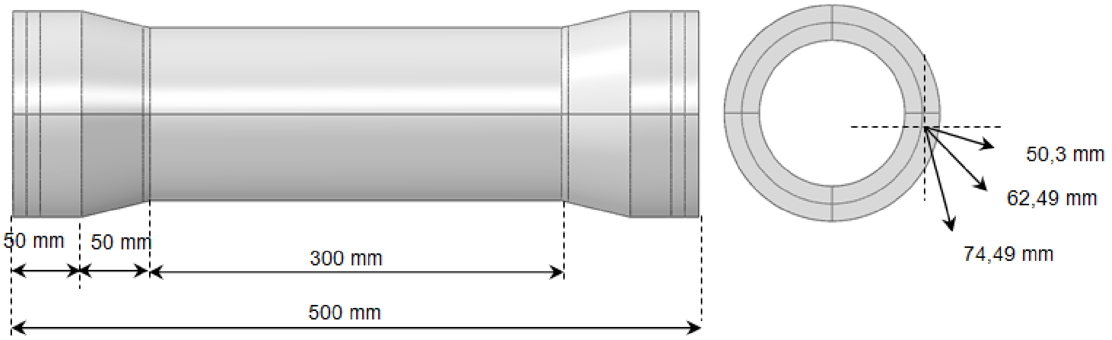

Figure II-A: Dimensions of the [0/±88] cylinder

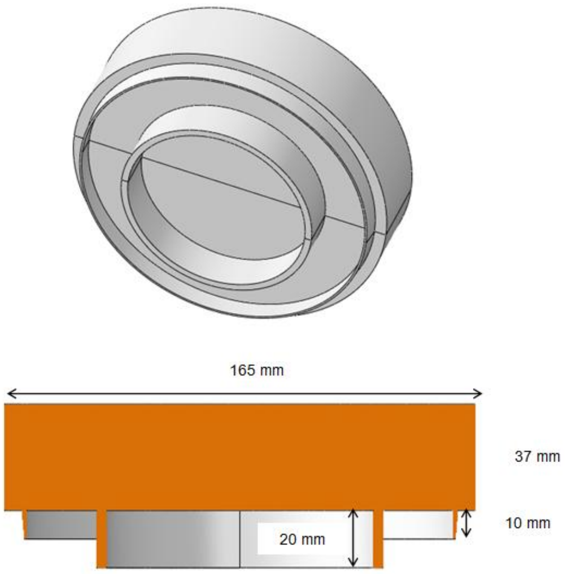

Figure II-B: Dimensions of the end covers

C – Mesh conditions

The composite cylinder is meshed using hexahedron elements (type C3D8R). It contains 7 through thicknesses elements of 5 mm, Figure II-C.a. The end covers are also meshed using hexahedron elements of 8 mm, Figure II-C.b.

(b)

(a)

Figure II-C: Mesh conditions (a) Composite tube (b) End covers

D – Boundary conditions

The composite tube and the end covers were subjected to an external pressure of 610 bar. The interface between the composite tube and the end covers is considered without friction.

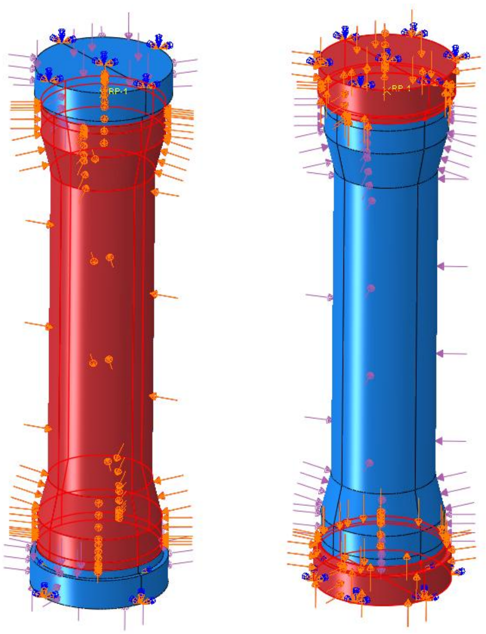

Figure II-D: Pressure conditions

E - Results from simulation (implosion)

The results from the simulation are presented in this section. It may be noted that the material properties used for the calculation are the same than in the previous appendix, i.e. shown in Table I-A.

First, the response in terms of strains as a function of hydrostatic pressure until failure is presented in Figure II-E. Experimental data are compared to the simulation.

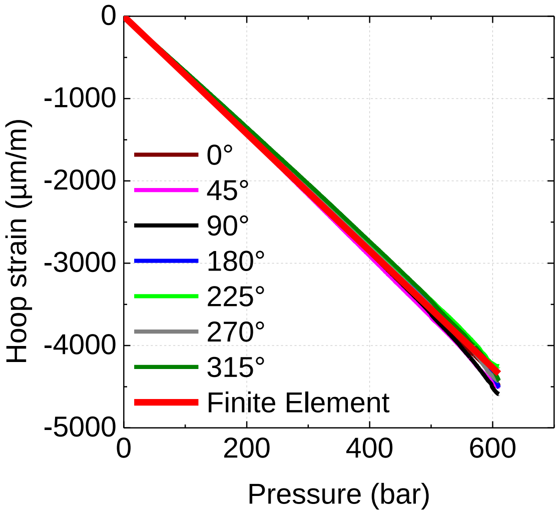

Figure II-E: Experimental hoop strains compared to the finite element simulation

The results show an excellent agreement between the experimental data and the finite element prediction. In addition, the through thickness compressive stresses contained within the tube at 610 bar are shown in Figure II-F. These represent the compressive stresses along the fibre direction.

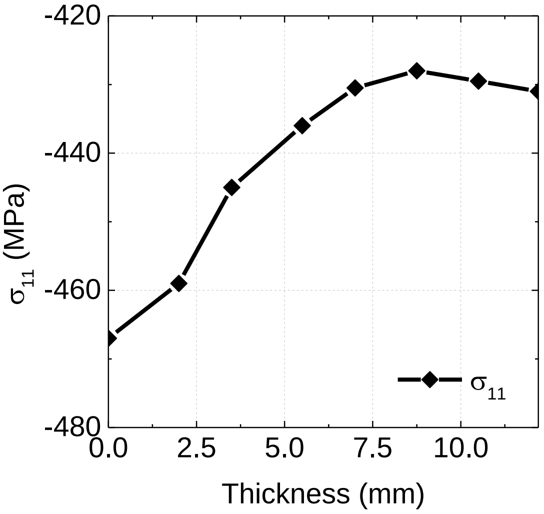

Figure II-F: Through thickness compressive stresses at 610 bar (Inner wall at 0 mm)

Results show that the maximal compressive stress is found on the inner wall and has a value of 466 MPa. This value obtained from the simulation is lower than those obtained from the experimental compression tests, presented in Chapter 4 (1385 MPa for the pin-ended buckling test and 513 MPa for the uniaxial compression test). Also, the through thickness stress gradient is quite low as the external stress is only 8 percent lower than that of the inner wall.

Finally, a simulation was performed in order to determine the pressure at which the composite tube starts to buckle. This simulation allows us to determine if the composite tube fails due to buckling or due to material failure. Results showed that the composite tube starts to buckle at 1348 bar (Figure II-H), which is much higher than the experimental implosion pressure. Therefore, this result suggests that in this case, the failure was due to pure material, which is in agreement which was what presented in Chapter 7.

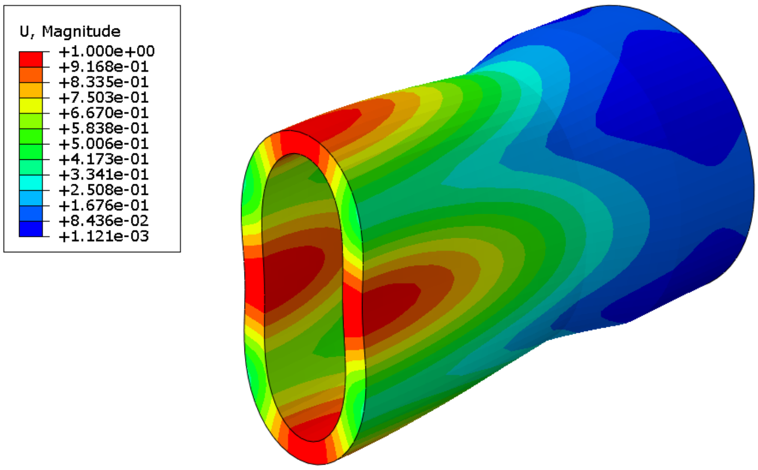

Figure II-H: Mode II buckling mode obtained at a pressure of 1348 bar

Appendix III: French Summary

Introduction

L’année 2015 a été reconnue comme étant l’année la plus chaude jamais enregistrée dans l’histoire moderne. Bien que cette information soit reliée à la température à la surface de la Terre, une des problématiques principales aujourd’hui concerne les océans qui absorbent plus de 90% de l’énergie liée au réchauffement climatique. Ce réchauffement climatique à long terme soulève de nombreuses questions, notamment comment celui-ci va t’il influer sur les changements climatiques futurs. Cependant, 70% de la surface des océans n’a pas encore été explorée et les masses d’eau profonde possèdent des propriétés très spécifiques (température, salinité) qui doivent être mesurées en temps réel. De ce fait, avec une profondeur moyenne des océans de 3800 mètres, il est devenu nécessaire de concevoir des engins d’exploration et des dispositifs de surveillance qui sont capables de supporter d’importantes pressions hydrostatiques.

Pendant de nombreuses années, les métaux ont été utilisés pour des applications sous-marines. Cependant, du à leurs excellentes propriétés spécifiques, les matériaux composites commencent à remplacer les structures actuelles. Ceux qui sont utilisés actuellement en milieu marin sont presque tous fabriqués avec des composites à matrice thermodurcissable (polyester, époxy). Ces enceintes sous marines, fabriquées par enroulement filamentaire, exigent de fortes épaisseurs (plus de 10mm). Obtenir de telles épaisseurs sans défauts est un réel challenge ; les contraintes résiduelles et les délaminages sont courants et mènent à une rupture prématurée de la structure.

Il existe aujourd’hui une alternative aux matrices thermodurcissables: les matrices thermoplastiques (polypropylène, polyamide, PPS, PEEK…). Celles-ci offrent la possibilité d’une mise en forme par placement de bandes pré-imprégnées par chauffage laser local associé à des propriétés mécaniques très intéressantes, une bonne résistance au vieillissement et un recyclage possible en fin de vie. Plus ductiles mais également réparables par fusion locale, elles offrent un réel potentiel pour des structures nettement améliorées. D’un point de vue scientifique, la plupart des études conduites sur ces matériaux se sont focalisées sur les structures aéronautiques, c'est-à-dire des structures minces. Dans ce contexte, plusieurs études ont abordé les liens entre mise en œuvre et microstructure, cependant l’influence sur les propriétés en compression dans des enceintes épaisses n’a pas été étudiée. En 2013, le CETIM (Centre Technique des Industries Mécaniques), situé à Nantes (France), a investi dans un équipement de placement de bandes pré-imprégnées par chauffage laser local. Le contrôle du procédé de fabrication et de ses paramètres (vitesse de dépôt, température, pression de consolidation, etc.) va permettre une évaluation approfondie du potentiel de ces matériaux pour de telles applications. Les composites à matrices thermoplastiques sont une famille de matériaux dont les paramètres de fabrication ont une forte influence sur la microstructure et les propriétés mécaniques. La compréhension et le contrôle de ces paramètres sont essentiels afin d’optimiser les différentes structures et cela demande une forte collaboration entre le fabriquant et le laboratoire, ce qui est la particularité de cette étude. De plus, très peu de travaux existent dans la littérature concernant le vieillissement de composites thermoplastiques renforcés de fibres longues de carbone. Leur durabilité en milieu marin requiert des études plus approfondies. En effet, comprendre et être capable de prédire l’effet de longues périodes d’immersion sur la diffusion d’eau et les conséquences sur les propriétés mécaniques est essentiel.

L’objectif principal de la présente étude est de fabriquer des cylindres épais en composites thermoplastiques par chauffage laser local de bandes pré-imprégnés qui sont capables de résister à de fortes pressions hydrostatiques (supérieures à 400 bar). Leur comportement sera comparé au profileur DEEP ARVOR utilisé actuellement à l’Ifremer pour des applications sous-marines et qui peut plonger à des profondeurs de 4500 mètres. Ces cylindres de référence font 1,2 mètres de long, ont un diamètre interne de 120 mm et une épaisseur de 12 mm. Afin d’atteindre un tel but, l’étude a été divisée en sept parties distinctes qui permettront une compréhension complète et globale du comportement de ces nouveaux composites thermoplastiques soumis à de fortes pressions hydrostatiques dans des conditions extrêmes (immersion à des basses températures couplée à de fortes pressions hydrostatiques).

Ce projet est une collaboration basée sur les compétences et connaissances de chacun des partenaires. Ainsi, le CETIM a l’expérience des procédés de fabrication, l’Ifremer possède les infrastructures d’essai et travaille sur le sujet depuis quelques années et l’Ecole Centrale de Nantes possède des moyens de caractérisation et des compétences permettant une caractérisation fine des matériaux.

Dans le premier chapitre, un accent particulier est mis sur les cylindres en composites pour applications sous-marines, concernant les composites thermodurcissables ainsi que les composites thermoplastiques. Plusieurs difficultés sont mises en évidence, associées au procédé de fabrication utilisé pour fabriquer les cylindres, la façon de mesurer les propriétés en compression ainsi que l’effet du vieillissement marin.

Dans le Chapitre 2, les différents matériaux et techniques expérimentales qui ont été utilisées au cours de cette étude sont présentés.

Dans le Chapitre 3, la diffusion de l’eau a été étudiée, tout d’abord sur la matrice pure puis étendue au matériau composite. Les cinétiques de diffusion ont été identifiées et ensuite utilisées pour prédire l'absorption d'eau dans la structure réelle, c'est-à-dire un cylindre en composite thermoplastique épais immergé à de basses températures pendant plusieurs années.

Dans le Chapitre 4, une étude expérimentale poussée est décrite dans le but d'étudier l'effet de l'eau sur les propriétés mécaniques en traction, compression et hors plan. Celles-ci sont ensuite utilisées pour prédire comment l'absorption d'eau peut limiter l'utilisation de cylindres en composite thermoplastique pour des applications sous-marines.

Dans le Chapitre 5, l'effet des conditions de fabrication sur les propriétés mécaniques et la microstructure est étudié. L'influence de la vitesse de refroidissement sur les cinétiques de cristallisation a été examinée et les modélisations associées sont également présentées. Ensuite, l'influence de la cristallinité sur les propriétés mécaniques est discutée. Enfin, les différences de propriétés mécaniques obtenues par Thermo-Compression et par placement de bandes pré-imprégnées sont discutées.

Dans le Chapitre 6, les contraintes et déformations résiduelles ont été étudiées sur des composites fabriqués par thermo-compression ainsi que par placement de bandes pré-imprégnées. L'effet des conditions environnementales (température et humidité) a également été étudié en détail selon différentes techniques.

Le Chapitre 7 décrit la fabrication de cylindres épais en composites thermoplastiques placement de bandes pré-imprégnées et présente les résultats d'implosion de ces enceintes sous-marines. Les pressions d'implosions obtenues sont ensuite comparées aux valeurs obtenues sur la référence en carbone/époxy utilisé actuellement à l'Ifremer.

Enfin, une conclusion générale présentant les résultats majeurs de l'étude est présentée ainsi que des pistes de travaux futurs.

La démarche décrivant l'étude est présentée ci-après :

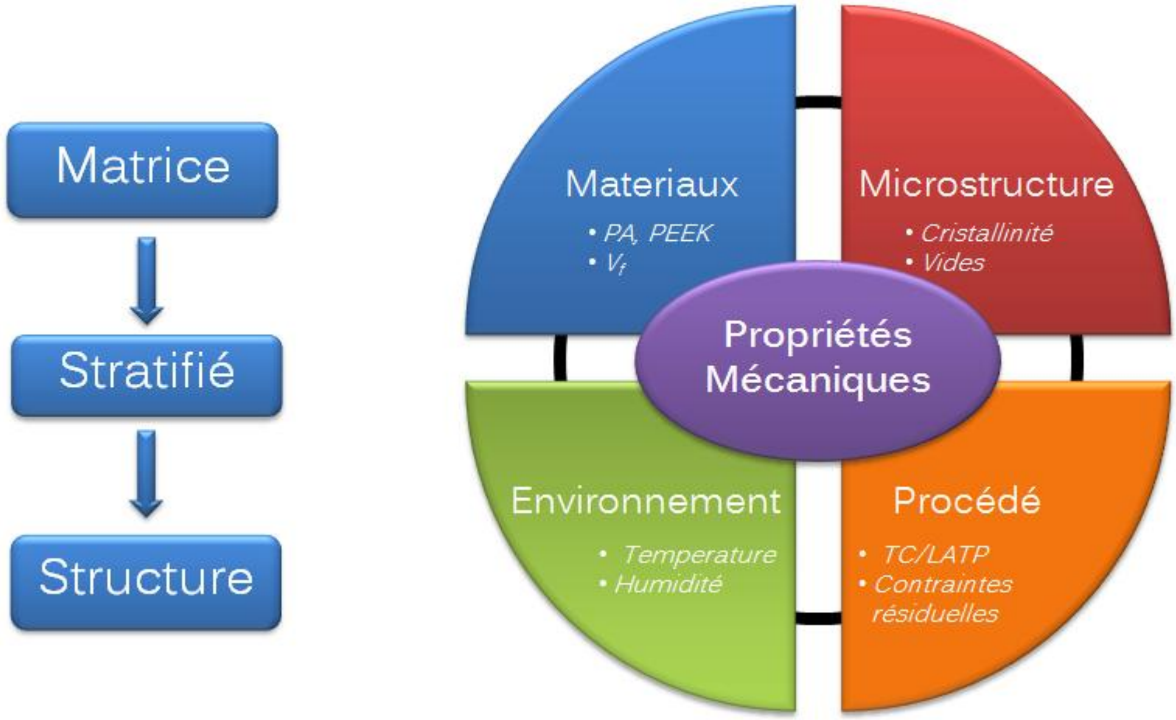

Démarche de l'étude

Résultats et conclusions

La plupart des études présentées dans la littérature sur l'implosion de cylindre en composites thermoplastiques concernent des composites hautes performances comme le C/PEEK ou le C/PEKK. Cependant, pour l'application visée, c'est-à-dire des profileurs océanographiques, ces matériaux sont bien trop chers comparés au C/Epoxy utilisé actuellement à l'Ifremer. De ce fait, des composites à matrice thermoplastique low-cost comme le C/PA6 sont particulièrement intéressants et ont été sélectionnés pour cette étude. Cependant, ces matériaux sont particulièrement sensibles au vieillissement marin. Lors d'une étude préliminaire, des composites en C/PA6 et C/PA12 ont été testés en flexion 4 points dans l'état sec et saturé en eau. Bien que les propriétés du C/PA12 à l'état saturé soient supérieures au C/PA6, les résultats dans l'état sec sont bien meilleurs pour le C/PA6, comme présenté dans la figure ci-après :

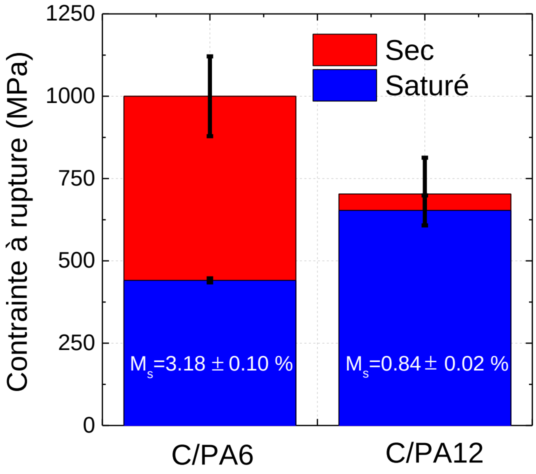

Contraintes à rupture obtenues en flexion 4 points sur des échantillons unidirectionnels de C/PA6 et C/PA12 à l'état sec et saturé en eau

Ce choix de matériau était justifié par le fait que les enceintes fabriquées sont épaisses (plus de 10 mm) et que de ce fait la diffusion d'eau peut-être considérée suffisamment lente pour ne pas affecter significativement les propriétés mécaniques du tube. Pour vérifier cette hypothèse, un modèle de diffusion s'avère nécessaire.

Tout d'abord, la cinétique de diffusion d'eau dans le PA6 pur ainsi que dans le C/PA6 a été étudiée sur une large gamme de température et de conditions d'humidités. Il a été montré que la cinétique de diffusion d'eau dans ces matériaux ne suivait pas un comportement de type Fickien du fait d'une augmentation de la diffusivité avec l'absorption d'eau lorsque le matériau passe de l'état vitreux à l'état caoutchoutique. Lorsque l'eau pénètre dans le matériau, la température de transition vitreuse T_g décroit et ce comportement change grandement les cinétiques de diffusion d'eau. Deux cas ont été identifiés ; un premier en dessous de T_g où la diffusivité peut être décrite suivant une loi d'Arrhénius et un second où la diffusivité peut être décrite par la théorie du volume libre. Ces deux cas ont ensuite été implémentés dans un modèle original afin de prédire la diffusion d'eau à différentes températures. Les résultats ont montré un excellent un accord entre les données expérimentales et les prédictions sont significativement plus précises que celles données par la loi Fickienne qui est, qui plus est, non conservative, plus particulièrement à basse température (15°C). Les résultats du modèle concernant l'absorption d'eau dans le PA6 pur à 15°C sont présentés ci-après :

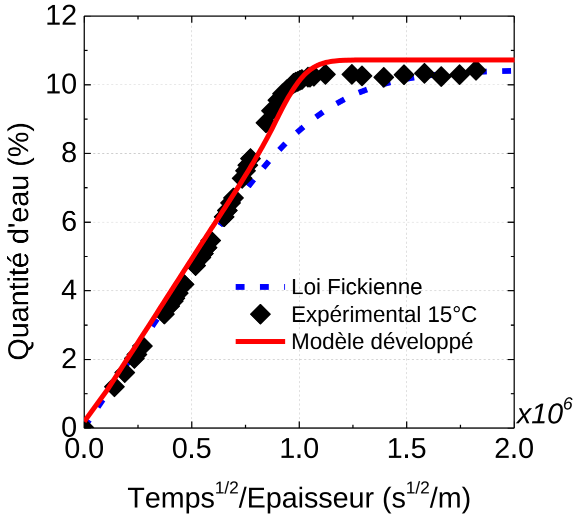

Comparaison des résultats du modèle spécifique développé avec les données expérimentales et la loi Fickienne à 15°C

Ce modèle est basé sur des considérations physiques et a ensuite été appliqué au matériau composite en utilisant des lois d'homogénéisation. Cela a permis de prédire l'absorption d'eau dans un tube en composite thermoplastique de 12 mm immergé à 15°C pendant plusieurs années. Les prédictions ont montré que l'eau n'était pas le problème majeur pour cette application à ces températures d'immersion car seulement 3 mm de la surface extérieure du tube est affectée par l'eau après deux ans d'immersion. Cependant, cette étude a concernait seulement la diffusion d'eau et l'étape suivante était d'étudier l'effet de l'absorption d'eau sur les propriétés mécaniques.

L'évolution des propriétés mécaniques sur des stratifiés C/PA6 de 2 mm d'épaisseur en fonction du vieillissement hydrique a ensuite été déterminée en traction, compression ainsi que hors plan sur des échantillons saturés à différents taux d'humidité. Cette étude a permis de comprendre quel était l'effet de l'eau sur les propriétés mécaniques de matériaux composites thermoplastiques immergés en eau. Il a été démontré que l'eau avait un effet très négatif sur les propriétés mécaniques dominées par le comportement de la matrice (diminuées de plus de 50%) comme présenté ci-dessous :

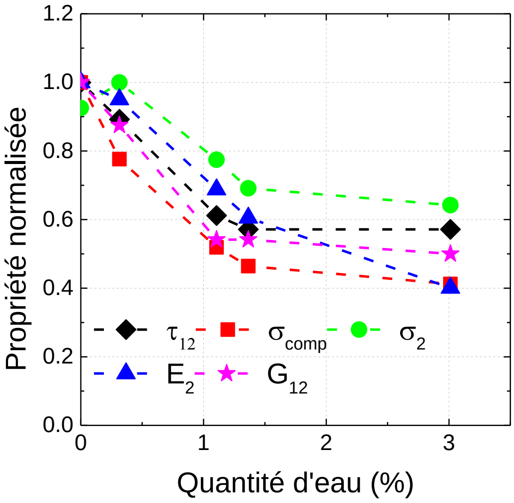

Chute des propriétés des mécaniques dominées par le comportement de la matrice en fonction de la quantité d'eau

Cette perte de propriétés a été liée à la diminution de la température de transition vitreuse (passant de 66°C à l'état sec à -12°C lorsque le matériau est complètement saturé en eau). Une relation semi-empirique entre les propriétés mécaniques et la quantité d'eau a été proposée. Couplé au modèle de diffusion d'eau développé précédemment, les résultats ont montré que la diffusion d'eau n'était pas le facteur limitant lorsque des cylindres épais en C/PA6 sont immergés en eau à 15°C pendant 2 ans.

L'étape suivante était de s'intéresser à l'effet des conditions de fabrication sur la cinétique de cristallisation et les propriétés mécaniques de composites en C/PA6. Du fait de la nature semi-cristalline du PA6, le développement d'un modèle de cristallisation était nécessaire. Le modèle a été appliqué pour décrire avec précision la cinétique non-isotherme de cristallisation dans la matrice PA6 pure ainsi que dans le composite. Ensuite, des panneaux de 2 mm d'épaisseur ont été fabriqués par thermo-compression à différentes vitesses de refroidissement (entre 1 et 20°C/min). Des essais de traction transverse ont été réalisés et les résultats ont montré que le degré de cristallinité de la matrice n'avait pas d'effet sur les propriétés mécaniques dans cette gamme de refroidissement. De plus, des panneaux et anneaux en C/PA6 ont été fabriqués par placement de bandes et ont ensuite été caractérisés mécaniquement afin d'identifier les différences pouvant exister entre ce procédé de fabrication et la thermo-compression en utilisant le même matériau de base. Les résultats ont montré que les propriétés mécaniques obtenues par placement de bandes étaient nettement inférieures à celles obtenues par thermo-compression. Ces différences ont été associées à des niveaux de contraintes résiduelles beaucoup plus importants dans le cas du procédé par placement de bandes. De ce fait, une étude spécifique sur la formation et la mesure des contraintes résiduelles a été conduite en utilisant différentes techniques.

Tout d'abord, un nouveau type de fibre optique a été intégré durant la fabrication de panneaux en C/PA6 fabriqués par thermo-compression. L'évolution des déformations résiduelles a été continuellement enregistrée durant le procédé (figure ci-après) de fabrication et la relaxation de ces dernières, induite par les conditions environnementales (température et humidité), a également été étudiée.

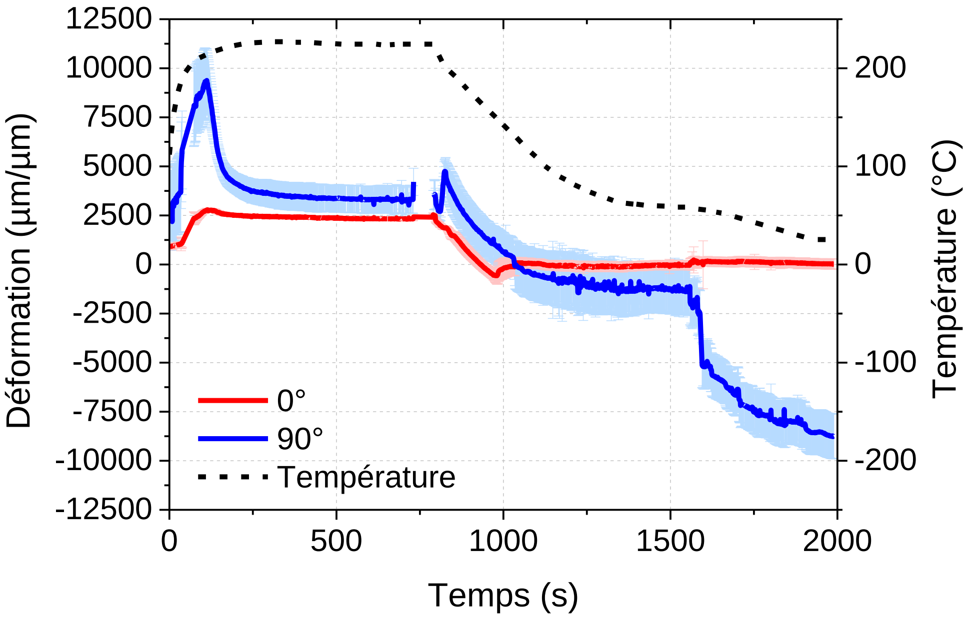

Evolution des déformations résiduelles lors de la fabrication de panneaux unidirectionnels en C/PA6 par thermo-compression

L'effet des conditions environnementales a également été étudié en détail en utilisant des stratifiés asymétriques. Les résultats d'essais gravimétriques de sorption et désorption ont montré que la relaxation des contraintes résiduelles induites par les conditions environnementales était un phénomène complètement réversible. Cependant, le modèle de diffusion d'eau spécifique qui a été développé précédemment n'a pas été en mesure de décrire la diffusion d'eau dans des stratifiés asymétriques. Cela est du au fait que la diffusion d'eau était beaucoup plus rapide que la prédiction, comme présenté dans la figure ci-après :

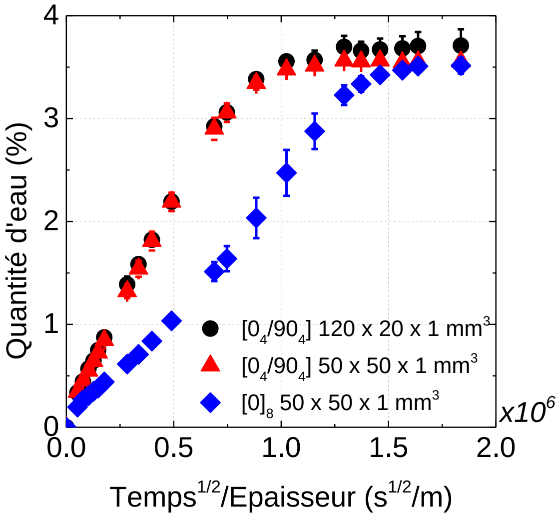

Comparaison des cinétiques de diffusion d'eau dans des échantillons asymétriques et unidirectionnels

Ce résultat suggère que les contraintes résiduelles ont un effet non négligeable sur la cinétique de diffusion d'eau. Enfin, les déformations résiduelles présentes dans des anneaux unidirectionnels en composite fabriqués par placement de bandes ont été étudiées et les résultats ont montré que ces dernières évoluaient linéairement avec l'augmentation de l'épaisseur des anneaux. Ce résultat suggère qu'un phénomène de couplage important pourrait se produire pour des tubes épais fabriqués par placement de bandes.

La dernière partie de cette étude concernait la performance de cylindres en composite thermoplastique épais fabriqués par placement de bandes soumis à de fortes pressions hydrostatiques. Les résultats obtenus ont ensuite été comparés aux tubes références en C/Epoxy utilisés actuellement à l'Ifremer. Premièrement, les résultats de contrôle qualité non destructifs (contrôle ultrasons, tomographie aux rayons X) ont montré que les cylindres en composites thermoplastiques étaient de bien meilleure qualité en terme de vide que le cylindre en C/Epoxy fabriqué par enroulement filamentaire, ce qui représente une nette amélioration.

Ensuite des tests d'implosion ont été réalisés sur les cylindres en C/PA6 et en C/Epoxy. Les résultats d'implosion ont montré que le cylindre en C/Epoxy implosait à la plus forte pression (772 bar). Son homologue en C/PA6 enroulé au même angle (±55°) a implosé à une pression bien plus faible (209 bar). Cette différence a été associée à un net défaut de circularité induit par le mandrin en deux parties utilisé pour fabriquer le tube. Ce type de défaut mène à un flambement prématuré de la structure et donc à une ruine précoce de cette dernière. De plus, cette faible pression d'implosion a également été associée aux propriétés mécaniques inférieures du PA6 par rapport à l'époxy. Ensuite, l'orientation des fibres a été optimisée [0/±88] dans le but d'obtenir un tube plus raide et dépendant peu des propriétés de la matrice, ce qui devrait permettre d'atteindre des pressions d'implosion bien plus élevées. Un nouveau mandrin a également utilisé pour obtenir un tube sans défaut de circularité. Les résultats du test d'implosion étaient bien plus proches du tube référence en C/Epoxy car celui-ci a implosé à une pression de 610 bar (bien que le diamètre du tube était plus faible, 100 mm). Les déformations résiduelles dans ces cylindres en composite épais ont également été étudiées et les résultats obtenus étaient étonnants car le niveau de déformations résiduelles le plus élevé était obtenu pour le tube en C/Epoxy. Cependant, il a également été montré que dans le cas du cylindre enroulé à [0/±88], les déformations résiduelles n'étaient pas uniformes dans longueur du cylindre, ce qui nécessiterait des études approfondies. Cependant, la pression d'implosion obtenue avec cette nouvelle séquence montre qu'il est en effet possible d'utiliser des tubes en C/PA6 pour des applications sous-marines à des profondeurs de 4000 mètres tout en prenant en compte un coefficient de sécurité de 1,5.

Perspectives

Les résultats présentés dans cette étude sont très prometteurs mais ont également soulevé plusieurs questions supplémentaires auxquelles des réponses pourraient être apportées lors de travaux futurs. Celles-ci peuvent être divisées en six parties.

Premièrement, il parait particulièrement intéressant d'utiliser le modèle de diffusion d'eau spécifique développé dans cette étude pour prédire la perte de propriété mécanique induite par l'absorption d'eau dans ces stratifiés C/PA6. A titre d'exemple, ce type de prédiction a été possible sur le polymère pur (PA6) mais doit encore être adapté aux matériaux composites. L'évaluation de la validation de ce modèle en immergeant des échantillons épais prélevés dans les différents cylindres a démarré, mais nécessite des temps d'immersion très longs.

Deuxièmement, il a été montré que le modèle de diffusion d'eau spécifique développé durant l'étude n'était pas en mesure de décrire l'absorption d'eau dans des stratifiés asymétriques. De ce fait, des études futures pourraient se focaliser sur l'adaptation du modèle à des stratifiés asymétriques. Tout d'abord, il est important de comprendre pourquoi le modèle n'est pas adapté à ce type de stratifié. Pour ce faire, il serait particulièrement intéressant de réaliser des essais DVS sur des stratifiés asymétriques fins dans de larges gammes de température et d'humidité, de la même façon que pour les essais réalisés afin de développer le modèle en premier lieu. Cela pourrait permettre de comprendre quelle propriété dévie par rapport à ce qui a été identifié dans le modèle (formation de cluster, valeur de T_g, évolution de la diffusivité) et donc de modifier le modèle en conséquence. Il serait également particulièrement intéressant de quantifier l'effet de couplage contrainte-diffusion d'eau pour ces matériaux. De telles études sont actuellement en cours dans une autre thèse à l'Ifremer

(C.Humeau) dont un des buts est de développer des modèles de couplage contrainte-diffusion d’eau.

Troisièmement, au cours de l’étude, une technique novatrice de mesure des déformations induites par le procédé de fabrication a été utilisée dans des panneaux en composites thermoplastiques fabriqués par thermo-compression. Il serait très intéressant d’adapter cette nouvelle technique à des pièces en composites thermoplastiques fabriquées par placement de bandes afin de comprendre les différences entre ces deux procédés de fabrication.

Quatrièmement, un nombre limité de cylindres (seulement un) a été testé jusqu’à implosion pour chaque condition. De ce fait, la reproductibilité de ces différents essais doit être évaluée. Cela n’a pas été réalisé durant l’étude car bien que le C/PA6 soit moins cher que le C/PEEK, il n’en reste pas moins que fabriquer et instrumenter des tubes de 12 mm d’épaisseur est assez cher. De ce fait, il serait particulièrement intéressant de réaliser des tests sur des tubes plus fins avec des rapports épaisseur/diamètre similaires. Cela permettrait de réduire significativement la quantité de matériaux utilisés pour chaque condition testée. De plus, il a été montré que prédire l’implosion de tubes soumis à des chargements hydrostatiques n’était pas simple et qu’utiliser les propriétés mécaniques déterminées par thermo-compression n’était peut-être pas la solution optimale. De ce fait, réaliser des essais comme de la compression axiale et diamétrale jusqu’à rupture sur des tubes fins fabriqués par placement de bandes pourrait améliorer la prédiction de la pression d’implosion. De plus, l’utilisation de matériaux composites encore moins chers comme du Verre/PP ou du Verre/PA pourrait également permettre de fabriquer des tubes de différentes épaisseurs et orientations qui permettrait une plus grande compréhension du procédé de placement de bandes et de l’effet de ses paramètres de fabrication sur la pression d’implosion. Ce type de matériau a été étudié lors de plusieurs travaux antérieurs, ainsi, des données concernant les propriétés matériaux ainsi que la diffusion d'eau sont disponibles.

Un autre aspect qui n'a pas été étudié durant ces travaux est le comportement en fluage de ces cylindres. Cet aspect pourrait avoir un effet non négligeable sur la pression d'implosion pour l'application visée et plus particulièrement concernant les défauts qui pourraient apparaitre. De ce fait, des travaux supplémentaires sont nécessaires afin de comprendre comment le comportement en fluage pourrait limiter l'utilisation de tels cylindres. De tels travaux sont actuellement en cours à l'ENS Cachan en collaboration avec le CETIM au travers d'une autre thèse.

Un dernier aspect qui nécessite des travaux supplémentaires concerne l'effet d'impacts sur la pression d'implosion. De nombreux composites à matrice thermoplastique possèdent des ténacités supérieures à celles de leurs homologues thermodurcissables. Cela suggère que l'utilisation des composites thermoplastiques pourrait grandement améliorer la résistance à l'impact de structures soumises à ce type de chargement. Cependant, lors d'une étude précédente réalisée à l'Ifremer, l'implosion résiduelle après impact a été étudiée sur des cylindres en C/Epoxy et en C/PEEK et les résultats ont montré que l'implosion après impact diminuait plus rapidement pour les tubes en C/PEEK que pour les tubes en C/Epoxy, malgré des zones d'impact plus faibles pour ce premier. Ces résultats ont montré que des études supplémentaires sont nécessaires dans le but de comprendre comment la ténacité du matériau est transférée à la structure.

Une quantité non négligeable de travail doit encore être fournie afin de qualifier ces cylindres en carbone/Polyamide 6 pour des applications sous-marines. Cependant, les premiers résultats obtenus sont très prometteurs. Un dernier aspect qui n'a pas été développé dans cette étude est la possibilité de recycler ces composites thermoplastiques. L'impact environnemental est désormais un aspect très important à prendre en compte dans le design de structures en matériaux composites et les composites thermoplastiques offrent une réelle solution à ce problème. Une analyse détaillée du cycle de vie pourrait aider à quantifier ces différents avantages.

UNIVERSITE
BRETAGNE
LOIRE

ECN
Centrale
Nantes

Thèse de Doctorat

Mael Arhant

Composites Thermoplastiques pour Enceintes Sous-Marines

Thermoplastic Composites for Underwater Applications

Résumé

Les matériaux composites utilisés actuellement en mer sont presque tous fabriqués avec des résines thermodurcissables (polyester, époxy). Il existe aujourd'hui une alternative aux matrices thermodurcissables: les matrices thermoplastiques (PP, PA, PPS, PEEK…). Celles-ci offrent la possibilité d'une mise en forme par chauffage local associée à des propriétés mécaniques très intéressantes et un recyclage possible en fin de vie. Les raisons pour l'adaptation lente de ces matériaux est qu'ils nécessitent une mise en œuvre complètement différente du fait de leur microstructure particulière et du manque d'expérience sur ce type de matériau pour des structures épaisses. Le but de ce projet est de designer, fabriquer et tester une enceinte en composite thermoplastique pour des profondeurs de 4500 mètres, afin d'établir l'intérêt technique, écologique et économique de ces matériaux sur ce marché. De nombreux matériaux existent mais des questions se posent concernant la sensibilité à l'eau de matériaux composites moins chers comme le C/PA6, plus particulièrement sur son effet sur les propriétés mécaniques. Dans cette étude, un modèle de diffusion spécifique a été développé et des relations semi-empiriques ont été proposées pour prendre en compte l'effet du vieillissement sur les propriétés mécaniques. L'effet des conditions de fabrication a également été étudié en détail et les résultats ont montré qu'il y avait un effet important de la mise en œuvre sur les propriétés. Enfin des cylindres épais en C/PA6 ont été fabriqués puis testés jusqu'à implosion. Les résultats ont montré qu'il était possible d'utiliser ce type de matériau pour des applications sous-marines car ceux-ci ont implosé à des pressions supérieures à 600 bar.

Mots Clés : Composites Thermoplastiques, Fibre de carbone, Vieillissement marin, compression, contraintes résiduelles

Abstract

The composite materials used at sea are today nearly all based on thermoset resins (polyester, epoxy). However, there is an increasing number of thermoplastic matrix polymers available on the market (PP, PA, PPS, PEEK…), which offer possibilities for forming by local heating, attractive mechanical properties and the potential for end of life recycling. The reasons for the slow adoption of these materials are that they require a completely different manufacturing route compared to the current materials, they have more complex microstructure, and that there is little experience with them, particularly for thick structures. The aim of this study is to design, manufacture and test thermoplastic composite pressure vessels for 4500 meter depth, in order to establish a technical, economic and ecological assessment of the use of these materials to replace traditional composites underwater. Various material options exist but there are questions concerning the water sensitivity of less expensive thermoplastic composites (C/PA6) for these applications, more especially concerning its effect on the mechanical properties. In this study, a specific water diffusion model has been developed and semi-empirical relationships have been proposed to account for the effect of water on the mechanical properties. The effect of processing conditions have also been addressed and have shown a strong effect on the mechanical properties. Finally, thick thermoplastic cylinders were manufactured and tested until implosion. Results showed that it is possible to use C/PA6 thermoplastic composite cylinders for deep sea applications as these imploded at pressures higher than 600 bar.

Key Words : Thermoplastic composites, Carbon fibres, Sea Water Aging, Compression, residual stresses

L'Université Nantes Angers Le Mans